



HAL
open science

Seismic and aseismic deformations in deep mines – Case of the Garpenberg mine, Sweden

Emeline Lhoumaud

► **To cite this version:**

Emeline Lhoumaud. Seismic and aseismic deformations in deep mines – Case of the Garpenberg mine, Sweden. Earth Sciences. Université de Lorraine, 2023. English. NNT: 2023LORR0200 . tel-04628818

HAL Id: tel-04628818

<https://hal.univ-lorraine.fr/tel-04628818>

Submitted on 28 Jun 2024

HAL is a multi-disciplinary open access archive for the deposit and dissemination of scientific research documents, whether they are published or not. The documents may come from teaching and research institutions in France or abroad, or from public or private research centers.

L'archive ouverte pluridisciplinaire **HAL**, est destinée au dépôt et à la diffusion de documents scientifiques de niveau recherche, publiés ou non, émanant des établissements d'enseignement et de recherche français ou étrangers, des laboratoires publics ou privés.



**UNIVERSITÉ
DE LORRAINE**

**BIBLIOTHÈQUES
UNIVERSITAIRES**

AVERTISSEMENT

Ce document est le fruit d'un long travail approuvé par le jury de soutenance et mis à disposition de l'ensemble de la communauté universitaire élargie.

Il est soumis à la propriété intellectuelle de l'auteur. Ceci implique une obligation de citation et de référencement lors de l'utilisation de ce document.

D'autre part, toute contrefaçon, plagiat, reproduction illicite encourt une poursuite pénale.

Contact bibliothèque : ddoc-theses-contact@univ-lorraine.fr
(Cette adresse ne permet pas de contacter les auteurs)

LIENS

Code de la Propriété Intellectuelle. articles L 122. 4

Code de la Propriété Intellectuelle. articles L 335.2- L 335.10

http://www.cfcopies.com/V2/leg/leg_droi.php

<http://www.culture.gouv.fr/culture/infos-pratiques/droits/protection.htm>



UNIVERSITÉ
DE LORRAINE

SIReNa



Université de Lorraine
Laboratoire GeoRessources
École doctorale SIReNa

Thèse

Présentée et soutenue publiquement pour l'obtention du titre de

DOCTEUR DE L'UNIVERSITÉ DE LORRAINE

en GEOSCIENCES

par **Emeline LHOUMAUD**

Seismic and aseismic deformations in deep mines –

Case of the Garpenberg mine, Sweden

Soutenue publiquement le 29 septembre 2023

Membres du jury :

Mme Mai-Linh DOAN	Maîtresse de conférences (HDR), ISTERre, Université Grenoble-Alpes, Grenoble, France	Rapporteur
Mr Pierre DUBLANCHET	Maître de conférences (HDR), Centre de Géosciences, Mines ParisTech, Fontainebleau, France	Rapporteur
Mr Frédéric CAPP	Professeur, Geoazur, Université Côte d'Azur, Valbonne, France	Président du jury
Mme Savka DINEVA	Professeure, Luleå University of Technology, Luleå, Sweden	Examineur
Mme Beata ORLECKA-SIKORA	Professeure, Institute of Geophysics, Polish Academy of Sciences, Warsaw, Poland	Examineur
Mr Yann GUNZBURGER	Professeur, GeoRessources, Université de Lorraine, Nancy, France	Directeur de thèse
Mr Jannes KINSCHER	Ingénieur (PhD), Institut national de l'environnement industriel et des risques (Ineris), Nancy, France	Co-directeur de thèse
Mme Marianne CONIN	Maîtresse de conférences, GeoRessources, Université de Lorraine, Nancy, France	Co-encadrante de thèse

Remerciements

Je commence mes remerciements dans l'avion pour le Chili, trois semaines après ma soutenance de thèse, pour travailler deux mois à l'Universidad tecnica federico santa maria de Santiago. Ces trois semaines montrent beaucoup de ces 3 ans de thèse. Une soutenance de thèse, une conférence internationale, une conférence nationale, un départ pour le Chili. Bien dynamique. Mais surtout... surtout beaucoup de fierté, de passion, de prise de conscience, de confiance et de rencontres avec de nombreux pairs. Alors sur cette touche positive... c'est parti pour les remerciements !

Honneur aux directeurs de thèse !! Tout d'abord merci Yann. Comme je te l'ai dit lors de la soutenance, tu as toute ma confiance, intellectuelle et humaine. J'admire la rigueur de tes raisonnements, et j'apprécie le soin et la précision que tu demandes au niveau du vocabulaire utilisé. Un mot mal employé, c'est un concept mal compris, et tu m'as aidé à construire des raisonnements plus solides et à clarifier des notions de base. J'adore tout ce processus, et je trouve passionnant de dérouler tout le fil intellectuel derrière l'utilisation d'un simple mot ! Au-delà de ça, merci de toujours t'assurer que tout aille bien, même avec un petit check rapide de temps en temps qui permet d'avoir l'opportunité de partager si quelque chose va mal. Merci d'avoir toujours répondu présent lorsque cela a été le cas, même si le moment où je décidais de partager ce qui me posait problème depuis des jours voire des semaines arrivait d'un coup un soir à 18h. Certaines fois, cela m'a vraiment beaucoup aidé. Merci de ton humour également, et pour tes blagues subtiles et bien dosées qui me font toujours beaucoup rire. Je suis ravie de se revoir d'ici un mois au Chili, visiter une ou des mines ensemble, en collègues cette fois !

Merci à toi Jannes. Merci pour tes multitudes d'idées, pour m'avoir connecté avec plein de gens différents. Ce n'était pas facile, à la fois car tu étais le seul sismologue de l'équipe et parce que tu avais un tout petit bout de chou qui ne faisait pas ses nuits ;) Beaucoup de mes interrogations de thèse sont nées de nos discussions, et elle aurait été extrêmement différente sans elles. Et je suis contente que ce soit avec toi que j'ai vécu la galère des quiproquos, des redéfinitions de termes 100000 de fois, car ta personnalité rend tout cela bien plus facile. Merci pour les deux heures de cours « sismo » qui resteront gravées dans ma mémoire. J'ai absolument adoré et tu as réussi à me communiquer un bout de conscience de la beauté de la physique derrière les concepts de toutes ces analyses sismos un peu obscures.

Et enfin merci Marianne. Déjà pour la journée la plus importante de ma thèse, même si tu n'en as peut-être pas conscience : celle où nous sommes allées faire des essais de cisaillement au labo. Où j'ai posé des questions et où tu as « refusé » de répondre, en me poussant à réfléchir. Cette journée, après des mois de covid confinée chez moi, a vraiment marqué un tournant décisif. C'est la journée où j'ai commencé à m'emparer scientifiquement de ma thèse. Merci pour ta passion, pour me montrer la beauté de ce métier particulier qui est celui de chercheur, et pour me pousser à toujours aller plus loin dans le raisonnement scientifique. Et merci pour ta disponibilité, ta gentillesse et tes valeurs féministes ! merci aussi d'oser dire les choses quand il faut les dire. Merci pour le concert aux NJP, pour toutes les tablettes de chocolat offertes pour mon anniversaire. Ce sont de petits gestes qui restent, et qui montrent beaucoup du soin et de l'attention que tu nous donnes.

En plus de mes directeurs de thèse, je vais remercier les personnes qui ont directement contribué à mes travaux de thèse. Tout d'abord merci Aurélien pour ton aide durant l'analyse des carottes de forages. J'ai beaucoup appris sur les différents types de linéations. Merci d'avoir vérifié certaines de mes mesures à la boussole, cela m'a permis d'être encore plus confiante sur leur validité. Merci aussi à toi Danièle, grâce à qui j'ai pu réaliser les analyses DRX. J'ai été épaté par ta patience, le soin et la délicatesse de tes gestes lors de la réalisation des analyses. Tu m'as donné de manière complètement désintéressée plusieurs heures de travail, et la nature des minéraux de remplissage était une donnée très précieuse dans ma thèse. Merci aussi à Guy-Aurèle et Laure : c'était un vrai plaisir d'être votre tutrice de projet labo et merci pour votre investissement !

Merci aux membres du comité de suivi individuel : David et Daniel. Sincèrement, chaque échange avec vous était extrêmement pertinent, et je ressortais toujours de chaque comité très motivée et avec des éléments concrets pour avancer. Merci à Daniel de m'avoir invitée à Lyon, de m'avoir accordé beaucoup de ton précieux temps durant cette semaine, et de m'avoir donné accès à une licence Itasca via le programme IEP research program. Merci à Rima pour toute l'aide apportée durant la semaine à Lyon, et à toute l'équipe Itasca pour leur formidable accueil.

Merci également aux membres du COPIL. A Pascal tout d'abord. Tes conseils et tes explications de sismologie étaient extrêmement précieux. Nous te devons l'idée du modèle de dislocation élastique qui est une analyse majeure de la thèse. Merci à Savka, que j'ai remerciée en tant que membre du jury mais qui a également participé à plusieurs COPILs. Merci beaucoup à Anders également pour la présence durant les COPILs et les informations données sur la mine.

Merci à Anders également pour ton temps durant mes missions à la mine qui font partie des meilleures expériences de ma thèse. J'adore descendre à 1km sous terre, être immergée dans l'univers minier, et encore plus dans une mine telle que celle de Garpenberg. J'étais émerveillée par la technologie et l'ambiance, et chaque visite de mine me confirme que je suis dans l'environnement qui me correspond. Toujours à la mine, merci aussi beaucoup à toute l'équipe de géologues qui m'a beaucoup aidée à comprendre le gisement de Lappberget mais aussi à analyser les carottes. La semaine à la carothèque reste un très bon souvenir, et un merci particulier à Morvan qui m'a aidé pour les carottes mais aussi pour classer les différents groupes lithologiques en début de thèse. Merci à l'équipe de Boliden qui a organisé l'envoi des carottes de forages également.

En dehors de l'équipe de travail, merci aussi à toi Darius, pour avoir pris le temps d'écouter ma présentation et pour tes conseils et encouragements. Je pense aussi à Rachida, merci pour ton temps également et pour ne jamais arrêter de me dire de faire des plannings !

Et puisque j'écris ces remerciements après ma soutenance, c'est l'occasion pour moi de remercier les membres du jury. Tout d'abord Mai-Linh et Pierre, mes deux rapporteurs. Merci pour vos rapports de très grande qualité, dans lesquels j'ai senti votre intérêt et le temps que vous avez consacré à cette lecture. Merci pour vos compliments, et pour vos suggestions qui m'ont aidée non seulement dans ma réflexion mais aussi dans la préparation de ma soutenance. Merci à Frédéric d'avoir présidé la séance, merci pour le sérieux et l'organisation, ainsi que la pertinence des questions. Et enfin merci à Savka et Beata, également pour la pertinence de vos questions et votre regard davantage orienté vers la mine, qui est mon environnement de prédilection. De manière générale, merci à tous les cinq pour votre dynamique de groupe, j'ai passé un magnifique moment.

Enfin, je vais finir par remercier tous les membres à la fois de l’Ineris et de Géoressources. Ma thèse a vraiment oscillé entre les deux, et je suis ravie d’avoir eu la place privilégiée de bénéficier des avantages des deux organismes !

Commençons par l’Ineris. Toute cette formidable installation à la mine, et toutes les données collectées ont été possibles grâce au partenariat entre Boliden et l’Ineris. Et c’était une chance incroyable d’avoir accès à toutes ces données. Tout d’abord merci Emmanuelle. De t’être battue pour que la thèse commence, pour ton rôle durant la totalité de la thèse, pour ton investissement lors des soucis de prolongation de thèse. Je suis restée principalement concentrée sur la production de données, mais je sais que cela n’a été possible que parce que encadrants et supérieurs, et en grande partie toi et Yann, faisaient le nécessaire administrativement pour m’épargner toute cette charge. Merci à toi Francesca. Tu as eu un rôle très important pour moi la première année de thèse, j’ai eu beaucoup de chance de prendre la suite d’un travail fait aussi sérieusement et j’ai eu beaucoup de chance que tu sois toujours disponible dès que j’avais une question. J’adore ton côté gauche féministe militante, et j’aurais sincèrement aimé te connaître et travailler avec toi encore davantage !! Merci Nicolas pour les missions en Suède, et pour ton investissement à chaque fois que j’avais une question sur les cellules CSIRO (aller chercher une cellule pour répondre à mes questions de mesures d’angle, sortir tous tes papiers de calibration pour m’expliquer le $5\mu\epsilon$ de précision et j’en passe)! Merci beaucoup à toi Nathalie. Tout est toujours simple dans nos échanges et c’est très agréable. Merci pour cette incroyable semaine passée à l’ISRM ! Et merci pour toujours essayer de me donner davantage confiance ! Et enfin merci Franz pour les moments à table échangés et ta gentillesse. Et merci à toutes celles et ceux que je croisais très régulièrement ou de temps en temps : Roxanne (pensée spéciale pour les pointés sismiques !!), Mountaka (merci pour tes petits mots gentils à chaque fois que l’on se croise), Vincent (j’aurais adoré travailler davantage sur la modélisation !), Marwan, Isabelle, Benoit, Regis, Regis, Cyrille, Stella, Catherine, Alice. Et je termine par Alain, ce qui me fait une excellente transition vers Georessources car tu es quand même un peu Géoressources dans nos cœurs ! Toutes les randonnées que tu proposais m’ont vraiment rempli d’énergie à chaque fois ! Elles étaient hyper précieuses et représentaient de vrais bouffées d’air frais au propre comme au figuré !! Et en plus, tu es extrêmement inspirant !

Maintenant merci à Georessources. Je vais commencer par toi Dalija. Tu as certainement été la personne la plus importante pour moi à Nancy pendant toute ma première année de thèse. On a vécu des moments vraiment particuliers en cette période de Covid, confinées ensemble pendant près d’1 an et demi, avec une fin de thèse pour toi et une arrivée bancaire pour moi. Tu resteras une personne vraiment primordiale dans cette thèse, et je suis contente qu’on soit restées en contact et qu’on suive ce que devient l’autre avec beaucoup de bienveillance.

Merci à mes nouveaux collègues de bureau : Antoine et Rachit ! Je vous souhaite vraiment à tous les deux de vivre une superbe aventure, avec beaucoup de plaisir durant le processus (un peu de galère aussi ne nous montons pas) et de fierté à la fin! Gardez la motivation, c’est le plus précieux. Merci Kamel. J’étais toujours trop contente quand on se voyait et qu’on discutait ensemble ! Vraiment tu as une force incroyable, ton expérience de thèse était loin d’être facile et tu peux être extrêmement extrêmement fier de toi !! C’est incroyable à quel point tu as évolué personnellement durant ces années de thèse, et les années à suivre ne peuvent qu’être plus faciles !

Merci Danielle. La conférence ISRM était vraiment géniale et je suis très contente d'avoir partagé cette semaine avec toi. J'ai beaucoup apprécié toutes nos discussions et notamment celles sur la famille !! Bon courage pour ces derniers mois, ça se termine un jour !!

Merci Nina <3 !! ça y est tu l'auras le fameux « Nina <3 » ! Merci pour toutes nos discussions sur la Guyane, un petit bout de mon cœur est encore là-bas et un gros bout de cœur est dans les mines artisanales. Alors merci pour nos échanges, ça me fait plaisir de suivre ton/tes projets au sens large : de thèse mais également tout ce qui gravite autour. J'adore la passion que tu mets dans ta thèse (mais prends soin de toi quand même). Cœur coeur féministe également, parce que ça fait juste du bien d'échanger avec toi ! Et cœur cœur pour cet amour des voyages partagé !

Et puis je te souhaite le meilleur Baptiste ! C'est toujours un réel plaisir de te parler quand tu es au bureau et voir ton point de vue thèse CIFRE ! J'ai hâte de voir tout ce que tu auras fait à la fin sur ton sujet passionnant, et comment tes positions auront évolué sur les différents sujets dont on a eu l'occasion de discuter ! Bon courage et merci !

Merci Delphine pour la bienveillance et la créativité que tu donnes à l'équipe. Tu apportes vraiment la touche « Delphine », et sans toi, il manquerait quelque chose !!

Merci Jacques, de me faire rêver avec tes projets en Chine et pour tes partages d'expériences et de connaissances toujours instructifs.

Merci Rasool de me faire saliver avec toutes tes succulentes recettes, pour la tarte le jour de mon anniversaire, pour tous tes conseils remplis de sagesse et pour tes blagues continuelles !

Merci Olivier : à chaque échange, on apprend quelque chose avec toi et je suis très admirative de ta pédagogie et de ta tranquillité apparente !

Merci Noémie également, arrivée vers la fin de ma thèse, avec l'expérience commune d'Alès !

Un immense merci à toi Audrey. T'entendre me répéter pendant 2 semaines avant ma soutenance que je suis une femme forte et que ma thèse est géniale, ça m'a vraiment beaucoup aidé !! Je ne peux que te retourner tous tes bons conseils. Merci pour ton empathie, pour ta générosité, pour ton énergie inépuisable.

Merci Mariam. Merci pour nos soirées pizzas/films, mais surtout pour nos promenades de nuit et dans les parcs. J'admire beaucoup de choses chez toi, et en particulier ta sensibilité artistique, ton courage et ton intelligence. Tu es devenue une personne proche à Nancy et une amie. On doit encore regarder le documentaire de Van Gogh ! Et vivement nos prochains appels avec Emilio !

Je tiens aussi à remercier nos très chers post-docs qui sont partis mais qui ont rythmé le labo pendant la moitié de ma thèse !

Tout d'abord un immense merci à toi Vincent. J'ai adoré notre confiance en tant que partenaires de bureau, et j'adore encore plus le fait qu'elle existe encore aujourd'hui autour d'un café parisien.

Merci pour toutes nos discussions que je valorise beaucoup.

Merci à Aurélien. J'ai beaucoup admiré ton courage et la force d'assumer tes convictions ! Je suis ravie de savoir que tu t'épanouis au BRGM ! merci aussi pour ton écoute.

Merci Guillaume bien sûr, et avec toi merci à Diane ! Je garde un super souvenir de tous nos moments partagés à 4 avec Emilio ! Merci pour la joie partagée lors de votre mariage, c'était un moment très spécial de cette thèse également ! Vous êtes un couple magnifique, et j'ai hâte de vous revoir autour d'un bon repas !

Et enfin personnellement, merci à toutes celles et ceux qui ont participé à ma vie à Nancy.

Merci Oura, Awal, Rayan et Farel. Des fois la vie nous fait des cadeaux ! Te retrouver ici Oura à Nancy, 15 ans après notre rencontre au Bénin ne peut pas être qualifié autrement qu'un cadeau de vie ! Ta petite famille est incroyable. Et aussi merci de m'avoir hébergé à mon arrivée (merci Rayan pour m'avoir prêté ta chambre !). J'ai adoré chacun de nos repas/goûter pendant ces 3 ans, je ressens toujours beaucoup de tranquillité et de confiance avec vous.

Merci à notre groupe de potes géromois : Marine, Martin, Chlotilde, Jarvis, Nathan, Emilio. La retraite d'écriture est vraiment un super souvenir !!! Je suis trop contente de vous avoir rencontré. J'adore la complémentarité de nos personnalités. Merci pour tous les précieux moments partagés, pour votre solidarité pendant l'écriture de thèse, et j'espère sincèrement qu'on refera des petits week-ends ensemble dans le futur !

Et je vais finir avec l'ami le plus important de cette thèse : Emilio ! merci merci merci, merci !! J'ai eu tellement de chance de tomber sur un partenaire de thèse comme toi ! C'est incroyable à quel point on se connaît après 3 ans presque 24h/24 ensemble ! Tu as la capacité d'anticiper et de me calmer en 2mns dès qu'un sujet me touche. Je valorise énormément le soutien qu'on s'est mutuellement apporté, avec nos portes respectives toujours ouvertes l'un pour l'autre. Si l'un de nous allait mal ou était contrarié pour quelque chose, l'autre arrêterait instantanément ce qu'il faisait, c'était un contrat tacite. Partager l'écriture de thèse avec toi était aussi une chance : avoir un partenaire pour manger des glaces à minuit au bureau, ça n'a pas de prix. Merci aussi pour tes petites attentions. En dehors de notre lien personnel, je valorise également nos discussions scientifiques. Tu es non seulement un ami, mais aussi un exemple pour moi. J'ai appris à tes côtés à oser devenir plus ambitieuse, à valoriser de rêver plus grand, à mettre davantage de « moi » dans mes travaux. Au-delà de ça, tu sais à quel point je valorise la personne que tu es et tes valeurs humaines. Alors MERCI. Et très sincèrement, j'espère que notre amitié restera encore très longtemps au-delà de la thèse.

Et enfin merci à ma famille. Merci d'abord à ma sœur. C'est quand même en tout premier lieu à travers toi que j'ai découvert le monde de la recherche, et je ne pense pas que l'idée de faire une thèse serait apparue si tu ne m'avais pas indirectement plongé dans ce milieu. Merci à toi et à Johan pour l'apparition dans ma vie de deux êtres qui me remplissent d'amour : ma petite Naélie et mon encore plus petit Elven. La naissance de Naélie a eu un énorme impact dans ma vie, devenir tata m'a fait découvrir une nouvelle manière d'aimer et c'est juste merveilleux. Et la naissance d'Elven sera certainement une des anecdotes de thèse les plus folles : avec un appel en plein milieu de mon écriture de chapitre de thèse à rendre le lendemain (et un autre à rendre 3 jours après), en mode « viens tout de suite à Paris, c'est pour aujourd'hui » ! Beaucoup d'émotions (et un peu de stress !), et je suis très fière et heureuse d'avoir été présente à la fois pour vous aider et pour partager ce magnifique moment de vie.

Et merci enfin à mes parents. Je n'avais pas du tout réalisé le niveau de stress dans lequel je vous ai plongé lors de cette thèse, avant le jour de la soutenance. Je suis super contente d'avoir partagé ce jour spécial avec vous, qui restera un des moments les plus forts et les plus positifs de ma vie. Merci encore à vous, car ce sont vos valeurs, votre dévouement et votre fantaisie qui font celle que je suis aujourd'hui et celle que j'aspire à être demain.

Résumé élargi

Le suivi sismique est couramment utilisé dans les mines profondes. A l'origine, son utilisation a été mise en place pour surveiller les coups de terrains, c'est-à-dire de violentes explosions de roches dans les mines associées à de la sismicité, responsables de nombreux accidents dans les mines (Cook, 1976; Kaiser et al., 1996; Mcgarr, 2002; Ortlepp & Stacey, 1994). Aujourd'hui encore, le suivi sismique est utilisé pour mieux prévenir les coups de terrain, mais a également étendu son utilisation pour d'autres objectifs tels qu'une amélioration de la compréhension du comportement du massif rocheux en réponse à l'excavation minière. (Cai et al., 2001; Hudyma et al., 2003). En général dans les mines profondes, les événements sismiques sont divisés en deux catégories : (i) des événements sismiques directement liés à la redistribution des contraintes induite par l'excavation minière, et qui suivent l'avancée de l'excavation et ii) des événements sismiques liés à un glissement le long de discontinuités majeurs ou des zones de cisaillement. Ces derniers sont plus difficiles à anticiper, et peuvent causer d'important dégâts. Parce que les sismologues étudient les séismes naturels depuis des décennies, ils ont accumulé un puissant savoir-faire, que ce soit au niveau de l'instrumentation, des outils d'analyses ou encore des modèles théoriques utilisés pour expliquer les séismes (Gibowicz & Kijko, 1994). En raison de ce savoir accumulé, mais également de l'opportunité qu'offre l'environnement minier pour mieux étudier les mécanismes impliqués dans les séismes, de plus en plus de collaboration sont engagées entre les entreprises minières et les scientifiques. Ainsi, les industriels bénéficient des compétences des scientifiques pour améliorer leur compréhension des déclenchements de séismes, dans un souci de sécurité et d'optimisation de la production dans la mine, alors que les mines profondes permettent aux scientifiques d'installer d' uniques réseaux d'étude pour étudier les environnements à la source et les propriétés de faille (Gibowicz, 2009; Ortlepp, 1997).

Dans ce contexte de collaboration, l'entreprise Boliden en Suède a développé différents partenariats avec différents organismes de recherche. En particulier, un partenariat existe depuis 2014 entre l'Ineris (Institut national de l'environnement industriel et des risques) en France et Boliden. Grâce à cette collaboration, une zone située à 1km de profondeur est instrumentée par l'Ineris depuis des années. L'analyse des événements sismiques dans la zone par Kinscher et al. (2020), avant le commencement de cette présente thèse, a mis en évidence la présence d'événements sismiques particuliers dans la mine : des répéteurs sismiques. Le concept de répéteurs sismiques provient du champ d'étude de la sismologie et fait référence à un type d'événements sismiques précis : ce sont des événements sismiques avec des formes d'onde extrêmement similaires, et sont associés à la rupture répétée de la même zone à des temps différents (Beroza et al., 1995; Mesimeri & Karakostas, 2018). La présence de répéteurs dans un contexte minier est notable, puisque cela montre que les mêmes zones sont activées à des temps différents dans la mine et malgré des zones exploitées différentes. De plus, les répéteurs sont rarement étudiés en contexte minier, et à ce jour une seule mine en Afrique du sud (mine Cooke 4) a identifié la présence de tels répéteurs avant la mine de Garpenberg. Ces répéteurs étaient associées à la

présence d'une large et bien connue zone de faille (Faille Zebra ~ 10 km de long) à 1km de profondeur, avec des magnitudes de moment comprises entre $-5.1 \leq M_w \leq -3.6$ (Naoi et al., 2015a; Naoi et al., 2015b; Yamaguchi et al., 2018). De manière similaire aux modèles bien connus en sismologie et décrits dans le paragraphe suivant, les auteurs associent la présence de ces répéteurs à des ruptures répéteurs de mêmes aspérités chargées par un glissement asismique dans les régions environnantes (Naoi et al., 2015a). A Garpenberg, le contexte est bien différent de la mine de Cooke 4, puisque la présence d'une large et bien connue faille telle que la faille Zebra n'est pas identifiée, et les familles de répéteurs sismiques sont associés avec des tailles de sources comprises entre 1 et 10m. Cette thèse représente donc un cas d'étude jamais étudié auparavant.

Alors que les répéteurs sismiques sont presque inconnus en contexte minier, ils ont été intensément étudiés par les sismologues à l'échelle géodynamique, et notamment aux niveaux des zones de subduction ou des plaques tectoniques. (Bohnhoff et al., 2017; Uchida, 2019). En particulier, la faille de San Andreas a été largement instrumentée à la suite de sept répéteurs sismiques enregistrés depuis 1987, avec une période de répétition d'environ 22 ans (Nadeau et al., 1995), au niveau du segment de Parkfield. Grâce à ce dense réseau d'instrumentation, un modèle d'interprétation a été élaboré, depuis largement adopté par la communauté des sismologues et appliqué à d'autres failles dans le monde. Le modèle associe la présence de répéteurs sismiques aux ruptures répétées d'une même patch bloqué chargé par un fluage environnant sur un plan de faille (Chen & Lapusta, 2009; Igarashi et al., 2003; Uchida et al., 2003; Yamaguchi et al., 2018). Généralement, le fluage est associé à la présence de phyllosilicates sur le plan de faille, susceptibles de fluer, alors que l'aspérité possède des propriétés rhéologiques différentes qui lui confèrent une nature sismogène (Ikari et al., 2011). Etudier l'origine des répéteurs sismiques dans un contexte de mine profonde est de large intérêt scientifique sur la compréhension générale du cycle sismiques et pour comprendre comment les séismes sont générés, que ce soient les séismes induits ou naturels, grâce à une unique échelle d'observation très rarement accessible : une échelle décamétrique, comprise entre l'échelle géodynamique et l'échelle du laboratoire. De plus, elle ouvre aussi des perspectives pour étudier les micromécanismes de fluage ainsi que le couplage entre fluage et sismicité, puisque la présence de répéteurs sismiques est classiquement associée à du fluage et questionne le mécanisme de chargement des zones sismiques. En plus de l'intérêt scientifique pour la compréhension des séismes, cette étude s'inscrit dans une démarche d'utilisation du suivi sismique pour mieux caractériser le comportement général du massif rocheux en réponse à l'excavation, dans un souci de gestion de risque et d'optimisation de la production durant l'exploitation minière.

Dans cette thèse, nous investiguons donc l'origine des répéteurs sismiques dans la mine de Garpenberg, en se basant sur le savoir accumulé par les sismologues au niveau des plaques tectoniques. En particulier, nous nous focalisons sur l'origine géologique et géomécanique des répéteurs, et nous questionnons l'applicabilité des modèles élaborés à l'échelle géodynamique dans un tel contexte. Plus particulièrement, nous proposons d'utiliser la multitude de données multi-échelle et multidisciplinaires disponibles dans le contexte minier de Garpenberg, pour explorer les différentes structures qui portent la sismicité (plan de faille, zones de cisaillement, massif rocheux), ainsi que les matériels et mécanismes qui chargent les zones sismiques (transfert de contraintes

statiques, fluage sur un plan de faille ou dans le massif rocheux). Une étude bibliographique présentée dans ce manuscrit montre la complexité d'une telle question, essentiellement car les notions mêmes d'aspérité et de zones de fluage dépendent considérablement des échelles et des champs d'études. Puisqu'une telle étude sur l'origine géologique et géomécanique des répéteurs sismiques n'a jamais été réalisée en contexte minier, nous développons notre propre méthodologie, basée sur les méthodes utilisées en sismologie, géologie et géomécanique.

Une première étude présentée dans le chapitre 3 a été réalisée à l'échelle du gisement (plusieurs centaines de mètres), en se focalisant sur deux types de données disponibles : des données lithologiques et des données géomécaniques. En analysant ces données, des corrélations statistiques entre lithologies et sismicité sont mises en évidence. En particulier, nous montrons que les répéteurs sismiques sont davantage associés à des roches contenant des minéraux type phyllosilicates, modérément fracturés et de bonne capacité à soutenir des contraintes. Au contraire, les événements sismiques isolés, c'est à dire qui n'appartiennent à aucune famille de répéteurs, sont associés à des roches sans minéraux de phyllosilicates et avec une résistance très élevée, ce qui suppose un mécanisme différent plutôt relié à de la fracturation induite directement par l'excavation. Pour les répéteurs, l'étude est toutefois limitée puisqu'ils sont présents dans des types de roches largement observés à l'échelle de la mine, ce qui suppose que d'autres éléments, telles que la présence de discontinuités, jouent également un rôle. En utilisant un modèle élastoplastique fourni par De Santis et al. (2020), nous montrons que dans certains cas, les changements de contraintes induits par l'excavation sont susceptibles d'activer des plans de faille orientés comme les plans nodaux déterminés par les analyses sismiques des familles de répéteurs. Toutefois, cela est seulement visible pour les données très proches de celles utilisées pour le calibrer le modèle. Ainsi, l'échelle d'étude, bien qu'elle fournisse des informations cohérentes avec le modèle des répéteurs donnés par les sismologues (i.e. répéteurs associés à la présence d'une aspérité rugueuse sur un plan de faille qui flue), reste insuffisante pour accéder au niveau de détails voulu sur l'origine des répéteurs (i.e. l'étude des structures portants les répéteurs ainsi que les mécanismes de chargement des zones sismiques).

En plus de cette étude à large échelle, deux études à échelle locale, chacune portant sur une famille de répéteurs singulière, ont été réalisées. Les deux familles de répéteurs sont localisées dans deux zones différentes du même bloc d'excavation et présentent des caractéristiques temporelles significativement différentes. La première est localisée dans le sill pillar juste au-dessus du bloc d'excavation instrumenté par l'Ineris (bloc 1250 à 1km de profondeur) alors que la deuxième est localisée au cœur de la zone d'excavation instrumentée. Temporellement, la première a été pour la première fois activée en 2016 et est toujours active aujourd'hui, avec des répéteurs sismiques encore régulièrement détectés par le réseau sismique (périodicité d'environ 35 jours entre les différents événements). La deuxième, au contraire, est restée active seulement 1 mois avec un nombre d'événements sismiques qui suit une loi d'Omori (décroissance en $1/t$, activée par 2 blasts différents).

Puisque que la première famille dans le sill pillar est toujours active aujourd'hui et grâce à sa localisation particulière proche des accès miniers, il a été possible d'installer un unique réseau de surveillance dans la zone source de la famille de répéteurs sismiques. Cette installation est la première installation de ce type en contexte minier, et reste extrêmement rare même à plus grande échelle, puisque la zone source d'événements sismiques est généralement très difficile d'accès. Elle vise à essayer d'atteindre la structure portant les répéteurs sismiques, ainsi que les matériaux potentiellement chargeant la zone. Des cellules permanentes de déformations ont été installées et des forages non destructifs ont été réalisés. Une fois les données de déformations et les carottes récupérées, une méthodologie a été développée pour analyser les données et enquêter sur l'origine de cette sismicité particulière. Cette méthodologie combine des connaissances à la fois géologiques, sismiques et géomécaniques. En particulier : les marqueurs de mouvement ont été observés sur les carottes, les orientations des familles de failles ont été déterminées, des analyses DRX ont été réalisées pour identifier la nature des minéraux de remplissage, les failles les plus favorablement orientées pour être activées ont été identifiées en considérant l'état de contrainte, et un modèle d'inversion a été réalisé à partir des données des cellules de déformations. En résultats, une famille de failles particulière a été identifiée dans les carottes, orientée de manière similaire au plan nodal attendu par les analyses sismiques. Les analyses DRX montre que cette famille présente un fin remplissage qui contient à la fois de la muscovite et de la chlorite. Ces deux minéraux sont des phyllosilicates, ce qui reste très cohérent avec la présence d'un plan de faille rempli de phyllosilicates attendu par le modèle de sismologie. Plusieurs marqueurs de glissement ont être identifiés. Toutefois, aucune famille n'avait à la fois l'orientation et la direction de glissement cohérentes avec le mécanisme focal donné par les données sismiques. En particulier, le marqueur de glissement observé sur la seule famille orientée comme le plan nodal était profondément incohérente avec le rake sismique. Ainsi, nous n'avons trouvé aucune évidence dans les forage qui nous permettrait d'identifier clairement une zone comme étant l'aspérité sismique. Cela révèle la difficulté d'identifier la zone sismogène malgré l'unicité et la précision de l'installation, pour d'aussi petites magnitudes.

Pour étudier plus en profondeur la localisation et les caractéristiques de l'aspérité sismique, un modèle d'inversion a alors été construit à partir des données des cellules CSIRO, et plus spécifiquement pour les données enregistrées lors d'une déformation cosismique associée à un événement de magnitude -1. L'aspérité est modélisée comme une dislocation rectangulaire dans un demi-espace élastique et isotrope et les formules d'Okada sont utilisées pour estimer les déformations aux localisations des cellules CSIRO. L'orientation et les dimensions de l'aspérité sont contraintes par les données sismiques, et une exploration est faite dans l'espace pour déterminer les possibles positions de l'aspérités, si elles existent, compatibles avec les orientations et valeurs des déformations principales calculées à partir des données des cellules CSIRO. Plusieurs localisations sont identifiées, ce qui montre une compatibilité entre données sismiques et géomécaniques. Toutefois, toutes les localisations se situent en dehors de la zone atteinte par les forages, ce qui peut expliquer pourquoi l'aspérité n'a pas été identifié dans les carottes de forages. En considérant le modèle théorique des répéteurs (i.e. la présence d'une aspérité qui rompt de

manière répétée sur un plan de faille, dû à un glissement continu sur ce plan de faille), il a été fait l'hypothèse que l'aspérité sismique est localisée sur un plan de faille plus grand. Ce plan de faille a alors été suffisamment étendu pour atteindre la zone traversée par les forages (15m*15m). De manière notable, une des zones de rencontres entre le plan et les forages est la zone de fracturation identifiée au préalable et qui contient la seule famille orientée comme le plan nodal et qui contient également des phyllosilicates. Ceci montre une excellente compatibilité entre données sismiques, géomécaniques et géologiques. Une proposition de modèle d'origine des répéteurs, cohérente avec le modèle classique de sismologie, est de considérer que les répéteurs sont dus à la présence d'une aspérité (3m*3m) environ sur un plan de faille plus large rempli de phyllosilicates. Bien que ce modèle soit compatible avec toutes les données disponibles, il est impossible de conclure sur l'exclusivité de ce modèle, et d'autres études sont prévues pour explorer plus en détails la présence ou non de fluage, ainsi que pour mieux localiser les événements sismiques et espérer atteindre l'aspérité sismique lors de prochains forages.

Alors que pour la famille quasi-périodique du sill-pillar, seule une déformation cosismique peut être analysée de manière fiable, la deuxième famille de répéteurs analysée dans le bloc d'excavation est localisée à côté de deux cellules CSIRO qui enregistrent une déformation temporelle pendant 1 mois complet. Durant le mois considéré, deux réponses à deux blasts différents sont enregistrées. Le premier blast est réalisé à distance de la famille de répéteurs (environ 60m) alors que le deuxième est plus proche (environ 25m). A partir des cellules CSIRO, les tenseurs de déformations ont été calculés, ce qui nous permet d'avoir des informations à la fois sur les valeurs et les orientations de déformations.

Le premier blast induit un saut soudain de déformation, suivi par une phase de deux jours d'augmentation de déformation (fluage), elle-même suivie par une séquence sismique. Les calculs montrent un changement soudain d'orientation de déformation après le blast sur la cellule CSIRO la plus proche de la famille de répéteurs (<2m du centroïde sismique). Les orientations des déformations restent constantes pendant toute la phase de fluage, puis une permutation entre les axes de déformations principales se produit lorsque commence la séquence sismique. Ces observations suggèrent que ces trois phases (réponse instantanée au blast, phase de fluage et phase sismique) sont associées à des structures et/ou des mécanismes différents. La cellule un peu plus distante de la famille (environ 13m) enregistre quant à elle très peu de fluage, ce qui montre que deux cellules à proximité peuvent enregistrer des réponses considérablement différentes.

La réponse au deuxième blast, plus proche de la cellule de déformation, présente une réponse significativement différente du premier blast. Dans ce cas, la réponse sismique est immédiate, et presque toute la déformation se produit instantanément lors du blast. De nouveau, cela montre la diversité des types de réponses et donc de mécanismes impliqués dans le déclenchement des différentes familles de répéteurs. Comme pour le premier blast, un changement de direction de déformation est observé lors du blast. Durant les cinq heures qui suivent le blast, un changement d'orientation est de nouveau visible et reste constant. Après cinq heures, un nouveau changement d'orientations est observé.

A partir de ces observations, deux principaux mécanismes sont proposés :

- 1) La présence d'un fluage localisé. Ceci est argumenté par le fait que le fluage soit principalement visible sur la cellule proche de la famille de répéteurs et non sur l'autre. Une possibilité est donc que le fluage se produise le long d'un plan de faille, et que la déformation enregistrée sur la cellule très proche du plan de faille soit représentative du glissement le long du plan de faille.
- 2) La présence d'une localisation progressive de la déformation. Dans ce cas, le fluage semble se produire premièrement dans le massif rocheux, puis progressivement se localiser le long d'une discontinuité. Ceci est soutenu par les différents changements d'orientation observés sur les cellules, qui peuvent être interprétés par le fait que le fluage se situe premièrement dans un volume de massif rocheux (par exemple sous forme de microfracturation), puis se localise progressivement. Ce mécanisme est très similaire à la fois aux nouveaux modèles de sismologie qui préconisent une relocalisation de la sismicité (Kato & Ben-Zion, 2021) ainsi qu'à la vision des géomécaniciens fondée sur des essais en laboratoire de fracturation de roches intactes, où une localisation progressive de la microrupture est observée (Renard et al., 2019).

De manière générale, ces analyses ouvrent des perspectives très intéressantes à la fois pour l'industrie minière et pour la communauté scientifique.

Pour l'industrie minière, elle met en avant : (i) la complexité des mécanismes qui peuvent induire des événements sismiques, (ii) le rôle du fluage dans le déclenchement de certains événements sismiques, (iii) le rôle de la lithologie et de l'excavation, (iv) l'importance des études à multi-échelles et multi-disciplines. Pour ce dernier point, l'importance des études locales pour mieux caractériser la nature des mécanismes, et donc espérer atteindre une connaissance plus pointue du rôle des différents facteurs connus pour influencer la sismicité (excavation, lithologie, discontinuités, etc) est particulièrement démontrée ici.

Pour la communauté scientifique, cette thèse montre que les données et observations sont pour la plupart cohérentes avec le modèle des sismologues préconisé lorsque des répéteurs sont observés, c'est-à-dire la présence d'un plan de faille rempli de phyllosilicates avec des aspérités sismogènes. Toutefois, malgré l'opportunité unique de forer à proximité de la zone source de répéteurs sismiques, il n'est pas possible de conclure sur la nature du mécanisme exact impliqué, ce qui souligne la complexité de clairement identifier les matériaux et mécanismes impliqués dans le déclenchement de séismes d'aussi petites magnitudes en contexte minier. Plusieurs mécanismes de déclenchement de la sismicité ont été mis en évidence, certains avec du fluage présismique et d'autres principalement caractérisés par une déformation cosismique suivi d'une déformation postsismique. L'étude ouvre également des perspectives cruciales pour étudier des questions scientifiques de haute importance telle que la présence d'un mécanisme de microfracturation volumétrique suivi d'une progressive localisation de la déformation et de la sismicité. Enfin, l'intérêt d'un travail multidisciplinaire pour étudier l'origine des séismes en contexte minier est largement démontré.

Une projet de recherche ANR (FIMOPTIC) a commencé durant les derniers mois de cette thèse. Bien qu'ils ne fassent pas l'objet du travail rendu ici, ce projet ouvre des perspectives précieuses

sur les limitations présentées dans cette thèse. En premier lieu, ce projet permettra de mieux localiser les événements sismiques, grâce à l'installation de nombreux géophones dans le sill pillar et de fibres optiques (Distributed Acoustic Sensing DAS), ce qui est crucial pour permettre de mieux localiser les forages et atteindre l'aspérité sismique recherchée. En deuxième temps, l'enregistrement de déformations en continu sera performé grâce à des strainmeters de haute résolution, ce qui permettra de suivre en continu à la fois dans le temps et dans l'espace les déformations, et ainsi détecter l'éventuelle présence de fluage presismique et mieux caractériser la déformation postsismique.

List of contents

Remerciements	i
Résumé élargi	vi
Introduction	1
Chapter 1 State of the art	3
1.1 Mining-induced seismicity	3
1.1.1 Interest of seismic monitoring	3
1.1.2 Types of seismic events and fault behaviors	4
1.1.3 Seismic repeaters	5
1.1.4 Seismicity and rockmass behavior	6
1.1.5 Factors influencing induced seismicity	7
1.1.6 Source mechanisms in seismology and in mining	8
1.2 Creep and asperities	9
1.2.1 How does a fault look like?	9
1.2.2 What is creep?	11
1.2.3 What is an asperity?	13
1.2.4 The largely studied example of the San Andreas Fault (SAF)	16
1.2.5 Strain measurements near excavation	19
1.3 Seismic triggering mechanisms	21
1.3.1 Seismic cycle	22
1.3.2 Fault slip behaviors and rate-and-state law	23
1.3.3 Triggering mechanisms of seismicity	25
1.3.4 Particular case of seismic repeaters	29
1.4 Conclusion and scientific questions	31
Chapter 2 Study area and previous analyses	33
2.1 Generalities	33
2.1.1 Presentation of the mine and area of study	33
2.1.2 Mining method in block 1250	34
2.1.3 Geological description	36
2.1.4 Influence of lithologies on the rockmass stability	38
2.1.5 Stress and rock properties	39

2.1.6 Seismicity in the mine	42
2.2 Seismicity in block 1250	43
2.2.1 Installation from 2015-2017	43
2.2.2 Geo-mechanical modeling: 2015-2016	43
2.2.3 Local and remote seismicity induced by mining.....	44
2.2.4 Migration of stresses after final stage of excavation stope 13	46
2.3 Seismicity driven by aseismic creep.....	46
2.3.1 Evidence for creep in the mine.....	46
2.3.2 Seismic repeaters in block 1250.....	48
2.3.3 Repeaters in the sill pillar.....	50
2.4 Conclusion.....	51
Chapter 3 Are repeaters correlated to specific lithologies or excavation sequences?.....	53
3.1 Statistical correlations between seismicity and lithologies	54
3.1.1 Lithological groups	54
3.1.2 Geomodelling of the different lithologies	58
3.1.3 Meshed cubes around seismic events.....	60
3.1.4 Results	62
3.1.5 Seismic repeaters.....	66
3.1.6 Hosting materials.....	69
3.1.7 Conclusions	72
3.2 Do stresses changes explain mine seismicity?	73
3.2.1 Method	73
3.2.2 Results	74
3.3 Conclusion.....	75
Chapter 4 Geological and geomechanical behavior of a repeater source zone	76
4.1 Local monitoring device.....	77
4.2 What are we looking for?	78
4.2.1 Seismic source mechanism.....	78
4.2.2 How would look like an asperity and creeping regions in cores?	79
4.3 Lithologies and fractures density.....	80
4.4 Orientations of fractures and nodal plane.....	83
4.4.1 Orientation of fractures	83

4.4.2 Influence of uncertainties of the measurements	85
4.5 Infilling mineralogy	86
4.6 Markers of movements and lineation	88
4.6.1 Identification of fractures with lineation	88
4.6.2 Comparison of geological and seismic source mechanisms	90
4.7 Stress state and fault activation	93
4.7.1 Measured state of stresses and fault activation	94
4.7.2 Inversion from source focal mechanism	96
4.8 Conclusions	97
Chapter 5 Triggering mechanisms of seismic repeaters.....	99
5.1 Transient and long-term periodic repeater rate.....	99
5.2 Long term period repeaters family	101
5.2.1 Coseismic Strain measured by BH4.....	101
5.2.2 Strain inversion to obtain stress variations.....	102
5.2.3 Location of the seismic nodal plane.....	103
5.2.4 Fault plane hosting the asperity.....	106
5.2.5 Activation of fractures with Coulomb stress changes.....	107
5.2.6 Geological and strain comparison	108
5.2.7 Perspectives: geomechanical model.....	109
5.2.8 Discussions.....	115
5.3 Example of a repeater transient	116
5.3.1 Description family 11 - seismicity	116
5.3.2 Comparison between post blast repeater rate and strain	118
5.3.3 Role of the excavation in the triggering of seismicity	122
5.3.4 Analyses and discussions	123
5.4 Conclusions	124
Conclusion and perspectives	126
Bibliography.....	129
Annex A	147
Annex B.....	148
Annex C.....	149

Introduction

Seismic monitoring is commonly used in deep mine. It has been originally developed to understand rockbursts phenomena, i.e. sudden and violent explosions of rocks associated with induced seismicity, after several major accidents (Cook, 1976; Kaiser et al., 1996; McGarr, 2002; Ortlepp & Stacey, 1994; Simser, 2019; Srinivasan et al., 1997). Even if rockbursts prevention is still an important topic, seismic monitoring is now used to understand a wider range of rockmass damage and failure mechanisms (Cai et al., 2001a; Hudyma et al., 2003) with a growing collaboration between mining companies and scientists (Gibowicz & Kijko, 1994). Studies of mine-induced seismicity benefit from the methods and physics developed over decades by seismologists. And while scientists offer a better understanding of the interplay between natural processes and engineering operations, which benefits production and safety decisions (McGarr, 2002), deep mines offer scientists unique opportunities to study seismic source processes and fault properties (Gibowicz, 2009; Ortlepp, 1997).

In deep mine, seismic events are commonly divided in two categories: (i) seismic events directly induced by mine excavation and the resulting redistribution of stresses (ii) seismic events related to slip on major discontinuities or shear zones. The former events follow the advance of the excavation front, while the latter can be distant and are mainly considered when they cause major seismic events and rockbursts (Malek et al., 2008; White & Whyatt, 1999). In the deep mine context of the Garpenberg mine, Sweden, an unusual type of microseismic events ($M_w < 1$), called repeaters, has been observed by Kinscher et al. (2020). They correspond to seismic events with highly similar waveforms, associated with a rupture area that remains at a constant location through times (Beroza et al., 1995; Mesimeri & Karakostas, 2018). The presence of these repeating earthquakes in a mining environment is surprising as it implies that it is always the same seismic asperities that rupture whereas the state of stress is constantly evolving as mining progresses. To my knowledge, only one case of microseismic repeaters has been monitored in a mining context before Garpenberg. They occurred on a major geological fault (Zebra fault $\sim 10\text{km}$ length) at 1km depth in the Cooke 4 mine, South Africa, with a moment magnitude comprises between $-5.1 \leq M_w \leq -3.6$ (Naoi et al., 2015a; Naoi et al., 2015b; Yamaguchi et al., 2018). The authors interpreted these events as repeat ruptures of same asperities loaded by aseismic slip on the surrounding regions (Naoi et al., 2015a). In the context of the Garpenberg mine, no major fault such as the Zebra fault is observed, and repeater families are associated with small-scale seismogenic sources comprised between 1-10m (Kinscher et al., 2020).

Whereas repeaters have only been reported in these two mines, they have been intensely observed and studied at plate boundaries, especially in subduction zones (Bohnhoff et al., 2017; Uchida, 2019). Most common model of interpretation of these repeaters is that they represent repeated ruptures of the same locked patch loaded by surrounding creep on the plate interface (Chen & Lapusta, 2009; Igarashi et al., 2003; Uchida et al., 2003; Yamaguchi et al., 2018). The triggering

of seismicity due to aseismic slip is also observed in fluid injection experiments. In these cases, seismicity is induced by creep on fault planes, previously caused by an increase of fluid pressure (Cappa et al., 2019; De Barros et al., 2020; Guglielmi et al., 2015). Considering that seismic moment of each repeater is related to the amount of background creep during the cycle of the repeater event, seismic repeaters moment are commonly used as a proxy to assess creep on plate boundaries (Nadeau & Johnson, 1998). **Here, it is questioned whether seismic repeaters in Garpenberg mine can also be used to assess the location and characteristics of a seismic asperity, as well as the mechanisms that lead to its loading, especially the occurrence and location of aseismic deformation prior and after their occurrence.** Studying the origin of repeaters in the context of a deep mine is therefore of scientific interest to improve general understanding of the seismic cycle and how earthquakes are triggered, using a rarely-used scale of observations. Results should also improve seismic hazards assessments during mine exploitation.

In this thesis, the origin of seismic repeaters is investigated in Garpenberg mine, based on seismological knowledge developed on plate boundary faults. The possible hosting materials and loading mechanisms are explored by combining different scales and fields of study, looking in details at evidences of creeping planes loading asperities, or at any other aseismic mechanism that could trigger them, such as creep² in talc lenses as mentioned by Kinscher et al. (2020). The manuscript is organized as follows:

A state of the art is first presented, which aims to define crucial concepts intrinsic to seismic repeaters, such as creep and seismogenic areas, and describe how seismic triggering is studied in mining and seismology. By doing so, the reader is encouraged to keep in mind that both scale of observation and field of study play a major role in the interpretation of the nature of seismic and aseismic mechanisms. In a second chapter, the Garpenberg mine is presented, as well as previous investigations on seismic repeaters in the mine. Third, fourth and fifth chapters describe investigations on the origin of repeaters in the Garpenberg mine. The third chapter focuses on investigations at the scale of the whole excavation. Both lithological and geomechanical data are analyzed, and statistical correlations between lithologies and seismicity are shown, as well as the limitation of a study at larger scale. The fourth chapter describes and analyzes data from boreholes and strain cells facilities installed in a sill pillar at 1km depth which aimed to target a specific repeater family. Drill cores analyses constrain the nature of both seismogenic and creeping areas. In the fifth chapter, local strain deformation are combined with seismic rate evolution, and the triggering mechanisms of seismic repeaters are discussed. Finally, the conclusion chapter sums up the main results regarding both structures hosting repeaters and mechanisms loading seismogenic regions.

Chapter 1

State of the art

1.1 Mining-induced seismicity

1.1.1 Interest of seismic monitoring

Mining induces local stress changes in the rockmass surrounding stopes. Two main types of inelastic deformation can occur: violent failures, or rockbursts, and aseismic (creep-like) movements (Malan, 1998). These two types of deformation are of interest in this study, as repeaters are commonly associated to the presence of seismic ruptures induced by aseismic deformation.

Seismic monitoring has been developed when the first rockbursts (i.e. violent explosion of rocks associated with seismicity) occurred. Today, with mines getting deeper, stresses increase in the rockmass which results in a higher risk of seismic events with large magnitude. Even though risk management has improved over the years, rockbursts are still responsible for many fatalities. Only in South Africa, where mine depths can reach 4km depth, they are still responsible for several tens of deaths per year (Foulger et al., 2018). Even in modern mines with performant monitoring, risks associated to rockbursts remain. As an example, a rockburst (Moment magnitude 4.2) occurred in Kiirunavaara mine in Sweden in May 2020, whereas it is the mine with the largest seismic monitoring system in the world, with 204 operational sensors in 2016 (Boskovic, 2022; Nordström et al., 2020). The rockburst caused important damage on several production levels. Understanding the source mechanisms of mine seismicity remains complex due to a multiple of involved factors, such as the orebody geometry, the geology and the stresses, mining sequencing and extracted volume (Ylmefors et al., 2022).

Seismic monitoring is still largely used to prevent rockbursts, but its use extends today to general rockmass studies, such as the understanding of rockmass failure and the location of highly stressed areas in the mine (Hudyma et al., 2003). This new use is justified by the easiness to install seismic monitoring compared to the installation of instruments to measure strains and stresses, such as extensometer and stress cells.

Amongst useful information for the miners, the characterization of aseismic deformation is of high interest, for two reasons. First, aseismic deformation is preferable to violent rockbursts, as it allows to dissipate energy in a stable manner (Malan, 1998). Then, understanding how energy is released in a stable manner would help to favor these conditions. Secondly, aseismic deformation can be

dangerous if large aseismic deformation is induced, and it is also necessary to follow its evolution. For these reasons, seismic repeaters raise new perspective in the use of seismic monitoring in the mine, as they are known in seismology to be good proxy to assess aseismic creep.

1.1.2 Types of seismic events and fault behaviors

Seismic events are caused by a release of energy within the rockmass during fracturing or when an instability arises on a pre-existing discontinuity (Urbancic & Trifu, 2000). Two different types of events have been distinguished in deep mines (Gibowicz & Kijko, 1994; Gibowicz, 2009; McGarr, 1976; Richardson & Jordan, 2002): (i) seismic events directly induced by mining excavation and with spatiotemporal characteristics following the advance of the mining front and (ii) seismic events associated with shear or rupture along discontinuities (*e.g.* fault plane, shear zones), which can be spatially and temporally distant from the excavation front (Malek et al., 2008; White & Whyatt, 1999). The latter usually induce seismic events with higher magnitude (Brown, 2021; Hudyma, 2008; McKinnon, 2006; Sainoki & Mitri, 2014). Interactions between seismic events also add complexity to the seismicity. This has been shown in the Rudna copper mine, Poland, where two large seismic events influenced seismic rate and location through Coulomb stress changes (Orlecka-Sikora et al., 2012). In Creighton mine, Canada, Marsan et al. (1999) highlighted that stress diffusion (propagation of stress away from the initial earthquake event) between events also played a role in the occurrence of stronger events.

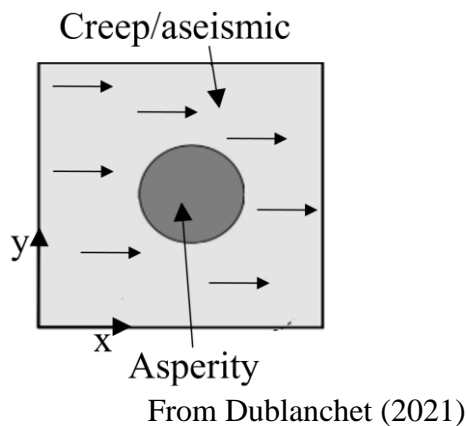
Whereas seismic events can be related to a fault plane, all fault planes are not necessarily seismic sources. This is important not only for the study of seismicity in deep and hard-rock mines, but also for the study of aseismic deformation occurring between or around seismic events. First of all, main geological structures can play a role in seismicity without being active structures. This might have been the case in the Creighton mine in Sudbury, Canada. Indeed, Snelling et al. (2013) observed no correlation between main geological structures and remotely-monitored seismicity, but suggest that main structures could play a role by redistributing the stresses, and then activate small fractures, or induce microfracturing. In other cases, faults can slip aseismically.

Identifying whether a fault plane is seismic or aseismic is of high importance to adapt the monitoring and the security measurements. As an example, Sainoki et al. (2017) showed that a fault in Copper Cliff Mine, Canada, slips aseismically, by the mean of a microseismic data base and a 3D numerical model. However, although aseismic slip is considered preferable to seismic slip which can lead to high magnitude events, it can induce aseismic deformations in the surrounding rockmass which could be risky if they become too important. Furthermore, it is known in seismology that an aseismic fault plane can become seismic if its friction angle or applied stresses change (Noël et al., 2019). Consequently, aseismic faults must not be disregarded in risk management in deep mine, which highlight the interest of studying further seismic repeaters which are a good proxy to assess creeping faults.

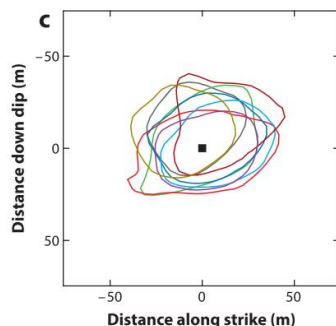
1.1.3 Seismic repeaters

Naoui et al. (2015) and Yamaguchi et al. (2018) highlighted the presence of very small microseismic repeaters ($M_w < -4$) in the Cooke 4 gold mine, South Africa. Repeaters are seismic signals with highly similar waveforms and same source location (Fig. 1.1b and c) (Geller & Mueller, 1980; Waldhauser & Schaff, 2021). They are well-known in natural seismology and are commonly associated to the shearing of asperities loaded by a continuous and aseismic slip on fault planes, also known as creep (Fig. 1.1a) (Bakun et al., 2013; Chen and Lapusta, 2009; Nadeau and McEvilly, 1999; Poupinet et al., 1984; Rice, 1993). Some famous examples where repeaters have been studied are the San Andreas Fault in California, USA (Nadeau et al., 1995), the North Anatolian fault in Turkey (Uchida et al., 2019), the Northeastern subduction zone in Japan (Igarashi et al., 2003). Repeaters and coupled seismic/aseismic deformation have also been observed in reservoirs and geothermal fields (Bourouis and Bernard, 2007; Guglielmi et al., 2015; Kinscher et al., 2023).

a) Theoretical model of repeaters



b) Same source location of the repeater families



c) Similar waveforms of a repeater family

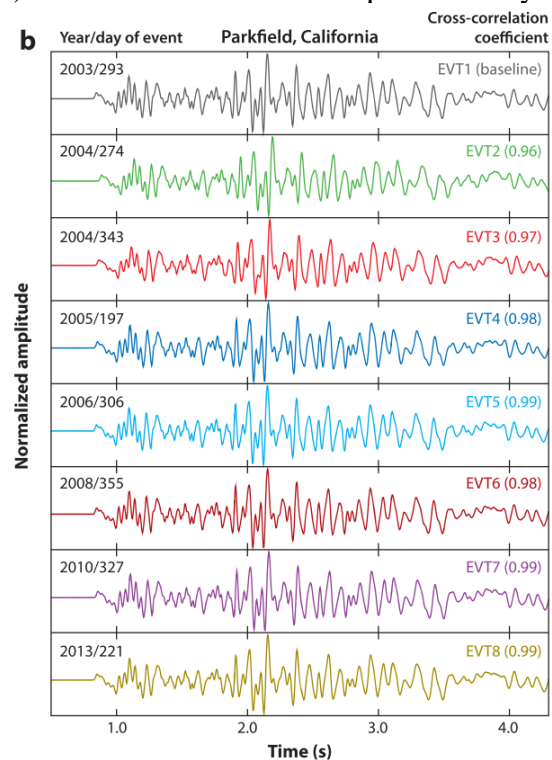


Fig. 1.1 - Characteristics of repeating earthquakes. By definition, they are seismic events with similar waveforms and same source location. a) shows theoretical model of repeaters, with an asperity embedded by creeping surrounding. From Dublanche (2021) b) and c) show a family of repeating earthquakes near Parkfield, California, with similar source location in b) and similar waveforms in c). From Uchida & Bürgmann (2019)

Contrary to seismic repeaters in Cooke 4 mine, no major fault plane described in Garpenberg mine is identified as hosting the monitored seismicity. Source size of each repeater family is assessed between 1-10m by Kinscher et al (2020) and size of each large fault plane hosting asperities is assumed to be several tens of meters, which could explain why they are not observed by mine geologists (personal communication, mine geologists). Then, small scale fault planes (i.e. several tens of meters) are of interest in this study. This is not common in mining context, where fault slips are usually considered when larger events ($M > 2$) are involved and associated with a major risk of rockbursts (Askaripour et al., 2022; Kaiser et al., 1996; Ortlepp & Stacey, 1994). Although usually overlooked, it is well known that small-scale discontinuities can play a higher role in mine design than larger structures (Glaser & Doolin; 2000). The monitored seismic repeaters represent then the opportunity to study how distant small-scale fractures (tens of meters scale) can also influence seismicity and aseismic deformation in the mine.

1.1.4 Seismicity and rockmass behavior

Andrieux et al. (2008) described the strain softening behavior typically associated with loading of a moderately jointed hard rock mass and described the phases during which seismicity is expected. The curve presented in Fig. 1.2 can be divided in five regions with different seismic behavior. First, the rockmass shows two stages of elastic deformation. Then, a third region corresponds to the brittle response, which occurs after the peak is reached. A fourth stage is the softening response and the last stage is the residual phase. The largest seismic events are expected within the third stage, as it is known that stressed rocks emit detectable seismic signals (Cai et al., 2001). Moderate seismic events can be monitored during the fourth stage. When residual stage is reached, no seismicity is expected anymore.

This curve helps to understand how seismic monitoring is used in mining to assess the mechanical state of the rockmass. By observing spatiotemporal seismicity at the scale of the excavation, the highly and moderately stresses regions can be located. When no seismicity is monitored in areas where seismicity was previously monitored, it can be an indication that the zone yielded or became highly fractured (Simser, 2019). This curve reproduces well the fracturing process of the rockmass, but several questions remain about the mechanisms monitored by seismic networks. In particular, fracturing in the rockmass can either be due to the formation of new fractures in the matrix (growth of microcracks), either due to slip on fractures. Main factors which influence the mechanism are: ratio from maximum stress compared to the strength of the rock, discontinuities spacing and orientations of the discontinuities. Geophysical analyses on seismic repeaters are commonly done for slip on well-known major faults (km scale) and not during study of rockmass fracturing. In a mining context, it is questioned whether seismic signals associated with rockmass fracturing (such as formation of new shear fractures) could also exhibit highly similar waveforms as observed for seismic repeaters (Moore & Lockner, 1995; Wong et al., 2002).

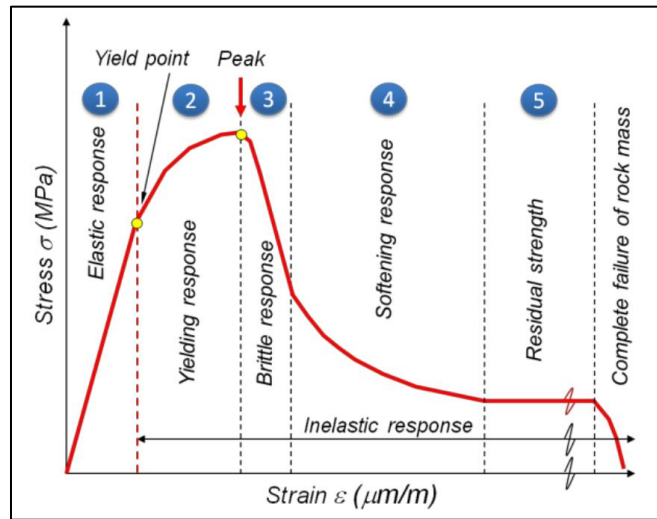


Fig. 1.2 - On the left: five regions of the strain-softening response of a moderately jointed rock mass. From Cotesta et al., (2014). On the right: Load-deformation curve for rock, which described the deformational response of rock to mechanical loading. From Fairhurst (2004).

1.1.5 Factors influencing induced seismicity

Several factors are known to contribute to rockbursts and to induce seismicity in deep hard-rock mines. They are commonly divided into two categories : (i) intrinsic rockmass and fault properties, and (ii) initial stresses and induced stress changes (Sainsbury & Kurucuk, 2020). Amongst these factors are found: stresses, excavation (mining method, sequencing and extracted volume), mineralogy, geomechanical contrasts between two rock types, and geological dykes or discontinuities.

Correlation between seismicity and mining activity has been recognized by numerous studies. As an example, Sibek (1963) showed a correlation between excavated volume and the number of rockbursts in the Brezove Hoty district, Czechoslovakia. Cook (1976) showed that the distribution of events is correlated with the distance from the excavation face, which is consistent with number of studies which showed that seismicity follow the newly formed mine excavation (Brown, 2018; Cook, 1976; Gibowicz & Kijko, 1994). Vallejos & McKinnon (2011) also showed a correlation between seismic decay time (i.e. decrease of the cumulative number of seismic events in function of time) after blast with different mining factors, such as the volume of mined rocks and depth, on Creighton and Macassa mines, Canada. Regarding excavation geometry, the greater and the closer to each other are the openings, the higher is the risk of rockburst occurrence, due to a reduction in loading stiffness (Kaiser & Cai, 2012).

Sainsbury & Kurucuk (2020) used geomechanical test data from 35 case studies and built a guide to identify types of rock masses most likely to burst, based on intrinsic rockmass properties. They

showed for example that Massive sulfides have violent fracturing failure mode whereas mafic rocks are more susceptible to squeeze and granite to present a high stress slabbing. Milev & Spottiswoode (2002) showed that seismicity in geotechnical areas with soft lava (volcanic rock of the Westonia) in the hanging wall was significantly lower than in geotechnical areas with hard lava (volcanic rock of the Alberton), which highlights the influence of rock properties on seismicity. De Santis et al. (2019) suggest that the proximity of weak lenses and stiff rocks at the eastern part of Garpenberg mine play a role in higher stress drops monitored during seismic events.

Seismicity is also favored by geological discontinuities, shear zones, or stress concentrators such as dykes (Keneti & Sainsbury, 2018). For example, Lucky Friday Mine, USA, is known to have hosted several rockbursts related to fault-slip. Slip displacements were observed along bedding planes, and it was shown that these displacements contributed to sudden failures of rocks (White & Whyatt, 1999).

1.1.6 Source mechanisms in seismology and in mining

In natural seismology, seismic sources are mainly described with double-couple (DC) mechanisms, which assume a shear faulting in an isotropic elastic medium (Julian et al., 1998). Then, the DC model as well as methods to interpret data based on this model were widely applied in mining context. Most common example is the determination of nodal planes from seismic signals, which can be compared to existing geological structures (Malovichko, 2012).

However in mining, other mechanisms than DC ones are found, due to the presence of voids and a stress field more complex than tectonic loading (Šílený & Milev, 2008). Hasegawa et al. (1989) classified mechanisms in mining into 6 main categories: cavity collapse, pillar burst, tensional fault, normal fault and deep and shallow thrust faults. The first 3 ones are associated to a non-double mechanisms, the 3 latter mechanisms with double couple mechanisms, which makes sense as they are the ones associated with discontinuities. As an example, Šílený & Milev (2008) studied 5 seismic events recorded in Driefontein gold mine, South Africa, and deduced the types of mine tremor associated with each of the event. 3 of the non-DC events were pillar burst tremors, 1 was a tensional fault, and the last one was a DC mechanism associated with a fault in the hanging wall. Ma et al. (2018) also used full wave form inversion for 8 events in the Yongshaba phosphate mine, China, to identify focal mechanisms. 4 events were recognized as fault slip events, 3 as cavity collapse events, and 1 as a tensional failure. Close to the excavation boundary and with no pre-existing faults, the main failure mechanism is expected to be tensile, with the creation of tension cracks (Vazaios et al., 2019). In this case, rock failure occurs mainly as a tension crack growing parallel to the excavation walls, producing predominantly P-waves (mode I - extensional fracture) (Cai et al., 2001b). This was confirmed by Cai et al. (2001) for a mine in South Africa. Using a shear DC model, they obtained source dimensions much larger than the size of visible fractures and cracks close to the excavation. By applying a tensile model, they obtained results similar to

those observed in the field. The presence of these non-DC mechanisms highlight the complexity of source mechanisms in the mine and show that DC models and interpretations derived from them are not applicable in each case. This must be kept in mind in the framework of this thesis, which focuses on a type of seismic events (repeaters) observed and characterized with methods and models developed in the case of plate boundaries where DC mechanisms are very common.

1.2 Creep and asperities

The presence of seismic repeaters in Garpenberg mine is the main subject of the thesis. In this context, I aim to better characterize the geological and geomechanical origin of these repeaters. Repeaters were originally studied in the case of large fault planes. They were described as representative of the rupture of asperities loaded by a surrounding creep (i.e. aseismic slip). In reality, the definition of both asperities and creeping material is far from obvious, and they differ depending on the scale and field of study. As Sornette (1999) said : “The fault of the geologists is not the same object as the fault of the rock mechanician which is itself a different structure than the fault of the seismologist”. In this thesis, I aim to characterize the origin of seismic repeaters by the use of geological, geomechanical and seismological data, models and tools. As with the fault definition, the concepts of asperities and creep differ from one field to another. Even for scientists working in similar fields, differences in scale play a major role, and a scientist working at field scale will have a different vision than a scientist working in a laboratory. It is therefore necessary to clearly define the notions of fault, asperity and creep, both to establish links between fields and to better characterize what we are looking for. Later in the thesis, data interpretation will be based on this state of the art to discuss the possible structures and materials hosting repeaters in the mine.

1.2.1 How does a fault look like?

The vision of a fault differs depending on the discipline, and Sornette (1999) explains well the differences in visions between geologists, seismologists and geomechanicians. Geologists see a fault as a large zone with different fractures and cataclastic deformations, and with a specific architecture: the central gouge and a complex damage zone (Fig. 1.3a). Geomechanicians focus mainly on the fragmented core of the fault and localized deformations. Seismologists see it as a well-defined fault plane with different patches and slip behaviors (Fig. 1.3b). Regarding earthquakes, seismologists consider the earthquake as a seismic source, usually with a double couple (DC) mechanism, and mainly study elastic waves from the source and their propagation in the medium generally considered as elastic and isotropic. For geomechanicians, a seismic event is a stick-slip event mainly due to frictional properties of the fault. They are mainly studied at the laboratory scale or with numerical models, using the notion of rupture criteria.

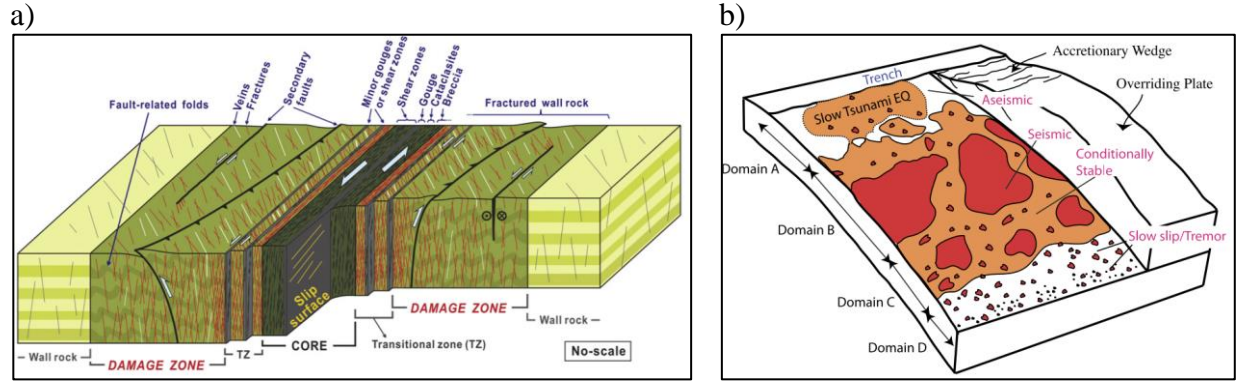


Fig. 1.3 - Two different conceptual visions of a fault plane. On the left, the “geological” vision, which represents the main components of a fault zone architecture, namely the fault core and the damage zone. From Choi et al. (2016). On the right, the “seismological” vision, with a fault represented as a fault plane with different slip behaviors: aseismic slip, seismic slip, slow slips. Asperities are represented as “patches” on a fault plane. The figure is taken from Lay (2015) and represents the subduction zone of the northeast coast of Honshu, Japan.

Scale also play a role in the vision of what is a fault or a fracture. Natural faults can be several hundreds of kilometers long and several kilometers or tens of kilometers wide (Rice, 1992; Zoback, 2006). In the vicinity of an excavation, civil engineers and miners consider that natural fracture systems exhibit a wide range of sizes described by a power law. As an example, Lei et al. (2017) use fracture sizes between 0.2 m and 2 km in their discrete fracture networks (DFN), when studying the impact of pre-existing fractures on damage evolution around a tunnel (Fig. 1.4a). In some cases, a specific larger fault plane with specific orientation is studied (Fig. 1.4b) to assess whether the excavation can induce slip on this fault, considering the change in stresses, rockmass strength and fault orientation (Sainoki & Mitri, 2017; White & Whyatt, 1999; Wu, 2021).

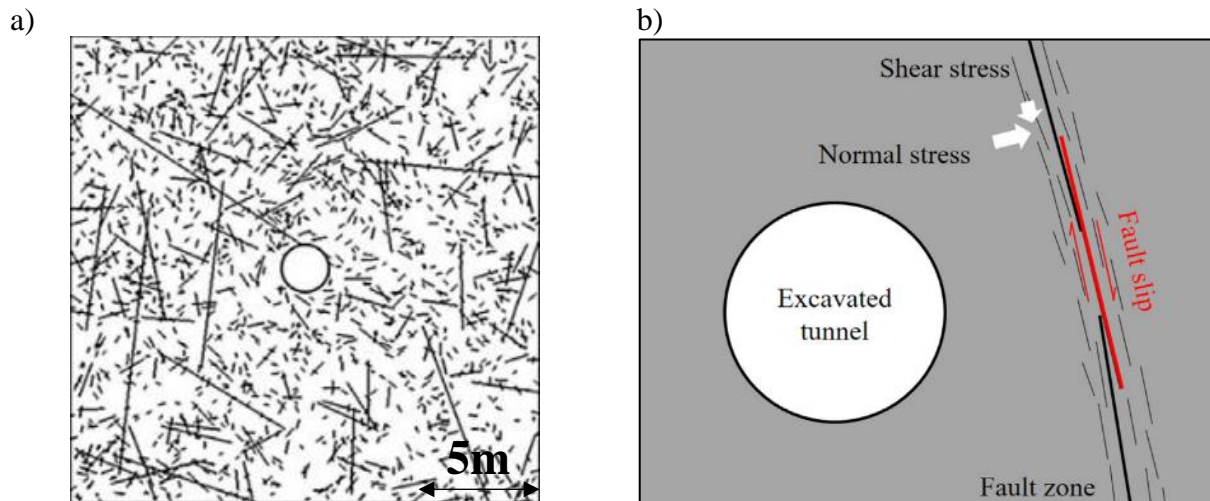


Fig. 1.4 - On the left: an example of a distribution of sizes of fractures around a tunnel excavation. From Lei et al. (2017). On the right: a fault slip at vicinity of an excavation, which is activated due to a change of stresses. From Wu (2021).

1.2.2 What is creep?

Creep is a concept used both by seismologists and geomechanicians, with a similar but not identical meaning. First, it should be noted that differences exist between creep and time-dependent deformation, although creep is commonly employed to designate time-dependent deformation in both geomechanical and seismological fields. Malan (1999) defines creep as “a continued deformation due to a constant applied stress” and time-dependent behavior as “a more general term encompassing concepts like creep of intact rock, creep of large-scale discontinuities, delayed failure and long-term strength”. The notion of constant load is essential in geomechanics in the creep definition. In laboratory, it is possible to study creep behavior because it is easy to apply a constant load. However, in reality, it is difficult to differentiate creep from time-dependent behavior, as a constant load is rarely applied. A third essential notion in geomechanics is that, due to time effect, a creeping rockmass will rupture at a shear stress smaller than the shear strength of the material. Similarly to the creep definition in rockmasses, Malan (1998) defines creep on discontinuities as a “time-dependent relative displacement of opposing discontinuity surfaces, caused by a shear stress smaller than the shear strength of the discontinuity”. This same definition is used in some constitutive laws in geomechanical softwares like 3DEC (Itasca). However, this definition differs from the definition commonly used in seismology. In seismology, creep is defined as a continuous and slow slip without any significant earthquake (Durand et al., 2022; Tocher, 1960). This definition is independent of the notion of constant loading or displacement of the discontinuity with a shear stress lower than the shear strength. Aseismic slip and creep are usually used in a same manner in seismology. In contrast, the creeping definition given by Malan is independent of the presence or absence of seismic events when the rockmass or the discontinuity creep. Then, a creeping rockmass or discontinuity still can host seismicity.

Creep in hard rockmass follows three stages: primary, secondary (steady-state) and tertiary phases (Boukharov, 1996) (Fig. 1.5). After application of the load, there is first an instantaneous elastic strain, followed by the primary phase characterized by a decelerating strain rate. During this phase, strain is recoverable on unloading, as a delayed process. Then a secondary steady-state phase starts in which deformation occurs at a constant strain rate. Finally, depending on the stress level, a tertiary phase can occur with an accelerating strain rate and failure.

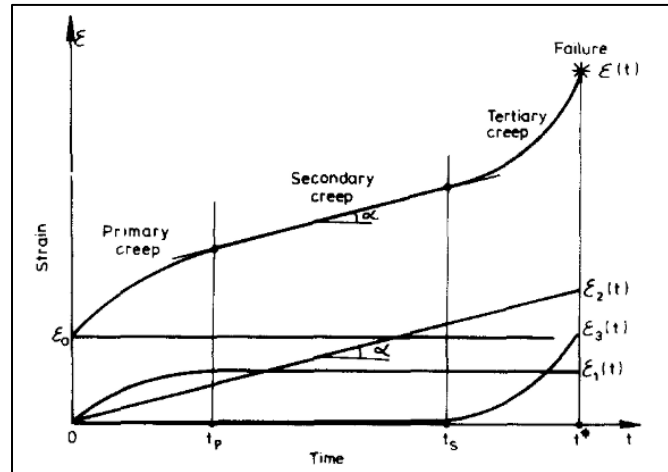


Fig. 1.5 - Three phases of creep. Primary, secondary and tertiary creep. From Boukharov (1996).

Whereas creep is known to play a major role in rockmass and fault plane behaviors and can be measured with geodetic or strain gauges tools (Malan, 1999; Savage & Burford, 1973; Titus et al., 2006), it is the macroscopic manifestation of mechanisms occurring at the scale of grains and fractures which are difficult to identify. In an intact rockmass, main mechanism related to creep is the time dependent micro-cracking of the matrix (Fig. 1.6a). In that case, macroscopic creep is the representation of microcrack extension under compressive stresses and a common model used to describe brittle creep is derived from the wing crack model of Ashby & Sammis (1990). In that case, primary phase can be seen as a decelerating crack growth and tertiary phase as an acceleration in crack growth due to crack interactions, and secondary phase as an intermediate between both (Brantut et al., 2012). In a jointed rockmass, creep is most of the time governed by discontinuities, although it is not always the case (for example if stresses are above the strength of the rockmass or discontinuities are unfavorably oriented to be activated). Several studies showed that the creep behavior of unfilled fractures is similar to that of an intact rock, but can reach larger strain magnitude if the ratio between shear stress and shear strength of the rockmass exceed some ratio (Glamheden & Hökmark, 2010). Main common mechanism to explain creep on unfilled rough discontinuity is the time-dependent shearing of asperities (or degradation of the asperities) (Fig. 1.6b). In this model, stresses concentrations occur on asperities, which induce a progressive yielding on the asperities and a slip on the joint surface, with shear stresses redistributed on other asperities (Glamheden & Hökmark, 2010). Other models such as extension of pre-existing fractures can also be involved, with models similar to the micro-cracks one, but at a different scale or with a different number of fractures (Na et al., 2022). Note that creep means here a long-time deformation under constant load. There is no need for the creep to be aseismic, as it is the case in the seismological definition.

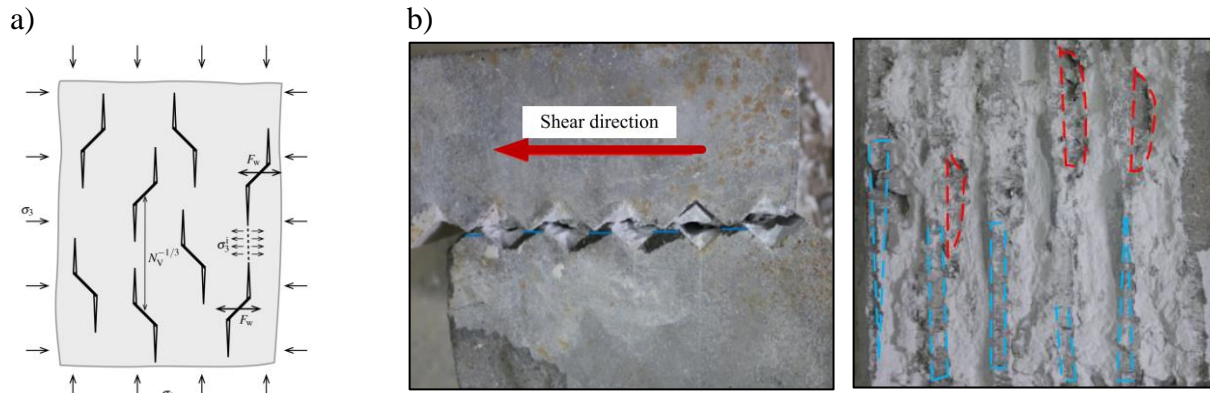


Fig. 1.6 - On the left: microcrack model of Ashby and Sammis, used by Brantut et al. (2012) to represent brittle creep in intact rocks. Cracks extend on top and bottom with the growth of “wing cracks”. On the right: Example of asperities degradation in an unfilled fracture. Figures from Wan et al. (2018).

Aseismic creep in natural fault planes is generally attributed to the presence of an infilling composed of key minerals such as clay and other phyllosilicates (Fig. 1.7). This is mainly due to the fact that these minerals exhibit both low shear strength and a rate strengthening behavior, which are favorable to stable sliding (French et al., 2015; Saffer & Marone, 2003). Pure clay gouges exhibit only stable sliding, and the percentages of clay in a mixed gouge can change the sliding behavior from stick-slip to stable sliding if they reach a certain amount in the mixture and under appropriate normal stresses (Saffer & Marone, 2003; Shimamoto & Logan, 1981). As shown by Malan (1998), creep in filled joints exhibits the same curve than for intact rock, with the three phases described above and with highest values of deformation.

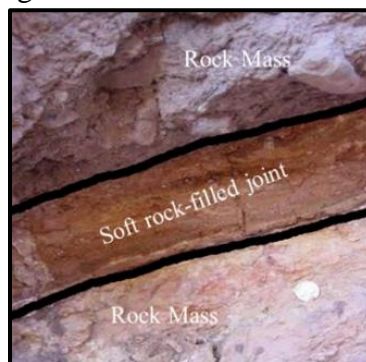


Fig. 1.7 - Example of soft rock-filled joint on a natural fault. From Wang et al. (2020).

1.2.3 What is an asperity?

The definitions of an asperity differ depending on whether we consider the geometry and the rheology of a fault zone, or the source of an earthquake.

An asperity can first be considered as a topographical irregularity on a fault plane, such as a bump, striation, undulation, or corrugation. This is the original definition, which can be applied at different scales, from laboratory experiments to natural fault planes. What represents such definition on different scales will be highlighted in next section with the example of the San Andreas Fault. With this definition, an asperity can be seen as an area of contact due to surface irregularities between two rough surfaces (Das & Kostrov, 1983). This is easily observable in laboratory experiments on rock friction, where several asperities are visible on two rough surfaces (Fig. 1.8a) (Huang et al., 1993; Zhang et al., 2019). When a fault slips, it can induce the rupture of many asperities of different sizes. An example is the fault zone near Klamath Falls, Oregon (USA) where asperities are 10-40m quasi-elliptical bumps (Fig. 1.8b) (Sagy & Brodsky, 2009a)

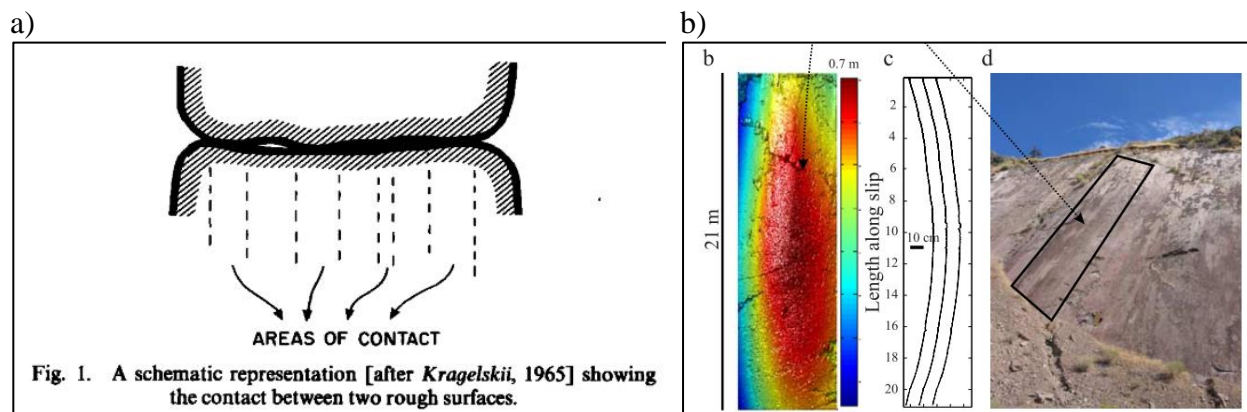


Fig. 1.8 - An asperity with a geometrical vision. On the left, the image shows areas of contact between two rough joints. From Das & Kostrov (1983). On the right: an example of a bump on the fault zone near Klamath Falls, Oregon USA). From Sagy & Brodsky (2009).

An asperity can also be a portion of a fault with a different rheology, capable of “accumulating” more stress than the surrounding environment. This vision is correlated with the definition of asperities as geometric irregularities, as these irregularities generally have higher frictional properties which allow the accumulation of stresses. For example, for the fault zone near Klamath Falls, Oregon (USA), asperities bumps are analogues to mullions and boudinage defined by Smith (1977), whose generation require two layers of different rheologies. In this case, asperities are then both geometrical and rheological inhomogeneities (Sagy & Brodsky, 2009a). By designing an injection experiment with a length of a few meters in a faulted shale layer, Barros et al. (2016) showed that most of the deformation is aseismic and that seismicity occurs on calcified structures in the damage zone. In this case, seismicity doesn’t occur on the same structures than the ones deforming aseismically (shale), but on neighboring fractures in the fault zone.

Lastly, an asperity can also be seen as the source of a strong seismic radiation or an earthquake (Zoback, 2006). This definition is mainly used in seismic studies. In this case, a single “seismic asperity” is seen as a “patch” on a fault and can correspond to many topographical asperities whose rupture corresponds to the seismic source (Das & Kostrov, 1983). The source is usually located from areas with high co-seismic slip (Chlieh et al., 2011; Mai et al., 2005; Sobiesiak et al., 2007).

During the interseismic period, the asperities can also be identified as the strongly coupled patches, i.e. locked patches with high deficit of slip or high moment deficit (Avouac, 2015; Chlieh et al., 2011) (Fig. 1.9a). In Garpenberg mine, Kinscher et al. (2020) used spatial distribution of relocated repeating earthquakes of separate families to define asperities (Fig. 1.9b). Note that in the case of deep mine, there is no surface geodetic measurement nor major fault plane, which explains why definitions of asperity based on high deficit of slip during interseismic period, such as in Fig. 1.9, is not applicable.

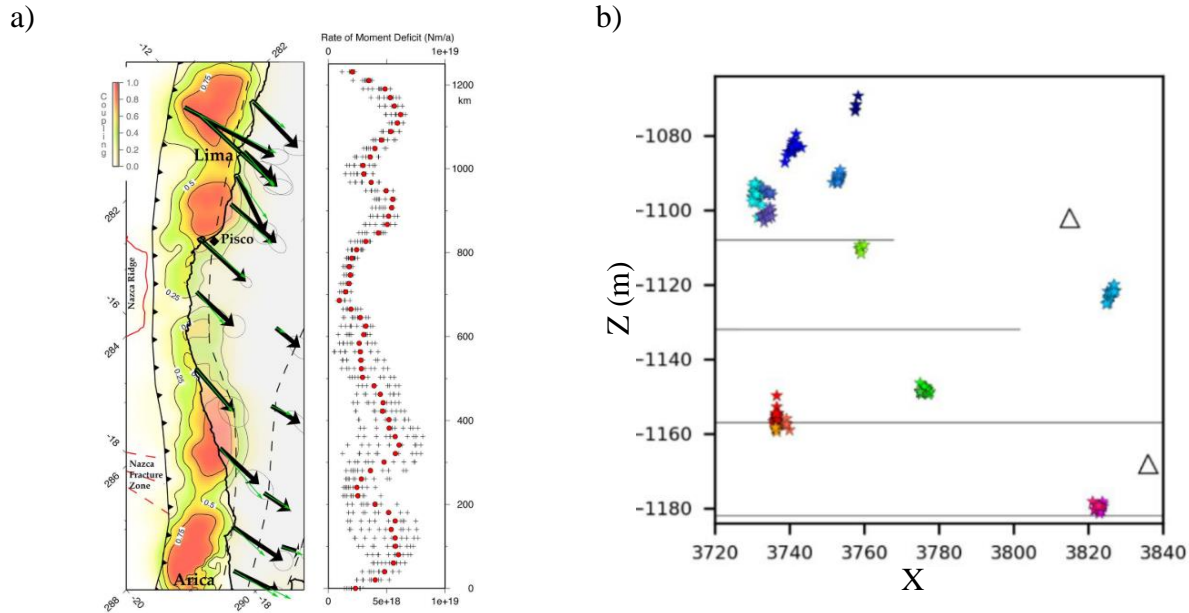


Fig. 1.9 - Two different examples of asperities defined in function of source location. On the left: a plane view of high coupling during interseismic period of the Central Andes subduction zone. Regions with high coupling (slip deficit during interseismic periods) are locked asperities. From Chlieh et al. (2011). On the right: a vertical view of an excavation panel of the Garpenberg mine. In this case, each cluster corresponds to an asperity of different repeaters families. From Kinscher et al. (2020).

Manthei & Plenkers (2018) present seismic parameters associated to different scales of seismic sources (Fig. 1.10). Major natural earthquakes can present moderate and large magnitudes ($M > 4$) with source radius of kilometer scale, whereas seismic events in the Garpenberg mine are micro-events ($M < 1$) with source radius of meter or tens of meter scales.

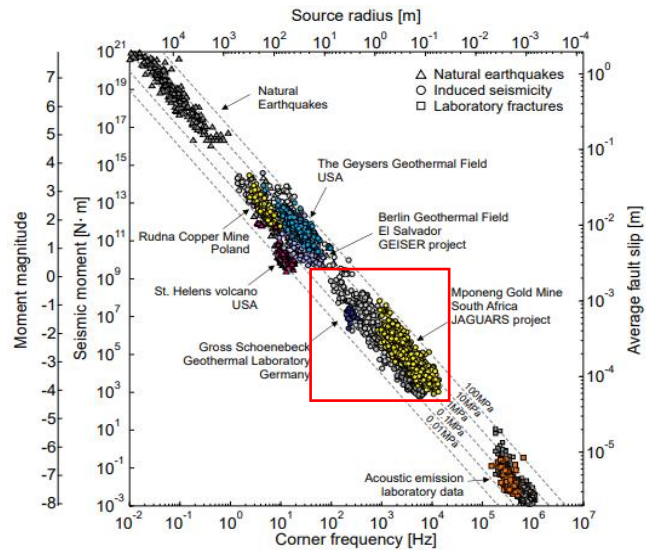


Fig. 1.10 - Relations between moment magnitude, source radius, corner frequency and average fault slip for different earthquakes at different scales. Stress drops values are also shown, calculated assuming a circular model of Madariaga, (1976). In red is shown the area which corresponds to values of mines such as Garpenberg mine. From Manthei & Plenkers (2018).

Because they host slip, asperities often present kinematics markers on their surfaces. Common marker is slickenlines, which indicates a relative displacement of opposing sides of a fault (Kirkpatrick & Brodsky, 2014; Macklin et al., 2021). From these slickenlines, it is possible to deduce the slip direction (rake on the plane) which occurred on this asperity during the earthquake (Fig. 1.11).



Fig. 1.11 - An example of slickenlines striation observed on the Corona Heights fault.

1.2.4 The largely studied example of the San Andreas Fault (SAF)

From a geological perspective, an asperity is defined as a bump or other irregularity on the fault topography, due to the non-planarity of the fault surface (Brown & Scholz, 1985; Kirkpatrick & Brodsky, 2014; Power et al., 1987). However, this definition is very large and can be applied at very different scales of observation.

The San Andreas Fault is a perfect example of the scale dependency of what is called an asperity. The fault is more than 1000 km long and is made of different segments. Some segments are locked sections which can host large and very large events at the northern and southern part. Between these locked sections, there is a creeping section and the Parkfield section. The latter is complex as it is a transition zone between creeping section and locked section (Fig. 1.12a). Two main types of seismic events are monitored on the San Andreas Fault: (i) large seismic events in northern and southern parts of fault, within locked sections, (ii) moderate and small repeating earthquakes in Parkfield segment. In function of the location and magnitude of seismic events which is studied, the asperity refers to objects with considerably different scales.

First, the term “asperity” can be used to design specific segments of plate boundaries of several tens of hundreds of kilometers where earthquakes can occur. In particular, the term “great asperities” has been used to refer to segments of plate boundaries where shear stresses required to induce fault slip higher than average (Sykes & Seeber, 1985). Consequently, magnitude of the induced earthquakes are also higher than average. Such a concentration of stresses can occur for different reasons, and a common one is the presence of geometric irregularities, such as a major bend, an intersection with other faults or a fault offset. Two “great asperities” are found in the big bend region of the southern San Andreas Fault, which induce large earthquakes (Fig. 1.12b). The eastern asperity is called the San Geronio-Cajon knot, and the western asperity is called Tejon knot. They are both larger than 100 km. The Tejon knot broke in 1857. The rupture extended along the fault, and was stopped to the northwest by a creeping zone, and to the southeast by the San Geronio-Cajon knot (Sykes & Seeber, 1985). At Wallace creek, which is part of the western asperity, slip during three great earthquakes ($M > 7.8$) that occurred in California during 200 years ranges between 9.5 to 12m.

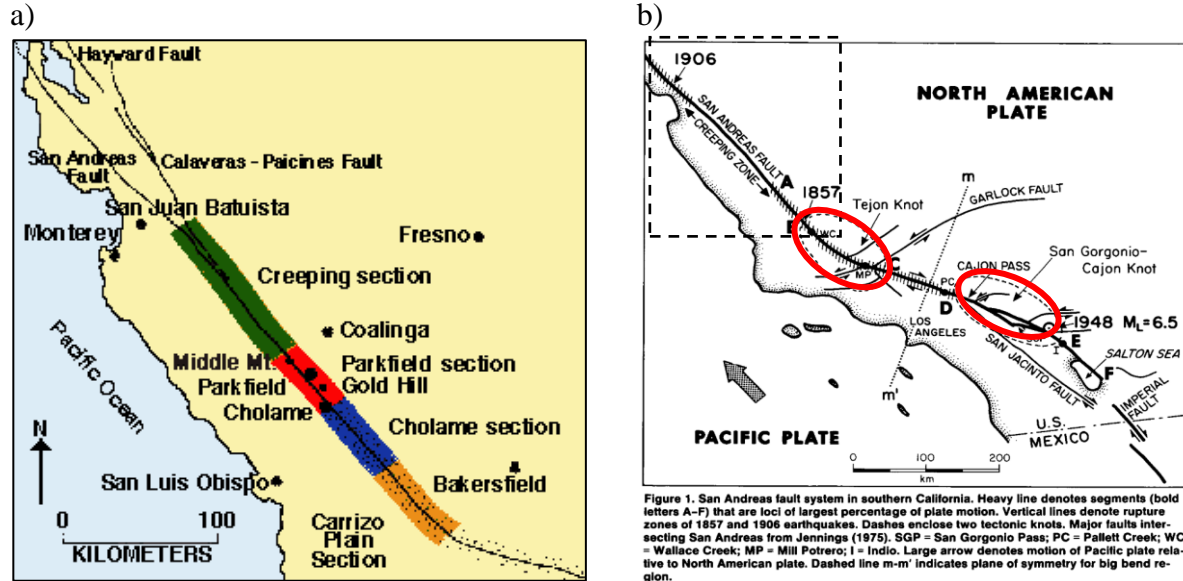


Fig. 1.12 - Portions of San Andreas Fault. On the left: a zoom on the Parkfield section, embedded between creeping section and locked southern part of the fault. Green segment shows the creeping section, red segment the Parkfield section, and blue and yellow segments on the locked section at the south-eastern part. Figure from USGS (United States Geological Survey). On the right: a view at larger scale of the fault plane. The dotted rectangle indicates the area of the figure on the left. Red ellipses show two 100km-scale asperities at the southern part of the fault.

Between the creeping and the southern portions of the San Andreas Fault, the Parkfield segment is a transition segment which has been and is still highly studied. A slow slip (creep) of around 25mm/yr have been measured from geodetic measurements in this segment (Titus et al., 2006). In this segment, 7 repeating earthquakes of magnitude $M=6$ have been monitored since 1987, with a period of 22 years (Nadeau et al., 1995). Geodetic measurements showed that rupture associated with these earthquakes propagated towards a few kilometers southeast. Main part of the monitored events are repeating micro-events with magnitude $M=3$ and smaller, with an average recurrence time of 3 years on seismic patches with a radius of 15-20m (Hadizadeh et al., 2012a). The smallest events occurred on small patches with a radius of 0.5m (Sammis et al., 1999). These geophysical observations show that asperities cover a broad range of sizes, with examples of centimeter scale, meter/decameter scale, and kilometer or tens of kilometers scale.

With the objective to better characterize the internal structure of a section of the fault with creep and seismic activity via direct observations, the exceptional San Andreas Fault Observatory at Depth (SAFOD) was drilled (Schleicher et al., 2012; Zoback et al., 2011). The analysis of drill cores gave precious information about what material was creeping in the fault gouge. First information is that creeping behavior in SAF is related to the presence of both key minerals and specific fluid-rock reaction processes. In fact, analyses of the drill cores revealed the presence of two narrow shear zones, named the Southwestern Deforming Zone and Central Deforming Zone (Bradbury et al., 2011; Zoback et al., 2011). Both zones are 1-2 meters wide zones within a 240 m wide broader damage zone (Holdsworth et al., 2011). They are serpentinite-bearing clay gouge,

whose location correspond to aseismic creep identified in the borehole from casing deformation. Hadizadeh et al. (2012) showed the abundance of phyllosilicate minerals, and proposed that fault creep occurs because the velocity-strengthening gouge is being sheared without strong sealing process. Velocity strengthening means that the friction coefficient increases with velocity, according to the rate and state law (Dieterich, 1979) further described in section 1.3.2. Hadizadeh et al. (2012) used microstructure analyses and showed that creeping is being caused by granular flow mechanisms with frictional sliding of microlithons (i.e. rock portion between parallel clivage plans, not affected by this clivage) along Riedel shears, combined with a stress-driven diffusive mass transfer (Fig. 1.13a). The surfaces exhibit slickenside striations produced by the creeping slip (Fig. 1.13b). Micro seismicity in these two narrow zones are interpreted as due to lithological contrasts or geometric undulations. Due to these specificities, local stresses accumulations could occur on patches with higher frictional strength (such as clasts) or on bumps in the topography. Alternatively, asperity patches can be fractures and seal-regions in the fault core where the pressure solution accommodates a portion of the current creep movement (Hadizadeh et al., 2012b).

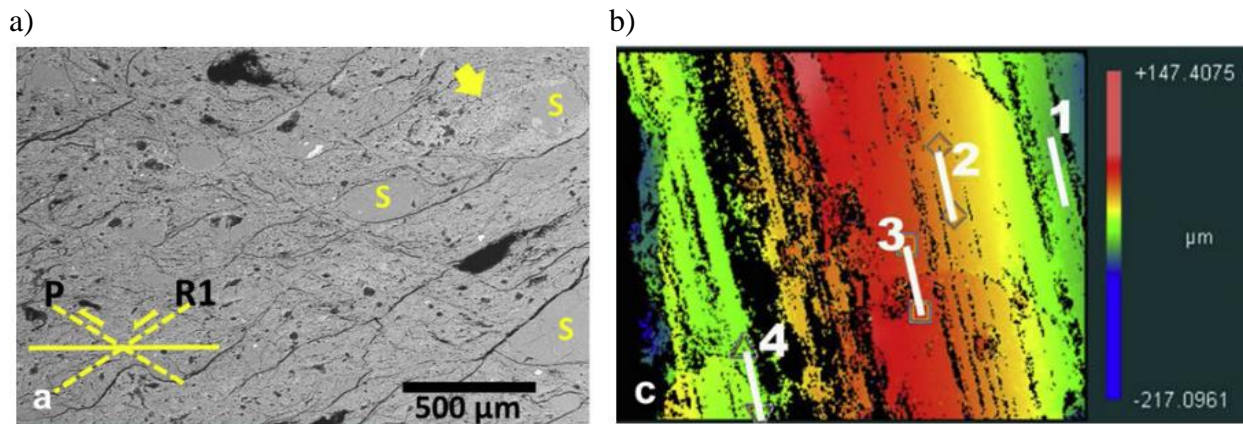


Fig. 1.13 - Evidence of frictional granular flow in the creeping shear zones. On the left: Riedel shears (P, R1) and clasts (S). On the right: Slickenside foliation surface on creeping shear zones (Hadizadeh et al., 2012b).

1.2.5 Strain measurements near excavation

In mining, strain and stress changes are most of the time assessed from numerical modeling and it is rare to obtain data from field measurements. A geotechnical monitoring in 1992 at the Brunswick Mine, Canada, gave information on the rockmass response after the excavation within a sill pillar at 725 m depth began. A strain cell located at 50 m from a 5000t blast shows that 70% of the total strain shift was monitored in the minute of the blast and 30% was monitored during several hours after the blast (Hudyma, 2008). The temporal strain curve clearly shows the presence of an instantaneous response at the time of the blast, a primary phase of decelerating strain (5hours) and a steady-state phase (Fig. 1.14a). No accelerating phase was observed. Another strain

measurements, located at 30m of the blast, shows that the rockmass started to yield (Fig. 1.14b). Hudyma (2008) attributed this phenomenon to the presence of localized crushing failure of quartz-porphry dyke, which redistributed stress away from the cell location. This shows how strain deformation can be locally affected by rockmass properties and specific lithologies. Malan (1999) also monitored creep deformation after blast and studied convergence of excavation during time. Similar curves were observed than the ones shown by Hudyma (2008), with an instantaneous response, a steady-state convergence phase. This pattern repeated at each blast.

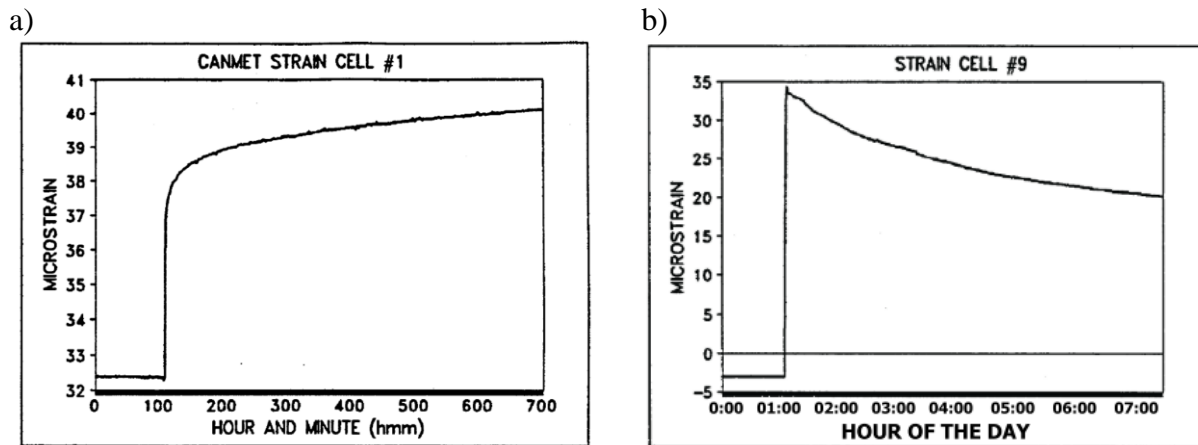


Fig. 1.14 - Time response of two gauges of strain cells at Brunswick Mine, respectively at 50m and 30m from the advancement blast.

Kaiser et al. (2001) carried out a more comprehensive study, by examining the evolution of stress paths with excavation, associated with different steps of excavation of a stope at Winston Lake mine, Canada (stope at 550 m depth). Data come from 4 CSIRO HI strain cells. They showed that the CSIRO cells are effective for monitoring stress shifts (Fig. 1.15). The cells were installed so that they were within the area of influence of two types of failures which occurred in the area: hangingwall delamination and collapse, and wedge-like failure of drifts. They highlighted the presence of significant stress rotations during steps of excavation. By comparison with failure criteria, they interpreted that these stresses rotations during steps of excavation can disturb pre-existing discontinuities and lead to the degradation of the rockmass.

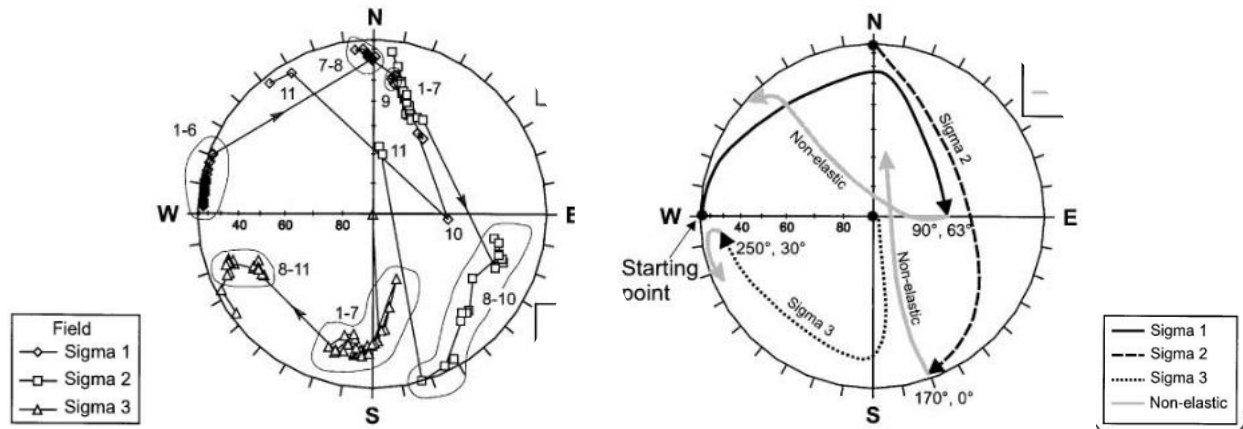


Fig. 1.15 - Principal stress orientations during steps of excavation of the studied stope, obtained from CSIRO cells data. On the left: data step by step, on the right: general tendency. From Kaiser et al. (2001).

1.3 Seismic triggering mechanisms

In the previous section, I investigated the nature of creeping and seismogenic materials. Here, I explore how seismicity is triggered and the relationships between seismic and aseismic deformation. While scaling and statistical laws are well known in seismology (Gutenberg-Richter, magnitude frequency distribution, Omori law, moment-duration scaling), the mechanical control of fault slip remains unclear (Dublanche, 2021). It depends mainly on triggering mechanisms of fault slip (i.e. stress redistributions, aseismic creep, fluid pressure) and on frictional heterogeneities of the fault, which both are difficult to identify and quantify. The fundamental understanding of such mechanics is a prerequisite for modelling seismic cycles with the long-term objective of forecasting earthquakes, since previous “black box” forecasting studies have failed (Smeraglia et al., 2017; Sornette, 1999). In mining, this understanding of triggering mechanism and rheological parameters is also a prerequisite to identify whether seismic events are related to microcracking and tensile fracturing, shear slip on pre-existing fractures via stress transfer, loading of an asperity on a fault via creeping process (in the rockmass or on the fault plane). At long term, such fundamental understanding would allow to identify seismic and creeping regions, i.e. their nature, their extension and their amount (magnitude, creep amount). This could be used to identify better regions that require higher level of monitoring, and to optimize system support and mine sequencing.

1.3.1 Seismic cycle

Considering the whole seismic cycle is necessary to further understand why, when, where and how are triggered seismic repeaters. At the scale of plate boundaries, the earthquake cycle is divided in interseismic, pre-seismic, coseismic and postseismic periods (Scholz, 1998) (Fig. 1.16). The interseismic period is characterized by a steady and stable slip loading the fault at depth. Then, starts the pre-seismic phase, also called the nucleation phase. During this phase, foreshocks can also occur. Slip accelerates until the earthquake occurs, which is the coseismic phase. Co-seismic motions extends in a deep region that hosts the post-seismic relaxation phase which lasts for several years or decades (Scholz, 1998). A second type of post-seismic deformation is the afterslip. It is a shallow relaxation phenomenon, where the fault slips aseismically following a logarithmic decay in function of time. Afterslip is particularly observed in subduction zones when an earthquake occurs on an unstable patch and triggers afterslip on neighboring stable regions (Scholz, 1998). The third post-seismic phenomena commonly observed is the aftershocks sequences. These aftershocks sequences have been well studied and exhibit a hyperbolic decay known as the Omori law.

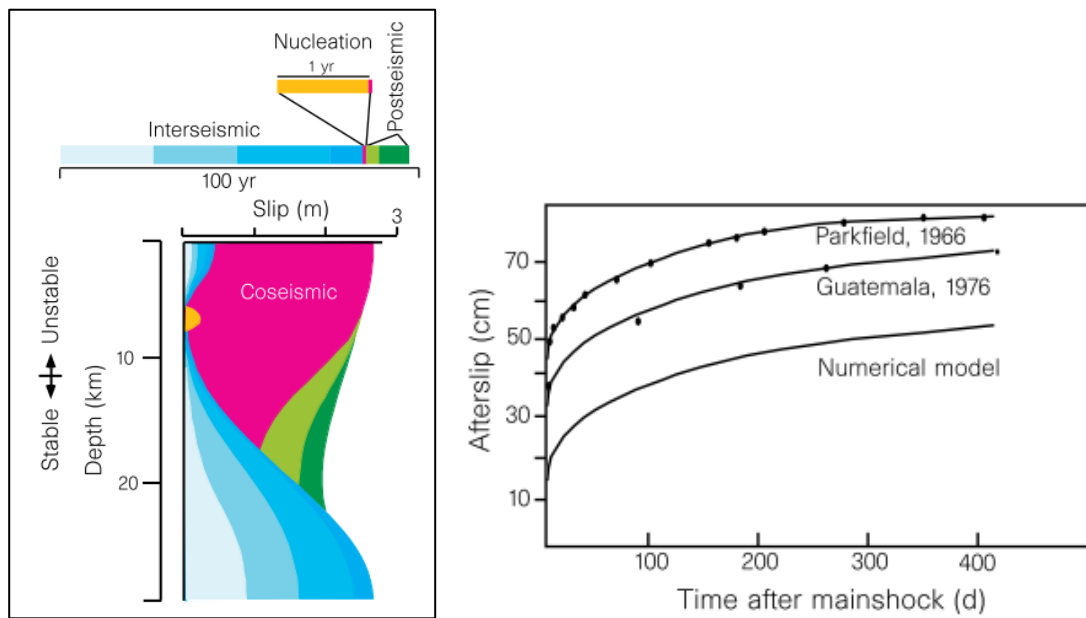


Fig. 1.16 - On the left: periods of a seismic cycle at a natural fault scale. The top of the image shows time periods of the five stages, and the bottom shows slip distribution in function of depth for each phase. On the right: logarithmic decay with time of afterslip. Both images come from Scholz (1998).

1.3.2 Fault slip behaviors and rate-and-state law

There are many different fault slip behaviors, ranging from classic earthquakes to aseismic slip. Classic earthquakes are elastodynamic ruptures, i.e. energy which has been stored in the rock and is released quickly. Aseismic slip, also called creep, was first discovered at the end of 1950s and refers to a continuous and slow slip, without seismic events. Between these two types of fault behaviors, several other types of seismic events are referred to as “slow earthquakes”, like tectonic tremor, “low and very low frequency earthquakes”, “long term slow slips”, “slow precursors” (Leeman et al., 2016a).

A well-known law commonly used to explain aseismic and seismic behavior is the rate-and-state law (Dieterich, 1979). This law describes the evolution of the friction coefficient depending on the velocity and a state parameter, via the relation : $\mu = \mu_0 + a \ln\left(\frac{V}{V^*}\right) + b \ln\left(\frac{V^* \theta}{D_c}\right)$, with μ_0 the friction coefficient for a reference velocity V^* , D_c the critical distance over which takes place the evolution of the friction coefficient after an immediate increase of velocity from V^* to V . The state parameter θ evolves with slip and time and is often interpreted as the average age of contacts on the fault (Helmstetter & Shaw, 2009). Two key parameters are used in the law: a and b , which are determined experimentally and are used to describe the velocity dependence of fault frictional strength (Chen & Spiers, 2016). Positive values of $a - b$ correspond to a velocity-strengthening behavior, which indicates stable sliding. Negative values of $a - b$ (velocity weakening) is a requirement for the nucleation of slip instability. In the first case, dynamic friction coefficient is higher than the static coefficient whereas in the second case, dynamic friction coefficient is lower than the static coefficient (Fig. 1.17a). This law highlights the importance of the frictional parameter $a - b$ for the fault frictional stability. A fault with a friction parameter $a - b < 0$ will exhibit creep, whereas a fault with a friction parameter $a - b > 0$ might be slipping in an unstable way.

Mineralogy plays an important role in the value of the frictional parameter. Faults with phyllosilicate infilling tend to have rate-strengthening behavior, with a parameter $a - b$ which increases with phyllosilicate amount, even though there is no theoretical relation between frictional strength and rate dependence (Ikari et al., 2011). Coefficients of friction are low for phyllosilicate materials, with values between 0.19 and 0.32. Ikari et al. (2009) attribute the strengthening behavior of clay-gouge to the saturation of contact area and the non-cohesive and unlithified (i.e. not converted into stone) nature of these gouges. Then, phyllosilicate gouges are generally expected to creep according to rate-and-state law, except if the mineralogy evolves or if restrengthening of the gouge occurs (Hadizadeh et al., 2012b; Ikari et al., 2011). However this is not always the case, as other parameters such as fluid pressure, composition of mineral phases within the slip zone, can also influence the frictional parameter (Bullock et al., 2014; Kang et al., 2019). Fig. 1.17b shows the evolution of the friction coefficient of smectites gouges, when different load velocities are

applied in a double-direct shear test. We see that smectites change from a weakening behavior to a strengthening behavior when normal stress $> 40\text{MPa}$ (Saffer & Marone, 2003).

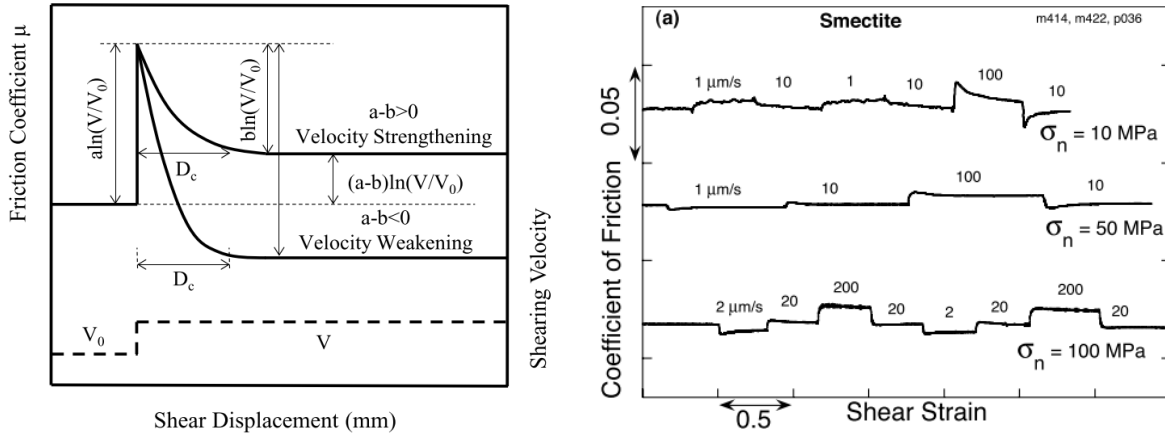


Fig. 1.17 - On the left: rate-and-state law, i.e. the evolution of the friction coefficient with an instantaneous change of velocity. For a velocity strengthening behavior, the friction coefficient increases. For a velocity weakening behavior, the friction coefficient decreases. From An et al. (2018). On the right: evolution of the friction coefficient for smectites, during a biaxial shear test, for different applied normal stresses and different velocities. For $\sigma_n > 40\text{MPa}$, friction coefficient increases with velocity increases and decreases when velocity decreases, which show a strengthening behavior. From Saffer & Marone (2003).

A criteria of instability has been defined when slip exhibits a rate-velocity weakening behavior (Leeman et al., 2016b; Rice, 1983; Ruina, 1983). In this case, sliding is potentially unstable and leads to stick slip when the equivalent stiffness K of the elastic medium is lower than a critical value K_c (Perfettini & Avouac, 2004). The criteria for slip instability was elaborated by combining elastic dislocation theory with friction laws. It means that the value of elastic stiffness of the loading system K must be inferior than a critical stiffness K_c defined by the properties of the fault. (Ikari et al., 2013). Then, the instability on the fault plane is defined both by internal properties of the fault plane and by external loading. The instability criterion is given by equation [1.1], with σ_n and D_c the normal stress and the critical distance, respectively. Parameter $a - b$ is defined experimentally by measuring the change in steady-state friction in response to a change in sliding velocity from V_0 to V .

$$K < K_c = \frac{-(a-b)*\sigma_n}{D_c} \quad [1.1]$$

Between aseismic and seismic slip is a whole spectrum of slow slip behaviors. They appear when the ratio K/K_c is at the limit between stable and unstable failure. These slow events involve different types of events, such as slow precursors, long term slow slip events, very low and low frequency earthquakes, tectonic tremor (Leeman et al., 2016b). These wide range of slow events are out of scope of this thesis, but they highlight the full spectrum of fault slip behaviors that can exist under different fault infillings and normal stresses, and how the fault behavior can evolve

when fault stiffness and frictional properties change, as well as when different loading stresses are applied (Mclasley & Yamashita, 2017; Peng & Gomberg, 2010).

This rate-and-state law is commonly used as laboratory scale and on large-scale field studies such as boundary plate models (Dieterich, 2007). It has also been used in induced seismicity context (Cappa et al., 2022; Heimisson et al., 2022; McClure & Horne, 2011). Its use in deep mines is uncommon, although it has already shown that the law is valid in some cases in mining-induced context (Kozłowska et al., 2015). Rate-and-state law describes how the fault behavior can change with evolution of frictional properties and external factors such as changes of stresses. This highlight the interest to explore how such law (and seismic repeaters) can be used further in mining to identify seismic and aseismic regions, and better characterize the relationships between both regions.

1.3.3 Triggering mechanisms of seismicity

Static stress transfer or creep?

Two models of triggering mechanisms of seismic events have been documented in the literature: (i) self-triggering of events by static or dynamic stress transfer (Stein, 1999) and (ii) creep or aseismic slip of faults which induces ruptures on asperities (Linde et al., 1996). In the context of the thesis, I don't consider the dynamic stress transfer, i.e. that I don't consider the strong shaking induced by an earthquake or a blast, but only the weak permanent stress changes (Stein, 1999). Here, static stress transfer is opposed to creep, in the sense that the static stress transfer is instantaneous whereas creep is a progressive process in time. Main difference between these two models is that seismic events following a major earthquake are the cause of the monitored post-seismic deformation when the triggering mechanism is static stress transfer, whereas they are induced by this afterslip in the second type of triggering mechanism.

Other models of triggering seismicity involve fluid pressure and poro-elastic deformation but they are out of scope in this thesis. Main reason to neglect water in the context of this thesis is that ground water is not connected to the mine openings in Lappberget. Then, Lappberget is considered dry. Only water from production is observed in the mine, but the pressure is usually very low. Note that there are areas in the mine away from Lappberget that holds ground water down to approximately 600 m depth (Anders Nystrom, Rock mechanician engineer from the mine, personal communication).

The first well-known model to explain aftershocks is the one proposed by Dieterich (1994). In this model, aftershocks are due to a direct effect of coseismic stress changes on neighboring faults. These faults exhibit a rate-weakening rheology and no rate-strengthening rheology is needed (Perfettini & Avouac, 2004). The model reproduces well the observed Omori-rate decay of aftershocks, by only considering the stress changes induced by previous earthquakes. Models based on stress changes are commonly used to reproduce observed data and assess risks of future

earthquakes. As an example, Murru et al. (2016) assumed a complete seismic coupling (i.e. cumulative seismic slip equal long-term slip, see Avouac (2015)) to assess the occurrence probability of future earthquakes in the next 30 years for the Sea of Marmara region, Turkey. They built a model based on multisegment ruptures, which incorporate interaction by stress transfer from neighboring faults. No aseismic creep was included. As results, they highlighted which segments are most likely to host a major seismic event in the next 30 years, such as the Gerede segment. In mining, Orlecka-Sikora et al. (2012) also used static stress transfer to investigate the impact of two large seismic events (local magnitude > 3) on the occurrence of subsequent events in the Rudna copper mine, Poland (Fig. 1.18). Based on values of Coulomb stress changes, they showed that these two large events induced a cumulative stress change which had a significant impact on the rate and location of subsequent seismic events. Another example of seismicity triggered by static stress changes commonly mentioned in rock mechanics is the unloading of a fault plane, which can induce slip with a progressive degradation of asperity (Sainoki & Mitri, 2015; Wu, 2021).

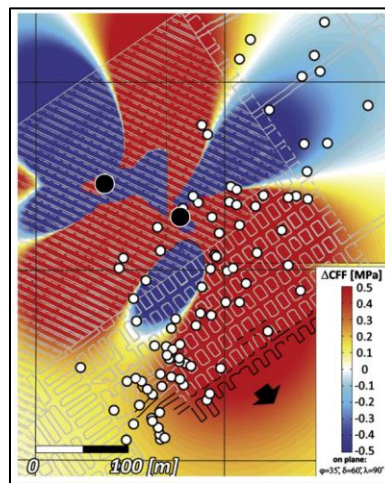


Fig. 1.18 - Coulomb stress changes due to the two strong tremors in the Rudna Copper mine in Poland, in 2005. The stress changes are calculated on receiving planes of strike/dip/rake $35^{\circ}/60^{\circ}/90^{\circ}$. Correlation between seismic events and increased stress is well evidenced. This shows that seismic events occurring after the two tremors are likely to be aftershocks induced by stress transfer. From Orlecka-Sikora et al. (2012).

The second classical model considers that seismic events are induced by aseismic slip (Marone et al., 1991; Perfettini & Avouac, 2004). It is based on the rate-and-state law, and consider a rate-strengthening behavior in some fault regions at shallow depths. Then, afterslip is caused by stress variation within the rate-strengthening region, after an earthquake occurred and propagated up to this region. Aftershocks are induced by this afterslip, instead of being the cause of post-seismic deformation as suggested by models based on static stress changes (Fig. 1.19). This model is consistent with field observations where cumulative moment of aftershocks are usually lower than the afterslip monitored by geodetic measurements. In particular, they exhibit Omori-law decay with

time. As an example, Perfettini & Avouac (2004) applied such model to the 1999 Chi-Chi earthquake (M7.6), Taiwan, and showed that their model reconcile time evolution of aftershocks decay with afterslip measured from geodesy (Fig. 1.20). One of the limitations of the model is that it does not take into account aftershocks with significant coseismic deformation, which can be secondary sources of geodetic displacements and stress transfers (Savage et al., 2007). Other examples where continuous fault aseismic slip after an earthquake has been identified as a main driven mechanism driving aftershocks are found all over the world, such as the Mw 8.8 2010 Maule earthquake in Chile (Bedford et al., 2013) and the Mw 5.8 2010 Collins Valley earthquake at the San Jacinto Fault (Inbal et al., 2017).

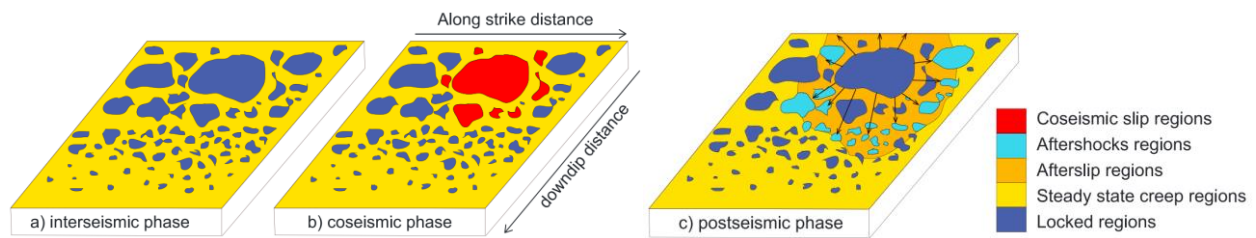


Fig. 1.19 - Conceptual model of aftershocks driven by afterslip. Asperities are locked during interseismic phase. Some of them slip during coseismic period. Then, an afterslip occur and loads aftershocks in the region at vicinity. From Perfettini et al., (2018).

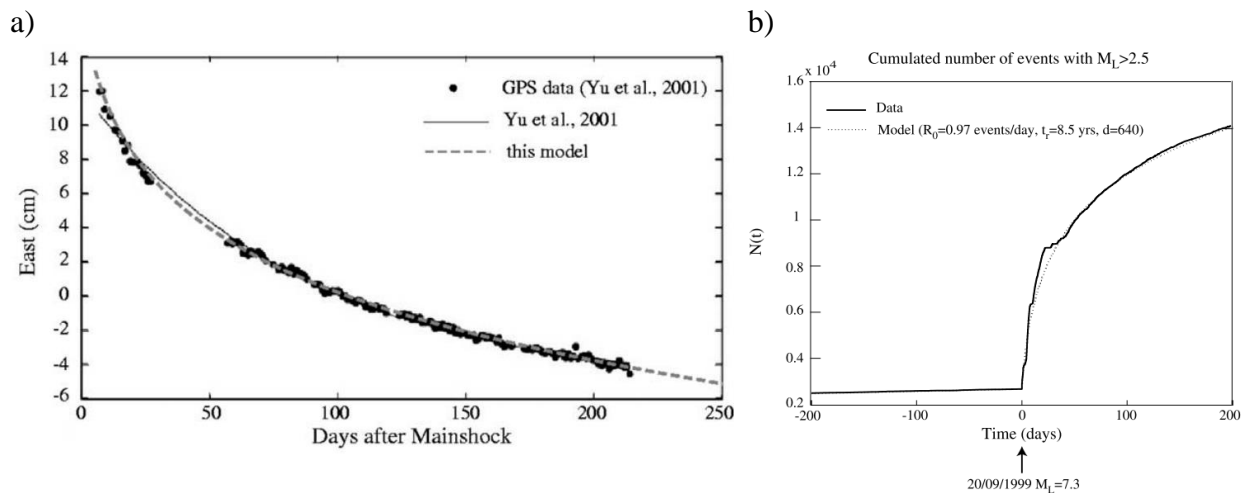


Fig. 1.20 - Afterslip and cumulative number of events for the Chi-Chi-earthquakes, both from field data and a model based on velocity-strengthening brittle creep rheology. From Perfettini & Avouac (2004).

Whereas these two models are well-known and accepted, identifying the mechanisms driving seismicity and creep, as well as calibrating mechanical models able to reproduce the coupling between aseismic and seismic observations, remain complex. For example, Martínez-Garzón et al. (2021) showed that the eastern Marmara region, Turkey, experienced both mechanisms after the Mw4.5 earthquake in 2018, based on microseismicity and strainmeters recordings during 100 days before the event and during 417days after. They observed that during 150 days after the main event, seismicity is driven by aseismic slip and/or fluids, whereas during second period, seismicity is

mainly driven by stress redistribution and ruptures of asperities. Aseismic slip during first period was deduced first from the logarithmic migration of aftershocks, identified as an indicative of afterslip-driven aftershock activity (Perfettini et al., 2018) and secondly because larger events did not occur at the beginning of the sequence and displayed a swarm-like behavior observed in presence of aseismic slip (Zaliapin & Ben-Zion, 2013). To the contrary, seismic events during the second period triggered aftershock clustered in space, with larger events occurring at the beginning of the seismic sequence, which is more similar to seismic events driven by stress redistribution (Martínez-Garzón et al., 2021). Dublanche et al. (2015) used mechanical fault models and a seismic cluster to investigate whether the northern end of the Corinth rift, Greece, is locked or slips aseismically (creeps). The fault is modeled as a rate-and-state frictional interface within an elastic medium; the seismogenic area as a patch with several asperities with a velocity-weakening behavior. They considered two scenarios: a cluster of asperities embedded in a creeping plane, or a cluster of asperities at the limit between a locked and a creeping segment (semi-locked model). They compared results of these models with real field data, and they showed that the creep model fits better the field parameters, such as the magnitude and the time-delays between events. These two examples from Martínez-Garzón et al. (2021) and Dublanche et al. (2015) show how different tools can be used to study the question of seismicity triggering, depending on the information that can be obtained in the field and the precision of the mechanical conditions sought.

Diffuse or localized mechanism?

The two triggering mechanisms described previously (i.e. stress transfer and aseismic slip) focus on processes occurring along a pre-existing large-scale fault surface (i.e. several kilometers or tens of kilometers). Investigation on progressive localization in the case of foreshocks raise additional questions on the triggering mechanisms of seismicity, and in particular whether this triggering mechanism is localized on a surface or acts as a progressive localization process in a volume (Kato & Ben-Zion, 2021). Indeed, on the contrary of other models which focus on processes occurring on pre-existing fault planes, the progressive localization model takes into account the deformation within the rockmass. Earthquake generation evolves from distributed volumetric deformation to shear localization, as it is commonly observed in laboratory experiments (Renard et al., 2019) . During the localization process, seismic events occur first within a whole volume with multiples fractures or faults, and then progressively align along specific planes (Fig. 1.21).

This progressive localization is of main interest for this thesis which aims to conciliate knowledge from seismological field at large scale (kilometric scale) with what occurs within a rockmass at excavation scale (meters to hundreds of meters scale). Indeed, a similar process was observed in laboratory experiments which aimed to study the failure mechanisms of intact or jointed rock masses, not dominated by a large and principal fault. In these experiments, a first distributed deformation phase is observed, followed by a progressive shear localization and finally a macroscopic failure along a specific fracture plane. Whether seismic repeaters could be loaded by

a volumetric process instead of a creep on a specific fault plane is a question addressed in this thesis.

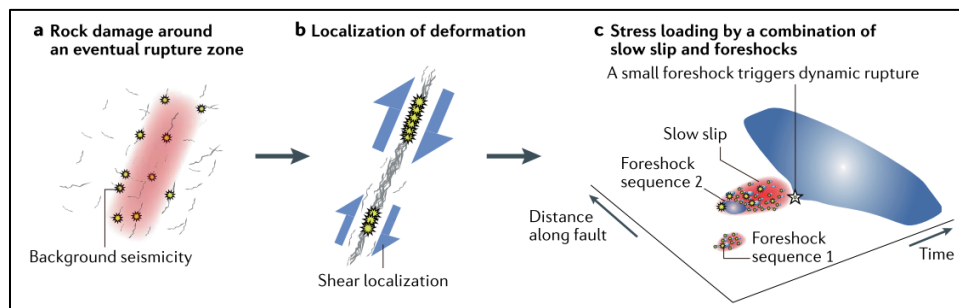


Fig. 1.21 - Progressive localization from seismological model during foreshocks triggering seismicity versus fracturing process from rock mechanical experiments, leading to failure. Top figure is from Kato & Ben-Zion, (2021). It shows a) a progressive localization of shear deformation and background seismicity, b) a shear localization and the foreshocks sequences, c) a major rupture induced by the final loading of a small foreshock. Bottom figure shows typical and well known processes of failure in rock sample at laboratory. The process involves growth of microcracks and formation of a principal plane which finally fails. Figure from Renard et al. (2019).

1.3.4 Particular case of seismic repeaters

In most studies, seismic repeaters are interpreted as the repetitive breakings of a single fault asperity loaded by aseismic slip (Burgmann et al., 2000; Matsuzawa et al., 2002; Nadeau & McEvilly, 1999; Schaff et al., 1998). Then, they are amongst the best examples of seismicity triggered by aseismic slip. Classical model to explain repeating earthquakes is based on laboratory-derived rate-and-state law, with a velocity-weakening law for the asperity and a velocity-strengthening law for the surrounding creeping material (Bourouis & Bernard, 2007b; Chen & Lapusta, 2009; Dublanchet et al., 2013; Uchida & Bürgmann, 2019).

Repeaters are strongly related to interactions between seismicity and aseismic deformations. They are for example commonly mentioned as a potential proxy to estimate the amount of aseismic slip

on a fault plane. Nadeau & Johnson (NJ) (1998) developed an empirical relationship between seismic events and aseismic slip (creep), based on geodetic observations near Parkfield, California. The law is given by equation [1.2]. The law has been shown to be applicable on different natural faults all over the world (Igarashi et al., 2003; Kimura et al., 2006; Matsuzawa et al., 2004; Uchida & Matsuzawa, 2013). However, the understanding of the deformation and creeping behavior is insufficient considering only NJ law or sum of coseismic slip, as this value only represents an amount of creep and doesn't give any information on how this amount of deformation is distributed, such as the creep extension zone or main strain orientations.

$$\log d_b = -2.36 + 0.17 \log M_o \quad [1.2]$$

In a few cases, repeaters have also been reported not to follow the Nadeau and Johnson (NJ) formula (Naoi et al., 2015). In these cases, the authors showed that creep was better estimated from a sum of coseismic slips, which means that repeater patches almost only slip seismically (Hayashi & Hiramatsu, 2013; Hiramatsu et al., 2011). The sum of coseismic slips was then calculated based on the hypothesis of constant shear drop (CSD) scaling, which means that coseismic shear stress drops are independent of their magnitudes, as classically used in seismology (Ide & Beroza, 2001; Kwiatek et al., 2011; McGarr, 1999; Naoi et al., 2015; Yoshimitsu et al., 2014). In other words, this means that repeaters show a higher seismic coupling, i.e. a higher ratio of slip calculated from seismic events to the total slip rate (Pacheco et al., 1993), than in the case of the NJ law (Naoi et al., 2015).

Repeating earthquakes are commonly thought as periodic events, which occur repetitively at the exact same place. For example, in San Andreas, California, a moderate event occurred every 22 years between 1857 and 1966. For these repetitive earthquakes to occur, an efficient and continuous loading is necessary. In some cases, and especially if asperities are sufficiently small, tectonic loading is sufficient to explain these repeating earthquakes. For most of cases, faster repeating earthquakes (faster than the tectonic loading) are commonly attributed to the presence of aseismic slip (Schmittbuhl et al., 2016). Lengliné & Marsan (2009) also showed how an external perturbation, such as a major earthquake, can influence the recurrence time of repeating sequences. This was the case for the Mw 6 Parkfield earthquake, which induced a perturbation in the periodic seismic sequences in the region. Just after the event, repeating sequences exhibited an Omori-Utsu curve law. This response was induced by an immediate coseismic stress change applied on the asperity (Fig. 1.22).

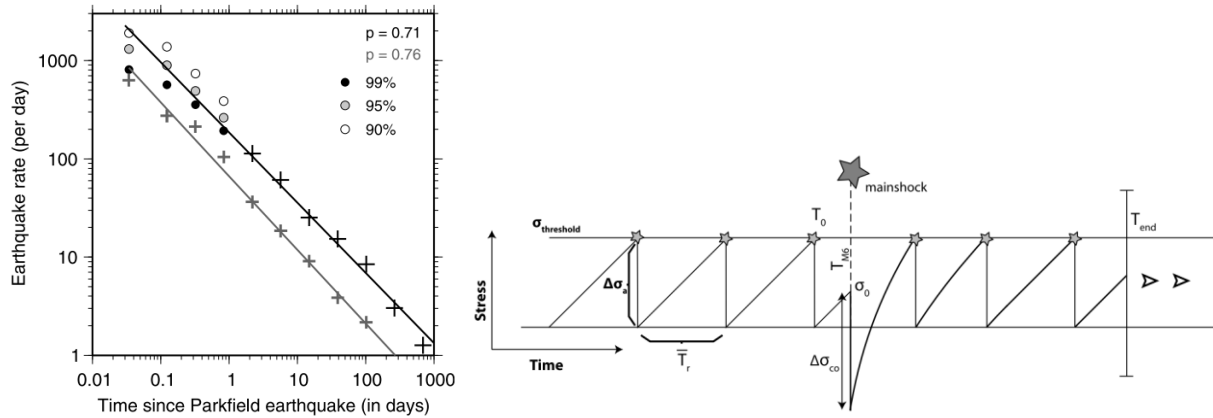


Fig. 1.22 - On the left: earthquake rate after the Mw 6 Parkfield earthquake. The decay is modeled by a power law (Omori-Utsu law) (different percentages are different coherency threshold). On the right: sketch of the earthquake model. It shows the periodicity of the repeating earthquake at Parkfield, with a perturbation induced by Mw 6 earthquake. Following the mainshock, an immediate coseismic stress change is applied. This induce a postseismic effect, which evolves logarithmically with time.

1.4 Conclusion and scientific questions

Seismological laws and models have been built from decades of observations and measurements done in laboratory and for large-scale faults. In particular, seismic repeaters have been identified on boundary plates and are modeled with rate-and-state law. They are directly related to the assumption of the presence of a seismogenic asperity on a large fault plane embedded by a surrounding aseismic creep (Chen & Lapusta, 2009; Igarashi et al., 2003). The presence of repeaters in Garpenberg mine raises then the question of relationships between seismic and aseismic deformation, i.e. what are the nature of seismic and aseismic areas in the mine and what roles play aseismic deformation in the triggering of seismicity.

Mine seismicity is commonly analyzed in terms of seismic parameters (i.e. location, time, magnitude of events), as well as in terms of qualitative source mechanisms (i.e. rockmass failure model: shear, tensile, implosive) (Hudyma, 2008). The notion “asperity” is rarely used in mining and seismic events are mostly seen as a micro-cracking process or as activations of well-oriented fractures. In some cases, the term asperity is employed for studies which focus on the behavior of a specific fault plane (Malek et al., 2008; Sainoki & Mitri, 2016). Creep is well-known in mines, and correlation between seismic and time-dependent rock behavior has been studied for years. For example, McGarr, (1976) exhibited a strong correlation between seismicity and rate of aseismic deformation in the East Rand Proprietary Mines, South Africa (Malan et al., 1997). The rockmass showed a logarithmic creep in response to stress changes. The authors interpreted this aseismic deformation as a consequence of progressive brittle failure of the rockmass. However, comparison

between creep and seismicity often remains qualitative, and law based on frictional properties similar to the seismological law rate-and-state is rarely considered. Therefore, these studies are far from studying mechanisms with such details on microscale behavior as it is the case in seismological laws.

Seismic repeaters in mines are remarkable as they suggest that seismicity is triggered by an aseismic creep. These repeaters show that seismic monitoring could be used in a mine to get information on aseismic deformation, and the question is raised on how to use known and studied seismological models in the context of a deep mine. Precursory to the use of seismic repeaters to further characterize relationships between seismicity and aseismic deformations, is the understanding of the origin of these repeaters, which is the subject of this thesis. By “origin”, I mean both the nature of the hosting material(s) and the triggering mechanism(s). In other words: what structures and materials host the seismic repeaters, and what mechanism loads the seismic regions? This state of the art highlighted the number of different interpretations which can be proposed for similar observations and the complexity to identify the origin of such repeaters. Most importantly, it was shown that the notion of asperity and creep are strongly scale and field dependent. This state of the art also exhibited what is commonly observed to distinguish and characterize seismic and creeping regions: lithologies, fracturing, mineralogy and kinematic markers; keeping in mind that same minerals or kinematic markers can be associated to different fault behaviors. Furthermore, the heterogeneity and the complexity of fault behaviors were shown, different triggering mechanisms that can trigger seismicity were evidenced, as well as the still ongoing development of different methods used to further correlate seismic and aseismic data as well as better characterize mechanical behavior of faults.

Chapter 2

Study area and previous analyses

2.1 Generalities

2.1.1 Presentation of the mine and area of study

The Garpenberg mine is a deep polymetallic mine located in central Sweden, operated by Boliden mining company. It is one of the oldest non-ferrous metal mine still in operation, with first extractions which started at the 13th century. Today, it is composed by several vertical ore bodies. The Lappberget deposit is currently the largest Zn-Pb-Ag-(Cu-Au) sulfide deposit in the mine. Its reserves are estimate of about 17MT at 5.5% of zinc, 2.3% lead, 104g/t of silver and 0.3g/t of gold (Ahmadi et al., 2013). Exploitation starts at a depth of about 450m below the surface until more than 1400m at the time of the writing of this manuscript. Stresses increase with depth, which increases risks of seismic events with larger magnitude and associated rock damage. The study area of this thesis is the block 1250 at more than 1km depth and its upper sill pillar (a left non- excavated pillar to support the weight of the overburden of upper levels) of 25meters height (Fig. 2.1). In the following of the thesis, except for the geological description in section 2.1.3, I will work in mine coordinates, with mine north oriented at N330° from the geographic north. The axis parallel to mine drifts is the Y-axis.

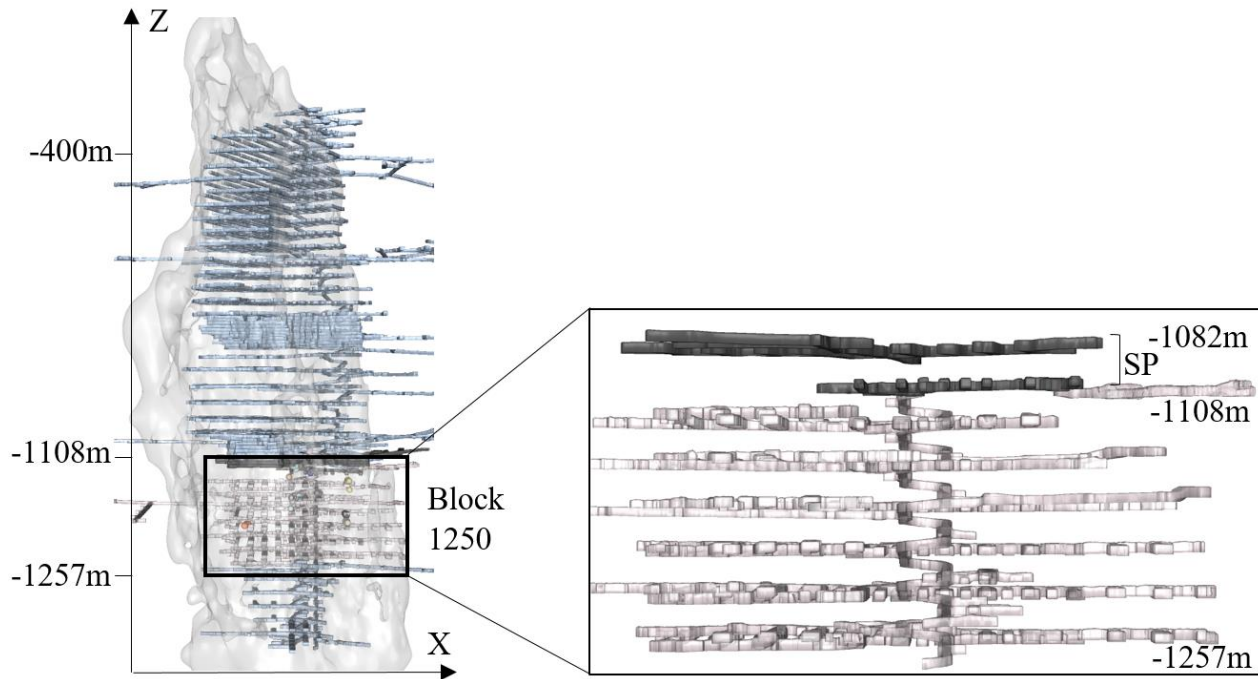


Fig. 2.1 - The orebody of Lappberget and the block 1250. On the left, a general view of the orebody (grey vertical lens) and horizontal access drifts (in blue). On the right: zoom on the area of study: the block 1250 and the upper sill pillar. The block 1250 consists of 7 levels of extraction (access horizontal drifts are shown on the figure). The sill pillar is a non-exploited pillar on the top of the block (between the levels -1082m and -1108m).

2.1.2 Mining method in block 1250

In the deepest area of Lappberget orebody, transversal open stoping mining method (highly similar to sublevel stoping method) is the main mining method. This is a high productivity method well adapted for vertical steep orebodies with regular shape and narrow width. It consists in excavating large vertical columns of rockmass, called stopes, between consecutive horizontal galleries, called drifts. A ramp is built from the surface to reach the orebody. At each level, a main horizontal drift is developed parallel to the orebody and cross drifts are developed perpendicular through the ore. From these drifts, vertical boreholes are drilled, explosives are installed, and the rockmass is mined out between two levels (Fig. 2.2).

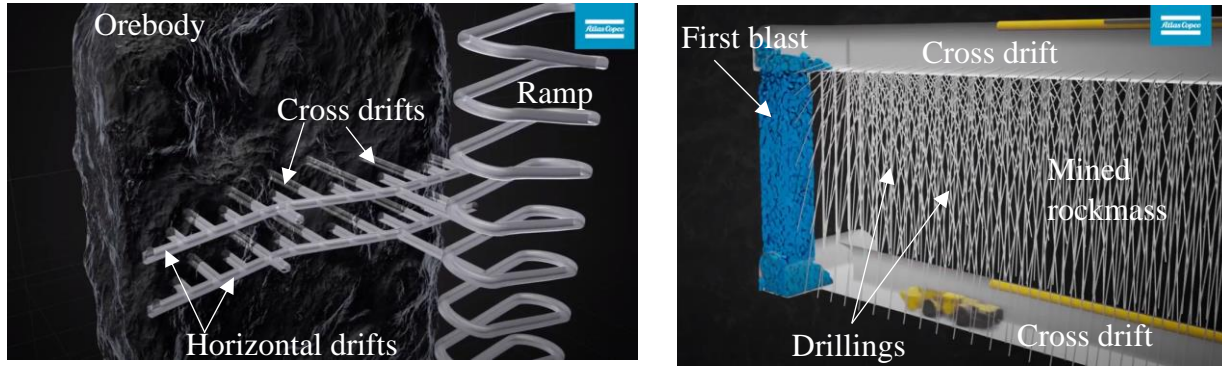


Fig. 2.2 - Transversal open stoping mining method. Images from Atlas Copco (YouTube video Epiroc).

In the block 1250, excavated stopes are 20-30 meters higher. A primary-secondary method is used. In this method, primary stopes are first excavated and secondary stopes, located between them, are excavated only when primary stopes have been mined and backfilled. This allows secondary stopes to give stability to the area while primary stopes are excavated (De Santis, 2019). The widths are around 10m for primary stopes, and 15m for secondary stopes. Stopes are extracted following a pyramid shape driven from the middle to the abutments, with both a top-down and a bottom-up sequencing, to avoid large stresses in the sill pillar. Stope 13 is the middle column and we'll see later that the final stages of the excavation of this stope play a major role in stress transfer through the upper sill pillar. The extraction of the rockmass between two different horizontal levels is done in three steps (Fig. 2.3).

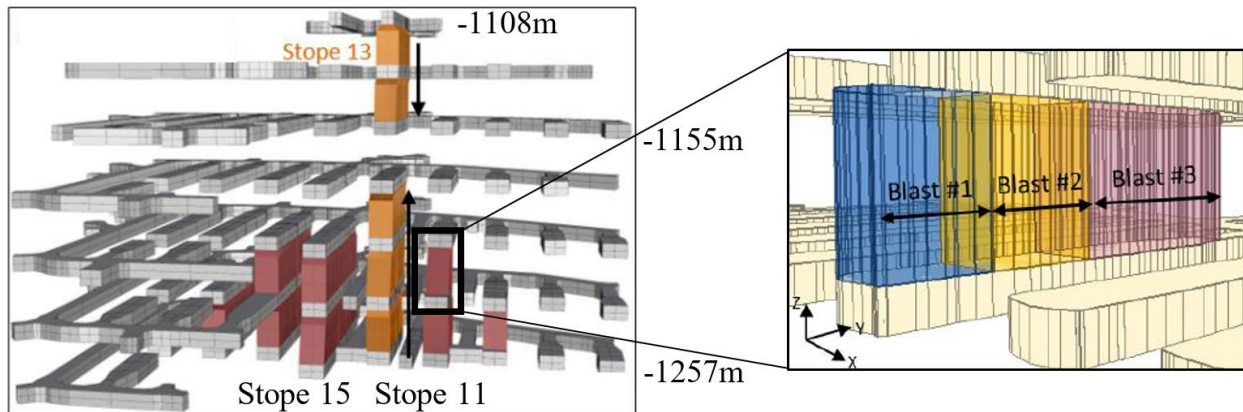


Fig. 2.3 - On the left: a view of the block 1250, with both horizontal drifts and vertical excavated stopes between drifts. The excavation of the stope 13 is shown, with top and bottom sequencing, which leaves a final non-excavated rockmass block in the middle. Note that the colored blocks are the excavated blocks, the blank areas represent the non-excavated rockmass. The sill pillar is not shown on the picture but is located just above the level -1108m. On the right: an example of the method to excavate the rockmass between two different horizontal levels, with three different blasts. From De Santis (2019).

2.1.3 Geological description

The Garpenberg mine is part of one of the most important mining areas in Sweden, known as the Bergslagen region. A wide variety of magmatic-hydrothermal deposits are found in the region, which have undergone strong metamorphism and deformation. Sulfide deposits in Garpenberg are stratabound, volcanic-associated marble- and skarn-hosted (SVALS) Zn-Pb-Ag-(Cu-Au) replacement deposits (Jansson et al., 2017). This means sulfide are associated with a submarine volcanic system and include subsea carbonate replacement (Kampmann et al., 2017). They are similar to volcanogenic Massive sulfides (VMS) deposits, which are formed by the interaction of hot mineral-rich fluids expelled from undersea volcanoes with cold seawater. After this complex process of formation, ore bodies in Garpenberg were modified by subsequent tectonic deformations and metamorphisms, which added even more complexity to the orebody (De Santis, 2019).

Garpenberg deposits are hosted by a strongly deformed and metamorphosed supracrustal inlier called Garpenberg supracrustal inlier (GSI) (Jansson, 2011). The major structure is a northeast-southwest trending, doubly plunging syncline with a sub-vertical axis referred as Garpenberg syncline, situated on the NW part of the inlier (Fig. 2.4a). Multiple tight folding resulted in a complex geology within the syncline. The southeastern part of the syncline limb is bordered by a major reverse zone known as Stora Jelken Zone, which is the major fault in the area (Tiu et al., 2021). This thrust fault is at more than 1km than the orebody of Lappberget.

The orebody of Lappberget is the largest of the sulfide deposits. It is hosted by an upright structural dome in the northwest limb of the Garpenberg syncline (Tiu et al., 2021). The dome is cored by intensely altered and metamorphosed felsic volcanic lithologies of the stratigraphic footwall whereas the ore host is overlain by less altered metamorphosed clastic rocks belonging to the stratigraphic hanging-wall. A unit dominated by calcitic to dolomitic marble overlies the felsic metavolcanites of intense K-Mg-Fe±Si-rich alteration expressed by mica and quartz (Jansson, 2011; Tiu et al., 2021). Mineralization occurs mainly as Massive to semi-Massive sulphide veins and breccias in calcitic to dolomitic marble (Fig. 2.4b), and impregnations and veins in felsic metavolcanic rocks. Tectonic ball ores and ore associated with skarn and quartz are also found (Jansson, 2011). The exploited orebody of Lappberget forms a subvertical lense, with a diameter around 200m and starts at 425m from the surface until more than 1500m depth (Ahmadi et al., 2013).

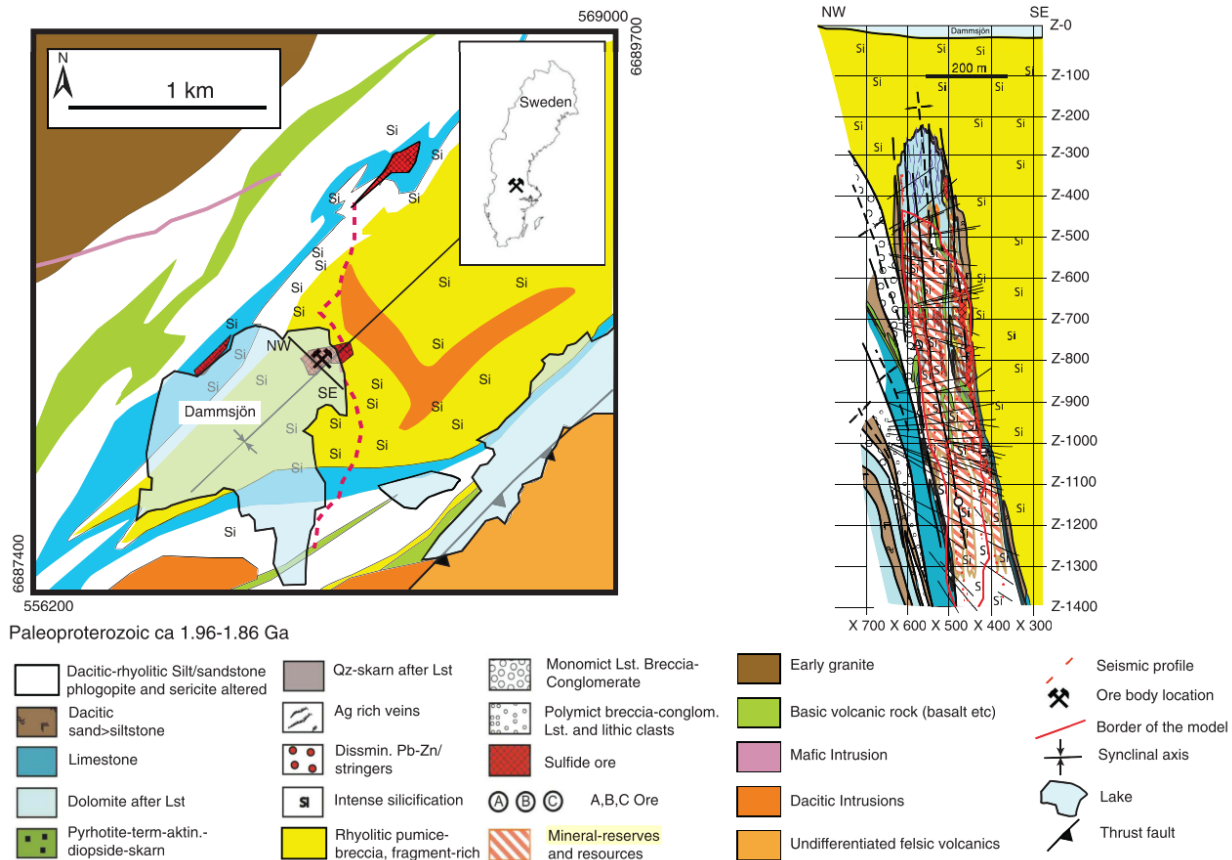


Fig. 2.4 - Geological map and cross-section of the Lappberget orebody. On the left, the Lappberget orebody emplacement is shown. The main thrust fault and the synclinal axis of the Garpenberg syncline are indicated. On the right, a cross section of the sulfide ore as a Massive sulfide form within dolomitic marble is shown. The stratigraphic hangingwall of volcanoclastic rocks is well visible (in yellow). From Ahmadi et al. (2013).

Step ENE-NE trending shear zones (foliation) are cross-cutting the Massive sulfide mineralization and are associated with talc and chlorite alteration. They form the main structures in the orebody and are subparallel to the strike of the orebody, which gives anisotropy to the rock mass. From the western part of the orebody to the eastern part, a change of orientation of foliation is observed (Fig. 2.5a). Sub-horizontal joints are also found (van Koppen, 2008). All along the orebody, weak zones are identified by geologists of the mine (Fig. 2.5b). They refer to unstable weak rock mass material which are ambiguous in terms of geological composition. They comprise lenses of schists characterized by Massive amount of soft minerals like talc and chlorite, some zones of contact between rock types, and areas characterized by intense natural and induced cracks (De Santis et al., 2019). In the western part, which is where most of the studies will be conducted in this thesis, weakness zones are mainly parallel to the foliation (van Koppen, 2008).

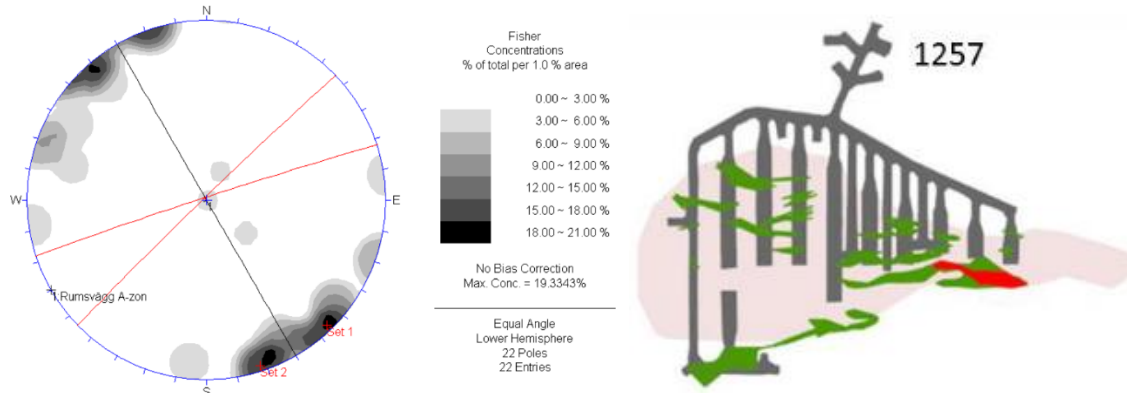


Fig. 2.5 - On the left, two main orientations of the foliation (in red) according to the geological north of the mine. Dark line is perpendicular to the strike within the western part of the mine. On the right, weak (in green) and very weak (in red) zones on a plane view of the level -1257 on the block 1250. Weak zones are almost parallel to the orebody. Figures from van Koppen (2008) and De Santis (2019).

2.1.4 Influence of lithologies on the rockmass stability

A rockburst observed in the mine at level -900m highlights the influence of lithological heterogeneities on the seismicity in the mine. This event has been shared via personal communication during a visit at the mine. The event occurred due to a mistake in the sequence of excavation, which didn't respect the usual pyramidal shape of excavation. As a consequence, a rock-burst appeared in the mine. Stope 13 (Fig. 2.3) is at the limit between the eastern part of the mine, characterized with Massive sulfides within dolomitic, and the western part of the mine, characterized with mineralized veins within felsic metavolcanic rocks, referred as Micaquartzites in the mine. Interestingly, two different behaviors appeared on each side of the stope 13. At the eastern part of the stope, one pillar failed (Fig. 2.6a). At the western part of the stope, the pillar stayed intact (Fig. 2.6b). This observation highlights the necessity to study better how differences of lithologies influence the seismicity and the rockmass damage.

a)



b)



Fig. 2.6 - Photos at the level 900m, after the rockburst in 2012. On the left, pillar at the western part of the stope 13, which has completely failed. On the right, pillar at the eastern part of the stope, where rockmass stayed perfectly intact. Note that in this area of the mine, the exploitation was in cut and fill method, which explains the presence of such pillars.

2.1.5 Stress and rock properties

A stress measurement campaign has been made far from the influence field of excavation, with LVDT-cell (Hakala, 2018). Measurements have been done at 1314m depth, at minimum 160m distance to the mined stopes (Fig. 2.7). Measured stresses can be considered as a proxy for the virgin stress state. Results show a major principal stress at the horizontal, with a trend of 155° from the Y-axis of the mine, a vertical intermediate principal stress, and a minor horizontal stress at a trend of 65° . Magnitudes of the principal stresses are respectively $\sigma_1 = 49\text{MPa}$, $\sigma_2 = 35\text{MPa}$ and $\sigma_3 = 25\text{MPa}$. In such a regime, model and extended model of Anderson predict a strike-slip faulting regime and/or a strike-slip/reverse faulting regime (Lund Snee & Zoback, 2019).

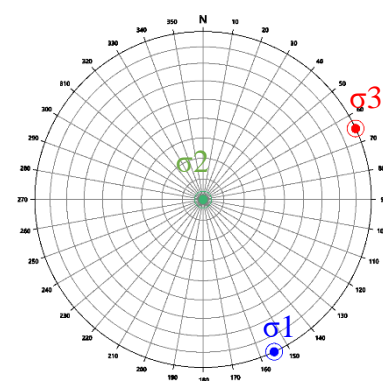
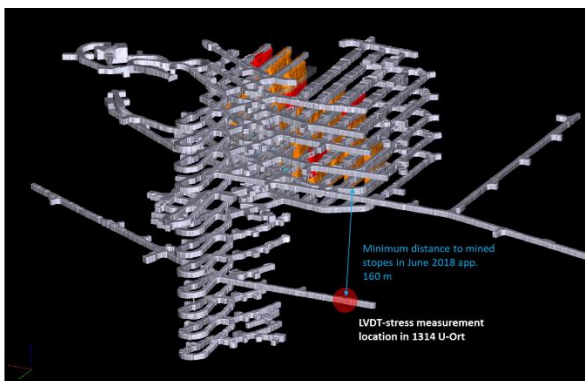
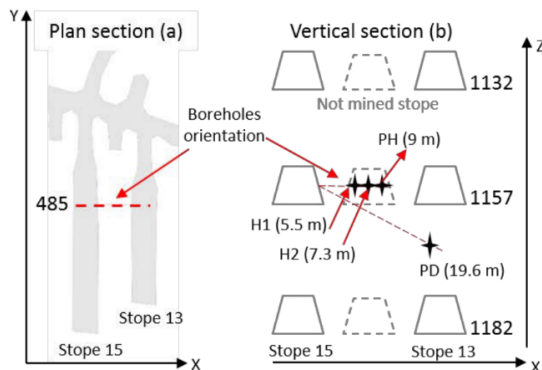


Fig. 2.7 - In situ stresses measurements with LVDT-cell, taken as virgin stress state, at 1314m level. On the left, the point of measurement, from Hakala (2018). On the right, orientations of principal stresses obtained from the measurements (north is Y-axis of the mine).

The geometry of the excavation influences the state of stresses. Two measurements (H1 and H2 cells) have been carried out by Ineris within block 1250 in December 2014 (Fig. 2.8). They were realized between two excavated stopes (stope 13 and 15) at -1155m depth. They were at around 2m from each other, with H1 closer from the excavation than H2. Values are similar but σ_1 orientation rotates at 40° , which is significant, especially as these two measurements are only at 2m from each other (Fig. 2.9). Interpretation of the differences of stresses can be due to different geological settings or due to the area of influence of the excavation.

a) Ineris measurements (2014)



b) Ineris and SINTEF values of principal stresses

Measurements	Depth [m]	Sample	σ_1 [MPa]	σ_2 [MPa]	σ_3 [MPa]
Ineris (2014)	1155	H1	57	46	26
		H2	56	40	28
SINTEF (2004)	883	level 883	45	24	20
	967	level 967	26	18	11

Fig. 2.8 - On the left: Ineris installation in 2014 on the level 1155m. H1 and H2 are CSIRO cells used for measurements on in situ stresses. On the right, values of the campaign of Ineris, and values from a previous campaign on highest level by SINTEF company on upper levels. From De Santis (2019).

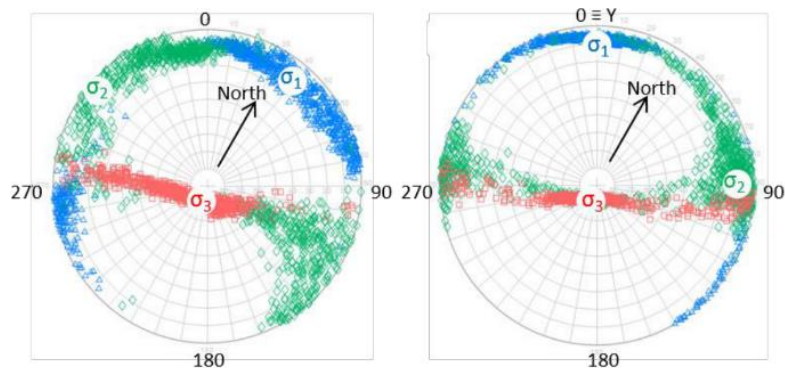


Fig. 2.9 - Orientations of Ineris measurements in the block 1250 (H1 on the left, H2 on the right). Figures are also in the mine coordinates system (north is Y-axis). The geological north was given for information. From De Santis (2019).

In 2005, the mine organized a geomechanical campaign and drill cores from 28 holes were analyzed, which represent a total length of almost 6km of cores. Both UCS (Uniaxial compressive strength) tests and RMR (Rock Mass Rating) classification were made (van Koppen, 2008). The campaign showed that most of rocks have UCS > 100MPa. From this detailed campaign, I sum up in Table 2.1 mean values of UCS for some lithologies of interest in the thesis. These groups will

be more detailed in chapter 3 and I describe them here to exhibit general properties of rocks in the mine and the variability between different rock types. Medium rocks are Dolomite and limestone (UCS between 50 and 100MPa), and weakest ones are talc/biotite micas (UCS < 50MPa). Micaquartzites show a large spread of UCS, with values from 60MPa until 200MPa (van Koppen, 2008), due to variability of mineral and especially micas minerals. Note that quartzite with very low amount of micas can be very strong. Massive sulfides are more homogeneous and quite stiff, with value around 120MPa (semi Massive sulfides can go below 100MPa).

	UCS (MPa)	RMR (0-100)
Mica-quartzites	60-200	40
Limestone – Dolomite – Sedimentary breccia	50-100	65-75
Massive and semi- Massive sulfides	70-140	50-90
Talc and biotite micas	30-60	40

Table 2.1 - UCS and RMR values of lithologies of main interest. Values come from a campaign of Boliden described in (van Koppen, 2008). RMR superior at 60 is good rock (very good if superior at 80). RMR below 40 is poor rock.

Ineris executed biaxial tests on the cores obtained from overcoring and results are shown in Table 2.2. Two other campaigns are shown for information. Ineris measurements were made within the orebody, and more particularly within Micaquartzites. SINTEF measurements were located in the limestone host rock unit at close proximity of the orebody. Few information is available on the third campaign, but it was done at the eastern part of the orebody, where semi and Massive sulfides are more represented (van Koppen, 2008). UCS values are consistent with values described in the previous table. In addition, biaxial tests give values of Young modulus, Poisson coefficient and density. Young modulus of Micaquartzites is heterogeneous, with values from 45GPa until 65GPa in the area of study. For limestone, it is homogenous with values around 55-60GPa and a Poisson coefficient of 0.12-0.17. Density of the orebody is highest than the surrounding limestone rocks.

Measurements	Sample	Depth [m]	Lithology	Young modulus [GPa]	Poisson's ratio	Density [kg/m ³]	UCS [MPa]
Ineris (2014)	H1	1155	Ore	44.9	0.23	3030*	150
	H2			64.1	0.23		
SINTEF (2004)	level 883	883	Limestone	55	0.17	2714	73
	level 967	967		60	0.12	2722	100
-	Hole 1	852	Ore	84.7	0.15	3331	196
	Hole 2			90.7	0.15	3270	146

*Density reported for Ineris measurements is the average value resulting from three laboratory tests.

Table 2.2 - Rockmass properties, from Ineris and two other campaigns. From De Santis (2019).

2.1.6 Seismicity in the mine

Seismicity in Lappberget is characterized by rather small magnitudes, with $-2 < M_w < 1$ on moment magnitude scale. In Lappberget, magnitudes of events are quite low comparatively to other deep mines. Large events are defined as events with $M > 0$, very large events as events with magnitude $M > 1$ (Erguncu Güçlü et al., 2020). Boliden has built a database of the main microseismic events occurring in Garpenberg mine from 2009, based on events recorded by a permanent monitoring network installed by the Institute of Mine Seismology (IMS). De Santis (2019) showed that most events have magnitudes < 1 and occur within 10 meters of distance from the excavation (Fig. 2.10b). Erguncu Güçlü et al. (2020) focused on upper levels of the mine and on large and very large events until 2018. They showed a frequency of larger events around 0.8 per month, and that most of large events are not related to blasts and don't show intense aftershocks series.

A major characteristic of the seismicity in Lappberget is a stronger seismic rate at the eastern part of the orebody (Fig. 2.10a). This is true for all levels of the orebody. This stronger rate is assumed to be due to specific lithological properties in the area, with both stiff and weak rocks at close vicinity (De Santis, 2019).

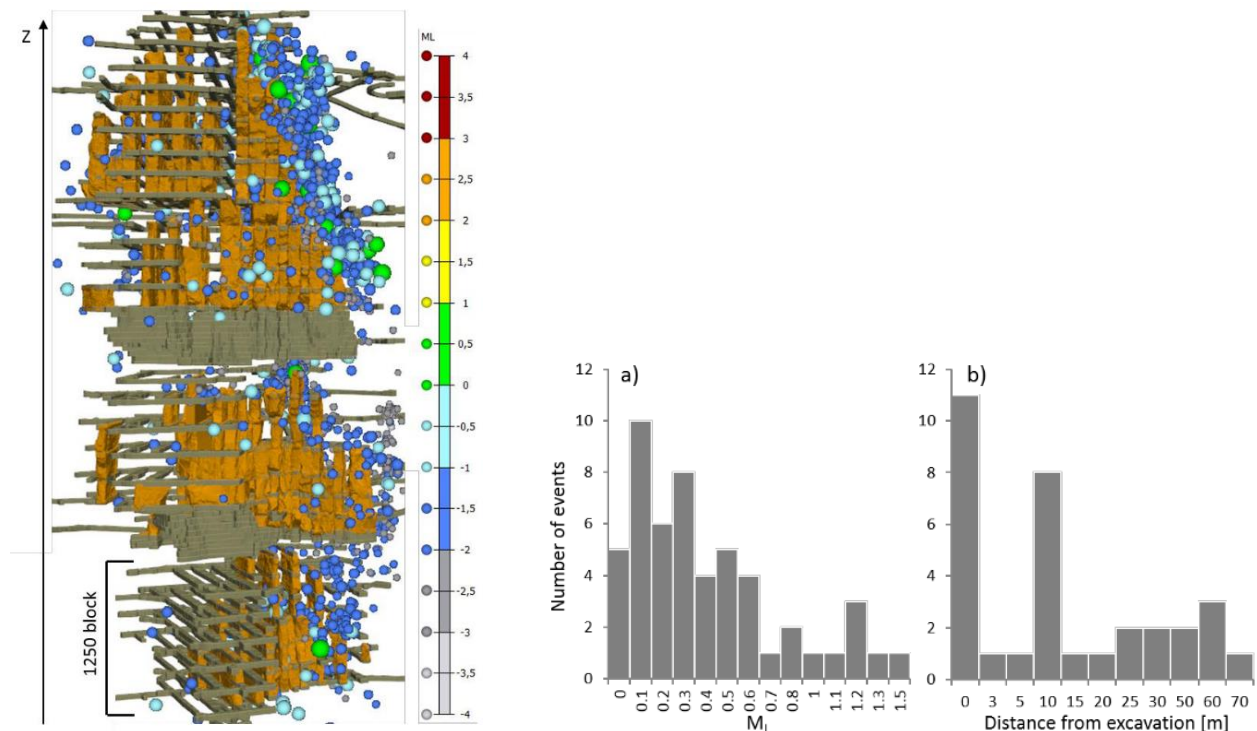


Fig. 2.10 - On the left, microseismicity at Lappberget between 2015 and 2016 monitored by IMS network. On the right, major seismic events ($M > 0$) of the Boliden database from 2012 until 2016. Figures from De Santis (2019).

2.2 Seismicity in block 1250

2.2.1 Installation from 2015-2017

The Lappberget orebody is instrumented by Ineris at deep level, within the block 1250. Previous analyses in the mine was based on a network installed between 2015 and 2017 throughout the entire block. It was composed by six 1-component and five 3-component 14Hz geophones, with a sampling frequency of 8kHz (Fig. 2.11). Some stations are still functional today (A02, A03, B05, B06 for example). It was completed with two strain cells and one extensometer.

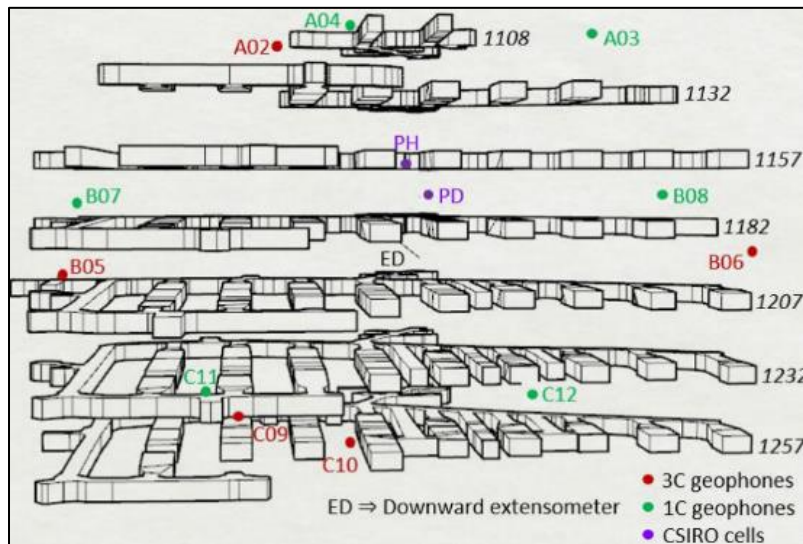


Fig. 2.11 - First network installed within the whole block 1250 during 2015-2017. From De Santis (2019).

2.2.2 Geo-mechanical modeling: 2015-2016

A continuous and elastoplastic 3D geomechanical modeling was built by De Santis et al. (2020), using FLAC3D software (Fig. 2.12). The model simulates 52 steps of excavation that were carried out during the 2015-2016 period in the block 1250. Four main geomechanical groups are represented: the orebody, the surrounding limestone (host rock), weak zones and very weak zones. The constitutive law used for the orebody is a non-linear constitutive law which modifies the Hoek and Brown criterion and takes into account the brittle behavior observed in hard rocks (Souley et al., 2018). Limestone, weak and very weak zones are modeled with Hoek and Brown criterion. The virgin stress state was back-computed with numerical modeling based on measurements of Ineris at -1155m. More information on the model can be found in De Santis (2019).

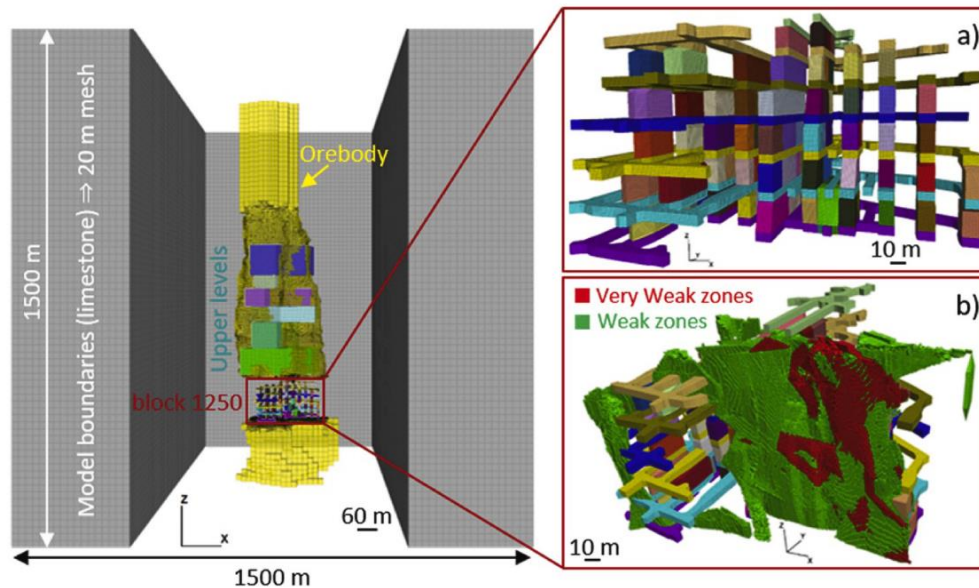


Fig. 2.12 - 3D elastoplastic model of the excavation of 52 steps of the block 1250. The zoom shows the block 1250 with excavation stopes and the weak zones. Figure from De Santis et al. (2020).

2.2.3 Local and remote seismicity induced by mining

Based on the recorded events between 2015 and 2016, De Santis et al. (2019) concluded that production blasts play a primary role in the microseismicity and that most events are a response to stress changes induced by blasting. De Santis et al. (2020) highlighted two main seismic behaviors inside the block 1250 (Fig. 2.13). First, a cluster of seismic events at proximity of the excavation, where spatiotemporal characteristics were strongly correlated with the excavation. Secondly, another cluster of seismicity remote from the excavation but still correlated temporally. This second cluster appeared later than the first cluster, once major part of the area of excavation have been excavated. The cluster at the central part of the excavation is called CC (central cluster) and the cluster at the eastern part is called RC (right cluster). Remote events have higher b-values and smaller source radii than the cluster at proximity of the excavation, which may evidence two different source dynamics. Remote events seem also more energetic and show higher apparent stresses and stress drops than events at proximity of the excavation. This difference is attributed to the fact that remote events are located within the area of strong lithological heterogeneities previously mentioned (stiff and weak rocks close to each other). Note that the 3D geomechanical model of the excavation also gives quantitative values of what is called “close” and “remote” from the excavation. The model gives a radius of influence of the excavation around 15m, which shows how local are stress changes induced by blast. Remote triggered seismicity can occur at more than 80m from the excavation, which is considerably larger than the influence area of the excavation (De Santis et al., 2020).

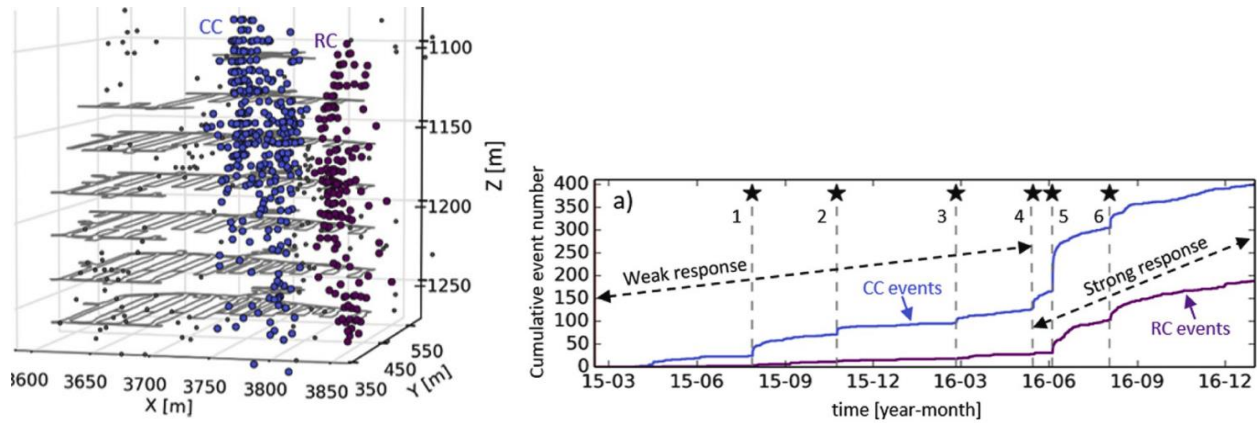


Fig. 2.13 - Spatial and temporal characteristics of the two clusters identified in 2015-2016 on the block 1250. CC is at proximity of the excavation, RC is the remote cluster. Two temporal responses are observed: a first weak response mainly close to the excavation, and one strong response with the additional remote cluster. The strong response starts after the excavation of the last stage of the excavation of the middle column of the block, which induced a large stress transfer. Figures from De Santis (2019).

At vicinity of the excavation, potential unstable areas in the 3D model (i.e. regions with high maximum shear stress variation) are consistent with areas where seismic events are monitored (Fig. 2.14a). This shows a good coherence between seismicity and stress changes induced by the excavation at vicinity of the excavation. However, unstable zones in the model are not spatially correlated with remote seismic area (Fig. 2.14b). This has been attributed to several factors not included in the model. Amongst them, the presence of creep was assumed to play a major role by transferring stresses and deformation through remote zones.

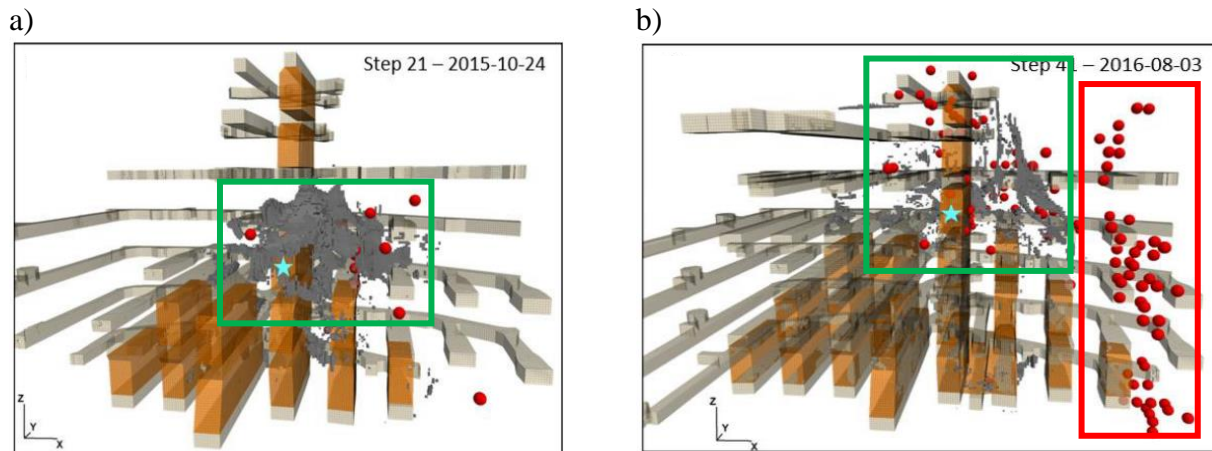


Fig. 2.14 - Predicted “unstable regions” based on maximum shear stress variation criterion ($\Delta\tau \geq 5$ MPa) are in grey. Blue stars indicate blast position and red spheres seismic events. Left image show one step of excavation where seismicity is mainly located at proximity of the excavation and well correlated with unstable regions. Right image shows unstable regions and seismicity when remote seismicity is observed. Remote seismicity is not correlated with unstable zones. Green rectangle show CC with good correlation between unstable areas of the model and seismicity. Red rectangle show the remote cluster RC, where seismicity is monitored but there is no unstable regions in the model. Figure adapted from De Santis (2019).

2.2.4 Migration of stresses after final stage of excavation stope 13

As already mentioned, the excavation follows a top-bottom pyramidal shape. One central area of Stope 13, between levels 1157 and 1182, was left as a pillar and exploited last (De Santis et al., 2019). Then, before the final excavation of this central block of the stope 13, stresses were accumulated in the remaining block. Once the final stage of excavation of stope 13 was made, stresses migrated through the sill pillar (Fig. 2.15). Seismic events then started in the sill pillar. The excavation of this last block induced a significant change of stresses and seismic distribution.

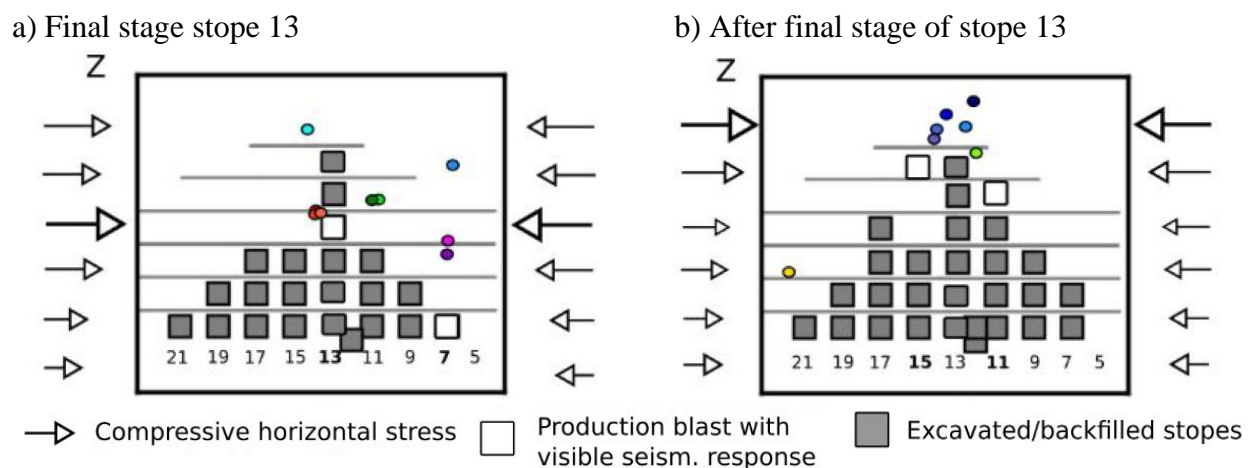


Fig. 2.15 - Final stage of excavation of stope 13 and migration of stresses until the sill pillar. From Kinscher et al. (2020). Dots indicates seismic events, which clearly migrated until the sill pillar after the final stage of excavation of stope 13.

2.3 Seismicity driven by aseismic creep

2.3.1 Evidence for creep in the mine

In addition to stress cells described in section 2.1.5, two permanent strain cells (PH and PD) have been installed in the block 1250 from 2015 and 2017. In some cases, they showed time dependent responses during several hours to several days or weeks after blasting. Significant strain responses to blast have maximum values between $20\mu\epsilon$ and more than $2000\mu\epsilon$. They are not proportional to the extracted volume rockmass, neither to the distance from the excavation (De Santis, 2019). During most of the strain responses, no seismicity is monitored, which suggests the presence of creep induced by blast in the mine (Fig. 2.16).

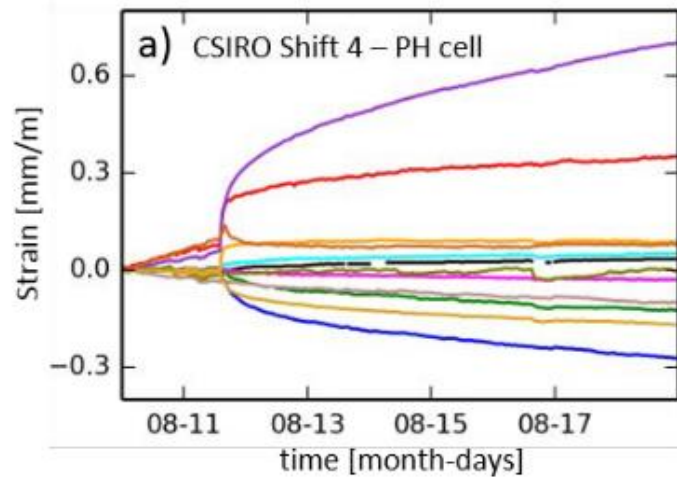


Fig. 2.16 – Time dependent response of the cell after blasting. Strain evolves gradual within the following days, which indicates the presence of creep induced by blast. The 12 curves represent strain monitored by 12 different gauges. From De Santis (2019).

For certain post-blast creep like strain sequence, a coincidence of remarkably similar seismic sequences (cumulative event number per time) was observed. This observation remains qualitative but suggests the existence of a coupling between seismicity and creep in the mine (Fig. 2.17).

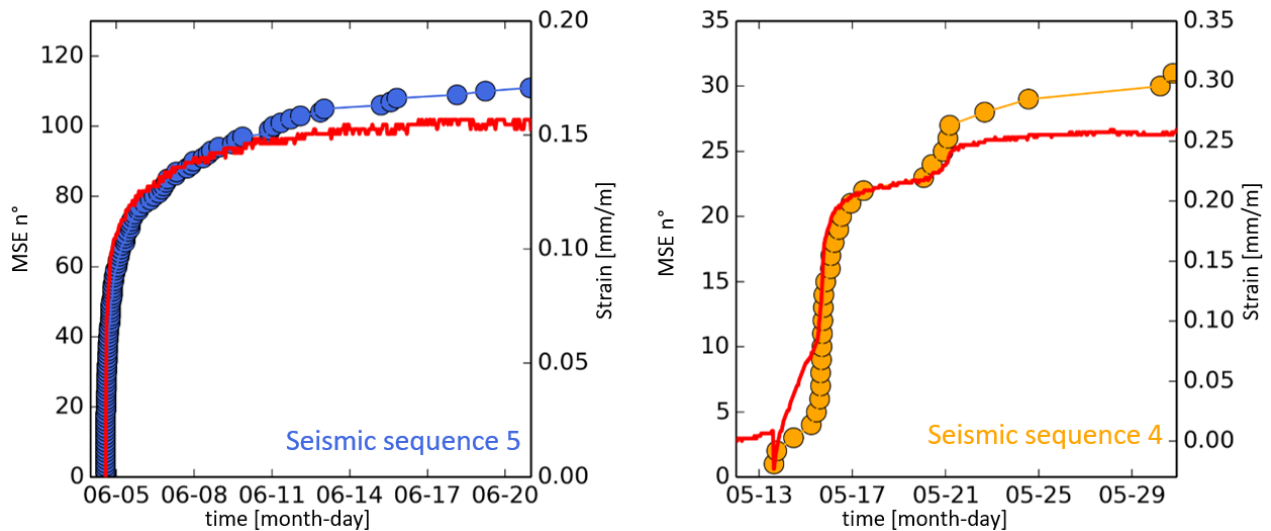


Fig. 2.17 - Proportionality between 2 strain gauges and seismic sequences. On the left, a seismic sequence directly induced by blast. On the right, the seismic sequence triggered 2 days after the blast. A reactivation of the sequence a few days later can be seen, also visible on one strain gauges. From De Santis (2019).

2.3.2 Seismic repeaters in block 1250

Based on seismic wave form similarity analyses for the 2015-2017 data set, Kinscher et al. (2020) demonstrated the presence of seventeen families of seismic repeaters in the mine (Fig. 2.18). As seismic repeaters are commonly associated to repeat rupture of brittle frictional asperities loaded by nearby creep (Chen & Lapusta, 2009), they provide evidence of creep in the mine. More specifically, they suggest the presence of seismicity driven by creep. Magnitudes of seismic events are between -1.2 and $0.2M_w$, stress drops range from 0.1MPa to 10MPa , and source radius between 1 and 10meters .

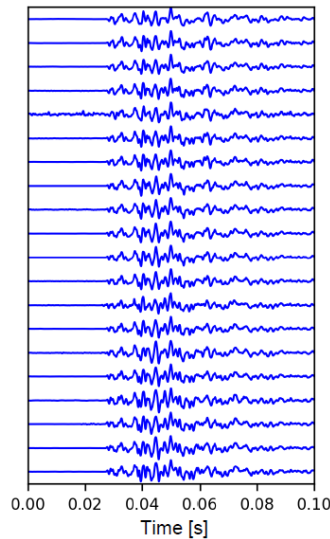


Fig. 2.18 - Example of similar waveforms of one family of repeaters. From Kinscher et al. (2020).

Same families of repeaters occur over long periods of time, ranging from days to years (Fig. 2.19). This is noticeable in the context of mining, as stress changes induced by mining evolve continuously and are expected to induce seismicity in different zones in the mine. When examining interevent times of repeater families, two patterns are observed: (i) a quasi-periodic time recurrence (long lasting repeater events) with periods around 35 days and (ii) transient repeaters following an Omori-type law (i.e. that the rate of aftershocks decays with time approximatively as $1/t$ following the main shock, see Parsons (2002)).

We observe a higher rate of seismicity just after the last stages of excavation of the stope 13, which accumulated a significant amount of stress. Prior to this period, most of the families are within the excavation block 1250. After this period, new families appeared within the upper sill pillar, exhibiting a more periodic pattern. Repeater occurrences are widely correlated in time and space with production blasts, even though temporal delays can be observed. For example, family 11 appeared two days after a blasting event (this family contains similar events than the sequence 4 described in Fig. 2.17). Family 37 located within the sill pillar and activated after the final stage of stope 13 is of main interest in this thesis and will be further described in more details.

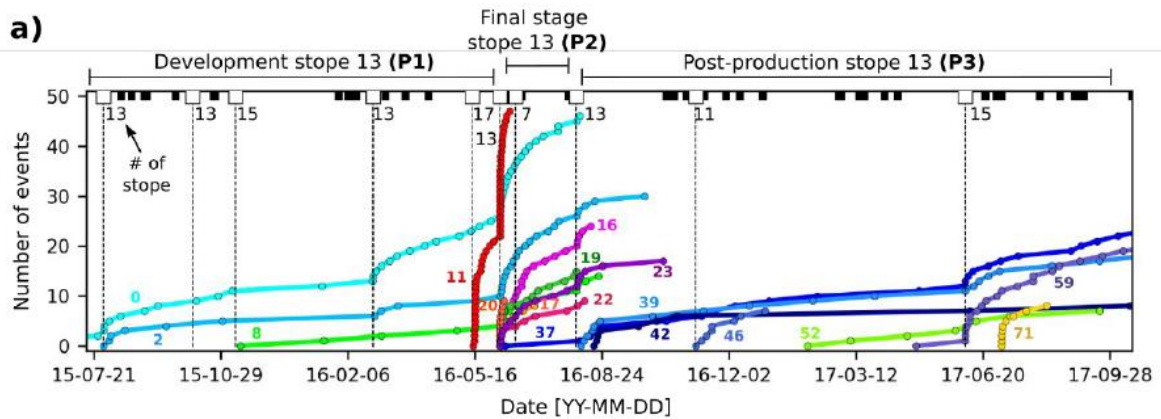


Fig. 2.19 - Temporality of the seventeen main repeater families. Each color represents a family and each point corresponds to a seismic event. Squares on top figure mark significant production blast occurrences. Most families are activated during the final stage of the middle column of the panel of excavation 1250 (slope 13). Some families, such as family 0, have been active for several years with several reactivations. We observe both long lasting and transient repeaters. From Kinscher et al. (2020).

Relocation of the 17 families using the double-difference principle shows that each family aligns along a plane slightly deviated from Y-direction (Fig. 2.20). These planes are approximately 70° from the main shear zones of the mine and they all have similar orientations. Same clusters than the two clusters shown in Fig. 2.13 are observed for seismic repeaters. Kinscher et al. (2020) highlighted that source mechanism of each repeater family is a strike-slip faulting with a significant reverse component. These results are consistent with state of stresses, as Anderson's theory preconize strike-slip faulting with reverse component in environments with major horizontal stress and minor and intermediate stresses with similar values. A good agreement between strike given by the focal mechanism and the alignment of seismic events was also found.

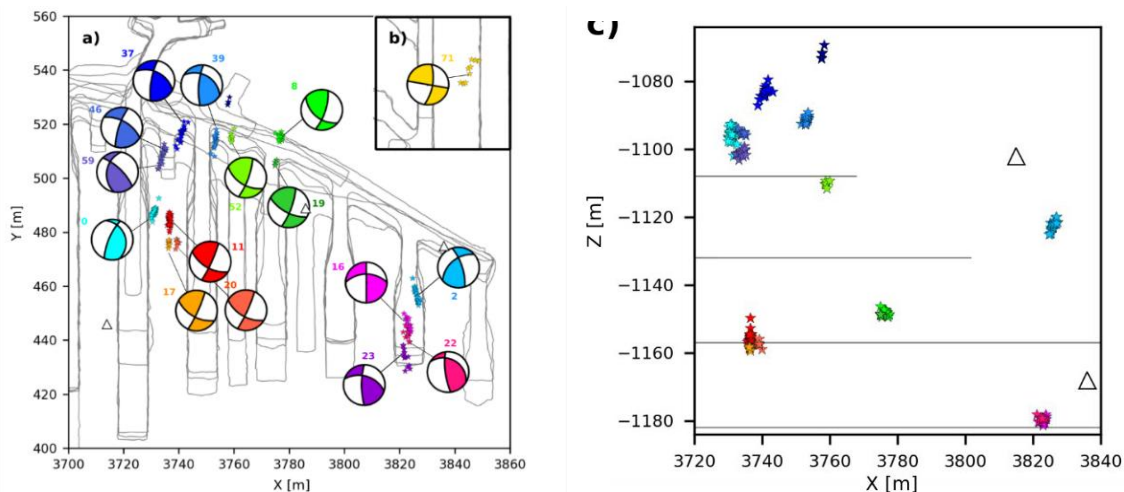


Fig. 2.20 - Spatiality of the seventeen main repeater families. On the left: plane view of the relocated events of each family, with the associated focal mechanisms. All families have similar strike that rotates slightly from Y-axis. Two clusters on the western and eastern part of the mine are visible. On the right: vertical view of the families (XZ plane). From Kinscher et al. (2020).

2.3.3 Repeaters in the sill pillar

Within the sill pillar of the block 1250, a local geophysical network was installed at the end of 2020 (Fig. 2.21). This network was composed by seven stations installed at the bottom and top of the Sill-Pillar. Full wave form based method was used to assure automatic seismic event detected and location (Palgunadi et al., 2019). This new and local network was completed by drillings and strain cells, which were installed one year after this geophysical network. This second step of installation will be further described in this thesis.

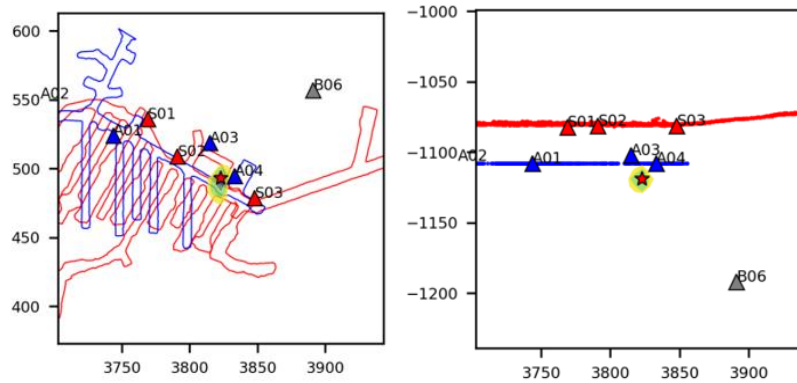


Fig. 2.21 - Seismic monitoring installed since 2020 within the sill pillar at the upper part of the block 1250 and still in activity today. Red and blue levels are the top and bottom levels of the sill pillar. Triangles show location of the geophysical sensors.

Among all the events monitored, seismic events belonging to the repeater families identified by the previous network (Fig. 2.11) were searched for. The main findings of the analysis of events in this new catalogue are summarized here. First, as observed previously at the scale of the entire block 1250, two spatial areas of seismicity are monitored in the sill pillar (CC and RC clusters). A focus is done here on the CC cluster and in particular on the family 37. As previously observed, two temporal trends are observed: long lasting and transient repeaters. Repeaters have usually low magnitude but some larger events ($M > 0$) can occur within repeater sequences. Events related to blasts are mainly located in the central area and little evidence is found for a correlation between seismic events and blasting activity in the RC cluster. Seismic rate increases are usually related to a blast but they seem to be delayed from blasts occurrence.

In the context of this thesis, a peculiar repeater family (family 37) within the central part of the sill pillar is of major interest. Seismic events of the new micro-seismic catalogue were examined to find new events belonging to the target family. The analyses revealed that this main family can be divided into nine subfamilies, based on waveform similarities (Fig. 2.22). Long lasting repeaters are mainly observed and some transient repeaters are sometimes induced by blast.

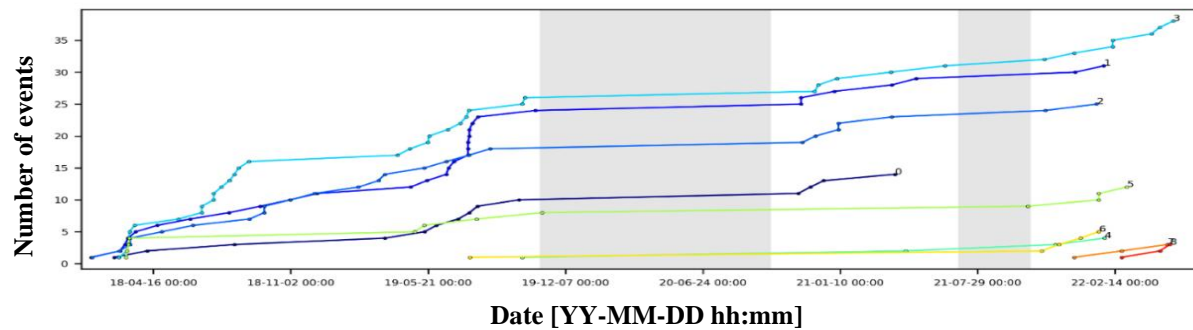


Fig. 2.22 – Temporal evolution of the rate of the nine seismic subfamilies of the target family 37, located in the central cluster of the sill pillar. Each curves is one of the subfamilies and each point corresponds to a seismic event.

2.4 Conclusion

In this chapter, lithologies, geomechanical properties, and seismic characteristics in the mine were described. Below, observations related to seismic repeaters are summarized, which are of major interest in this thesis.

- Seismic repeaters have been observed in the mine. They are of major concern as they suggest creep as a driven mechanism of the seismicity.
- Repeaters are localized in two regions: one central cluster and one eastern cluster. This is consistent with general distribution of seismicity, with intense seismicity at the eastern part of the whole orebody.
- Different patterns in seismicity on central and eastern clusters might be related to lithological heterogeneities.
- Same repeater families are activated over days or years, even if the excavation is evolving. Two different temporality are also observed: long lasting repeating events with a periodicity of 35 days and transient repeaters with short repeating time evolving with time.
- Qualitative fit has been observed between seismic and individual strain gauges. This encourages to pursue studies on how to correlate both types of data.
- Large events ($M > 0$) are more associated with isolated events than with repeater families, but some large events occur sometimes within repeater families.
- For most cases, seismic sequences are mainly related to blasts, with sometimes time-delays between blast and seismicity. In the eastern cluster of the sill pillar and for larger events in the upper levels, there is however very little correlation between blasts and seismicity.

These observations on previous studies related to seismicity in the mine give more information on why it is necessary to study seismic repeaters in the mine. Some of them are : (i) understanding the

different triggering mechanisms associated with different types of seismicity in the mine, (ii) assessing the use of seismic repeaters as a proxy for aseismic deformation in the mine (iii) evaluating the risk of an aseismic area of the mine to become seismic (aseismic to seismic faulting transition) (iv) further exploring general questions in the mine, such as remote seismicity, intense seismicity at the eastern part of the mine, temporal and spatial persistency of events in same regions, and delayed response after blasting.

In the context of the thesis, I focus on the origin of these repeaters, i.e. on the hosting structure(s) and the loading mechanism of seismogenic regions. Previous results gave factors to study: (i) lithologies might play a role (shear drops differ in two regions with different lithologies) and (ii) repeaters could be associated with creeping fault planes loading asperities. These two hypotheses were built only on geophysical analyses on repeaters and need to be study further with field data. In particular, a local network was installed in the framework of this thesis, close to a repeater family within a sill pillar at 1km depth. These new data allow to explore deeper the origin of seismic repeaters combining local geophysical, geological and geomechanical data. In particular, this thesis aims to:

- 1) Investigate whether simple statistical relationships exist between specific lithological groups and the distribution of seismicity at the scale of the whole orebody, and whether the lithologies of seismic repeaters differ from those of other types of events.
- 2) Study what can be learned from a local network targeting a specific repeater family, regarding the geological nature of creeping and seismic areas involved in the occurrence of repeaters.
- 3) Explore how local geological, geomechanical and geophysical data can be used to obtain information on the source location and triggering mechanisms of seismic repeaters. More precisely, It will be studied how to combine fault activations, global stresses and local deformation, in a direct and indirect approach.

Chapter 3

Are repeaters correlated to specific lithologies or excavation sequences?

The main objective of this thesis is to investigate hosting materials and triggering mechanisms of seismic repeaters monitored in the mine. In this chapter, these questions are investigated at large-scale, i.e. at the scale of the orebody and of the panel of excavation 1250, by considering both lithological and geomechanical information.

From seismological models, it is expected to find creeping regions that load neighboring regions with geometrical irregularities or higher friction properties, the most common model being weakly-filled faults loading brittle frictional asperities (Bourouis & Bernard, 2007; Nadeau et al., 1995; Peng & Ben-Zion, 2005). As mentioned in chapter 1, Sainsbury & Kurucuk (2020) showed that seismicity and rockbursts can be correlated with types of rocks due to intrinsic properties of some types of rocks. Then, I first question whether seismic repeaters are more statistically correlated with some lithologies than other ones, and whether these lithologies present specific properties consistent with seismic repeaters (such as the presence of weak minerals or rocks susceptible to creep). I also investigate differences between seismic repeaters and other types of seismic events monitored in the mine (multiplets and isolated events): are they associated with different types of rocks which could explain different triggering mechanisms? In particular, as discussed in chapter 1, seismicity in mine is mainly related to pre-existing structures or to fracturing close to excavation, induced by changes of stresses (Gibowicz & Kijko, 1994; Malek et al., 2008). In this case, could isolated events be located with stiff rocks capable of storing sufficient energy and fracture, whereas repeaters would be correlated with rocks susceptible to creep? In a second step, I also question the influence of stress changes induced by the excavation, a fundamental well-known “external” factor influencing seismicity in addition to intrinsic properties of the rocks and geological intensifiers (Sainsbury & Kurucuk, 2020).

I focus on two types of available data to explore hosting materials of repeaters and other seismic events: lithological data (drill cores and 2D maps) in the entire orebody, and an elastoplastic geomechanical model simulating stress changes induced by excavation steps of block 1250 (De Santis et al. 2020). Fracture data is not available at the scale of the mine, as no fractures survey is realized by mine geologists. By identifying in which lithologies seismic repeaters are mostly located, hosting materials and triggering mechanisms can be constrained. In particular, it is discussed whether seismic events are located in lithologies largely present in the orebody or in

veins and intrusion patches, in stiff and intact rock or fractured rocks with weak minerals, within Massive rock type or at the contact between two rock types. These observations can lead to different interpretations regarding the triggering mechanisms. By studying stress changes induced by excavations, it is also possible to discuss whether these stress changes can activate pre-existing fractures hosting repeaters or whether additional mechanisms such as creep must be taken into account.

The first section of this chapter investigates in which lithologies seismic events are located. Spatial statistical correlations between seismic events and lithological groups are studied, both for repeaters and other seismic events. To study these correlations, a 3D geometrical model based on lithological drill cores data and 2D geological maps was built. Possible mechanisms are discussed considering geomechanical properties of lithological groups hosting seismic events and uncertainties of the model. The second section investigates whether seismic repeaters can be explained by stresses changes induced by the excavation or whether more complex mechanisms must be taken into account. This study is based on the calculation of stress paths on fault planes oriented like the nodal planes of repeaters, made from stress tensors extracted from the elastoplastic model of De Santis et al. (2020).

3.1 Statistical correlations between seismicity and lithologies

3.1.1 Lithological groups

More than 190 different lithologies are identified into the mine from drillings and 2D geological maps. I gathered data in 11 main lithological groups, based on discussions with geologists of the mine (Fig. 3.1 and Annex A). In this chapter, I use the nomenclature of the mine, which may differ from classical rock denomination in some cases, and I provide a brief description of the main groups to clarify their geological nature and their spatial distribution in the mine. I use majuscules to name lithological groups with mine nomenclature.

The eleven groups of rockmasses are metamorphosed rocks with different levels and types of alteration. The so-called limestone rocks are actually marble rocks. They are white rocks with medium-size grains which come from a first metamorphism from the limestone protolite, which was present before mineralization occurs. Dolomite rocks result from a second alteration of the marble rocks located at vicinity of the ore, due to magnesium alteration. They have smaller grains than marble and can contain green talc alteration. Skarn rocks also result from metamorphism of limestone or Dolomite. Sedimentary breccia (mainly limestone breccia or breccia conglomerates) are matrix rocks hosting sedimentary fragments.

The so-called “Quartzites and Mica-quartzites” (MQZTE) is the most heterogeneous group and gather different metamorphosed felsic volcanic rocks from same origin but with different types and levels of alteration. This group can be divided in two subgroups: silicified rocks with no mica (i.e. Chert, Siltstone and Quartzite), and silicified rocks with different types of micas, resulting from metamorphism and alteration of quartzite rocks (Sericite, Phlogopite, Biotite Quartzites and others). I will refer to Quartzite the sub-group which gathers Chert, Siltstone and Quartzite. I will refer to Micaquartzite the sub-group with mica alteration and foliation.

Highly foliated rocks are called Schists. Because of their mechanical weakness, they are avoided during the extraction and are known as “death zones” by the miners. The group Quartz refers to quartz veins found in the orebody. Mafics and Dacite are magmatic rocks. Dacite is the main rock of a dyke intrusion at the eastern part of the orebody. Its characteristics are similar to quartzite subgroup (composed mainly by quartz). Volcanoclastics are sedimentary rocks with fragments of volcanic rocks. Finally, the Massive sulfides group includes both Massive and semi-Massive sulfides. They form the main mineralized zones in the orebody.

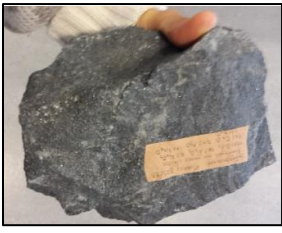
<p>Limestone (marble)</p> 	<p>Breccia</p> 	<p><u>Dolomite</u></p> 
<p><u>Skarns</u></p> 	<p><u>Massive Sulfides</u></p> 	<p>Schists</p> 
<p><u>Quartzites and Micaquartzites (QMOTZE)</u></p> 	<p><u>Quartz veins</u></p> 	<p><u>Dacite</u></p> 
<p>Mafics</p> 	<p>Volcanoclastic rock</p> 	

Fig. 3.1 - Photos of the eleven main lithological groups. In blue: rocks of different levels of metamorphisms from the originate limestone protolite. Light blue are the rock types in the orebody, dark blue are the ones in the host rock. In red, Massive sulfides. In brown: Schists. In yellow: rocks with significant amount of quartz. First: Quartzites and Micaquartzites are the main group in the orebody. They are composed by two subgroups: Quartzite and Micaquartzite. An example of the latter is shown, with foliation induced by the alignment of micas. Quartz veins are found in the orebody and Dacite is an intrusion of magmatic rock rich in quartz. In bold: groups which are represented or included in groups in Fig. 3.2. Except for Dacite, they are part of the orebody. Other are mainly part of the host rocks or are avoided during extraction (Schists).

Fig. 3.2a shows the orebody geometry modeled by the geologists of the mine from the drillings data. Limestone, sedimentary breccia, volcano sediments and mafic rocks are part of the hosting rocks (rocks surrounding the exploited orebody) and are not represented. Five lenses of mineralization are modeled: the blue lens for Dolomite and Skarn; the green lens for Dacite intrusion; the red and orange lenses for Massive sulfides and semi Massive sulfides respectively, the yellow lens for Mica-quartzites. The four first groups are located in the eastern part of the orebody and the latter one in the western part. Shale schists are also present within and at proximity of the orebody, but are not modelled by geologists. They are mainly found in the eastern part of the orebody, at proximity of Massive sulfides and Dolomite.

Proportion of each of the eleven groups has been calculated from drillcores below 900m depth (Fig. 3.2b). Mica-Quartzites is the most represented group in the area, with more than 40% of the cores, followed by limestone with more than 20% and breccia with more than 10%. On the contrary, Mafics is almost inexistent in the area of study and Quartz veins represent only a small proportion. Other groups: Skarn, Schists, Dacite, Dolomite, Volcanoclastics and Massive Sulfides are equally represented with proportion comprised between 3% and 5%.

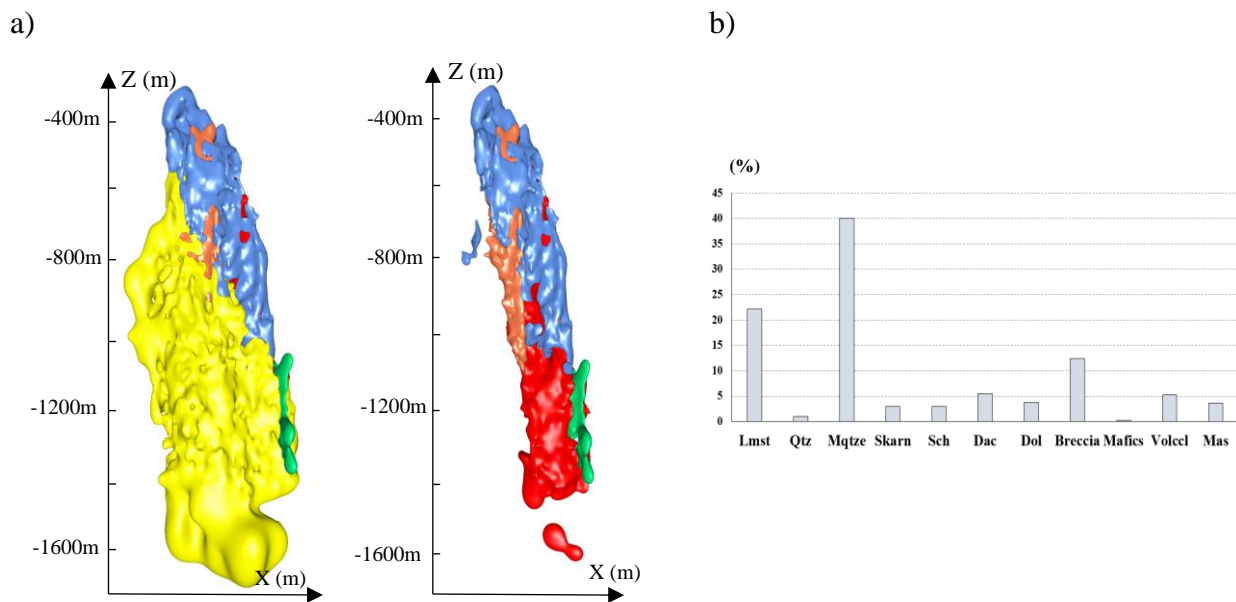


Fig. 3.2 - On the left, 5 lenses representing: Massive and semi Massive sulfides (red and orange), Dolomite/Skarn (blue), Dacite dyke (green) and Micaquartzites (yellow), modeled by the geologists of the mine from the drill cores. Middle and right image are same view, but Micaquartzites are hidden on the right image to visualize better the lithological groups at the eastern part of the orebody. On the right, percentages of the main lithological groups within the cores (below 900m). Each abbreviation refers to the name of a lithological group: Limestone, Quartz veins, Quartzites and Micaquartzites, Skarn, Schist, Dacite, Dolomite, Breccia, Mafics, Volcanoclastics, Massive Sulfides.

3.1.2 Geomodelling of the different lithologies

To gather all available lithological data and examine their correlation with seismicity, a simplified geometrical geomodel is built under the Skua-Gocad® software (Paradigm Geophysical, 2009). Below, I present the elaboration of the geometrical lithological model, the importation of seismic data and the extraction of lithological information.

Dimensions of the model cover the entire area of excavation on the whole orebody: X (3600m, 3900m); Y (350m, 600m); Z (-300m, -1300m). Lithological information comes from 659 drillings (total length is almost 100kms, only drillings within the area of the model are considered) and 2D geological maps drawn by geologists (format dxf) (Fig. 3.3). The resolution of the model is 1 m³. This resolution was chosen as fine as possible to take into lithological variations which sometimes occur on a few meters, and to consider the influence of minor intrusion of rocks or minerals (such as quartz veins or skarn minerals). High variability between lithologies is mainly seen at the eastern part of the orebody, in the area with Dolomite, Skarn, Massive sulfides and Schists. Lithology of each cell of the model crossed by the drillings is directly assigned with the lithology of the drilling which first crosses the cell. Lithologies of other cells are calculated with the method of interpolation of the nearest neighbor (Fig. 3.3, Fig. 3.4). All cells were interpolated, even the ones in regions where less data was available. This choice was motivated with the intention to get information also on seismic events within host rocks, where less data is available since drillings made by the miners aim to reach the orebody. However, host rocks are more homogeneous than the orebody, with mainly limestone and breccia in the footwall, and volcano-sediments in the hanging wall, and interpolated data are considered still reliable.

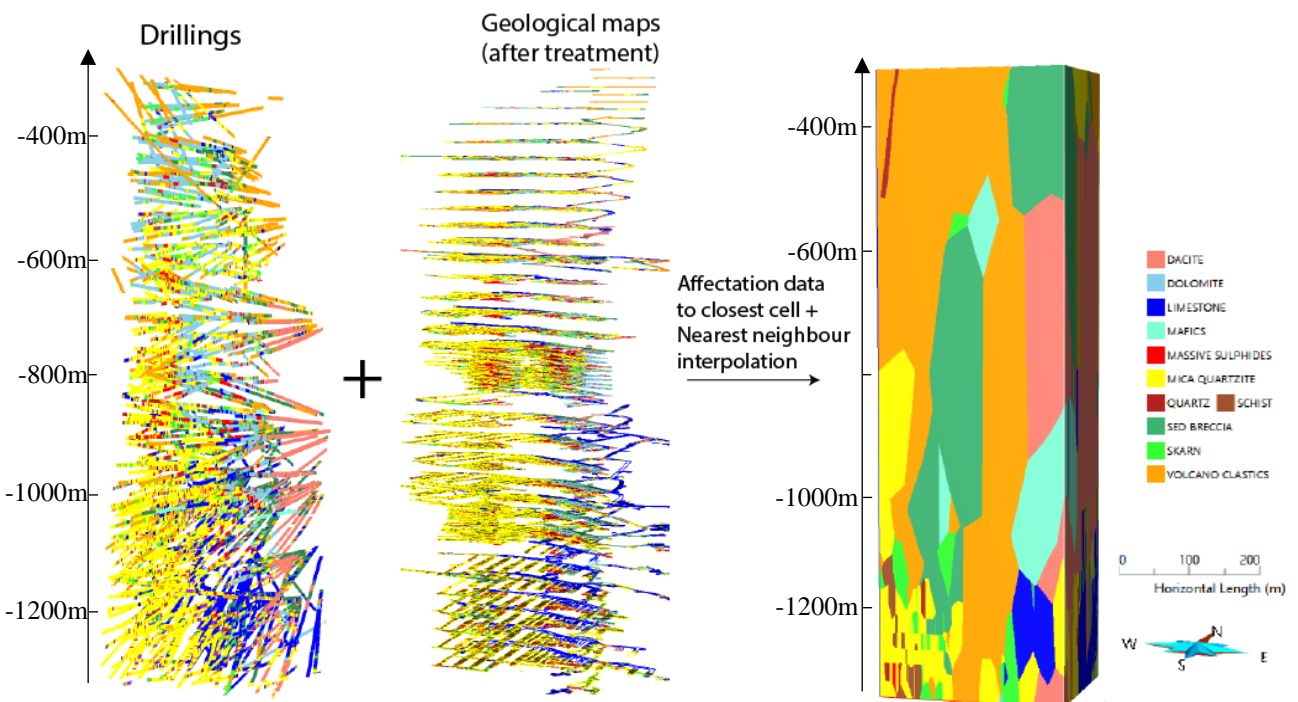


Fig. 3.3 - Vertical view of lithological data, and the model after interpolation with nearest neighbor using the geomodelling software Gocad.

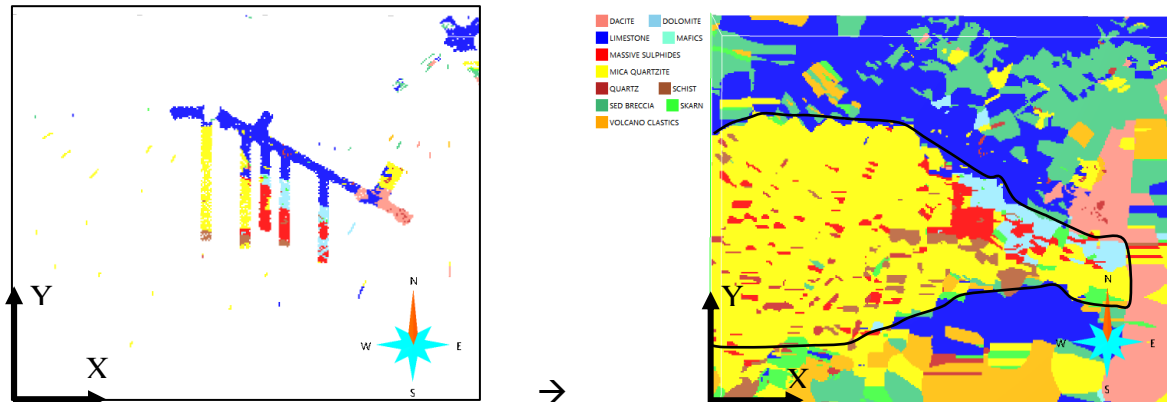


Fig. 3.4. - Plane view of the horizontal level at -1108m (lower level of the sill-pillar of the panel of excavation 1250 presented in chapter2). On the left, colors represent areas which have been directly assigned to the closest lithological group. Blank area are not assigned to any lithology. On the right, the same level after interpolation by nearest neighbor. We observe the tendency previously described: eastern part has stronger Dolomite (light blue), Schists (brown) and Massive sulfides (red) content. Western part is mainly Quartzites and Mica Quartzites (yellow). Around the orebody, we find Limestone (dark blue), Breccia (in dark green), Volcanoclastics (orange), and Dacite intrusion (pink). In dark, approximate outline of the exploited orebody.

To assess the data sensibility of the model, the model was rebuilt five times removing a different drilling each time (Fig. 3.5). For each model, lithologies of five different cells located at equal distance along the path of the removed drilling were observed and compared to the lithologies of the same cells but from the model with all the drillings. By doing so, we observe whether the model assesses correctly the lithologies of the removed drilling. 65% of the cells in models with a removed drilling exhibited same lithologies as the cells in the model with all the drillings. This shows that the model is quite sensitive to the lack of data, but still reproduce correctly two thirds of the data and can reasonably be used for the objective of this study, which is to identify in which lithologies population of seismic events are more statistically located.

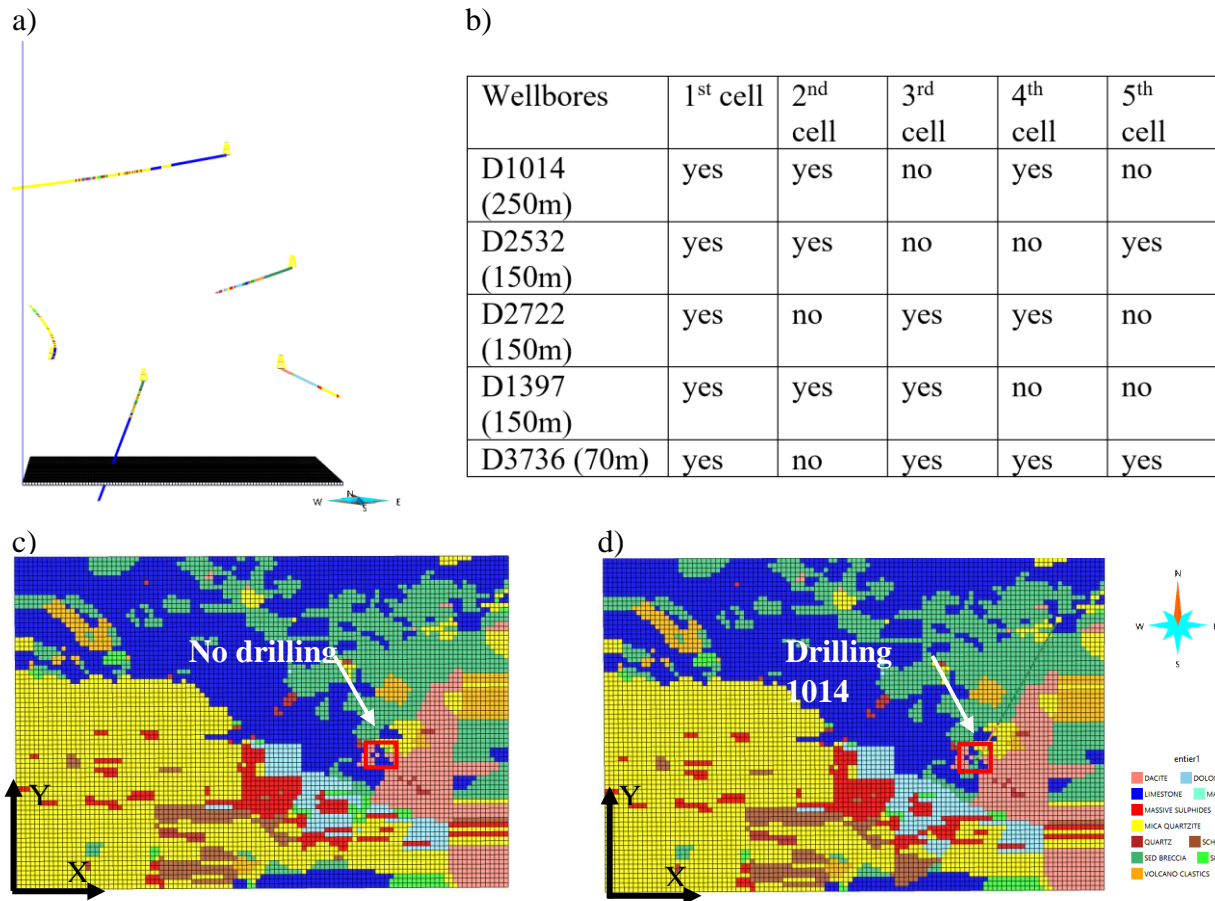


Fig. 3.5 - a) Five wellbores used to estimate uncertainties of the model. The model has been rebuilt five times, removing each of these drillings. b) For each model, five cells on the path of the removed drilling are compared with the model interpolated with all the drillings. “yes” means cells have same lithologies, “no” means they have different lithologies. Cells have been observed at equal intervals along the drilling. In images c) and d), an example of comparison is shown. On the left, plane view of the model interpolated without the drilling 1014 at -1104m. On the right, plane view of the model with the drilling at -1104m. Red squares show different lithologies on the cell at the intersection of the drilling with the level -1104m. In this case, interpolated model with the removed drilling is not able to reproduce real values on the drilling.

3.1.3 Meshed cubes around seismic events

All seismic events from IMS network, which cover the entire orebody, are imported (11 166 events). Sizes of the sources are estimated between 1 and 10 m by Kinscher et al. (2020). Lithologies are extracted in cubes of 10m^3 around each event (Fig. 3.6 and Fig. 3.7). Note that the choice of a cube and not a sphere is due to the possibilities of construction in the software. Each

meshed cube is built with same resolution than the entire model (1m^3), and lithologies from the entire model are upscaled to the cubes. Seismic events from Ineris network are also imported and same method is used to identify in which lithologies they are located. In this case, seismic events are divided into 3 categories defined by Kinscher et al. (2020): seismic repeaters (17 families), seismic multiplets (61 families) and isolated events (138 in total). For repeater and multiplet families, the centroid is imported. By considering these three families, I aim to observe lithologies close to seismic repeaters and observe whether different types of seismicity are associated to different lithologies. This will give precious information to constrain and discuss possible hosting materials and triggering mechanisms. In particular, I want to observe whether repeaters are located within or close to lithologies susceptible to creep, such as phyllosilicates or talc.

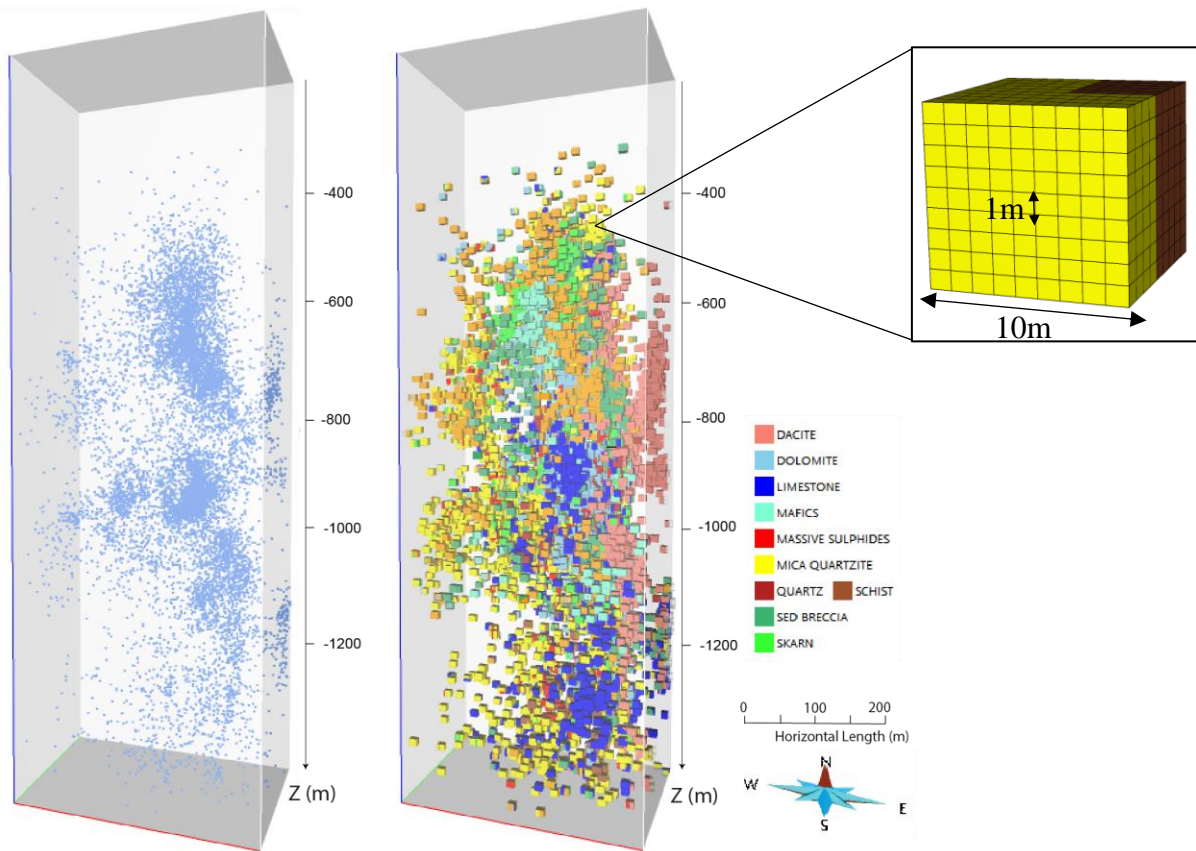


Fig. 3.6. On the left: seismic events imported within the entire model (blue dots). On the right: small meshed cubes (10m^3) around each event and the associated lithologies after upscaling from the entire interpolated model.

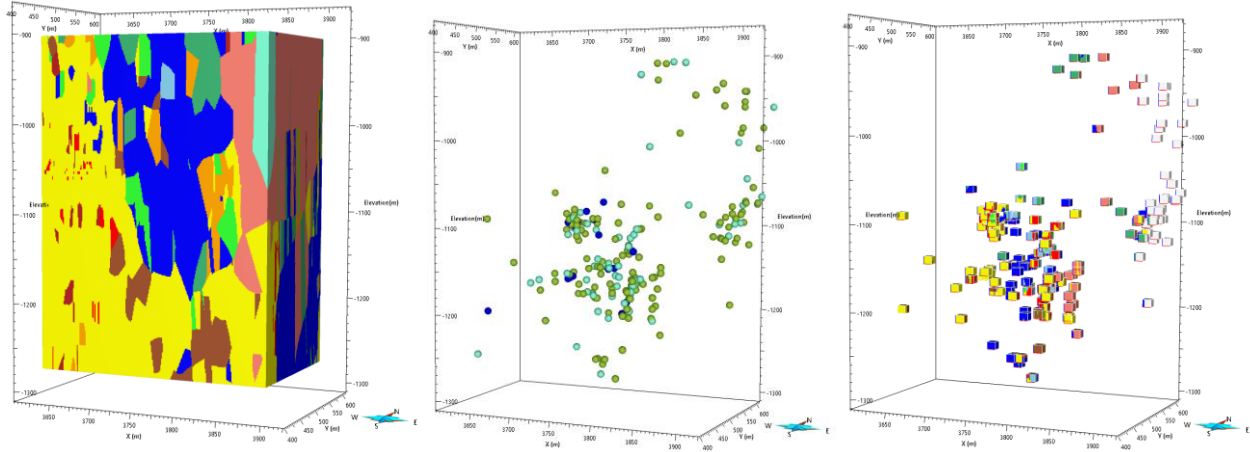


Fig. 3.7. On the left: lithological model in the area covered by Ineris network after interpolation (block 1250 presented in chapter 2). In the middle: imported seismic events from Ineris. Green dots are isolated events, light blue dots are centroids of multiplets families and dark blue dots are centroids of repeater families. On the right: meshed cubes around each seismic event and the upscaled lithologies. Same legend is used than for Fig. 3.6. Blank cubes are no data (outside the model).

3.1.4 Results

Statistical correlation between seismic events and lithologies

Percentages of each lithology in the small meshed cubes are extracted. To avoid biases due to over or under representation of some lithologies in the orebody, percentages of each lithology around seismic events are divided by percentages of this same lithology in the entire area covered by the network, which gives a ratio value. A ratio of 2 indicates that there is twice as much of the lithology around seismic events as compared to the rest of the area. This ratio was calculated for all seismic events of IMS and for the three types of seismic events monitored by Ineris.

Two lithological groups more represented around all seismic events from IMS than in the entire orebody. These groups are Dolomite and Massive sulfides, with ratios of more than 2.5. This means there is 2.5 times more Dolomite and Massive sulfides around seismic events than within the entire orebody (Fig. 3.8). The major advantage of considering a ratio instead of an absolute percentage of lithologies is to observe whether lithologies in small amount in the orebody are correlated with repeaters.

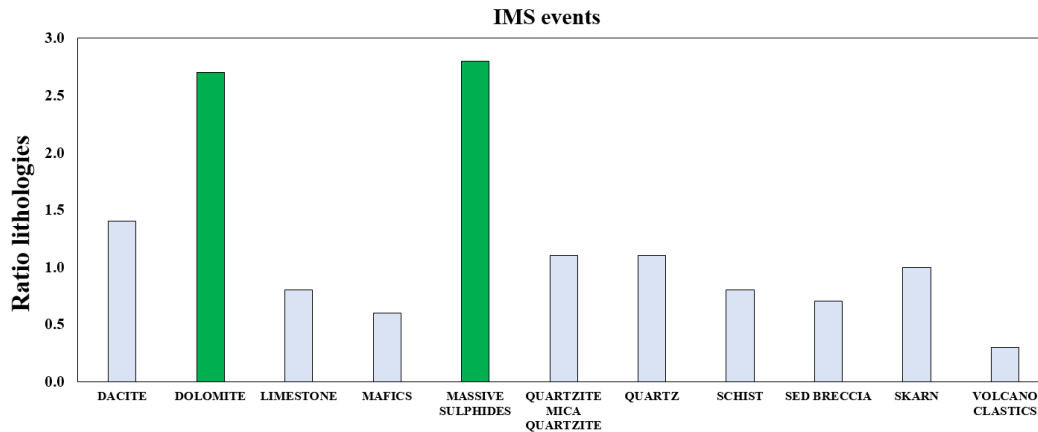


Fig. 3.8. Representativeness of lithologies around IMS events, within the whole orebody. For each lithological group, the ratio represents percentage of this lithology within all the small meshes around IMS seismic events divided by the percentage of the same lithology in the global mesh.

Seismic events of Ineris network have been separated in three different types by Kinscher et al. (2020): seismic repeaters, seismic multiplets and isolated events. Main explanation to explain these differences between types of events is that they are associated to different mechanisms of rupture. By separating these three types in this study, it is possible to observe whether they are located in different lithologies which could explain different triggering mechanisms. Around seismic repeaters, there is a clear overrepresentation of Dolomite compared to other lithological groups (Fig. 3.9). For multiplets families and isolated events, Massive sulfides are more represented around the events.

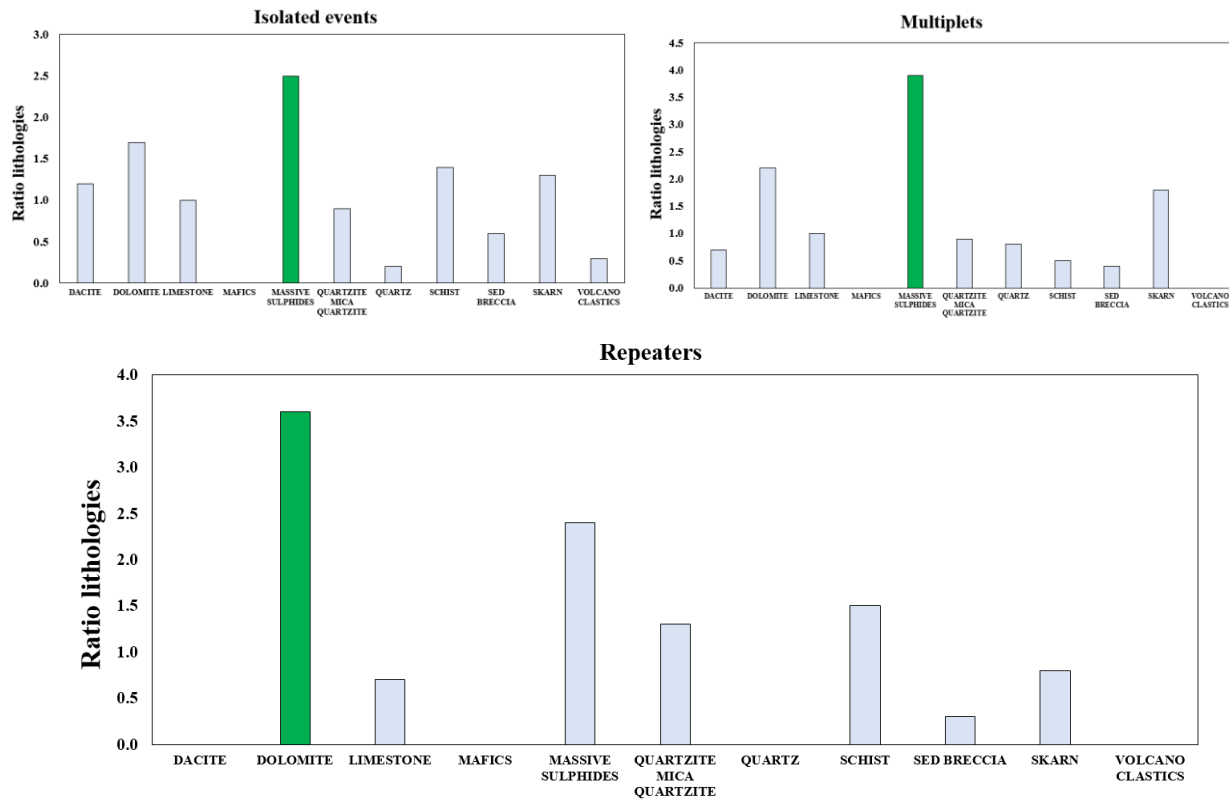


Fig. 3.9. Ratios between percentages of lithologies within meshes around seismic events and percentages of lithologies within the area covered by Ineris network. Calculation has been done separately for isolated events, multiplets and repeaters. The most overrepresented group for each case is shown in green.

Influence of size of the cubes on results

Meshed cubes of 10m^3 were created around seismic events. This choice was made based on the size of the seismic source estimated between 1-10 meters by Kinscher et al. (2020). Here, the influence of the size of the meshed cubes on the results is assessed, with a focus on seismic repeaters. Three different sizes of meshes are tested: $2*2*2\text{m}^3$ and $5*5*5\text{m}^3$ and $20*20*20\text{m}^3$. Results are considered reliable if Dolomite is still overrepresented around repeaters, which is the case for all sizes of the meshed cubes (Fig. 3.10). Therefore, the size of the meshed cubes does not have a strong influence on the results. However, a decrease in the overrepresentation of Dolomite is observed when the size of the meshed cubes increases. This suggests that the reliability is stronger when the meshed cubes are smaller. It is worth noting that the resolution of the meshing can also influence the reliability of the results. In this present case, a very fine resolution of 1m^3 was chosen, so its influence is considered to be minimal.

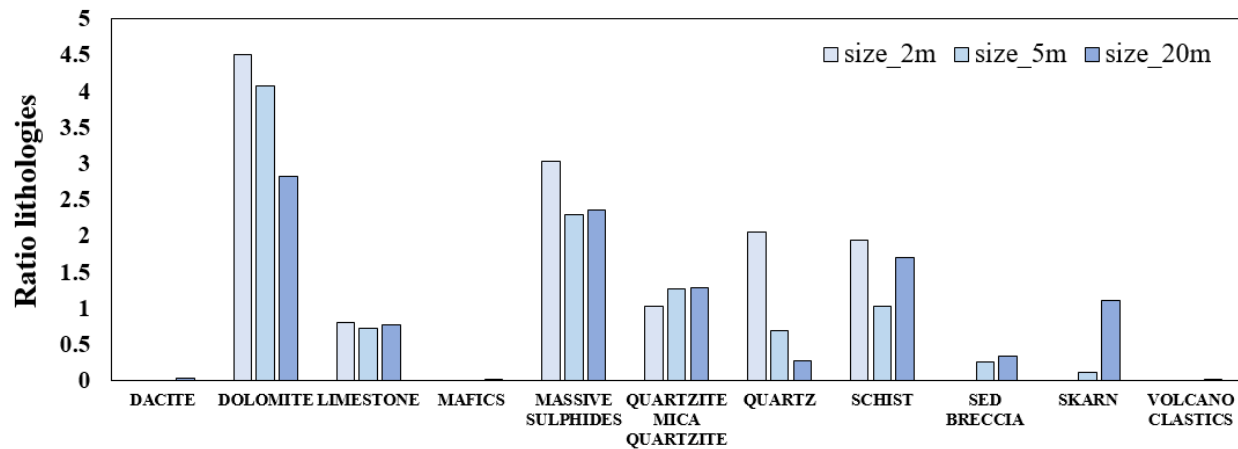


Fig. 3.10. Ratios of each lithology for different sizes of meshed cubes in the case of seismic repeaters (percentages of each lithology within the cubes are divided by percentages of the same lithology within the whole area covered by Ineris). Different colors represent different sizes.

Influence of errors of location of seismic events on results

Locations uncertainties for the seismic network is estimated between 10-20m. In order to evaluate the impact of errors on seismic event locations, the centroids of seismic events were shifted between 5m and 30m from the origin, along three different planes: the XY plane, the XZ plane, and the YZ plane. This resulted in a total of 213 locations, with 71 locations on each plane. The estimation doesn't cover the entire sphere around the centroid, as it is limited to these three planes, but it provides a useful way to visualize the effects of location errors in the X, Y and Z directions (Fig. 3.11). A focus is done on seismic repeaters and results are considered reliable if Dolomite is overrepresented around these events. Results are separated in three cases to assess the impact of location errors on the results: case 1 is when Dolomite is the most represented group in the meshed cubes, case 2 is when Dolomite is not the most represented group but the ratio is greater than 2, case 3 is when Dolomite is not overrepresented. For cases 1 and 2, seismic source location errors have little to no influence on the results, in case 3 they influence the results.

For uncertainties of 5m, Dolomite remains the most represented group around repeaters. For uncertainties of 10m, 85% of the values show an overrepresentation of Dolomite in repeater families. For uncertainties of 20m and 30m, 75% and 60% of the values show an overrepresentation of Dolomite, respectively. Thus, the reliability of the results decreased with increasing location error, from 85% for 10m uncertainties to 60% for 30m uncertainties. Results are considered reliable for errors of 10-20meters, which is the estimate error range of seismic data. However, it is important to note that the impact of errors varies with direction. While locations errors of 10m have little influence along the XZ and YZ planes, they have significant impact along the XY plane when the centroid is shifted towards the south direction (Y negative).

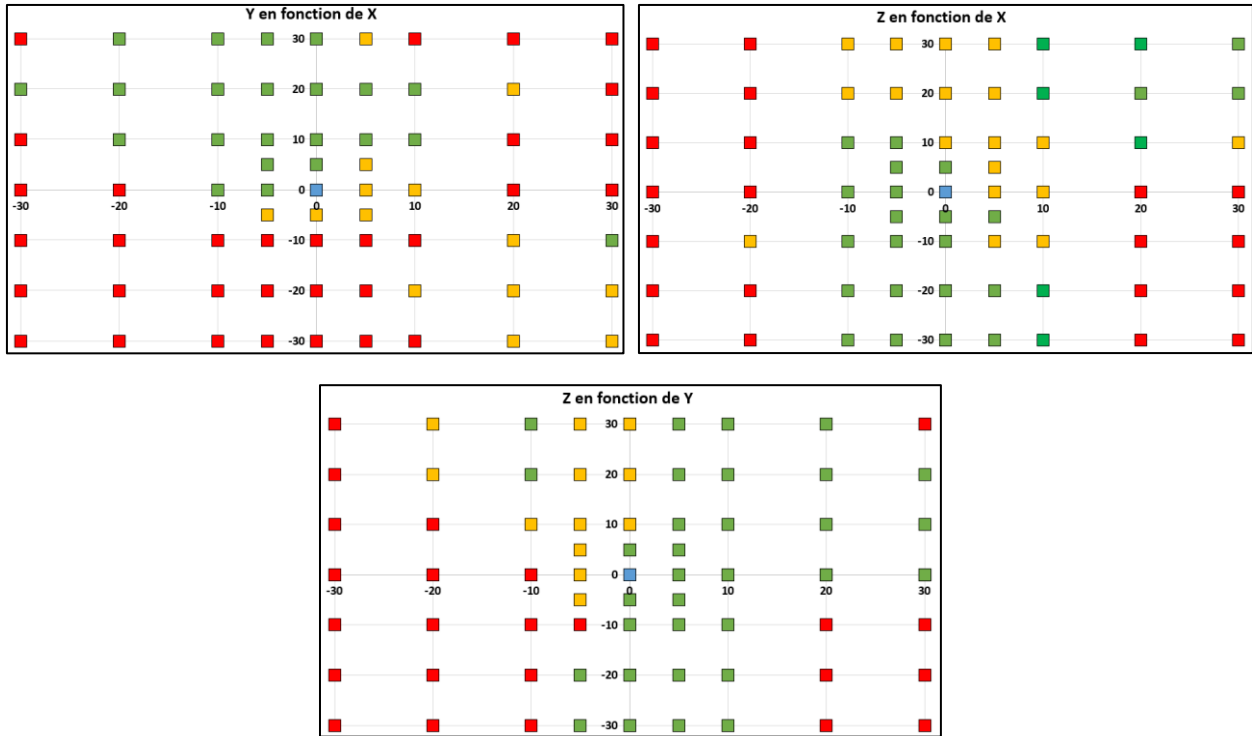


Fig. 3.11. Influence of the error of location of the seismic source on the results. (0, 0, 0) is the seismic source location given by seismologists. The seismic source is moved at 5, 10, 20 and 30 meters from the origin, along to three planes (XY), (YZ) and (XZ). Each point represents one position on the plane. As an example, the point at (-10, 20) of the plane (YX) means that the seismic source was moved at 10 meters to the west and at 20 meters to the north. Green color indicates Dolomite is the most represented group in the sphere of 10m³ at this position, orange indicates that Dolomite is not the most represented group but is at least twice more represented than in the rest of the area. Red means neither of them, which signifies that Dolomite is not overrepresented and that there is significant change in the results if the seismic source is moved at this position.

3.1.5 Seismic repeaters

Dolomite is overrepresented in regions with repeaters, which shows Dolomite must play a role in the occurrence of repeaters. However, this doesn't mean that Dolomite is the only lithology involved in repeaters. Indeed, the ratio calculation was chosen to identify whether lithologies in a small or moderate amount were associated to repeaters. However, it is limited in the case where repeaters are located in lithologies highly represented all over the orebody, as the ratio calculation doesn't highlight the presence of such lithologies around repeaters. To better identify lithologies hosting repeaters, the ratio calculation was completed by absolute observations (Fig. 3.12). Lithologies around repeaters were extracted individually and no ratio was calculated. Results show that seismic repeaters are located in two main lithologies: Dolomite and Quartzites/Micaquartzites.

The whole orebody is mainly composed by Quartzites/Mica Quartzites, especially at the western part (40% of the drill cores, see figure 2), which explains why the presence of Micaquartzites was not highlighted by the ratio calculation.

Families within Dolomite are predominantly located in the eastern part of the area (families 2, 16, 22), with the exception of family 42 located in the western part of the sill-pillar. Repeater families within Micaquartzites belong to the western part of the orebody (families 0, 11, 17, 20, 37, 46, 59, 71). This difference is consistent because Dolomite is mainly found in the eastern part whereas Micaquartzites are mainly found in the western part. Then, seismic repeaters are related to two different lithologies, in function of whether they occur at the eastern part or at the western part of the orebody.

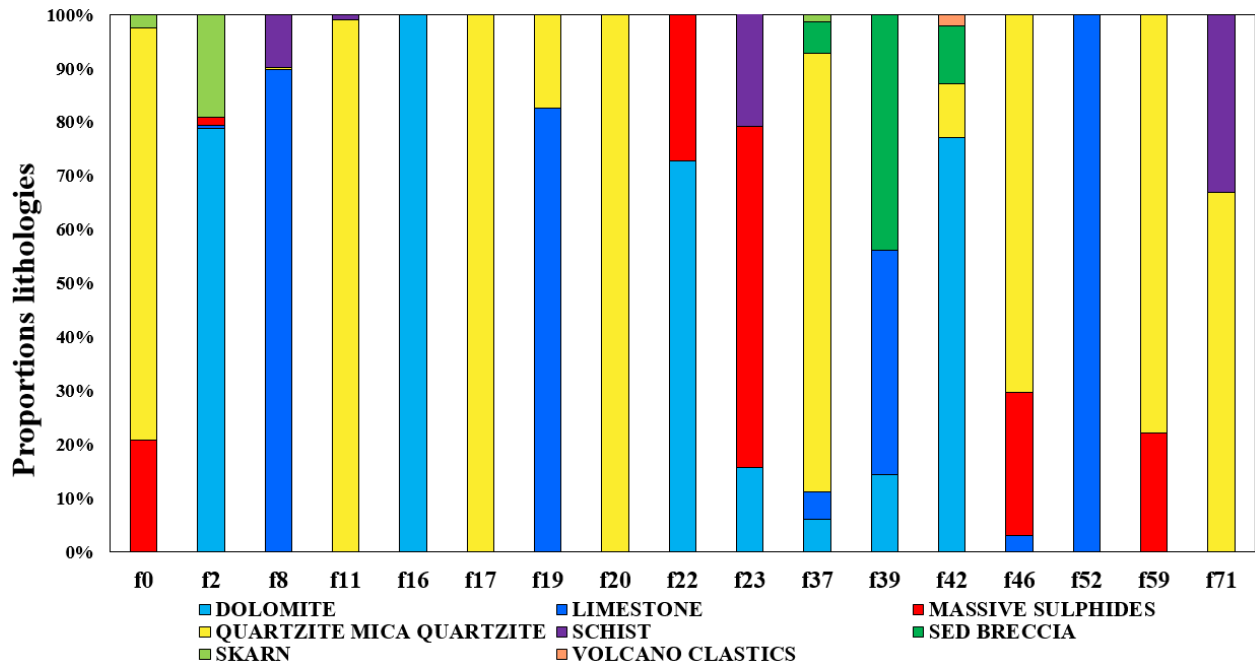


Fig. 3.12. Proportions of lithologies for each of the seventeen seismic repeater family. Each color refer to one lithological group. Most families are in Dolomite or Micaquartzites. Five families are found within limestone and Massive sulfides. They are in close proximity of micaquartzite and/or Dolomite, and location uncertainties of the events can play a role.

The orebody is widely composed by Quartzites and Micaquartzites (more than 45% of the drill cores are Quartzites and Micaquartzites, see Figure 2), whereas repeaters are localized in specific areas. Then, it was needed to explore further whether a mineral, alteration level, texture or structure inside this lithological group could be hosting repeaters. In literature, it has been shown that not all micas show exactly similar characteristics, and that some of them are more likely to creep than other ones (Saffer & Marone, 2003). This is due to different mineralogy (types and amount of minerals, grains arrangement) but also to other processes like cementation, consolidation which can influence frictional properties (Saffer & Marone, 2003). Furthermore, some minerals could be located in thick veins and other ones in narrow veins, which can also influence frictional properties

(Ikari, Niemeijer, et al., 2011). A second set of drill cores data with a distinction of types of micas in the drill cores is used, to explore further whether specific types of micas are involved in the origin of seismic repeaters. By doing so, it is considered that different minerals can be representative of different frictional properties and would provide a clue to the interpretation of the hosting minerals and triggering mechanisms involved in repeaters.

Quartzites and Micaquartzites are divided into seventeen different subgroups as a function of the main mica they contain (Fig. 3.13). Some of them are protolithe with no alteration, such as quartzite and siltstone. Most of them are metavolcanic rocks that have passed through different types of alteration, and contain micas mainly located in moderately foliated sub-vertical planes. When there is no predominant mica, the general term “Micaquartzite” is used. This undifferentiated group represents more than 40% of the drillcores. Phlogopite and sericite Quartzites represent each 10% of the drill cores. Quartzite and siltstone, which are both strong and competent rocks with no mica alteration, represent also both 10% each of the drill cores. Except these five groups which represent more than 80% of the drill cores, biotite and chlorite quartzite are found (strongly altered rocks), as well as sandstone (no mica alteration).

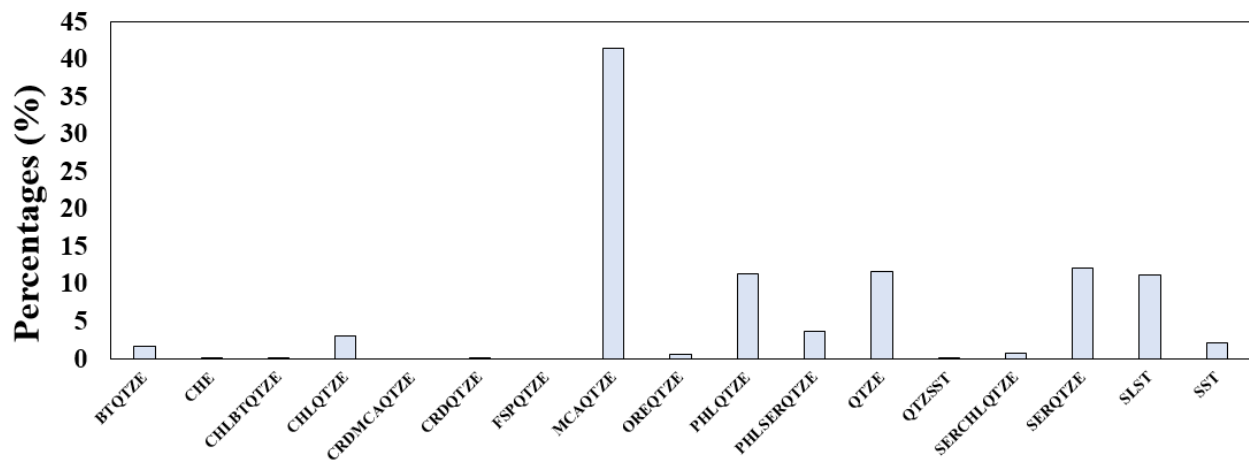


Fig. 3.13. Seventeen types of Micaquartzites within the drill cores below 900m depth (area covered by Ineris network), and their proportions in the drill cores. Lithologies are from left to right: Biotite Quartzite, Cert, Chlorite and Biotite Quartzite, Chlorite Quartzite, Cordierite and Micas Quartzite, Cordierite Quartzite, Feldspath Quartzite, Mica Quartzite, Ore Quartzite, Phlogopite Quartzite, Phlogopite and Sericite Quartzite, Quartzite, Sandstone with quartz, Sericite Chlorite Quartzite, Siltstone, Sandstone.

A lithological geometrical geomodel was rebuilt considering the seventeen subgroups in the drillings. To improve reliability of the models, 2D geological maps were used for interpolation but not for calculation, as the seventeen subgroups are undifferentiated in the maps. Results show that repeaters are located in only four subgroups on the seventeen subgroups: phlogopite quartzite, sericite quartzite, mica quartzite, and siltstone (Fig. 3.14). These are four of the five main subgroups identified in the entire area (Fig. 3.13). Noticeably, Quartzite is not found around repeaters, even though this group is highly present in the drill cores. Calculating ratios between percentages of these four types of lithologies around repeaters and percentages of lithologies in the whole area of

study, the undifferentiated micaquartzite subgroup is the only overrepresented subgroup. Then, repeaters are mostly located in felsic volcanic rocks with mica alteration (Mica-Quartzites), whether it is undifferentiated Micaquartzite group or Phlogopite and Sericite quartzites. However, these groups are widely found in the orebody, which means further studies on alteration degree, texture or structures are needed.

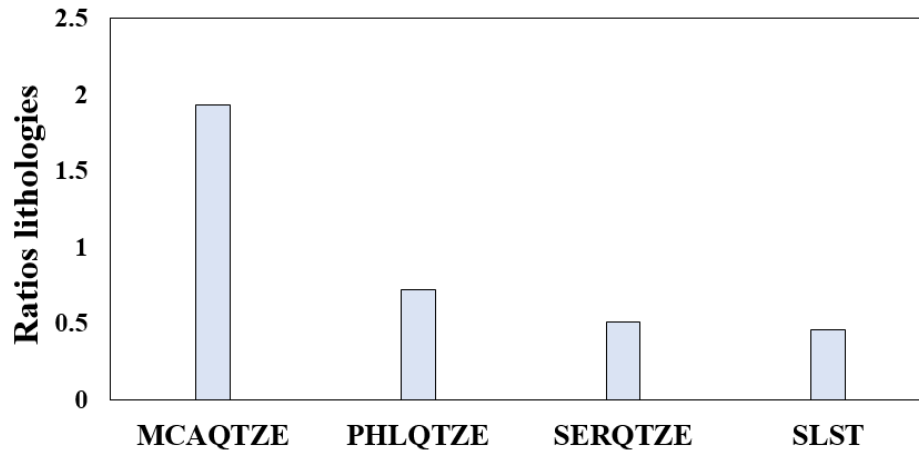


Fig. 3.14. Ratios represent percentages of each subgroup around repeaters divided by percentages of each subgroup in the entire area. Then, a ratio of 2 means that this group is twice as abundant amongst the seventeen subgroups around repeaters as amongst the seventeen subgroups in the entire area. From left to right: undifferentiated Micaquartzite, Phlogopite Quartzite, Sericite Quartzite, and Siltstone.

3.1.6 Hosting materials

Repeaters are mostly located within Dolomite and Micaquartzites, multiplets and isolated events within Massive sulfides. Here, I want to: (i) investigate whether the properties of Dolomite and Micaquartzites are consistent with the occurrence of repeaters, (ii) explore whether Massive sulfides present different properties explaining why they host different seismic events, and (iii) compare these three groups with all other groups to investigate required properties to host seismic repeaters. I investigate types of structures, secondary minerals, RMR values and Young modulus of the groups. I focus in particular on phyllosilicates minerals and fractures, as repeaters are commonly associated to creeping phyllosilicates materials loading brittle frictional asperities (Nadeau et al., 1995).

Statistics calculations were done based on drill cores data. Dolomite and Micaquartzites contain both fractures and phyllosilicate minerals as second minerals. Dolomite host mostly talc, Micaquartzites host mostly sericite and phlogopite types of micas (Table 3.1). Dolomite is moderately stiff and is qualified as good rock quality (van Koppen, 2008). Micaquartzite is more heterogeneous and considered as a fair rock. Between 3-5% of the drill cores are fractured for these two groups, which is moderate compared to the other groups (Fig. 3.16). Massive sulfide has different properties from the previous two groups. It contains almost no fracture nor phyllosilicate

minerals, even if some amount of talc can be found in semi-Massive sulfides. It is a very stiff rock (70-90GPa) with quartz as its main second mineral, and it is classified as good to very good rocks. Then, Dolomite and Micaquartzites are consistent with what is expected in presence of repeaters, as they contain both phyllosilicates and fractures. Phyllosilicates are able to creep and slip can occur on fractures. At the contrary, Massive sulfides are less likely to host these repeaters, as they are very stiff rocks with almost no fracture nor phyllosilicates.

Amongst other groups, Dacite contains lots of fractures, with almost 20% of drill cores which are fractured (Fig. 3.16), but has a very low amount of phyllosilicates (they are found in less than 5% of the drill cores, see Fig. 3.15). On the other hand, limestone and mafic rocks are protolithe rocks which contain lots of phyllosilicates (more than 25% of the drill cores contain them) but almost no fracture. Phyllosilicates are interpreted as primary minerals distributed in large regions of the rocks, which differs from mica alteration in felsic metavolcanic which come from fluid infiltration in fractures and are then expected to be more localized. Schist rocks also contain significant amount of fractures and phyllosilicates, but their RMR and Young modulus are very low (Young modulus around 20GPa). Schists show high anisotropy with large vertical bedding foliation planes filled with flat, sheet like phyllosilicates.

Based on these observations, three characteristics observed in lithologies that host repeaters are identified:

- 1) Rocks of good consistency (i.e., good RMR/UCS/Young modulus).
- 2) A moderate amount of fractures.
- 3) The presence of talc or other phyllosilicates.

	Fractured drill cores	Drill cores with talc or phyllosilicates	Main “second” mineral	Young Modulus	RMR
Dolomite	3%	17%	Talc	57GPa	60-80 : Good rock
Micaquartzites	5%	20%	Sericite and phlogopite	45-65GPa	30-60: Fair rock
Semi-Massive and Massive sulfides	1%	7%	Quartz	87GPa	50-90: Good rock to very good rock

Table 3.1. Properties of the three groups more represented around seismic events. Fractures and mineral information result from analyses realized from drill cores data given by mine geologists. Young modulus and RMR information can be found in De Santis et al. (2020) and van Koppen (2008). Young modulus of Dolomite and Massive sulfides are mean values.

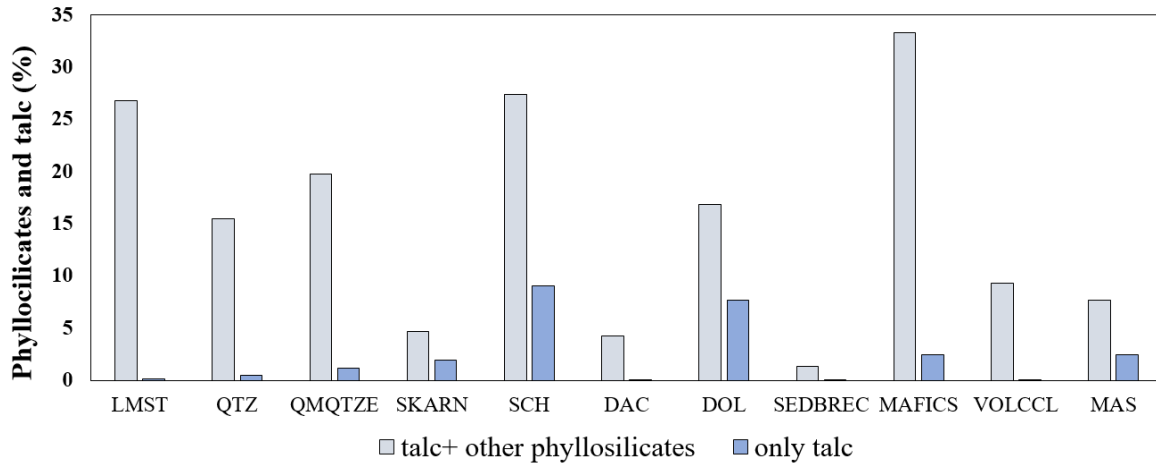


Fig. 3.15. Mineral data from drill cores calculated from drill cores data of mine geologists. Percentages of phyllosilicates (talc + other phyllosilicates) and talc alone are shown for each lithology. This percentage represents the length of drill cores in the lithology which contains talc or phyllosilicates as a second mineral, on the total length of drill cores in the same lithology. From left to right: Limestone, Quartz veins, Quartzite/Micaquartzite, Skarn, Schists, Dacite, Dolomite, Sedimentary breccia, Mafics, Volcanoclastic sediments, Massive Sulfides.

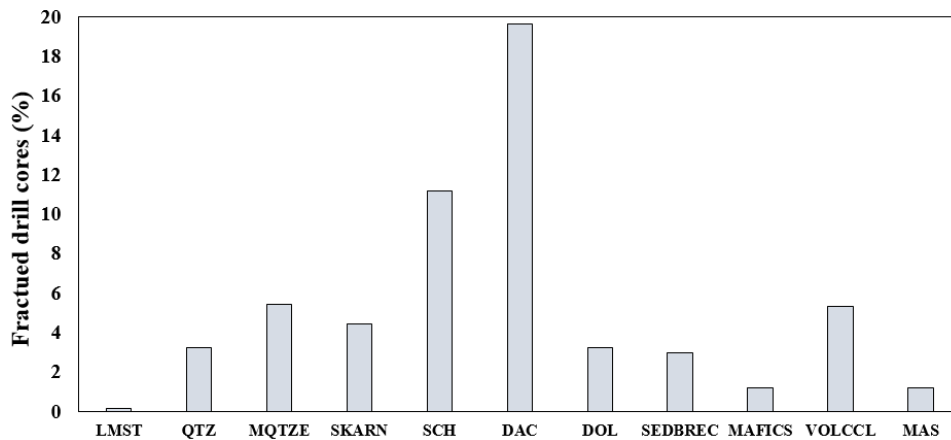


Fig. 3.16. Percentages of fractured drill cores on the total length of drill cores within each lithology. They are calculated from drill cores data of mine geologists. Note that qualifying rocks as little, moderately and highly fractured is relative. Dacite is considered as highly fractured and limestone as no fractured.

While it was shown that the seismic repeaters are associated with moderately fractured rock masses containing talc (as well as other phyllosilicates), the statistical analyses give no information on the form in which these minerals are present. More specifically, there is no evidence that the repeaters are associated with talc-filled faults as suggested by seismological models (Uchida & Bürgmann, 2019). To investigate the presence of such talc-filled faults, I examined three available drillings that contained both talc and Dolomite in the orebody. I observed the form in which talc is present in the rockmass, and especially if talc-filled fractures could be found. Two different cases were observed: talc minerals are either part of the rockmass (Fig. 3.17a), or are present as infilling within fractures (Fig. 3.17b and c). The infilling in talc-filled fractures can be very thin (<1mm) and up to 5mm. The proof of the existence of talc-filled fractures is highly noticeable, as they are perfectly

consistent with the model of repeaters known in seismology, where repeaters are repetitive ruptures of asperities loaded by a creeping material on a fault plane. Then, these observations give more confidence to the statistical correlations presented in this chapter. They allow to give a possible triggering mechanism for seismic repeaters, which is the presence of phyllosilicates-filled fractures in the orebody. However, it was not possible to check whether such fractures are found in repeater areas, since no drilling is available in these regions. Another option is also that creep (assuming it exists) would be related to talc minerals inside the matrix such as shown in Fig. 3.17a.



Fig. 3.17. Three photos of talc mineral within Dolomite in the drill cores. On the left, an example of talc minerals within rock matrix. Middle and right photos show talc-filled fractures. Middle one shows a very thin infilling whereas the right figure show an infilling of several millimeters.

3.1.7 Conclusions

From this large-scale study (i.e. at the scale of the orebody), several observations are made:

- Most of repeaters are found within two lithological groups. The eastern cluster is located with Dolomite, and the western cluster within Quartzites/Micaquartzites.
- Isolated events are mainly found in Massive Sulfides.
- Dolomite and Micaquartzites are moderately fractured good quality rocks containing talc or phyllosilicates. Talc is either under the form of mineral incrustation or infilling material in fractures. Massive sulfides are stiff rocks with almost no fracture and only little phyllosilicates.
- Repeaters in Quartzites/Micaquartzites group are mainly found in undifferentiated micas quartzites, as well as within phlogopite quartzites, sericite quartzites, and siltstones which are widely found in the entire orebody.

Lithologies differ from repeaters and other events, which suggests these events are related to different hosting materials and then different triggering mechanisms. A possible triggering mechanisms for repeaters, consistent with seismological models and lithological observations, is that repeaters occur on brittle frictional asperities loaded by a continuous and slow slip on talc or phyllosilicate infilling. This was sustained by the proof that such filled fractures exist in the orebody. However, other hosting materials are also possible regarding lithological observations,

such as creep due to talc minerals inside rock matrix or creep in weak rock types close to stiff rocks (Schists close to Massive Sulfides). Then, although this study at large scale gives valuable information on materials hosting repeaters and give elements to discuss possible triggering mechanisms, the conclusions are limited. In particular, lithologies alone are insufficient to explain the seismic triggering mechanisms and no data close to seismic repeaters is available to observe in more details the hosting materials. In next section, the influence of external factors on triggering mechanism is studied; i.e. stresses changes induced by the excavation, at the scale of the panel of excavation 1250.

3.2 Do stresses changes explain mine seismicity?

Both intrinsic properties of hosting materials and external factors such as initial and stresses changes play a major role in inducing seismicity (Sainsbury & Kurucuk, 2020). Common model in seismology is that repeaters are located on brittle frictional asperities loaded by the creep of phyllosilicate-filled fractures. I showed that such model is consistent with lithological observations at the scale of the orebody, although it was not possible to prove the existence of such fractures at the location of the repeaters since no drillings crossed these areas. In addition to internal properties of rockmass, seismicity in mining is commonly attributed as a result of stress changes in the rockmass close to mining excavations (S. Gibowicz, 2009). Assuming repeaters are located on fault planes, I investigated whether stress changes induced by the excavation alone can induce slip on such fault planes, or whether an additional mechanism (such as creep) must be involved.

3.2.1 Method

To do so, the large-scale elastoplastic model developed by De Santis et al. (2020) was used, which simulates the excavation of 52 steps of excavation in the bloc 1250. This model was presented in chapter 2. For each of the 52 excavation steps, the stress tensors were extracted from the model at the seismic centroids of the 17 repeater families. Repeaters are considered located on fault planes oriented like the nodal planes determined by Kinscher et al. (2020), and the stress vectors acting on these planes were calculated. Finally, the stress vectors were projected to the planes, which gives both shear and normal stresses. Stresses paths are represented in Mohr plane, for each family of repeaters; the display how normal and shear stress changes with time. The Coulomb criterion is used: $\tau = \mu * \sigma_n$, with zero cohesion. A friction angle of 20° ($\mu = 0.36$) is considered, which corresponds to a high value in the range of coefficients of friction observed for phyllosilicates (Ikari et al., 2009). Note that fault planes are not included in the model of De Santis et al. (2020) and values of stresses do not take into account the eventual influence of these fault planes on the local stress field.

3.2.2 Results

Stress paths remain below the rupture criteria for most of the families (Fig. 3.18). Fig. 3.18a shows the example of family 0, where no difference is observed during excavation steps where seismicity was activated. For families close to strain cells used to calibrate the model, stress paths can reach the criteria of rupture. This is the case for the family 11 (Fig. 3.18b), where stress paths are above the considered Coulomb criteria for all steps of excavation after step 11. When seismicity is observed, i.e. during steps 34 and 37, stress path is above the criteria. However, stress path is also above the criteria for all steps after step 11, and none of the other steps induced seismicity, which shows limits on such model to explain the temporality of seismicity. Especially, seismic events didn't occur for step 11, which significantly moved the fault closer to criteria, as shown in figure 3.18, neither on step 41 which also induced a noticeable change of stresses.

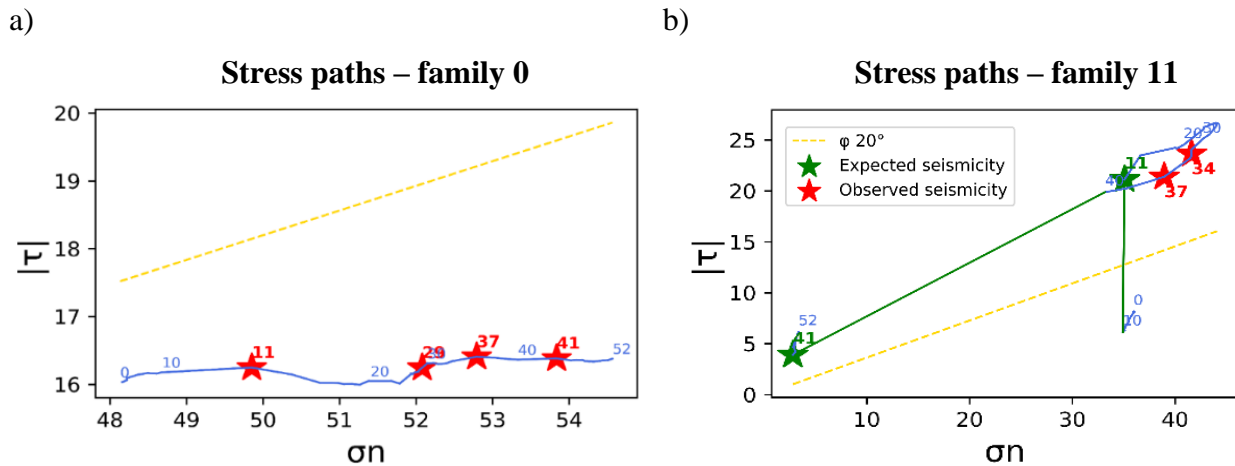


Fig. 3.18. Path stresses for the family 0 (on the left) and the family 11 (on the right). Conventions are chosen positive compressions. Numbers indicate the steps of excavation, red stars the steps where seismicity is observed. Yellow line is the criterion of rupture considering a phyllosilicate infilling. In green: expected seismicity due to stress paths getting closer to criterion of rupture. Values need to be read carefully, as fault planes are not considered into the model of excavation and stress paths can then reach values above the criteria of rupture, which is physically impossible.

As a first conclusion, a 3D large-scale excavation doesn't seem to be sufficiently precise to observe a local mechanism far from the cells used to calibrate the model. A second conclusion is that, for a family at less than 5 m away from a cell used to calibrate the model, stresses changes induced by the excavation from the elastoplastic model are able to activate slip on the plane. However, there is no explanation why seismicity occurs at steps 34 and 37, and not during other steps sometimes more expected to induce seismicity. This can be explained by the presence of creep, either on the fault plane (due to creeping mineral infilling) or within the rockmass.

3.3 Conclusion

In this chapter, I investigated the origin of repeaters, and more specifically the hosting materials and triggering mechanisms, considering both lithological types and stress changes induced by mining. I focused on data available from the mine and I studied factors at the scale of the orebody and a panel of excavation (block 1250). I showed that seismic repeaters and isolated events are related to different lithologies, and that properties of the lithological groups are consistent with the existence of different mechanisms. In particular, isolated events display a higher correlation with fractures in Massive sulfides, whereas repeaters are likely to be related to fractures and creeping materials within Micaquartzites or Dolomite. A possible model is the presence of phyllosilicate filled fractures with brittle frictional asperities, which is consistent with the presence of talc-filled fractures observed elsewhere in the orebody. In this model, seismic repeaters are due to repeater ruptures of brittle friction asperities loaded by creep on phyllosilicate material. However, this study also shows that studying the origin of repeaters at large scale is limited. Especially, no drilling crossed any repeater family, and it is unknown if such talc-filled fractures are found in repeater areas. Furthermore, western repeaters are located in Micaquartzites (and more specifically in sericite, phlogopite and undifferentiated micas), which is the most common lithological group found in the area. This shows that only considering lithologies is insufficient to clearly identify the origin of repeaters and that other elements such as discontinuities must be considered. Furthermore, considering stress changes induced by mining, it was shown that seismic events can occur on fault planes oriented like the nodal planes of repeater families. However, a large-scale elastoplastic model is not adapted to reproduce local stress changes for fault planes far from data used to calibrate the model. In addition, the model can't explain the temporality of the seismic events, i.e. that seismic events are not observed for changes of stresses which significantly moved the fault planes closer to criteria of rupture.

To study further the nature of the hosting materials and triggering mechanisms, a very local network was installed at vicinity of a singular repeater family. In next chapter, the installation and what can be learnt from a local network at the scale of a peculiar repeater family is described, in addition to this large-scale study.

Chapter 4

Geological and geomechanical behavior of a repeater source zone

In previous chapter, it was shown that repeaters are mostly observed in Micaquartzites (silicified felsic metavolcanites) on the western part of the orebody and in Dolomite on the eastern part of the orebody. However, these two lithologies are largely represented elsewhere in the mine and they can't alone explain the origin of repeaters. Other elements such as discontinuities or regions with specific geomechanical properties must host repeaters inside these two lithological groups. As the study at large scale doesn't allow to get more information on the origin of seismic repeaters, their origin is then explored at local scale, i.e., at the scale of a singular family of repeaters (source size estimated between 1 and 10meters).

In the framework of this thesis, we had the opportunity to drill and install strain cells close to the repeater family 37 identified by Kinscher et al. (2020) within the sill-pillar of the block 1250, at 1 km depth. The choice of this target repeater family amongst the 17 families monitored by Kinscher et al. (2020) has been motivated by two reasons: (i) seismicity migrated through the sill-pillar after the excavation of a highly stressed stope in the underlying excavation panel (stope 13, see chapter 2) and (ii) this family was accessible from mine drifts. This installation aims to try to reach the structure(s) and/or material hosting and loading repeaters. From seismological models and insitu observations described in chapter 1, more specific questions can be raised, such as: (i) can we find in the drill cores phyllosilicates filled fractures, as commonly observed in creeping regions at the scale of boundary plates? (ii) Can we observe a brittle frictional fracture oriented like the seismic nodal plane, with kinematic markers indicating a slip orientation similar to seismic rake, which could be the seismic asperity?

I focus on characteristics susceptible to constrain what hosts and loads seismic repeaters: lithologies, density of fractures, orientation of fractures, mineralogy, markers of movement, state of stresses (see chapter 1). In particular, I want to check whether a family of fracture has similar orientation than the nodal plane (unknown by mine geologists); whether minerals commonly associated with repeaters (phyllosilicates) are found in filled fractures, whether kinematic markers indicates slip direction similar to seismic rake.

4.1 Local monitoring device

The design of the local installation was done in collaboration with Ineris and Boliden, with the objective to optimize chances of reaching the structure(s) hosting and/or loading the repeaters. The main points to both optimize chances of reaching the target family and take into account the accessibility constraints are the following:

- Drillings must start from accessible areas in the mine.
- Inclinations, lengths and diameters of the drillings must respect machine limitations.
- Different orientations and inclinations for the drillings are needed to reduce instrumentation biases and to allow the crossing of fractures with all orientations.
- Drillings should be spaced to take into account possible error of locations of seismic events.

The installation is presented in Fig. 4.1. It was set up at the end of November 2021. Three permanent CSIRO Hollow Inclusion (HI12) strain cells were installed at the bottom of 10-meters long boreholes BH1, BH3 and BH4. Each cell measures strains every minute with an accuracy about ± 5 micro-strains ($\mu\epsilon$). Two additional boreholes (DI and DH, respectively 30 and 35 meters long) were drilled to get lithological and structural information. One is sub-horizontal (inclination of 15°), and the other one has an inclination of 35° . In addition, an optic fiber (BOTDR) was installed during two weeks in January 2022, as part of a preliminary installation of a larger project conducted by Ineris and IPGP (Institut de Physique du Globe de Paris).

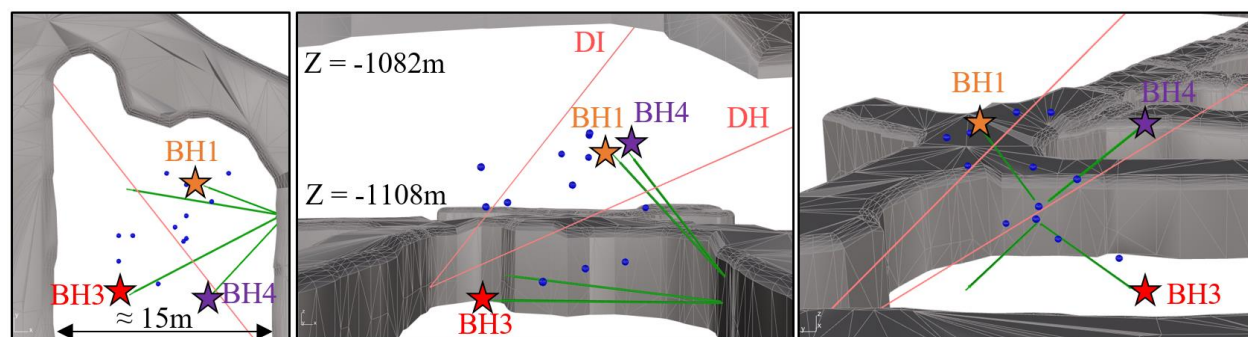


Fig. 4.1 - Local monitoring network installed in the sill pillar. From left to right: plane view, front view and side view. Excavated drifts are in grey. Blue dots represent the repeaters active between October 2020 and November 2021, from the repeater family 37. BH1, BH3 and BH4 refer to the 3 installed CSIRO cells (colored stars) and the associated drillings (in green). In red: additional drillings DH (subhorizontal drilling) and DI (inclined drilling).

CSIRO cells were installed inside a small hole, at the bottom of a borehole of larger diameter (Fig. 4.2). Each cell includes 12 strain gauges with different orientations, providing the complete strain tensor at the location of the cell. For further calculation, parameters of the cells are determined in the field: length of the drillings is determined by laser sensor, orientation with a compass and inclination of the CSIRO cells with an inclinometer. Note that another CSIRO cell (BH2) was also

installed but is not presented here as the cell was not correctly installed. The dysfunction of the cell has been identified first due to very noisy signals and secondly looking at videos from endoscopes inside the drilling, which show the cell is not correctly glued in the small hole.

An event of the repeater family was detected by the cell BH4 (strain of around $6\mu\epsilon$ for an event of M -1). This confirms we are sufficiently close from the seismic asperity to be detected by at least one cell and that the repeater family is still active, even after having drilled in the area.

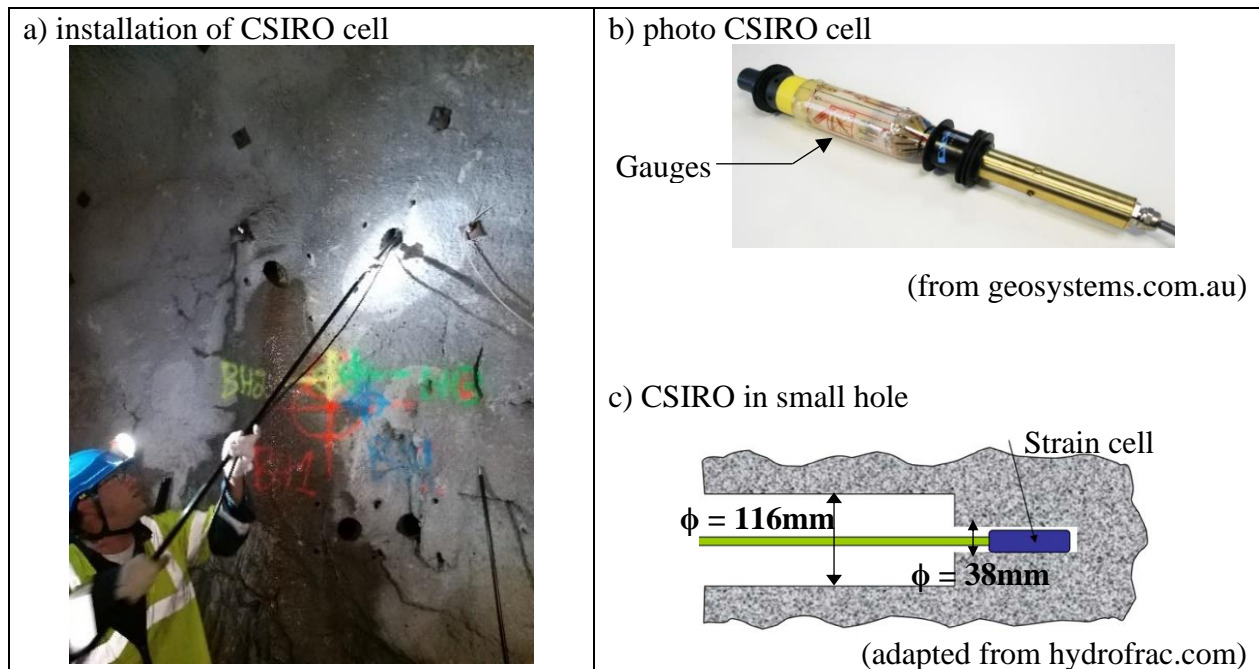


Fig. 4.2 - CSIRO cell and method of installation in the mine: a) shows the installation in the mine b) shows a photo of CSIRO cell with its 12 strain gauges and c) shows a strain cell glued in a smaller pilot hole at the bottom of the drilling.

4.2 What are we looking for?

4.2.1 Seismic source mechanism

The source mechanism of family 37 is given by Kinscher et al. (2020). Source mechanism gives two possible plane orientations and Kinscher et al. (2020) chose the nodal plane based on the alignment of seismic events. Stress drops are estimated between 1 and 10 MPa, and magnitudes are $M_w < 1$ on moment scale magnitude. As for all families in the mine, source mechanism indicates a strike-slip faulting mechanism, with a reverse component. The size of the seismic asperity is estimated between 1 and 10 meters. The nodal plane is a sub-vertical fault plane (dip = 75°), slightly inclined from Y-axis (Strike = 190°). Source mechanism is a strike slip with a reverse component (rake = 130) (Table 4.1). The auxiliary nodal plane is also indicated. These information

will be compared to the insitu observations, to discuss and constrain better the geological origin of repeaters. The source mechanism of family 37 is similar to the 17 other repeater families in the mine.

Strike	Dip	Rake	<i>Strike2</i>	<i>Dip2</i>	<i>Rake2</i>	Source mechanism	Mw average	Slip maximum
190°	75°	130°	297°	42°	22°	Strike-slip with reverse component	-0.3	1mm

Table 4.1 - Characteristics of the nodal plane associated with the targeted family, and the auxiliary nodal plane (*in italic*). Strike is defined clockwise from Y-axis of the mine and follows the right-hand rule. The rake corresponds to the slip direction on the fault plane, defined with Aki Richards convention. Mw-average is the average moment magnitude of the events and slip-average is the maximum amount of seismic slip during one seismic event.

Hypotheses to find seismic source mechanism must be kept in mind, as geological and geomechanical observations are compared with the expected nodal plane given by geophysical analyses. First, inversion method (i.e. the method which allows to come back to the source from displacement of the medium) assumes a point source model, and a far field displacement, and we are at the limit of these two hypotheses. In the framework of these two hypotheses, the displacement in the medium was expressed as a convolution product between the Green tensor (which describes the propagation of the signal) and the moment tensor (which describes the source). To determine the Green function, the medium was considered as a layered media and the homogeneous velocity model of De Santis (2019) was used. Last but not least, the moment tensor of the source was determined with the assumption of a Double Couple mechanism. The latter was object of discussions, as a tensile mechanism would be more expected for seismic families in the panel of excavation as they are almost parallel to drifts (see chapter 1). However, three main arguments are in favor of a DC mechanism: (i) seismic waves are mainly shear waves (S-waves), (ii) same source mechanisms were also found in the non-excavated sill pillar, (iii) the nodal plane calculated from the DC hypothesis is consistent with the alignment of seismic events determined independently of DC hypothesis. Then, the presence of shearing discontinuities almost parallel to drifts is the plausible to explain the monitored seismicity.

4.2.2 How would look like an asperity and creeping regions in cores?

It was shown in chapter 1 that the definition of an asperity strongly differs from scale and field of study. In particular, geometrical and rheological definitions of asperities, which refers to bumps or corrugations, were distinguished from seismological definition, which refer to the source location of seismic events. In this chapter, I use the term “seismic asperity” to refer to the target source location of seismic repeaters from family 37, and the term “geological asperity” to refer to a bump

or other geometrical irregularity which can be observed in the cores. The size of the seismic asperity is estimated between 1-10m from geophysical analyses.

In field, this seismic asperity can be (i) a large bump of 1-10m of radius or (ii) several centrimetric bumps close to each other in a radius of 1-10m. Then in the drill cores, the target asperity can be seen as: (i) centrimetric bumps observed in fractures with thin infilling, or (ii) an unfilled fracture (or a fracture filled with a non-ductile material). The latter is explained by the fact that the diameter of the drillings ($\phi 1 = 116\text{mm}$ or $\phi 2 = 38\text{mm}$) is smaller than the diameter of a 1-10m bump ($\phi = 1-10\text{m}$). Then, a bore hole drilled through a bump with a radius 1-10m is expected to appear as an unfilled fracture, probably with kinematic markers as a testimony that movement occurred.

a) A “small bump” on a filled fracture



b) An unfilled fracture (large bump) with stries



Fig. 4.3 - On the left: a centrimetric “bump” on a filled fracture. On the right: an unfilled fracture with kinematic markers.

For creeping regions, it is expected to find fractures filled with a weak mineral such as talc or other phyllosilicates, commonly associated in literature with creep. Other options can be patches of a weak lithology or contact between different lithologies.

4.3 Lithologies and fractures density

Drill cores, with a total length of about 100 meters and with different orientations, provide a representative view of the study area. The area is located within non-altered and mica-altered silicified metavolcanites (i.e., Micaquartzites with the mine nomenclature used in chapter 3), at the boundary with the hosting rock, i.e. Limestone (marble) and Breccia. More precisely, mica minerals within mica-altered silicified metavolcanites (Micaquartzites) are phlogopite and sericite (Fig. 4.4).

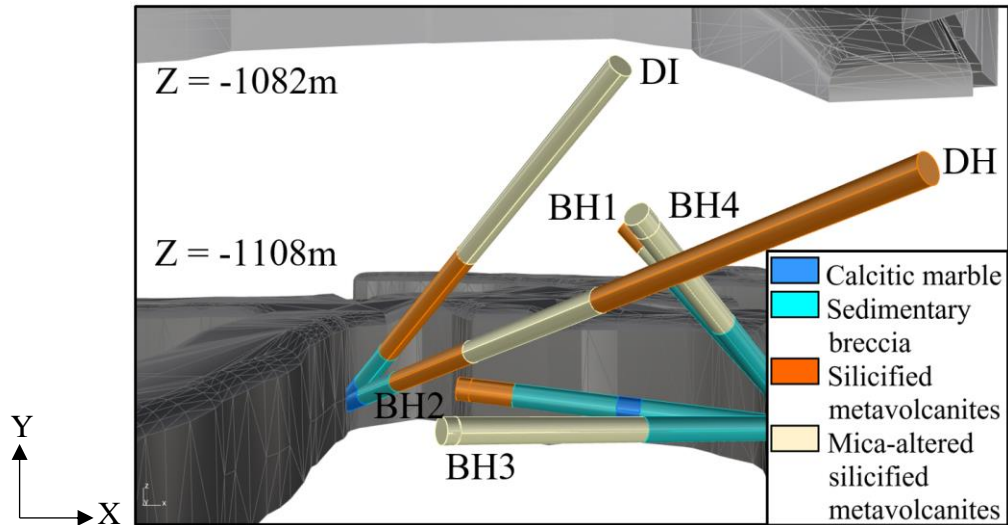


Fig. 4.4 - Lithologies within the boreholes in the sill pillar. Grey drifts are top and bottom levels of the sill pillar. North of the mine is the Y-axis.

First, these lithologies are similar to what was expected from the geometrical lithological model presented in chapter 3. Indeed, the lithological model around the family predicted: 85% of silicified metavolcanites (both non-altered and altered rocks), 10% of sedimentary breccia, 5% of Dolomite and 2% of calcitic marble. This is highly coherent with what is observed (71% of silicified metavolcanites, 19% sedimentary breccia, 10% limestone).

No lithological groups other than what was predicted by the geological model is observed, such as the presence of a specific rock type (intrusion of Dolomite for example) which would have been missed by the large-scale study. This confirms lithologies associated with repeaters in this area of the mine are Mica-quartzites, which are highly represented in the mine. This confirms that lithologies alone can't explain the presence of repeaters and that other elements have to be considered, such as discontinuities.

In geological maps, there is a contact zone between Limestone and Micaquartzites in the map oriented like the seismic nodal plane (red square in Fig. 4.5a). This raises the question on whether such contacts between different rock types may be the seismogenic areas. However, there is no fracture in contact zones between different types of lithologies in the drill cores which can sustain this hypothesis (Fig. 4.5b). The transition is continuous between lithologies and no marker indicates that any movement occurred (such as an offset between veins crossing both lithologies).

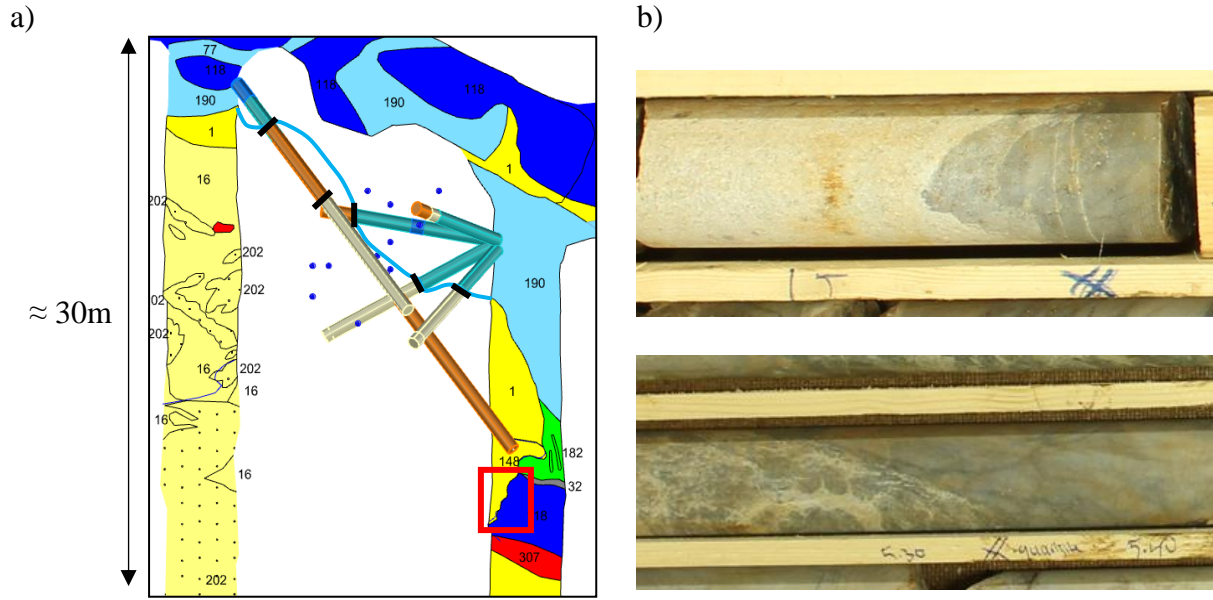


Fig. 4.5 - Contacts between different lithological groups. On the left: a plane view of the installation with a 2D geological map of the lower level of the sill pillar ($Z = -1108\text{m}$). The red square indicates a contact between Micaquartzites and Dolomite with an azimuth similar to the seismic nodal. Yellow surfaces indicate Micaquartzites (different numbers refer to different types), light and dark blue refer to sedimentary breccia and marble. Red and green are Massive sulfides and skarn. On the right: two examples of contact on the drill cores. Top figure is a contact between marble and silicified metavolcanic rocks; bottom one is a contact between breccia and silicified metavolcanic rocks. None of the contacts in the drill cores shows any fracture or marker of movement, and then there is no indication that lithological contacts might be hosting repeaters.

In seismological models, repeaters are assumed to be hosted by pre-existing faults, loaded by the surrounding creep. In addition to lithologies, the linear density of natural faults was measured in order to assess the level of fracturing in the region and to identify areas of greatest fracturing. To distinguish between induced and natural fractures, both the filling and the geometry of the fracturing were observed. If fractures are ragged, contain no fill and are almost perpendicular to the borehole, they are considered to be drilling-induced. On the contrary, if the fractures contain fracture cement (minerals that have been precipitated), are vein-like and/or contain lineation on the fracture faces, they are considered natural faults (Kulander et al., 1990).

Linear density shows that the area is slightly fractured, with values between 1 and 10 fractures per meter (Fig. 4.6a). However, two zones of higher fracturing (linear density > 10 per meter) are found. Fracture zone Z1 is the most fractured area and is made of unfilled fractures with marker of movements (Fig. 4.6b). Z2 fracture zone contain several fractures with similar orientation and filled with thin white material ($< 1\text{mm}$) which will be further identified with DRX analyses (Fig. 4.6c).

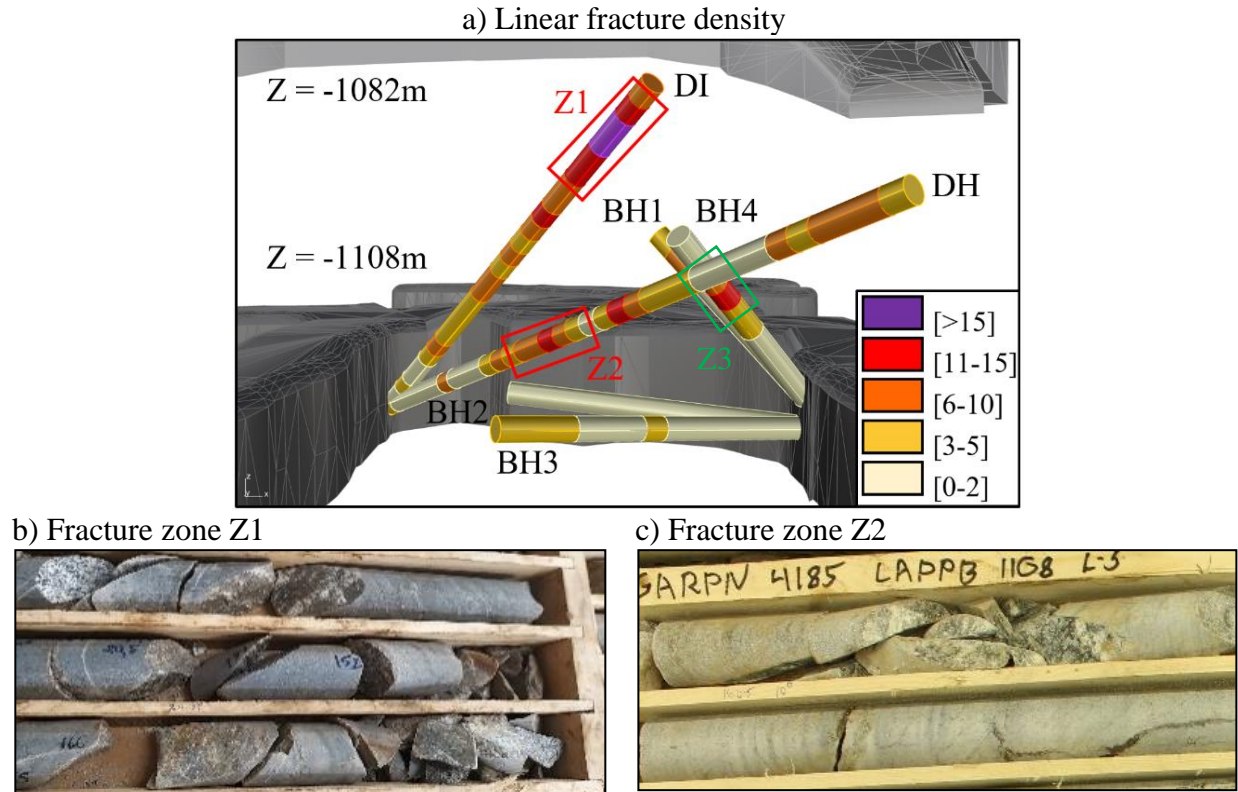


Fig. 4.6 - Linear density of fracturing in the drillings. The two zones of highest fracture density are shown in red, the third area of fracturing (with moderate amount + spun) is shown in green.

4.4 Orientations of fractures and nodal plane

4.4.1 Orientation of fractures

Mine geologists identified two major orientations of structures: foliation and sub-horizontal fractures. First one is almost perpendicular to the drifts. None of them is oriented like the seismic nodal plane (sub-vertical and almost parallel to the drifts), given by geophysical analyses. No other families of fractures oriented like the nodal plane is known by mine geologists (personal communication). The orientations of different families of fractures on the cores were measured with the objective to better characterize the different families of fractures in the area and observe whether at least one of them is oriented like the nodal plane.

To determine the orientation of the different fractures observed on the drill cores, drill cores have been first cautiously oriented using endoscope images (Fig. 4.7a). Then, orientations of the fractures were determined using the method proposed by Holcombe (2013). The method is widely used and is based on the measurement of two angles on the cores (α and β), measured with protractor templates, which give the orientation of fractures with respect to the drill core axis and to a

reference line along the core (Fig. 4.7b). α is the acute angle between the long axis of the fracture and the core axis, and β is the angle (measured clockwise) between a reference line along the core (in the figures the reference line is the top of the borehole) and the lower inflexion point of the ellipse (fracture) on the borehole. The angles and their measurement are shown in Fig. 4.7c.

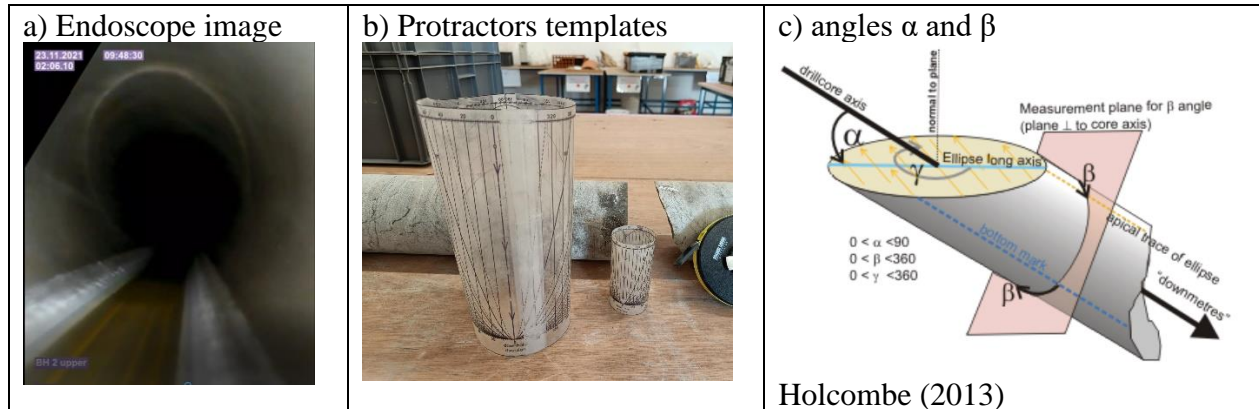


Fig. 4.7 - An example of the endoscope images which were used to orientate the drillcore and get the reference bottom line. Measurements on protractors allow to find the angle alpha and beta.

The detailed procedure to obtain orientation of the fractures from the drill cores is given by Stigsson & Munier (2013). The calculation is based on the determination of the normal vector of the plane, and uses 4 different parameters: bearing and inclination of the drilling, and α and β angles measured on the drill cores. Coordinates of the normal vector is first determined inside a local coordinate system of the drilling, as a function of α and β angles. Then, it is converted within the general coordinate system using matrices of rotation, which depends of trend and plunge of the drilling. Measurements and conventions have been checked by manual measurements of dip and strike with compass and rocket launcher and with the software Geocalculator (Holcombe, 2013). The three methods gave same results, which assures reliability of the measurements.

The orientation of all the fractures logged in the drill cores were plotted on stereonet (Fig. 4.8). From the results, two main families of fractures are observed: F1 (in light green), subparallel to foliation, and F2 (in red) sub-horizontal. These two families are the ones already known by mine geologists. In addition, five secondary families are found. They are called “secondary families” as they are not part of the well-known major structures, which can be explained because they are smaller in size, rarer in the orebody and/or with an orientation unfavorable to be observed by geologists (parallel to drifts).

A major result is the presence of a unique family of fracture oriented like the nodal plane: SF5 (blue one) family. Most fractures of the family are oriented between 10 and 20° from the nodal plane, which is an acceptable uncertainty considering both uncertainties in strike of the nodal plane (10-20°) and in the measurements in the cores. This family is mainly observed in Z2 fracture zone on DH bore hole (Fig. 4.9).

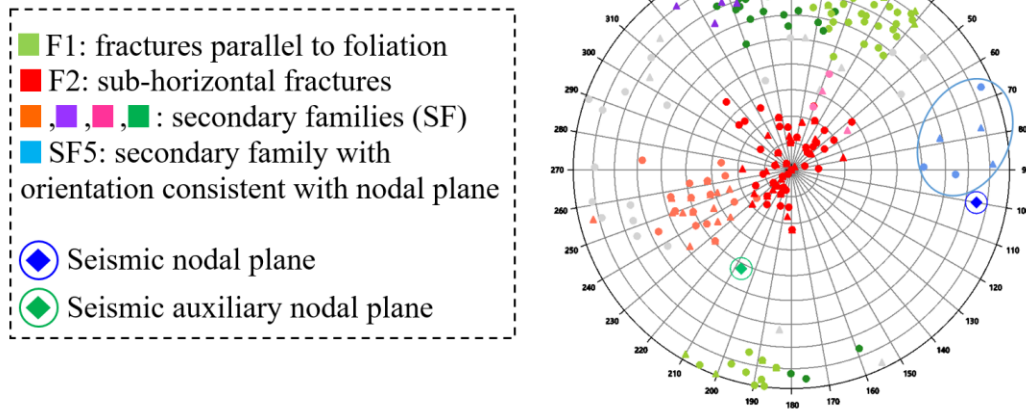


Fig. 4.8 - All natural fractures on all the drill cores. The dark blue diamond represents the nodal plane orientation, the dark green diamond the auxiliary nodal plane. Grey dots are fractures not belonging to any family.

F1 fractures (light green)	F2 fractures (red)	SF2 (dark green)
 2cm	 *SF1 are similar	
SF3 (pink)	SF4 (purple)	SF5 (blue)
		

Fig. 4.9 - One example of fractures for each of the seven identified families (SF1 and F2 are shown in same figure because they have same infilling).

4.4.2 Influence of uncertainties of the measurements

The question of the reliability of the measurements was raised due to the complexity to orientate the drill cores using endoscopes. To study the influence of the uncertainty of α and β measurements on the orientation of the families, I followed the method elaborated by Stigsson & Munier (2013) and I used the VBA code in open access written by the authors (Fig. 4.10). I also added uncertainties regarding the seismic nodal plane orientation: I chose values of uncertainties of 20° for the strike and 30° for the dip. SF5 is the only family for which the uncertainty surface meets the incertitude

surface of the seismic nodal plane. This confirms the seismic asperity is not part of any other family of fractures observed in the drill cores.

It should be noted that this method is more reliable than simply taking into account the range of possible orientations in Fig. 4.8, as it includes the uncertainties of drilling orientation using endoscope images and not just the uncertainties of measurements with protractors. An uncertainty of $\pm 5^\circ$ is chosen for angle α , which depends only on the uncertainty of measurements with protractors, while an uncertainty of $\pm 20^\circ$ is considered for angle β , which also takes into account errors on drilling orientation.

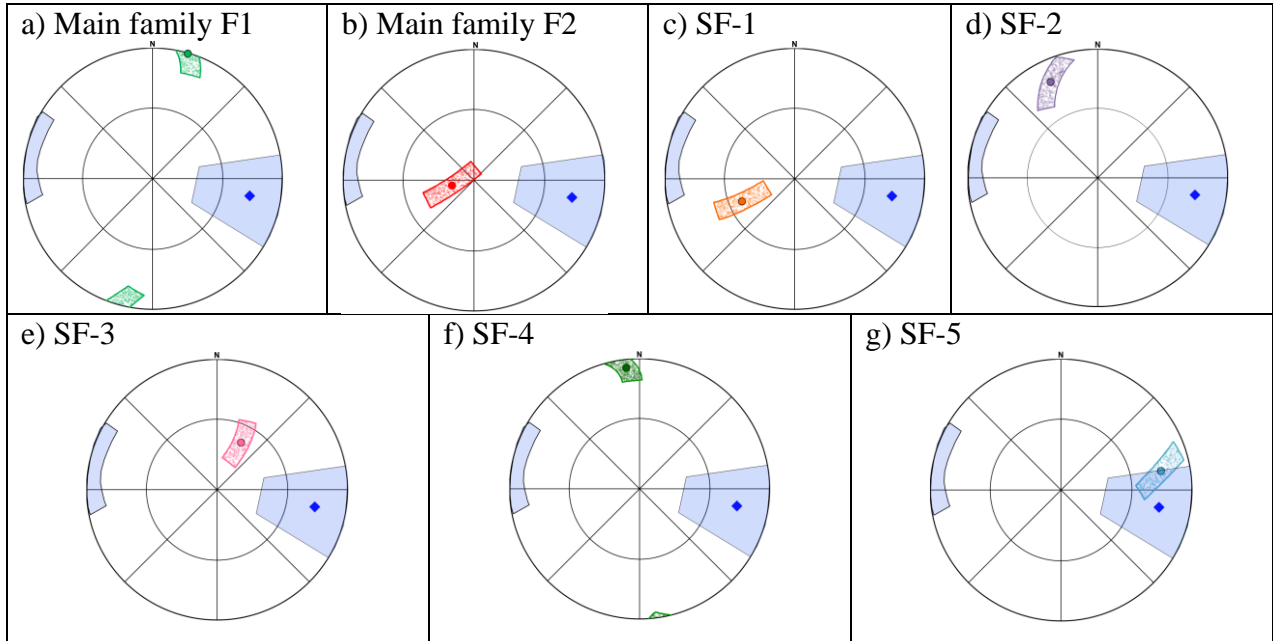


Fig. 4.10 - Uncertainties on fractures and nodal plane orientation considering $\alpha \pm 5^\circ$ and $\beta \pm 20^\circ$ in the Holcombe (2013) method, $\pm 20^\circ$ for the strike and of $\pm 30^\circ$ for the dip angle of the nodal plane. (Holcombe, 2013). Dark blue dot represents the nodal plane, blue surface covers uncertainties of the nodal plane and dots cover uncertainties of the measurements.

4.5 Infilling mineralogy

Creep is commonly associated to the presence of minerals such as clay and/or other phyllosilicates (Carpenter et al., 2011; Saffer & Marone, 2003). Here, I aim at observing whether some families of fractures contain that type of mineral of infilling. In that case, this would be an indicator these fractures might creep. Three families present some infilling: F1 family (fractures parallel to foliation), F2 family (sub-horizontal fractures) and SF5 family (similar orientation than nodal plane).

To determine nature of their infillings, X-ray diffraction was used (Fig. 4.11). This is a common technique to identify minerals and other crystalline materials (Al-Jaroudi et al., 2007; Hillier, 2009). The method is based on the fact that X-rays are diffracted differently by each mineral. A sample of mineral is placed is exposed to a beam of X-rays, and signals from the sample are recorded by a detector. X-rays are diffracted differently by each mineral, as diffraction depends on the nature of the atoms and their arrangement inside the crystal lattice. In the recorded signal for an X-ray scan, peaks of intensity are observed for different positions (position 2θ , with θ the angle of incidence of the X-ray beam) which represent positions where the X-ray beam has been diffracted. The characteristic set of peaks in a typical X-ray provides a unique “fingerprint” of the minerals in the sample. By comparing the signal with standard reference patterns, the mineral can be identified.



Fig. 4.11 - On the left: the instrument used during the analyses. On the right: an example of sample installed in the equipment. The sample remains immobile while the X-ray tube and detector move through the angle theta. Mineral of infilling was extracted from the cores using a spatula. This operation was delicate since the infilling is very thin. The use of a binocular loupe was needed to facilitate the extraction. The powder was crushed to make a powder the most homogeneous as possible. The mineral was mixed in a solution of acetone and placed on a silicon slide.

For mineral inside fractures, two different types of infilling were found. For sub-horizontal fractures (F2 and SF1), the infilling is quite thick (several millimeters) and composed by laumontite (zeolite). F1 (parallel to foliation) and SF5 fractures have very thin infilling, usually $< 1\text{mm}$. The infilling of SF5 and F1 families contain muscovite and chlorite (and laumontite), which are both phyllosilicates. Phyllosilicates are commonly associated to creep (Fig. 4.12), although creep tests would be needed to confirm this is the case here. Then, creep loading asperities in the area might be attributed to chlorite and muscovite infilling, either in F1 or SF5 families. The latter is the only family with fractures oriented like the nodal plane.

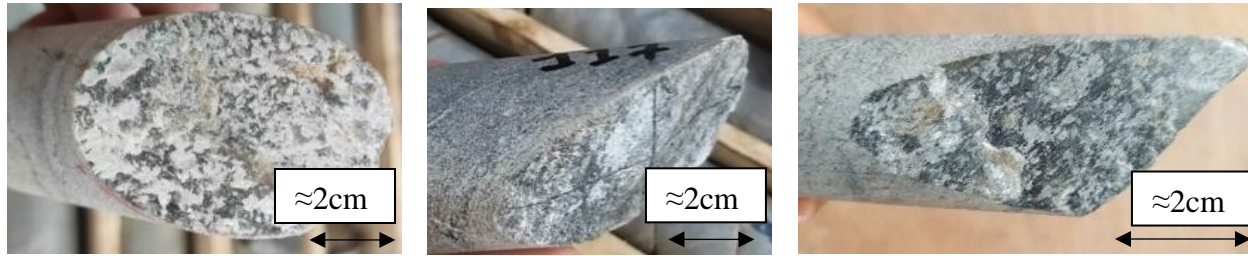


Fig. 4.12 - Infilling minerals within sub-horizontal fractures, fractures parallel to foliation and SF5 fractures. From left to right: laumontite in F1 family, chlorite/muscovite in F2 family and chlorite/muscovite in SF5 family.

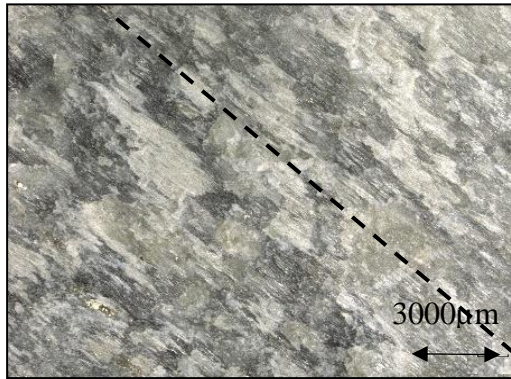
4.6 Markers of movements and lineation

4.6.1 Identification of fractures with lineation

As mentioned in chapter 1, kinematic markers are commonly observed in seismogenic and creeping sections and can give indication on movements occurring within these regions. While all faults with marker of movements in the cores are not the seismic asperity or the creeping region, it is expected that these two regions would show such lineation features if they have been reached by the drillings.

Two major types of lineation are observed on fractures: (i) slickenside lineation (or stries), (ii) stretching lineation. Slickensided fractures are polished surfaces and are created by friction between the opposite sides of the fractures (Fig. 4.13). Slickenlines indicate there has been slip movement on the fracture (Hudson & Harrison, 2000) and can be used to deduce fault slip direction (Doblas, 1998; Petit, 1987). They are usually associated to seismic areas, but can also be associated with continuous and aseismic slip in presence of phyllosilicates, as shown in the case of the San Andreas Fault in chapter 1. Second type of lineation (stretching lineation) is a symbol of ductile deformation. These are only visible in filled fractures and are related to the anisotropy of mineral infilling. In some cases, it has been shown that low strain rate creep can align phyllosilicate grains during interseismic periods (Wintsch et al., 1995). Then, it is worthy to identify slickensided and stretched fractures in the drill cores, as potential asperities and creeping fractures. However, nothing proves kinematic markers are indicators of present movement and further comparison between geological measurements and seismic source mechanism will be done in next section to study further whether one of these lineated fractures could be hosting seismic repeaters.

a) SF5 – Slickenside lineation



c) F2 - No lineation



Fig. 4.13 - Examples of a slickenside lineation and of an infilling without any lineation, from the cores. Photos were done with scanning electron microscope.

Four fractures have noticeable slickenside lineation and have been named in function of the family and their location. Their position is shown in Fig. 4.14, as well as the position of two stretching fractures at proximity of Z1 zone. SF5 is located in Z2 fracture zone. To be precise, not only one but several fractures of this family with slickenlines are observed, close to each other. They are filled with phyllosilicates. F1-below is also filled with phyllosilicates and is at proximity of BH4. The fracture contain both stretching and slickenside lineation. Finally, SF2 and F1-upper are unfilled fractures within Z1 fracture zone (Fig. 4.14d).

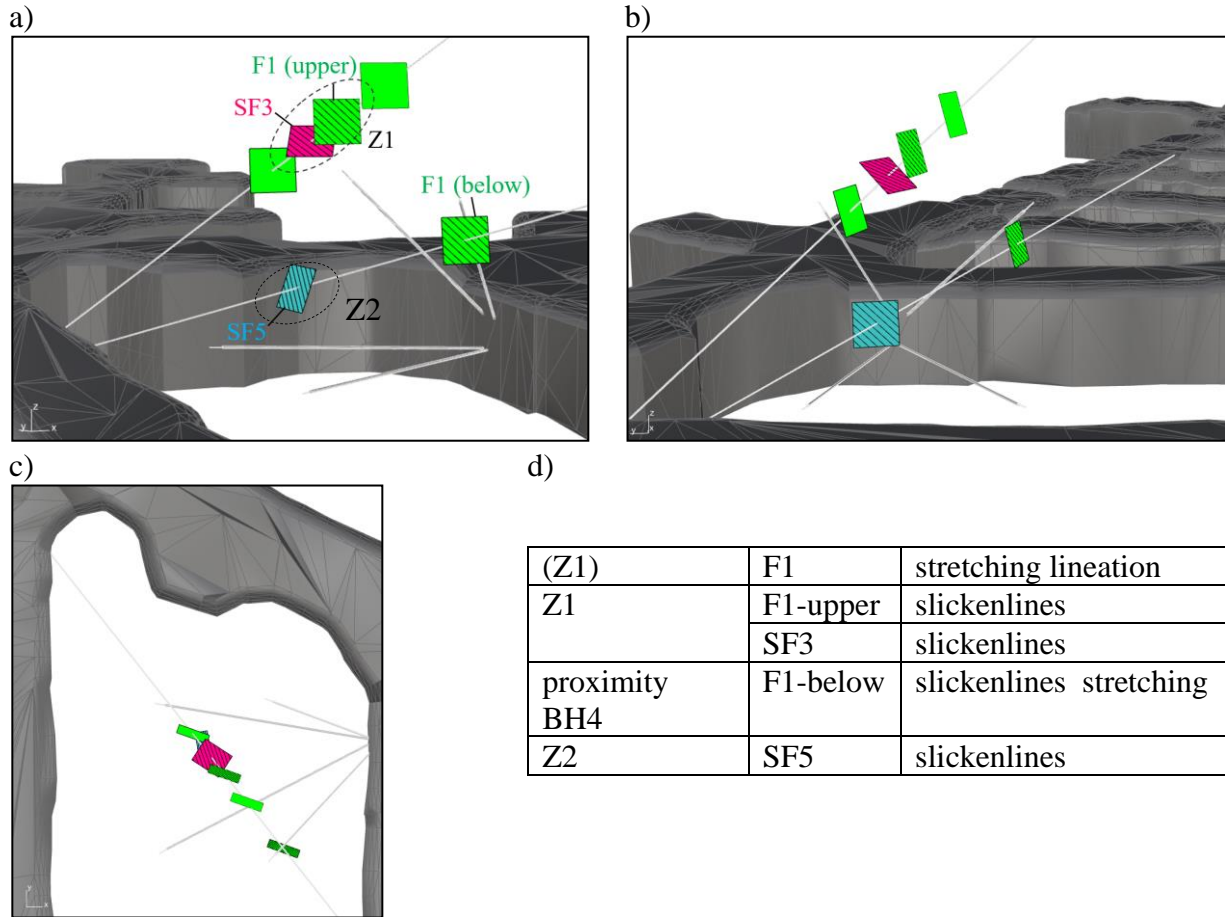


Fig. 4.14 - Fractures with visible lineation in the drillings. Colors refer to the family: Green fractures belong to F1 family, the blue fracture belongs to SF5 family, and the pink fracture belongs to SF3 family. If lineation is of type of slickenside lineation, hatched surfaces are shown. If lineation is of stretching type, no hatch is represented. Note that several stretching lineation type exists and only two of them are shown on each side of the fracture zone.

4.6.2 Comparison of geological and seismic source mechanisms

Here, I focus on the fractures with lineation and I compare their orientations (strike, dip) and slip direction (rake) with seismic source mechanism of the repeater family.

SF5 fractures and seismic nodal have similar orientations, and their slip orientations can be easily compared. A rake of 60° was measured on the drill cores for SF5 whereas seismic rake from seismic source mechanism is 130° . First one indicate a left lateral movement and second one a right lateral movement (Fig. 4.15). This represents a clear incompatibility between the seismic nodal plane and the SF5 family. None of the SF5 fracture in the cores is the seismic asperity, except under the hypothesis that seismic slip doesn't leave any visible indicator of movement due to very small displacement. SF5 fractures, or at least one of them, is most probably part of the creeping portion

of the fault plane hosting the seismic asperity. In this case, the observed striation could be an indicator of a past movement independent of what occurs today.

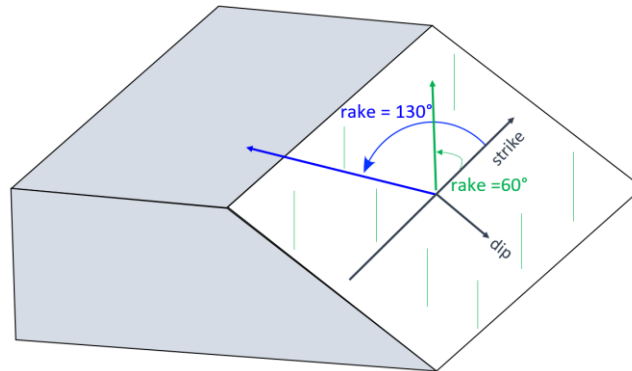


Fig. 4.15 - Orientation and rake of the SF5 fracture (rake = 60°) and the seismic nodal plane (rake = 130°), considering their orientation is the same. This scheme highlights the incompatibility of the slip direction on SF5 with the nodal plane, as one is left lateral and the other one right lateral (figure adapted from Allmendinger (2019)).

The orientations of the other fractures with lineation differ from the orientation of the nodal plan. A method to compare these fractures and the seismic focal mechanism is the determination of pseudo focal mechanisms from geological measurements (strike, dip and rake), as described by Angelier & Mechler (1977) (Cirillo et al., 2022; Kinscher et al., 2013; Schulz & Evans, 2000). Similarly to seismic focal mechanism, the construction of the pseudo focal mechanism (i.e. “beach ball”) is based on the calculation of the auxiliary plane, which is possible thanks to the symmetry of the moment tensor associated with a double couple focal mechanism (Cronin, 2004). To determine the pseudo beach balls from geological measurements, I used the software FaultKin (Allmendinger et al., 2012; Marrett & Allmendinger, 1990).

To compare pseudo beach balls and seismic focal mechanism, I used a quantitative method based on the calculation of the Kagan angle (Kagan, 1991). This angle is commonly used to compare focal mechanisms, whether it is the comparison of real and synthetic moment tensors, moment tensors from different earthquakes, or moment tensors from same events determined with different methods (Tape & Tape, 2012). This angle represents the minimum rotation angle between two focal mechanism solutions, i.e., the minimum rotation angle which will transform the first focal mechanism into the second one. The angle ranges from 0° (identical focal mechanisms) to 120° (total disagreement between the focal mechanisms). Values below 60° indicate a good similarity while above 60° indicate a mismatch (Pondrelli et al., 2006). Here, I calculated the Kagan angle between the seismic beach ball and each of the pseudo beach balls obtained from geological measurements, using an open access code based on the algorithms developed by Kagan (2007) .

For each pseudo beach ball associated with slickensided lineation, values of Kagan angles are above 60°, which indicates pseudo focal mechanisms are incompatible with the seismic focal mechanism (Fig. 4.17). Then, the asperity is unlikely to be hosted by any of the slickensided fractures observed in the drill cores. For one fracture with stretching lineation, pseudo focal

mechanism is compatible with the seismic focal mechanisms. This fracture belongs to F1 family (parallel to foliation) and the stretching lination is due to stretching of phyllosilicate minerals. Such fracture is likely to host creep with slow slip aligned with the anisotropy of the grain minerals (Wintsch et al., 1995). In this case, seismic repeaters can represent the breakings of micro asperities (centimeter scale) on these creeping zones, similar to what was described in San Andreas Fault in chapter 1. The presence of both seismic and creeping zones in fractures parallel to foliation is consistent with field observations, where 35% of the fractures parallel to foliation contain chlorite and muscovite, with the remainder showing no infill at all. This shows that both ductile and brittle behavior could be hosted by such fractures. However, this hypothesis is not coherent with the alignment of seismic events, perpendicular to these fractures and aligned with the nodal plane calculated from focal mechanism. A possible explanation of the alignment of seismic events could be related to the rupture of rock bridges between the shear planes, as proposed by Malek et al. (2008) in their conceptual models of rockbursts elaborated in the study of seismicity in the Creighton mine (Fig. 4.16). However, such models stay very qualitative.

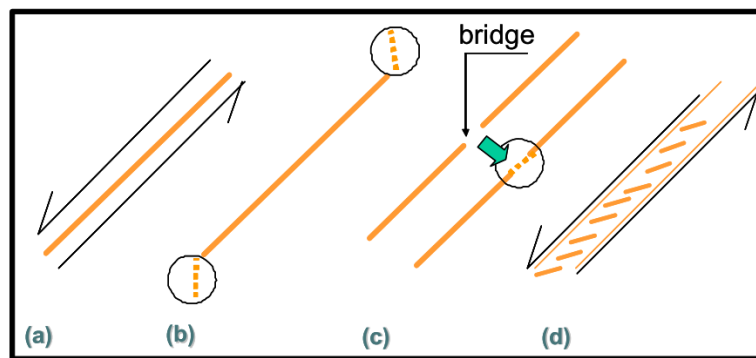


Fig. 4.16 – Conceptual models of rockbursts. (a) fault slip (b) fault propagation (c) damage of rockbridges linear with shear zones (d) damage of en-echelon relay faults. From Malek et al. (2008).

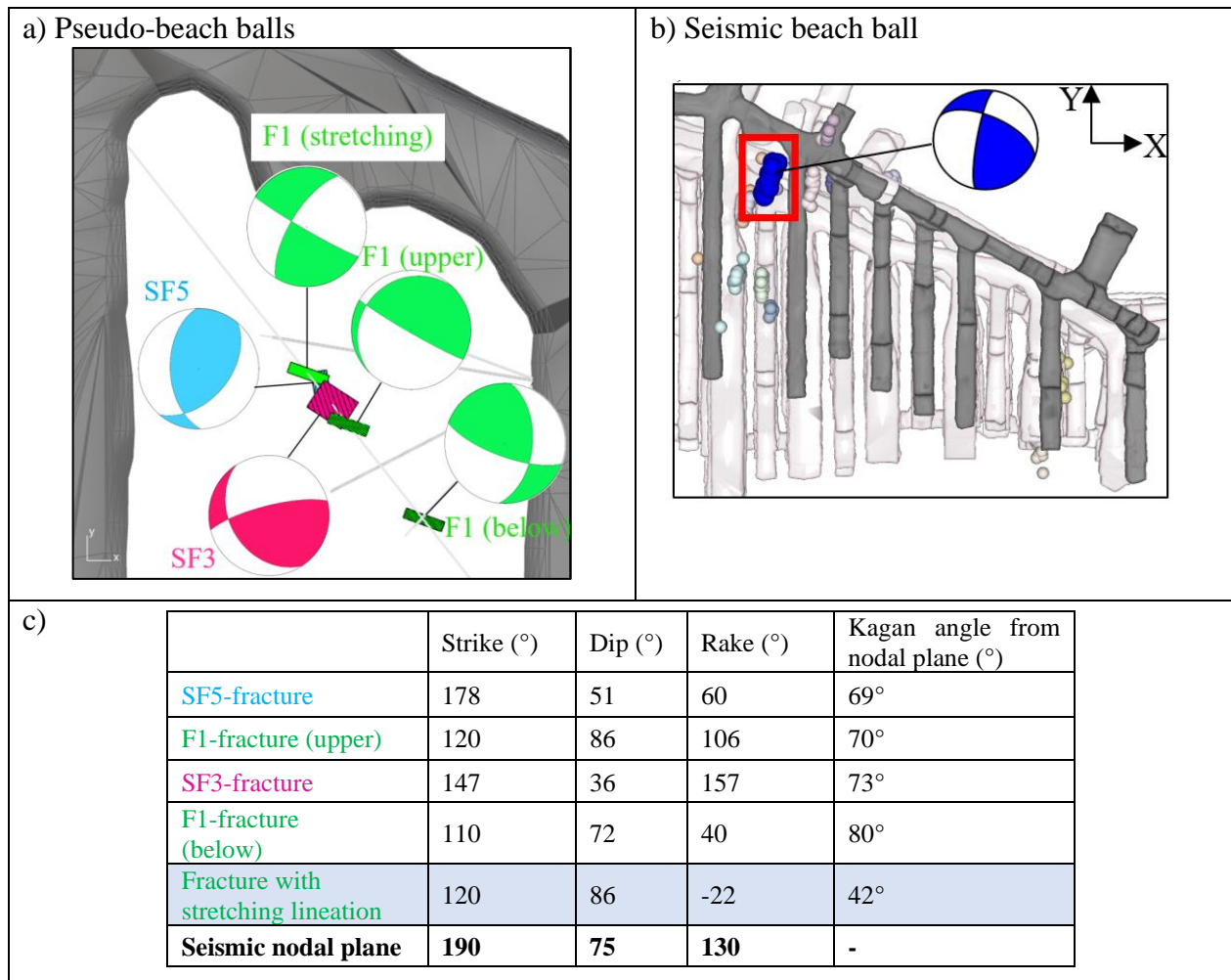


Fig. 4.17 - Comparison between pseudo beach balls from geological measurements and seismic beach ball. Figure a) show fractures with slickenside lineation and pseudo beach ball determined from measurements of strike, dip and rake. The figure only show the sill-pillar in a plane view. Figure b) shows seismic beach ball determined by Kinscher et al. (2020). It is also a plane view and all drifts of excavation can be seen. Table c) shows the values associated with the geological and seismic beach balls, and the calculation of Kagan angle between each geological beach ball and the seismic beach ball.

4.7 Stress state and fault activation

Here, I study whether families of fractures on the drill cores and the seismic nodal plane are likely to be activated, considering the local state of stresses. No stress measurement is available in the sill pillar. Thus, I study this question with two different approaches. First, I consider available stress measurements (see chapter 2), even if they are not located within the sill pillar. Secondly, I use the inversion of the seismic focal mechanism in the sill pillar, assuming an elastic and isotropic medium, to determine a state of stresses consistent with seismic measurements and I discuss its consistency with expected state of stresses in the mine.

4.7.1 Measured state of stresses and fault activation

We use the two measurements by Ineris in the block of excavation below the sill pillar and one measurement outside the area of influence of the excavation (see chapter 2). The two measurements by Ineris are very disturbed by the presence of galleries, and I first chose to infer the stress state with the measurement outside the area of influence of the excavation. Principal stresses σ_1 and σ_3 of these measurements are horizontal and oriented at 155° and 65° from the Y axis, respectively, while σ_2 is vertical. Normal and shear stresses on all the fracture planes measured in the drill cores were calculated by projection of the stress vector on the fault planes. The stress vector was calculated by applying the stress tensor to the normal of the fault planes using Cauchy's law : $\vec{T} = \bar{\sigma} \cdot \vec{n}$. Results are plotted on Fig. 4.18. The seismic nodal plane was also plotted. Next, I included a Coulomb friction criteria for different coefficients of friction. To do so, I first assessed coefficients of friction of the fractures in the drill cores, using the nature of their infilling obtained from DRX analyses and what is known in literature (Table 4.2).

For the chosen stress measurement, seismic nodal plane appears to be favorably oriented to slip under the assumed stress state. All fractures with coefficients of friction higher than 0.35 are unable to slip, which correspond to all fractures except F1 and SF5 fractures which have chlorite and muscovite infilling (Table 4.2). If a coefficient of friction of 0.27 is considered consistent with chlorite infilling, the seismic nodal plane, the major part of F1 fractures and half of the SF5 fractures are susceptible to slip.

	Mineral	Coefficient of friction (estimated)
Family F1	infilling : chlorite/muscovite (laumontite)	0,27-0.32
Secondary family SF5	infilling : chlorite/muscovite (laumontite)	0,27-0,32
Family F2	infilling : laumontite	0,8
Secondary family SF1	laumontite	0,8
Secondary family SF2	? (only veins)	?
Secondary family SF3	no infilling	0,6-0,8
Secondary family SF4	no infilling	0,6-0,8

Table 4.2 - Estimated coefficient of friction for the seven families of fractures identified in the drill cores. Values come from Ikari et al. (2009) for chlorite, from Morrow et al. (2000) for laumontite, from Byerlee (1978) and Goldsby & Tullis (2002) for rocks with quartz.

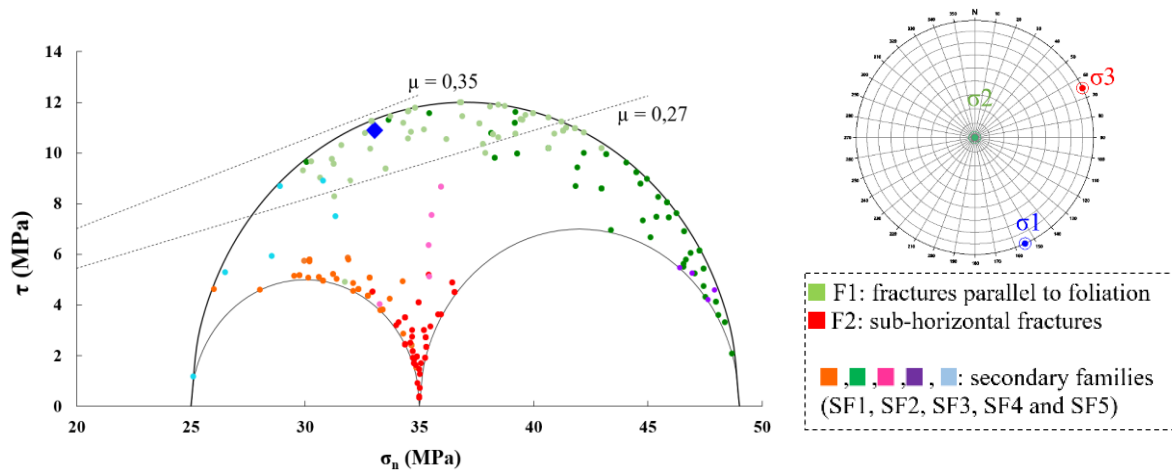


Fig. 4.18 - Mohr circles for the considered measurement. Dots represent all the fractures from drill cores measurements. Each color refers to a family. Stress orientations are shown upper side above.

We also studied the potential of activation of fault planes considering the two stress measurements by Ineris, within the panel of excavation below the sill pillar (Fig. 4.19). These two measurements are only a few meters from each other but differ strongly, probably due to the influence of the excavation. Similarly to previous stress measurement, coefficient of friction must be below 0.4 for the fractures to be activated, which is only the case for F1 and SF5 fractures. For both measurements, the seismic nodal plane is not activated, even for low coefficient of friction, as well as most F1 fractures. Then, these two state of stresses are inconsistent with seismic repeaters.

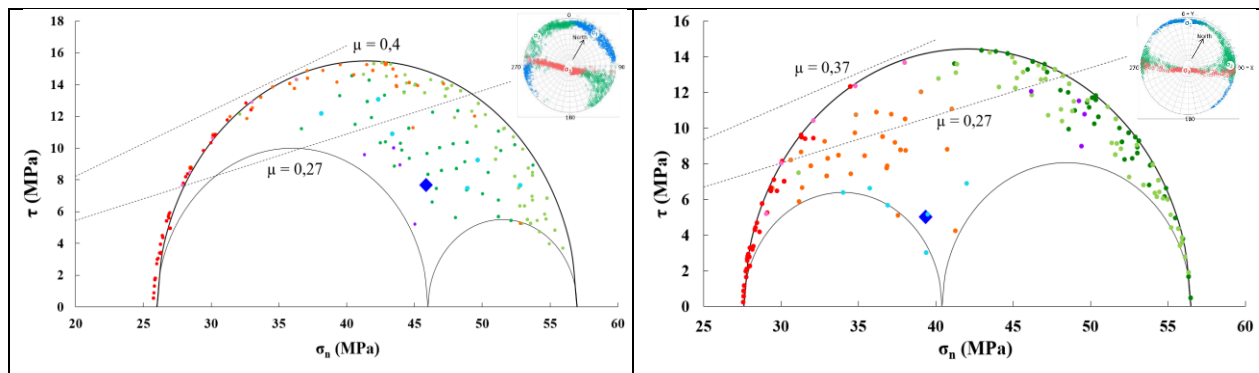


Fig. 4.19 - Mohr circles for the considered stress measurements. On the left, H1 measurement and on the right H2 measurement (see chapter 1 for locations). Dots represent all the fractures from drill cores measurements. Each color refer to a family. Same colors are used than for Fig. 4.18. Dotted lines represent coulomb criteria for two different values of coefficient of friction. First value is 0,27 which is chosen as a low value coherent with phyllosilicates infilling. Second value (0,37 and 0,4) are the maximum values which allow some fractures to slip. All values above these coefficient of frictions can't slip considering the state of stresses. This is the case for all fractures, except the seismic nodal plane (dark blue dot) and the two families with phyllosilicates infilling (SF5 and F1, in light blue and light green).

Then, the three stress measurements show that only fractures with low coefficients of friction can be activated. Then, a brittle frictional asperity is unlikely to slip due only to state of stresses. In literature, creeping material is often associated to minerals with low coefficient of friction, although

not all minerals with low coefficient of friction exhibit creep. Then, the most probable explanation to justify that seismic asperity (with higher friction coefficient) is loaded by a surrounding creep on the fault plane hosting the asperity. This is highly consistent with models associated with repeaters. Note that I considered that both asperity and the creeping fault plane hosting the asperity are oriented like the nodal plane.

Whereas stress measurement outside the area of influence of the excavation is consistent with the activation of the nodal plane, direction of slip differ from the seismic rake. Rake obtained by projection of the stress vector is 92° and the seismic rake is 130° , which indicates a complete reverse fault mechanism rather than a strike/slip mechanism with reverse component. A first explanation is that slip on the asperity is not aligned with shear stress orientation, which means Wallace-Bott hypothesis (i.e. slip on fault occurs in the direction of maximum resolved shear stress) is not applicable. This can be due to striation on the asperity which orientate the displacement on the asperity (Kirkpatrick & Brodsky, 2014; R. Lisle, 2015). Second explanation is that the stress of state is not entirely representative of the state of stresses within the sill-pillar, which is highly plausible as the stress measurement was not made in the sill pillar.

4.7.2 Inversion from source focal mechanism

We estimated a possible state of stresses from the focal mechanism of the repeater family, based on the P- T axis method (Angelier & Mechler, 1977). The term P-T axis refers to the definition of P axis (pression) and T axis (tension), which are the centers of the dilatational and compressive quadrants of the focal mechanism. This method is based on two hypotheses: (i) fault planes are assumed to be due to a mean and uniform state of stress in the rockmass (σ_1 , σ_2 , σ_3 being the maximum, intermediate and minimal principal stresses, respectively) and (ii) direction of slip is the same than shear stresses, referred as the Wallace- Bott hypothesis (Bott, 1959; Wallace, 1951). Four dihedra separate fault plans and its auxiliary plane. Two quadrants are compressional quadrants, and two quadrants are dilatational quadrants. In that case, σ_1 and σ_3 are located within dilatational and compressive quadrants, respectively (Lisle, 1992). A first observation is the incompatibility of the state of stresses measured outside the area of influence of the excavation with this theory. Indeed, σ_1 is within the compressive quadrant and σ_3 in the dilatational quadrant, which confirms that this state of stresses is probably not the one which activates the asperity. In an environment purely isotropic and elastic and considering σ_1 is at 45° of the fault plane, σ_1 is same axis than P axis and σ_3 is same axis as T axis. P and T axes were determined using FaultKin software. Values must respect the following relation: $Rake = \frac{(\sigma_1 - \sigma_2)}{(\sigma_2 - \sigma_3)}$ (Lisle, 1992). A set of possible values which give a rake of 130° is: $\sigma_1 = 57\text{MPa}$, $\sigma_2 = 36\text{MPa}$ and $\sigma_3 = 26\text{MPa}$. These values are in the order of scale of stress measurements from Ineris (chapter 2). Under this state of stresses, SF5 fractures and seismic nodal plane are well oriented to slip (Fig. 4.20). F1 fractures are not well oriented on the contrary. This state of stresses is consistent with general tendencies in

the mine, with a sub horizontal maximum principal stress, and the intermediate and minimum ones which are vertical and sub horizontal.

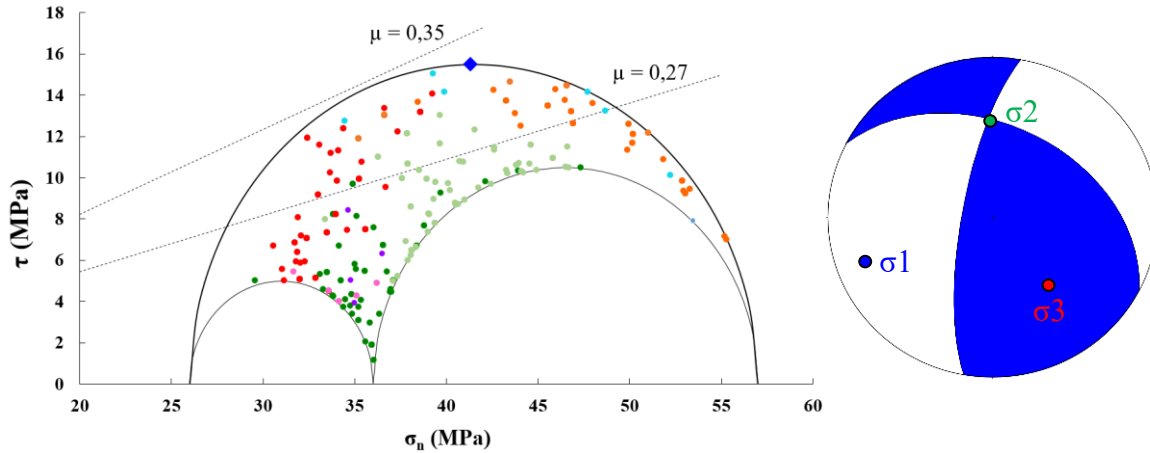


Fig. 4.20 - Mohr coulomb for the state of stresses deduced from focal mechanism, assuming elastic and isotropic environment.

To conclude, It was shown that only fractures with low coefficient of friction can be activated under state of stresses measurement in the mine. One stress measurement, made outside the area of influence of the excavation, could explain slip on the nodal plane, but not the slip direction. A state of stresses (not exhaustive) consistent with focal mechanism was proposed, calculated from P-T axis method. Under this state of stresses, SF5 family and the nodal plane are activated for friction coefficient lower than 0.35. Other fractures were not activated. A fault plane or a portion of a fault plane with high friction coefficient (>0.35) can't be activated under the state of stresses measurement, which suggests slip on the asperity was not directly induced by the state of stresses. This is very consistent with the presence of seismic repeaters, which assume asperities are loaded by a continuous and aseismic slip which modifies the local state of stresses until the asperity breaks. A continuous and slow slip on a fracture of SF5 family can be activated under this state of stresses, and load a locked portion of the fault (asperity), inducing repeating ruptures.

4.8 Conclusions

This chapter highlighted the interest of using local data to study the geological origin of seismic repeaters in a deep mine, i.e. what hosts and loads the seismic asperities. I looked at lithologies, orientation of fractures, mineralogy, kinematic markers, and state of stresses.

Thanks to this installation, the presence of both materials susceptible to creep and material likely to be seismogenic was highlighted, i.e. phyllosilicate infilling and fractures with slickenlines. The geological nature of both creeping and seismic materials was also constrained, and the areas

potentially involved. First of all, creep is probably associated with chlorite and muscovite infilling. The fault plane hosting creep might be one of the fault planes oriented like the nodal plane (SF5 family) and filled with such creeping material. This option is consistent with state of stresses, insufficient to induce slip on brittle frictional asperities but sufficient to activate slip on a fault plane with low friction coefficient. Assuming this low friction coefficient is due to phyllosilicate infilling, as observed on SF5 family, state of stresses could induce creep on the fault plane (Ikari et al., 2011). This creep can then change the local state of stresses on the frictional asperity and induce a seismic slip. This is highly consistent with the presence of repeaters and common seismological models. However, the seismic asperity was not identified in the drill cores, as no fracture oriented like the nodal plane exhibited kinematic markers consistent with the slip direction given by the focal source mechanism. This shows that reaching and/or identifying a seismic asperity for such small events is not obvious, even for such a local installation targeting a singular repeater family.

Chapter 5

Triggering mechanisms of seismic repeaters

Time-dependent post-blast deformation was identified on strain cells in the panel of excavation 1250 between 2015 and 2017 by De Santis (2019). Most of the time, they were not accompanied with seismicity. When seismicity occurred, a qualitative fit was observed between temporal evolution of seismic rate and temporal evolution of deformation of individual gauges (see Fig. 2.17 in chapter 2). This suggests a relationships between seismicity and strain deformation. Although these observations are valuable as they suggest seismicity driven by creep in the mine, they remain very qualitative as they are based on a simple fit between random curves. The nature of the creeping material remain uncertain, although previous chapter showed that creep is probably related to chlorite and muscovite filled fractures. The seismic asperity was also not identified in the cores. In this chapter, I propose to combine strain data with geological and seismic data, to further constrain location and dimensions of the asperity, as well as further characterize strain deformations (values and orientations of principal strains) and relationships between strain data and seismic observations. By doing so, I aim to discuss further the possible triggering mechanisms of seismic repeaters.

When questions on the nature of the triggering mechanism and relationships between seismicity and aseismic deformation are raised, displacement values from geodetic measurements are usually compared with temporal evolution of seismicity (Savage, 2010; Lohman & McGuire, 2007; Miyazaki et al., 2004; Perfettini et al., 2010). In this present case, no displacement value such as GPS data is available. However, local strains were monitored by strain cells. To correlate strain and displacement, it is proposed to use an inversion model based on a model of elastic dislocation (Okada, 1992).

5.1 Transient and long-term periodic repeater rate

Two different repeater families are located close to CSIRO Hi12 strain cells (a few meters) and represent exceptional opportunities to study relationships between seismic and strain data, and the mechanical loading of seismic asperities. The two families are: family 37 and family 11. The numbering of these families corresponds to the numbering of the seventeen repeater families given by Kinscher et al. (2020). The two families are located within block 1250. Family 37 is located in

the upper sill pillar; family 11 is within the underlying excavation panel (Fig. 5.1). Different loading mechanisms are expected for both families: family 37 is expected to have a more constant loading mainly influenced by initial state of stresses, family 11 is expected to be influenced by the excavation of individual stopes of excavation.

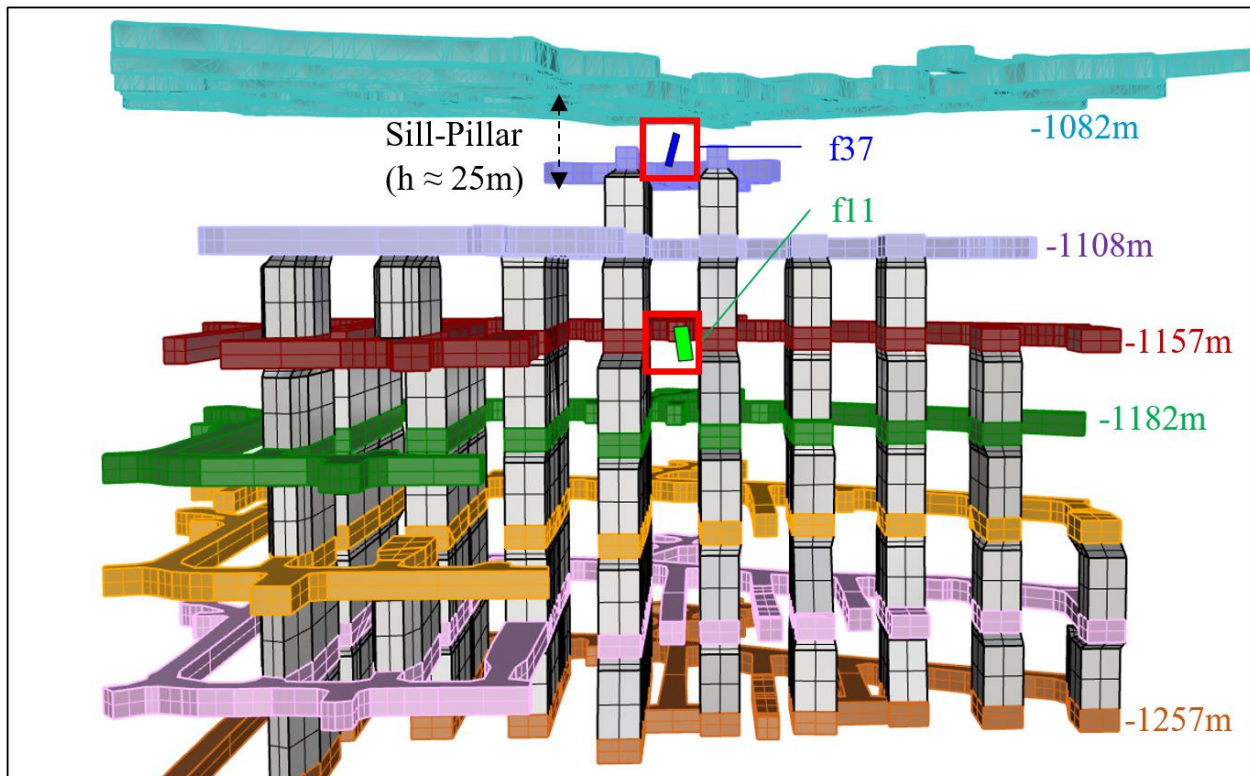


Fig. 5.1 - Location of the retractor families 11 and 37, in the excavation panel (block 1250) and in the sill pillar, respectively. For each family of retractors, the nodal plane is determined using a double couple seismic analysis (Kinscher et al., 2020). Planes of the two families are represented in the figure, with an arbitrary size of 10m x 10m.

Both families are located in Micaquartzites and have similar source mechanism: a strike-slip focal mechanism with a reverse component, oriented at 10-24° eastwards from the Y-axis of the mine (Table 5.1). This suggests that similarly oriented discontinuities are hosting retractors independently of their location (anisotropy of initial stress might also have a strong influence). This observation is all the stronger that almost all retractor families in the mine have similar source focal mechanisms (Kinscher et al., 2020). Such strike-slip faulting mechanism associated with a reverse component indicates a dominant compressional stress in the horizontal plane (Anderson, 1905), which is consistent with insitu stresses measurements (Tonnelier et al., 2016).

	Strike	Dip	Rake	Strike2	Dip2	Rake2	Source mechanism	Mw	Slip
fam37	190°	75°	130°	297	42	22°	Strike-slip with reverse component	-1 (max)	1mm (max)
fam11	24°	81°	144°	120°	55°	10°	Strike-slip with reverse component	-0.7 (average)	0.2mm (average)

Table 5.1 - Characteristics of the nodal and auxiliary nodal associated with families 37 and 11. Strike is defined clockwise from Y-axis of the mine and follows the right-hand rule. The rake corresponds to the slip direction on the fault plane, defined with Aki Richards's convention. Mw is the moment magnitude of the events and slip is the amount of seismic slip during one seismic event.

As discussed in chapter 2, the seventeen repeater families monitored by Kinscher et al., (2020) exhibit two different recurrence time: (i) a classical Omori-like law and (ii) quasi-periodic events (Fig. 5.11). Family 11 presents a typical Omori-like response, with two different responses induced by two blasts. Family 37 is mainly characterized by quasi-periodic events (time recurrence of around 35 days between seismic events), not directly induced by blast. Omori-like response was also sometimes observed in family 37 just after a blast (stope 15 on 18th of June 2017). Note that family 11 was active during a month whereas the family in the sill pillar started in 2016 and is still active today.

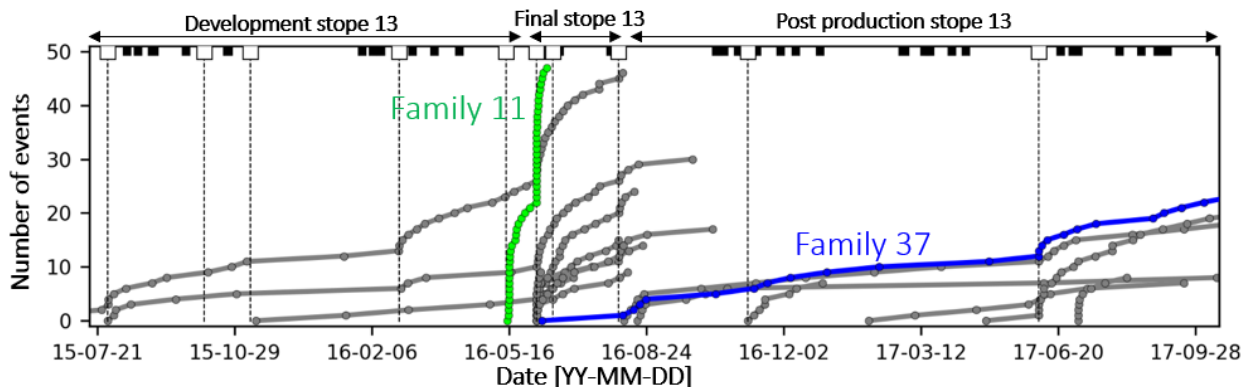


Fig. 5.2 - Number of seismic events as a function of time, for the 17 families of repeaters identified by Kinscher et al. (2020). Curves are highlighted for the family 11 (in green) and the family 37 (in blue). At the top of the figure, excavated stopes are shown. Family 11 is induced by two different blasts. Family 37 starts just after the final stage of excavation of stope 13, which induced a transfer of stress towards the overlaying sill pillar (see chapter 2, section 2.2.4). Figure adapted from Kinscher et al. (2020).

5.2 Long term period repeaters family

5.2.1 Coseismic Strain measured by BH4

A seismic event of magnitude of one order of magnitude higher than the other seismic events monitored during an 8-month period ($M_w = -1$) occurred on January 18, 2022. Static concomitant deformation was detected by one of the strain cell (BH4). The correlation between the seismic waveforms of this event and the family 37 (target family of the installation described in chapter 4) show that it belongs to the family 37 (the method of comparison between seismic signals is described by (Kinscher et al., 2020)). The event was not followed by any subsequent event, and was considered as part of the periodic trend in the sill pillar where interevent periods of around 35 days are observed between 2 events. It was the only event detected, probably due to its larger magnitude.

The coseismic strain monitored by BH4 ($6 \mu\epsilon$) is sudden and no time dependent deformation was observed on the monitored data (Fig. 5.3). However, the resolution of the cell is only $5 \mu\epsilon$ for a coseismic shift of $6 \mu\epsilon$, which suggests that the resolution of the cell doesn't allow to observe whether creep occurred or not. Note that the deviation observed in figure 5.3 is the deviation due to creep of the glue and doesn't represent any creep in the rockmass or on a fault plane (typical creep glue curves where orthoradial deformation is high whereas almost no axial deformation is monitored - (Lahaie et al., 2010)). Whereas BH4 monitored a coseismic shift, BH1 did not monitor any deformation and BH3 monitored a tiny shift of around $0.8 \mu\epsilon$ (see Annex B). Assuming that the deformation monitored during the shift is mainly caused by the rupture of the asperity, this suggests that the seismic area is located very close to BH4, not too far from BH3 and far enough from BH1 not to be detected.

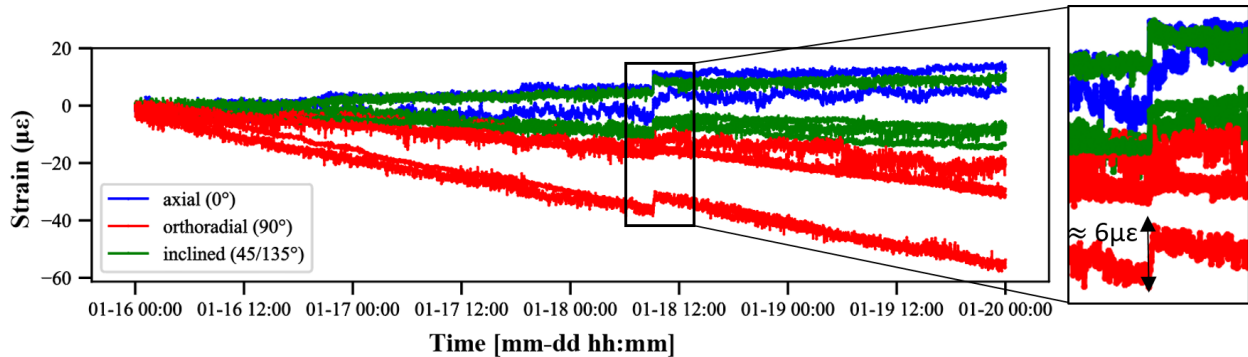


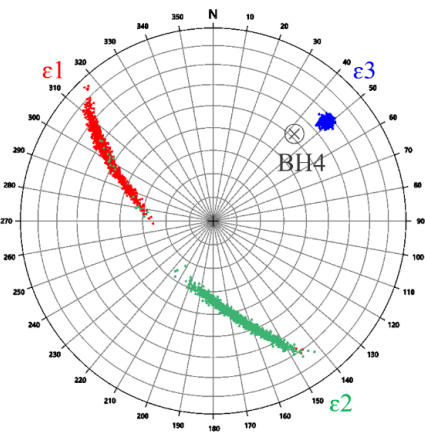
Fig. 5.3 - Recordings of the 12 strain gauges of the BH4 CSIRO cell, between the January 16 and 20, 2022. In blue: the axial gauges, in red: the orthoradial gauges and in green: the inclined gauges. The instantaneous increase of deformation occurred the 18th of January between 9:08am and 9:09am, i.e. the same minute that the seismic event. Here, only the co-seismic strain is of interest and the influence of creep of the glue is neglected during the coseismic shift, as the strain shift occurs over a very short period compared to the creep characteristic timescale.

5.2.2 Strain inversion to obtain stress variations

From the 12 strain gauges of BH4, I calculated a co-seismic strain tensor, and a co-seismic “variations of stresses” tensor, following the inversion method described by Worotnicki (1993). To

determine variations of stresses from strain measurements, the medium is assumed to be elastic and isotropic. Note that in that case, the tensor of variation of stresses is obtained and not the final stress tensor, as the initial state of stresses was not measured in the sill pillar. Conventions are chosen compression positive.

The amplitudes and orientations of the three principal strain axes (Fig. 5.4) show a major elongation ϵ_3 ($-6,6\mu\epsilon$) with an azimuth of 48° from Y-direction and a dip of 22° , i.e. close to the direction of the borehole. A decrease of stresses of $0,37\text{MPa}$ is collinear with the extension ϵ_3 (assuming the medium is assumed elastic and isotropic). The orientation of the major extension is well-constrained, whereas the orientations of ϵ_1 and ϵ_2 exhibit a higher range of uncertainties.



Principal variations of stresses (MPa)	Principal strains ($\mu\epsilon$)	Azimuth ($^\circ$)	Dip ($^\circ$)
$(\Delta\sigma)_3 = -0,37$	$\epsilon_3 = -6,6$	49	23
$(\Delta\sigma)_2 = -0,03$	$\epsilon_2 = +0,94$	166	47
$(\Delta\sigma)_1 = -0,0001$	$\epsilon_1 = +1,7$	302	34

Fig. 5.4. Principal co-seismic strain orientations during the shift of the 18th of January. Dots on the figure come from a random set of other potential solutions considering the error attached to the estimation of the tensor. Values are shown in the table on the right: $\epsilon_3 = -6,6\mu\epsilon$ (extension), $\epsilon_2 = +0,96\mu\epsilon$ (shortening), $\epsilon_1 = +1,7\mu\epsilon$ (shortening).

5.2.3 Location of the seismic nodal plane

In this section, the seismic asperity is defined as a rectangular portion (i.e. a patch) of a fault plane where occurred the seismic slip. The coseismic strain (i.e. permanent and concomitant static strain induced by slip on the asperity) can be used to locate and constrain the dimensions of the asperity. To do so, I used an inverse model based on Okada's formulas (Okada, 1992). This model is based on dislocation theory introduced first in 1958 by the seismologist Steketee (1958), who calculated surface displacement due to a point source vertical strike-slip. Further studies lead to calculation of strain fields at depth for inclined finite shear fault (Iwasaki & Sato, 1979; Sato & Matsu'ura, 1974). This is the case of Okada model, which allows the calculation of strains and displacements based on either point sources or finite rectangular fault sources models. Point source model can be used to estimate far-field deformation. Finite rectangular model gives the strain tensors in the vicinity of a fault plane, based on an analytical calculation of static stress changes caused by slip on a finite rectangular fault. Okada model is commonly used to analyze co-seismic displacement,

mainly because it is a fast method compared to more detailed methods (Hasegawa et al., 2012; Koketsu et al., 2011; Yoshida et al., 2014). The medium is a homogenous half-space and is supposed to be elastic and isotropic. Details on the method can be found in Van Zwieten et al. (2013).

We used the *Coulomb3* software, based on Okada formulas, to calculate static stress changes induced by slip on the asperity (Toda et al., 2011). Geometry is chosen according to the dimensions of the sill pillar (X between 3500 and 3900 m, Y between 450 and 550 m, Z until depth of -1108 m) and the rock parameters come from biaxial tests performed on samples from the excavation panel underlying the sill pillar (Bouffier et al., 2015). A finite rectangular plane was included in the model. Because only slip on the asperity is considered responsible for the co-seismic strain monitored on BH4 cell, the rectangular plane represents only the seismic asperity and not the entire fault plane. This plane is called the asperity and I set its location, area (width = length), strike, and dip, as well as the slip amount and the rake, based on the results of Kinscher et al. (2020). Once slip is simulated, the strain tensors are extracted and compared with CSIRO measurements (Fig. 5.5). A mesh resolution of 0,5 m is used to calculate the strain tensors. I varied the length of the asperity from 1 meter to 10 meters.

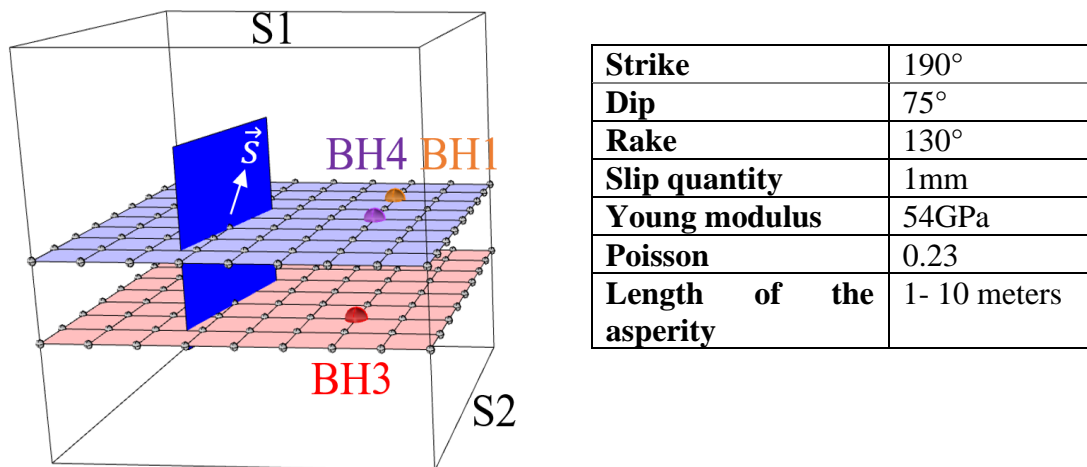


Fig. 5.5 - Conceptual scheme of the elastic model of dislocation represented in *Coulomb3*, and the input parameters. The planar free surface (S1) of the medium is traction-free and the borders of the half space (S2) are displacement-free. The asperity is represented by the blue rectangular surface, \vec{s} is the slip vector on the asperity with specific orientation (rake) and value (1mm). Purple and red surfaces indicate horizontal surfaces at BH4 and BH3 levels. Strain tensors are extracted at BH1, BH3 and BH4 cells (orange, red and purple dots). Strike is the most reliable data, dip uncertainty is approximately 30°, rake uncertainty cover values which give strike-slip and/or right lateral movements, the amount of slip can be up to a few mm. A few tests, by varying each parameter individually, have shown no significant changes in the interpretation of the results presented next section.

To account for uncertainties on location of the seismic nodal plane with respect to the cell, different scenarios were tested, by changing the location of the asperity centroid from one grid point to another, within a sphere of 10 m radius (a total of 34248 points for a 0.5 m mesh). For each

configuration, strain tensors are extracted at the strain cell positions and compared with monitored data, after calculation of principal strains. As BH4 cell is the most reliable data, values and orientations of the calculated principal strains must be within the range of uncertainties of the cell. The principal strains extracted at BH1 and BH3 must be below the detection threshold of the cells, as no reliable shift was detected by them.

The results show that possible asperity locations are concentrated in two zones (Fig. 5.6). The western cluster is closer to the seismic event location and is thus assumed to be the most likely asperity location. Average distance between the possible asperities locations within the cluster is 2m and the maximal distance is 8m, which shows the cluster is small and that possible locations are close to each other. Blue plane in Figure 5 shows one possible location of the asperity within the cluster, which was chosen qualitatively to fit best the orientations and values of the cell. The asperity is located at 6m from the seismic event of the 18th of January, which is reasonable considering error location, and its dimensions are 3m*3m. None of these zones is intersected by the drillings, what eventually explains the asperity was not identified in the drill cores.

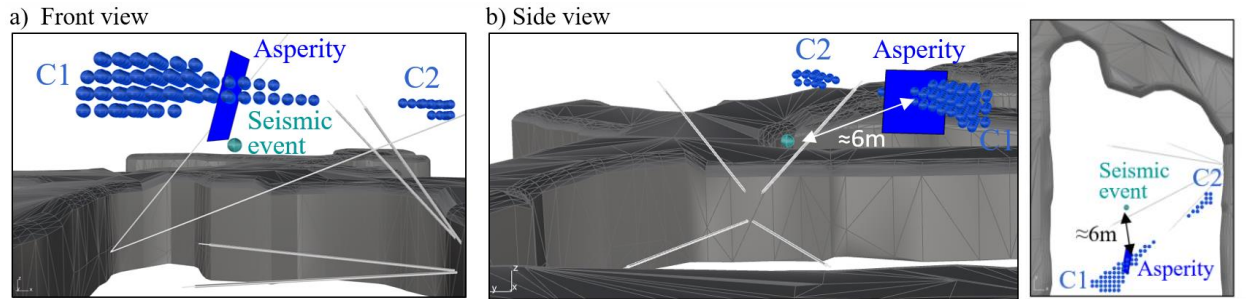


Fig. 5.6 - Clusters of locations of the seismic asperity compatible with the cells (centroids in dark blue). The monitored seismic event is shown in light blue. The dark blue surface show one possible asperity. Size is 3m*3m and is located at 6m from the event. Borehole and mine drifts are shown in grey.

For the chosen asperity, orientations of the main strains are within the ranges of uncertainties of the BH4 cell (Fig. 5.11). At the depth of BH4 cell, BH4 is located in the area of extensive deformation lobe, which is consistent with the main extensive component observed in the cell. Main extensive value is the same. Only the scalar ratio between the main elongation and the main shortening of the principal strains differs, since the ratio between the modeled values is around two whereas it is four for the cells. Anisotropy of the medium, not considered in the model, may influence this ratio.

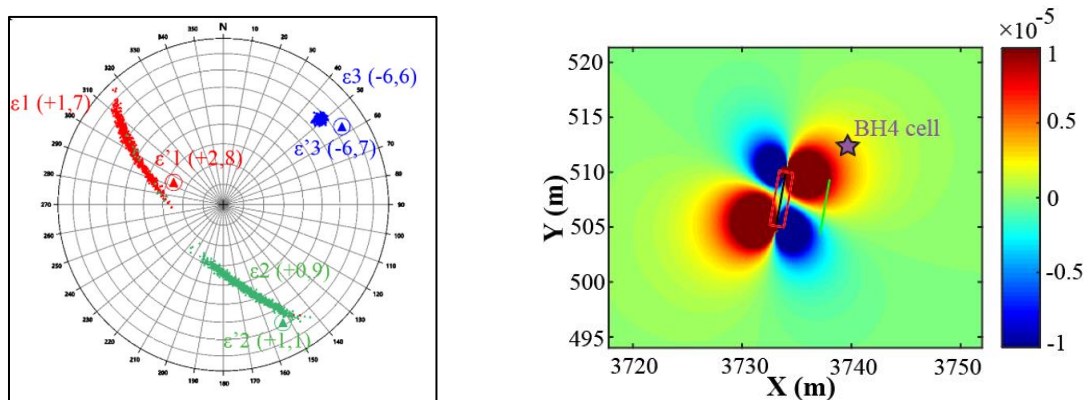


Fig. 5.7 - On the left: orientations of principal strains at BH4 cell, extracted from the model of Okada with the relocated asperity ($\epsilon'1$, $\epsilon'2$ and $\epsilon'3$) compared with real values of the cell ($\epsilon1$, $\epsilon2$ and $\epsilon3$). On the right: plane view of the asperity and its lobes of dilatation, at the depth of BH4 cell. Positive values are extension zones and blue values are shortening zones. Red rectangle represents the asperity at this depth. The purple star shows the BH4 cell, located within the extensive lobe.

5.2.4 Fault plane hosting the asperity

Combining Okada's model and strain data, I showed that it exists a solution to the inverse problem, i.e., that at least one location of seismic asperity, consistent with both geophysical analyses and strain data, can be found. The asperity is located outside the area reached by the drillings, which can explain why it was not observed in the drill cores.

If the asperity (3m*3m) is considered part of a larger fault plane, this fault plane can be extended until the zone reached by the drillings (Fig. 5.8). The minimum size of the fault to reach the drillings is 15m*15m. In this case, the fault plane meets the DH drilling exactly in Z2 fracture zone, where the only fault planes oriented like the nodal plane were observed in the drill cores (family SF5, see chapter 4). Then, the fault plane hosting the asperity is likely to be one of the fault planes of this family observed in the drill cores. As presented in chapter 4, this fault plane is filled with chlorite and muscovite. This represents a high compatibility between the location of the asperity obtained from the inversion problem (based on geophysical analyses and strain data) and the observations in the drill cores. The fault plane also meets DI drilling exactly at Z1 fracture zone, where mostly unfilled fractures with slickenlines were observed. In Z1, no fracture was oriented like the nodal plane but there was significant core loss.

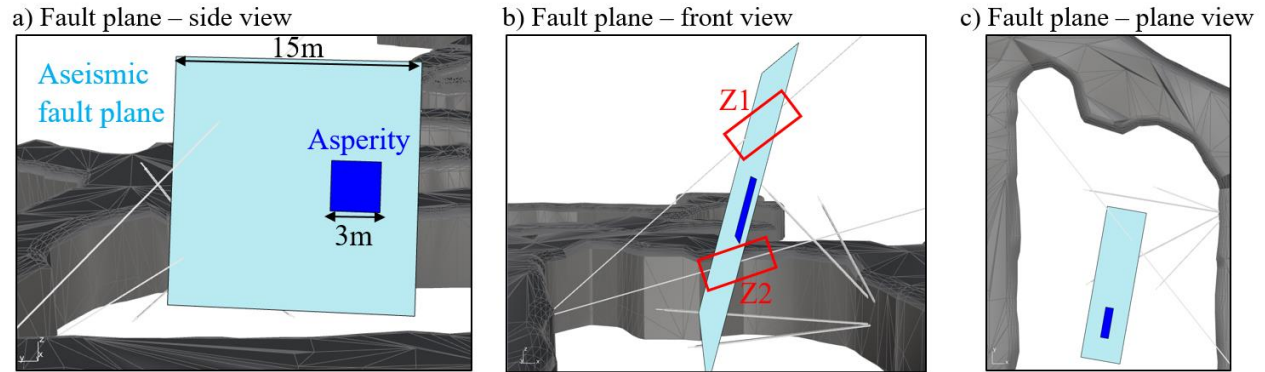


Fig. 5.8 - Fault plane hosting the asperity. The fault plane is chosen with same orientation than the asperity, and sufficiently large to meet the drillings. Z1 and Z1 fracture zones identified in the drill cores are shown in red rectangles. The fault plane crosses the drillings exactly in these two zones.

Based on these observations, it can be assumed that the asperity responsible for the coseismic shift of deformation monitored by BH4 cell may correspond to a portion (3m*3m) of a larger fault plane (15m*15m) filled with chlorite and muscovite (infilling of 1mm), at least one some portions (Z2 fracture zone). Different mechanisms are proposed to explain slip on the asperity. Firstly, the asperity can accumulate stresses due to the heterogeneity of the fault, eventually rupturing based on a simple Coulomb criterion. The repeat rupture on the fault plane is attributed to the accumulation of stresses in the same area with higher frictional properties. The heterogeneity of the fault planes is evidenced by the contrasting characteristics between Z1 and Z2 fracture zones that both intersect the fault plane. A second possible mechanism involves the presence of creep that loads the asperity. In this scenario, creep may occur within the lenses of the fault plane filled with chlorite and muscovite, and load continuously the asperity (i.e., a brittle frictional patch on the plane). The continuous and aseismic slip on the creeping portions of the fault leads to repeat rupture of the asperity. Creep can also occur on several fault planes within a wider fault zone, as suggested by the presence of several filled fault planes on the DI drilling, or even within the matrix of the rockmass itself.

5.2.5 Activation of fractures with Coulomb stress changes

In chapter 4, fractures with striation were observed in the drill cores. Considering the nodal plane given by geophysical analysis is reliable, it was shown that none of the fracture in Z1 zone is the seismic asperity. This was evidenced by the difference between their pseudo source mechanisms (i.e focal mechanisms calculated from strike, dip and rake measured on the drill cores) and the seismic source mechanism (for more detailed information, refer to chapter 4). Here, I show that slip on these fractures may have been triggered by stress Coulomb changes induced by slip on the seismic asperity. To demonstrate this, I used the concepts of receiver faults and Coulomb stress changes (CFF). The coulomb stress change is defined with the Coulomb Failure Function: ΔCFF

$= \Delta\tau + \mu\Delta\sigma_n$, where $\Delta\tau$ and $\Delta\sigma_n$ are the changes in shear and normal stresses on a plane respectively. When an earthquake occurs, coulomb stress changes can be calculated on “receiver fault planes” with specified orientation and rake direction (Lin & Stein, 2004). A positive value of ΔCFF means that the receiver fault becomes closer to failure whereas a negative value tends to move away the fault from Coulomb criteria of rupture (Orlecka-Sikora et al., 2012). Here, at least one receiver fracture (SF3 in chapter 4, see 4.6.1) within Z1 zone has a positive value of ΔCFF when slip is simulated on the asperity within Coulomb3 software (Fig. 5.9). This positive value of ΔCFF means that slip on the seismic asperity gets SF3 fracture closer from failure. Then, whereas none of the unfilled fractures in Z1 appears to be the loci of the seismic asperity, they could be activated by the stress coulomb changes caused by slip on the seismic asperity. This can explain why the optic fiber monitored strain in Z1 fracture zone after the coseismic shift of deformation monitored by the cells.

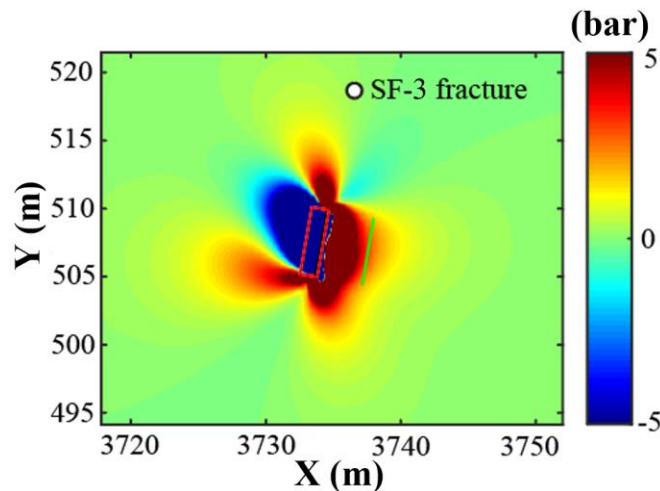


Fig. 5.9 - Plane view of ΔCFF on fault receivers oriented like SF3 fracture, at depth of SF3 fracture. The location of SF3 is shown by the dot. At this location, $\Delta\text{CFF} > 0$, which means SF3 gets closer to failure and might slip if it moves sufficiently far to reach the failure criteria.

5.2.6 Geological and strain comparison

Based on geological and seismic data, It was shown in chapter 4 that the seismic asperity is probably located outside the zone reached by the drilling. However, the geophysical data contain strong assumptions (point source model, far displacement), and I examined whether movements on planes badly oriented compared to the nodal plane can give possible scenari to explain strain values observed in the strain cells. I focused on the faults with lineation identified in the cores in chapter 4. I show that same conclusions are reached by comparing strain and geological data than in chapter 4 comparing seismic and geophysical data.

First, each of the four striated fractures were included in Coulomb3, and strain tensor was extracted at BH4 position and compared with strain cell measurements. Same method as described in 5.2.2 was used. In all cases, none of the obtained strain tensor were compatible with strain cell data (i.e.

that orientations of the extracted tensor were not in the range of uncertainties of the strain cell), confirming that none of those fractures is the seismic asperity. However, results differ from the fracture parallel to foliation with stretching lineation. This fracture has focal mechanism in agreement with seismic focal mechanism (see chapter 4), even though this fracture is not oriented like the nodal plane. The inversion method based on Okada model shows that two clusters of location of an asperity with similar orientation and slip direction than this fracture, are consistent with principal strain's orientations given by the strain cell (Fig. 5.10). One cluster is at very close vicinity from Z3 fracture zone, where fractures parallel to foliation were found. This shows that same interpretations are obtained by considering strain and geological data than when I considered seismic and geological data. The seismic asperity was probably not reached by the drilling. Although this model with asperities parallel to foliation is worthy to study further, I favor here the hypothesis than seismic events are hosted by a plane oriented like the nodal plane and that the asperity was not reached. This choice was done because a plane oriented like the nodal plane was actually observed in the cores.

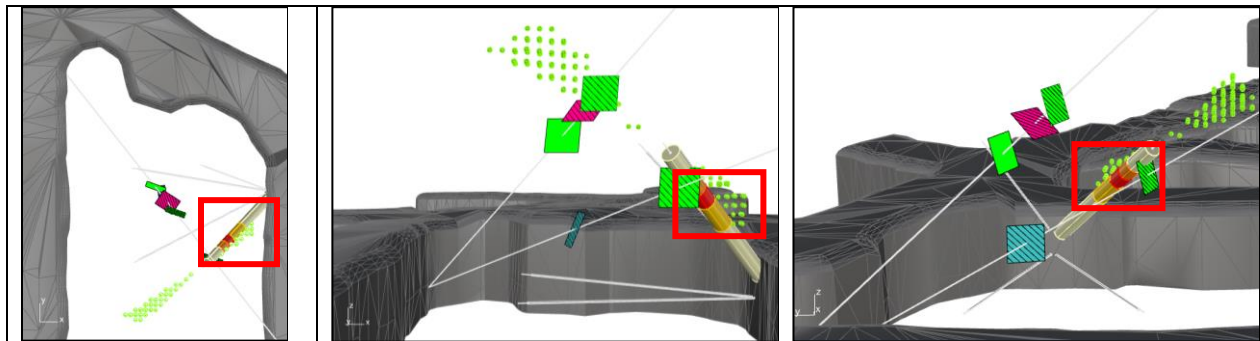


Fig. 5.10 - Clusters of location within a radius of 10 meters, around seismic centroid of the event, considering an asperity oriented like the stretching fracture observed in the drill cores consistent with seismic focal mechanism. It can be seen that, in the case such asperity was hosting seismic repeaters, it would be located at less than one meter from the Z3 fracture zone observed in BH4 borehole (area of core loss in the drill cores).

5.2.7 Perspectives: geomechanical model

From geophysical, geological and strain data, It was proposed that seismic repeaters in the sill pillar are due to the presence of a creeping fault plane loading an asperity. Creep is induced by initial stresses in the sill pillar. Here, I propose to use geomechanical model as a perspective to study further the validity of such model. The chosen software is 3DEC (Itasca), based on Distinct Element Method (discontinuous modeling approach). 3DEC is adapted to local study on joint behaviors, as a wide range of interface laws available. I aim to reproduce quasi-periodic activation of the asperity, loaded by creep on a fault plane induced by initial stresses in the sill pillar. The model described here is a preliminary model and is presented as a perspective to further geomechanical models.

Model geometry

A circular creeping plane with an asperity is included inside an isotropic and elastic medium. The plane is oriented like the nodal plane given by geophysical analyses. Sizes (areas) of the creeping fault plane and the asperity are chosen to be the same than the ones obtained from the inversion model and observations on the cores. The only difference is that the creeping fault and the asperity have cylindrical shapes instead of rectangular shapes, with the objective to limit border effects. The asperity has a radius of 1.5 m (area of 9 m²) and the creeping fault plane a radius of 8 m (area of 200 m²) (Fig. 5.11). Dimensions of the model (40m*40m*40m) are chosen sufficiently large to avoid border conditions on the creeping shape, i.e. 5 times larger than the radius of the creeping fault (radius = 8m). Location of the CSIRO cell is chosen from relative distance between the asperity and the cell after relocation of the asperity from the inversion model based on Okada formulas.

A particularity of the model is the inclusion of an external fault plane around the creeping plane, which is a construction plane imposed by the method of modeling but doesn't aim to represent any physical reality. Properties on this external plane need to be chosen to limit its influence at maximum.

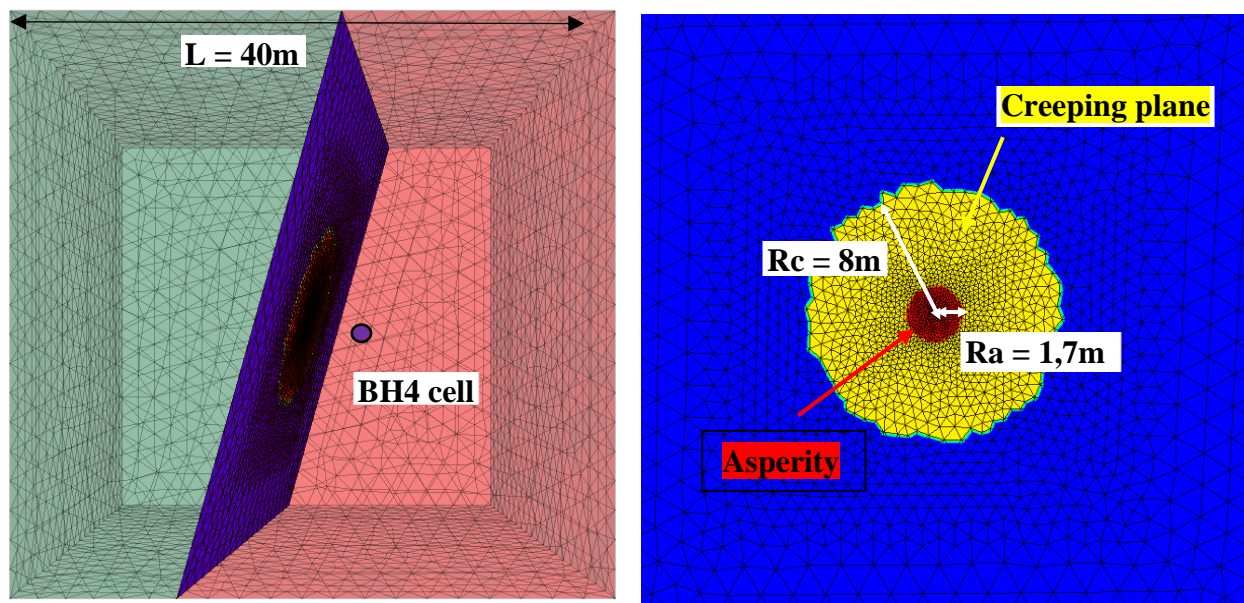


Fig. 5.11 - Geometry of the 3D model and the interface. The creeping fracture is represented in yellow (circular shape to facilitate construction) and the asperity in red. The whole fault plane is here for construction reason and doesn't have a physical reason. Size of the creeping fracture is a circular shape with a radius of 8m. The asperity is a circular patch with a radius of 1,7m.

Mechanical properties and behavior of rockmass and interface

The chosen medium is an elastic medium, with same properties than the one used in the Okada model, i.e. with a Young modulus of 54GPa and a Poisson coefficient of 0.23.

For the asperity, a softening-healing Mohr-Coulomb law available in 3DEC is employed. The softening-healing law is based on a Mohr-Coulomb criterion and allows stick-slip behavior. Once shear strength is reached and the joint starts to slip, the shear strength reduces from the peak value until a residual value over a critical distance of displacement D_c . Once slip stops, the shear strength raises instantaneously to the peak value. The creeping plane is modeled with a power creeping law, based on an adaptation of Norton's law, commonly used to model the creep behavior of soft rocks subjected to shear load (source: Itasca). The considerable advantage of this law is that it includes a time component. In a simplified formula, the creep rate is given by $\dot{\epsilon} = A * \sigma^n$, with A and n the power-law constants and exponents defined by the user. A friction coefficient of 15° is chosen for the creeping plane, which is consistent with phyllosilicates infilling. A value of 20° is chosen for the asperity to simulate the presence of a brittle frictional bump in an infilled fault plane, as observed in the drill cores. Parameters of the creep law, A and n , are given in Table 5.2. They represent a set of possible values chosen to allow a quasi-periodic time recurrence of 35 days between cyclic ruptures of the asperity. This proposal is not exhaustive, and further parametrical investigations are needed to test the influence of different parameters influencing time recurrence of the seismic events.

	Normal stiffness (Pa)	Shear stiffness (Pa)	Friction angle ($^\circ$)	residual friction angle ($^\circ$)	Dc (m)	A	n
asperity	100e9	10e9	20	15	0.000001	NC	NC
creeping fault	100e9	10e9	15	NC	NC	1.2e-17	1

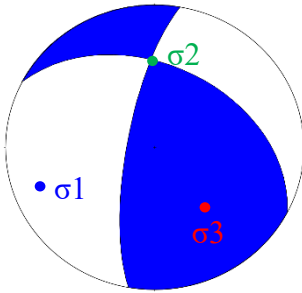
Table 5.2 - Properties of the asperity and the creeping fault plane hosting the asperity in the geomechanical model.

The external fault plane (i.e. the construction plane) is modeled as elastic and properties are chosen as proximate as possible from the elastic medium, with a first approximation based on the use of equivalent formulas given by Itasca : $k_n = \frac{K + \frac{4}{3}G}{edge_min}$ and $k_s = \frac{G}{0.01}$, with K and G the bulk and shear modulus, respectively and $edge_min$ the minimal mesh size (Daniel Billiaux, personal communication). From this first approximation, stiffnesses values are modified in order to respect the two additional following aspects: the construction plane must be sufficiently stiff to avoid the plane to slip artificially when creep starts, and it must not be too stiff so that the criteria the surrounding stiffness stays inferior to the stiffness of the asperity, which is a condition for stick-slip behavior to occur ($K_{surrounding} < Kc$, see chapter 1). In 3DEC, the criteria of instability (i.e. criteria for instability on a portion of a fault exhibiting velocity-weakening behavior) is: $Kc = \frac{\sigma_n * (\tan(\varphi_{peak}) - \tan(\varphi_{res}))}{D_c}$. The lower factor applied to stiffnesses k_n and k_s which allows the

construction plane to stay locked when creep starts on the plane is a factor of 100. Final stiffnesses are: $626e^{11}$ and $219e^{11}$.

In situ stress state, boundary conditions

The model aims to reproduce creep on the plane loaded by initial stresses in the sill pillar. Then, in a first step, in situ stresses and boundary conditions are chosen based on the state of stresses in the sill pillar calculated in chapter 4 from the focal mechanism of the repeater family. Slip on the creeping plane and the asperity are assumed to be in same direction according to Wallace-Bott hypothesis. In this case, the chosen state of stresses will induce creep and slip on the asperity with similar direction (similar rake) than the seismic rake given by geophysical analyses (Fig. 5.12). Boundary conditions are equal to in situ stresses and properties of the creeping and on the asperity are chosen close but inferior to criteria of rupture under this state of stresses. By doing so, the model reaches the equilibrium and the model converges.



	Azimuth (°)	Dip angle (°)	Value (MPa)
σ_1	251	20	57
σ_2	358	38	36
σ_3	140	45	26

Fig. 5.12 - State of stresses applied to the model. Orientations were calculated from the seismic focal mechanisms and stresses values, as described in chapter 4 section 4.3.7.

Creep activation

In a second step, creep is activated. In this case, and according to the creep definition in 3DEC the creeping plane starts to shear due to the time effect, even though stresses are below the shear strength. While creep occurs, the asperity is locked and loaded until rupture.

Results

From the results, shear stresses and shear displacements are extracted at the center of the asperity and at a point on the creeping plane, and strain deformation at the location of BH4 cell. First, it is observed that the model reproduces cyclic repeating ruptures of the asperity loaded by creep on the fault plane.

Shear stresses on the creeping plane progressively decrease whereas shear stresses on the asperity progressively increase until a peak value of 14MPa (). During this period, the asperity is locked and stresses are redistributed on the interface. Once the peak value is reached, a shear stress drop of 3.7MPa occurs, which corresponds to the rupture of the asperity. During rupture, friction coefficient drops until its residual value. Once slip has stopped, the friction coefficient returns from residual value to peak value (strengthening-healing law in 3DEC), and the asperity is loaded again

and the shear stresses increase again. Stress drop is 3.7MPa (Fig. 5.13a). A set of parameters of the power law was calibrated such as time recurrence is close to 35days, which is the value given by Kinscher et al. (2020). Shear displacement on the creeping plane increases progressively whereas slip on the asperity is divided in two phases: (i) a slow increase of displacement when the asperity is loaded, and (ii) a sudden increase of displacement when the asperity breaks (Fig. 5.13b). Seismic slip (i.e. slip which occurs when the asperity breaks) is 0.4mm per cycle, for a total slip of 0.8mm. Results are in agreement with geophysical parameters given by Kinscher et al. (2020), with a shear stress between 1 and 10MPa and millimetric slip values.

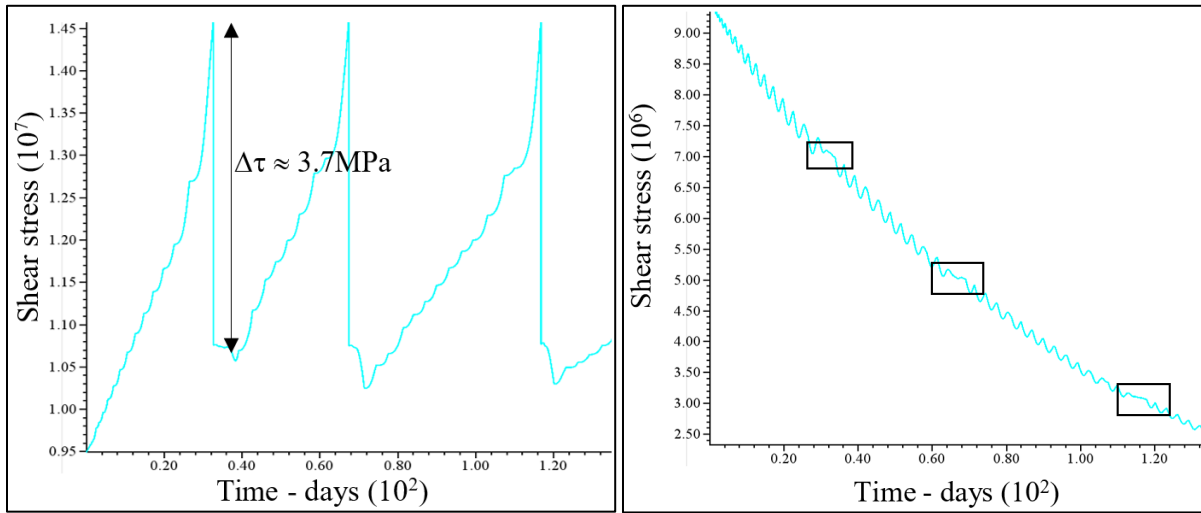


Fig. 5.13 – Time evolution of shear stress for two points: a point at the middle of the asperity (on the left) and another one on the creeping plane (on the right). Shear stress drop is indicated on the left figure. On the right, square rectangles represent periods of constant shear stress during the shear stress drops.

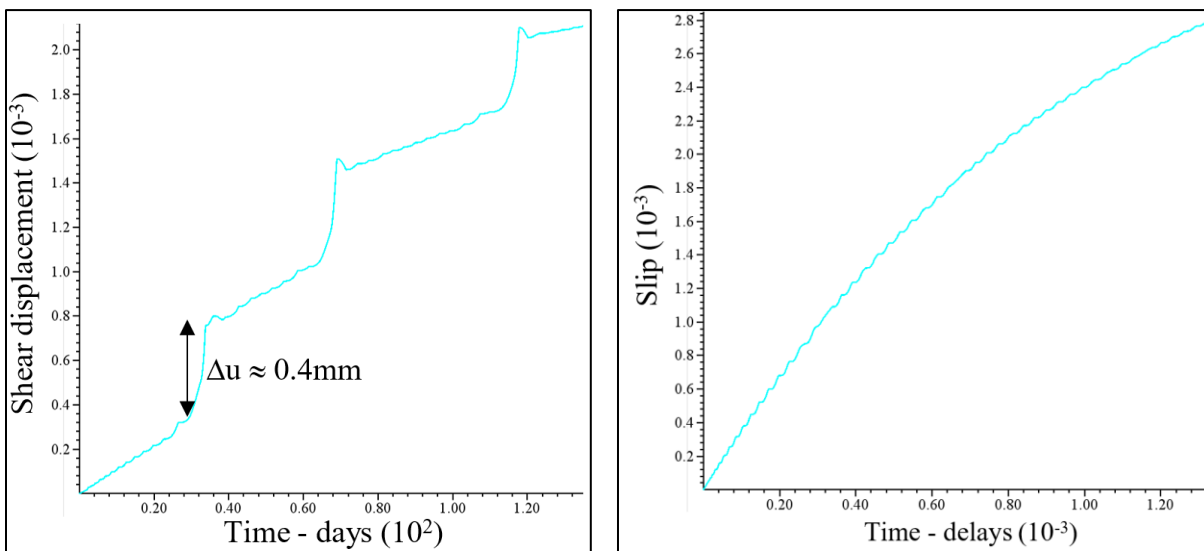


Fig. 5.14 - Time evolution of shear displacement for two points: a point at the middle of the asperity (on the left) and a point on the creeping plane (on the right). Shear displacement during the shear stress drop is shown.

Strain data was extracted at the location of BH4 and compared with data located at BH4 from Okada model and with strain monitored by the BH4 cell (Fig. 5.16). Strain increases are visible for each rupture of the asperity (Fig. 5.15). Principal strains are calculated and compared with values from the inversion model (Okada) and values measured on field (Fig. 5.16). They show similar orientations, with a main sub-horizontal extension (ϵ_3) with similar azimuth than field measurement. Intermediate strain orientation is also similar, rotated by less than 20° , and ϵ_1 has very similar dip although azimuth differ (rotation 40°). In conclusion, the geomechanical model reproduces well field measurements. Further parameter study would allow to adjust better the dimensions, location and properties of the asperity and of the entire fault plane to get closer from field measurements.

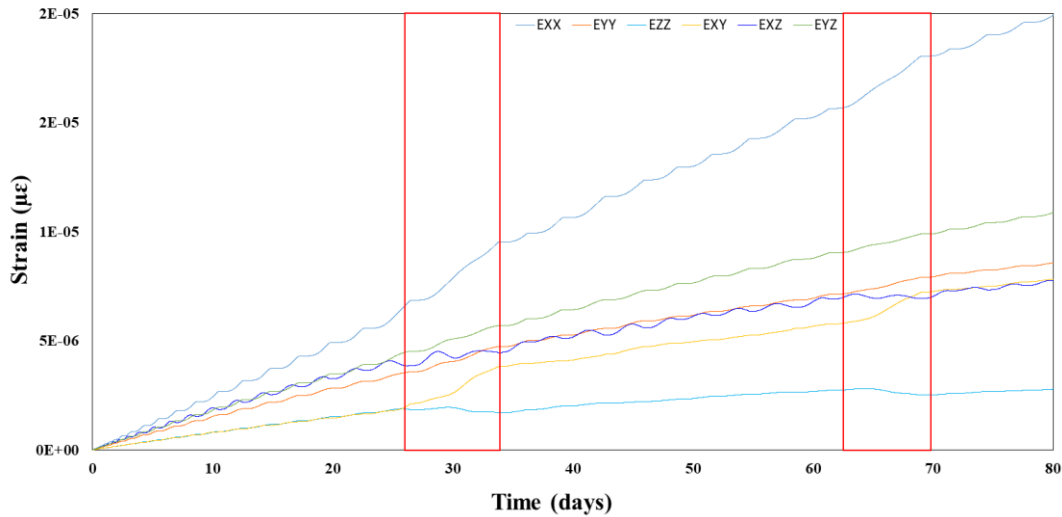


Fig. 5.15 – Time evolution of the components of the strain tensor at BH4 cell. Each curve represents a component of the strain tensor (ϵ_{xx} , ϵ_{yy} , ϵ_{zz} , ϵ_{xy} , ϵ_{xz} , ϵ_{yz}). The two red squares show two strain increase corresponding to the two first ruptures of the asperity.

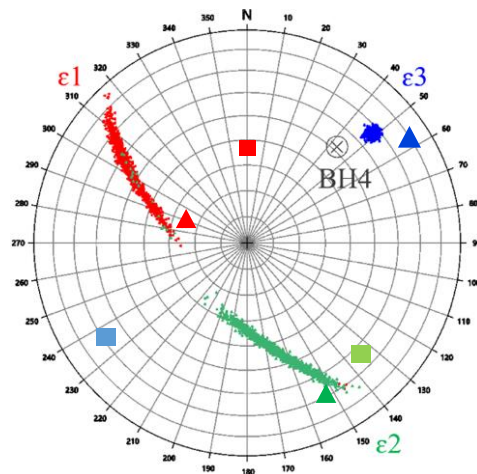


Fig. 5.16 – Principal strain measurements at BH4 cell, calculated from the 12 gauges. Data with range of uncertainties come from BH4 cell. Triangles are values from Okada model. Squares are values from the 3DEC model.

Then, such geomechanical model seems promising for further study on better characterization of the repeat rupture of a seismic asperity loaded by creep on a fault plane, and further work need to be carried out to better characterize the influence of the chosen parameters. However, the influence of construction planes is the main limitation on this model. The presence of a fault construction plane is acceptable with a careful on parameters, but they might become a major limitation in the case of the inclusion of a bloc of excavation which will include more of these construction planes. Several tests have been done with the inclusion of an excavated bloc, all unsuccessful at this stage of the study due to the reactivation of construction fault planes which don't represent any physical reality. The limit of such modeling method might have been reached.

5.2.8 Discussions

In the sill pillar, strain data was used with two objectives: (i) study deeper the location, dimensions and orientations of the seismic asperity, not reached by the drillings and (ii) study the loading mechanism of the seismic asperity. One seismic event of M-1 was monitored during the period of installation. The temporal response was immediate: only an instantaneous coseismic shift of deformation ($6\mu\epsilon$) was monitored by one cell. This event is unique, not followed by sequence of other repeaters, which is consistent with long interevent intervals observed in the sill pillar by Kinscher et al. (2020).

First, the asperity was localized using an inversion model based on the coseismic shift of deformation monitored by BH4 cell. The asperity was assumed to be hosted by a larger fault plane. The asperity was considered as a rectangular dislocation plane and Okada's model (elastic model of dislocation) was used to calculate the near quasi static strains in a semi-infinite elastic and isotropic medium (Okada, 1992; Ryosuke & Mitsushiro, 1974). The asperity was oriented like the nodal plane given by the focal source mechanism calculated by Kinscher et al. (2020). The results of the inversion model show that the asperity is located outside the area reached by the drillings, which explains why it was not observed in the drill cores. Using this inversion model and the geological data, it is proposed that repeaters might be associated with the presence of a 3m*3m asperity located on a larger 15m*15m fault plane, filled with chlorite and muscovite. An alternative orientation and location of the asperity is also proposed: the asperity could be a portion of a plane parallel to foliation (in the shear zones), close to a zone of core loss observed on BH4 drilling. Such model is also consistent with the seismic source focal mechanism and strain data.

This inversion model provides valuable information for discussing the loading mechanisms of seismogenic zones. Based on the observations, several mechanisms can be proposed. The asperity can be considered as a portion of a fault plane that accumulates stresses due to the heterogeneity of the fault plane. No creep is involved and the loading is due to high stresses in the sill pillar. This portion fails repeatedly with a simple Coulomb criterion. In this case, the filling of the fault plane plays a role in reducing the shear strength of the fault plane. Other models propose that the asperity

is loaded by creep, either on the surrounding fault plane, or within the surrounding rockmass, or on several planes in the fault zone or shear zones. The first model is most commonly used in studies of boundary plates, where seismic repeaters are generally interpreted as repeated ruptures of a brittle frictional patch on a creeping fault plane. A rate-and-state law is used to describe both behaviors: a rate-weakening behavior is given to the asperity, while creep on the surrounding plane is modeled with a rate-strengthening law (Bourouis & Bernard, 2007; T. Chen & Lapusta, 2009; Uchida & Bürgmann, 2019). The second model might induce normal stress relaxation or stress stress accumulation on the asperity. The last one is sustained by the presence of a few planes (between 2 and 4) oriented like the nodal planes observed in the drill cores and concentrated in a fracture zone. In all models, creep is constant in the sill pillar because it is induced by constant insitu stresses, rarely directly affected by the excavation of a single stope. I also proposed an alternative triggering mechanism, in which the asperity represents an unfilled portion of a plane parallel to the foliation (shear zones) embedded in chlorite-filled portions. This model is compatible with most observations, with the exception of the alignment of seismic events perpendicular to the shear zones, as shown by Kinscher et al. (2020). A possible explanation for the alignment of seismic events, perpendicular to these fractures, is an echelon mechanism. This an echelon mechanism can correspond to the linear rupture of rock bridges, or slip on relay faults between shear zones (Malek et al., 2008).

However, while this installation provides valuable clues for interpreting and listing possible mechanisms, the available data do not allow to conclude on the nature of the seismic and creeping materials, or to identify the actual triggering mechanism. This underlines the difficulty of concluding on the origin of seismic repeaters, even with such a local installation. I am however convinced that determining the triggering mechanisms is essential to understanding what is being measured by the repeaters in the perspective of using them to assess creep in the mine. In the sill pillar, the presence of a seismicity driven by creep is so far unproven, although both geological structures and mineralogy are consistent with what is expected in the presence of creep.

5.3 Example of a repeater transient

5.3.1 Description family 11 - seismicity

Centroid of Family 11 has been located at only 2,5meters from a strain cell (PH cell) and at 15meters from a second one (PD cell). Kinscher et al. (2020) highlighted two different responses after two blasts: first one was monitored the 14th of May, and is probably induced by a blast occurring the 13th of May. A second blast on 4th of June induced an instantaneous reactivation of the family (Fig. 5.2). First blast was done at almost 50m from the centroid of the repeater family, second one at less than 25 meters (Fig. 5.17). First blast extracted a volume of 7000m³ and second blast extracted a volume of 4300m³. Magnitudes of this family range between Mw -0.9 and -0.4

(moment scale magnitude). Strain evolves in function of time, which suggests the presence of creep if the load is constant. Note that for repeaters, the Nadeau and Johnson law presented in chapter 2 (Nadeau & Johnson, 1998) is usually used to quantify aseismic slip from moment of repeaters. However here, I've shown that NJ law is not applicable by calculating creep from seismic moment of a repeating sequence. NJ law gave a creep amount of 36 cm, which is highly improbable as such displacement at the vicinity of excavation would clearly be visible in the drifts. Then, no immediate correlation exist between seismic and strain data, and I study further rockmass deformation based on values and orientations of the two strain cells.

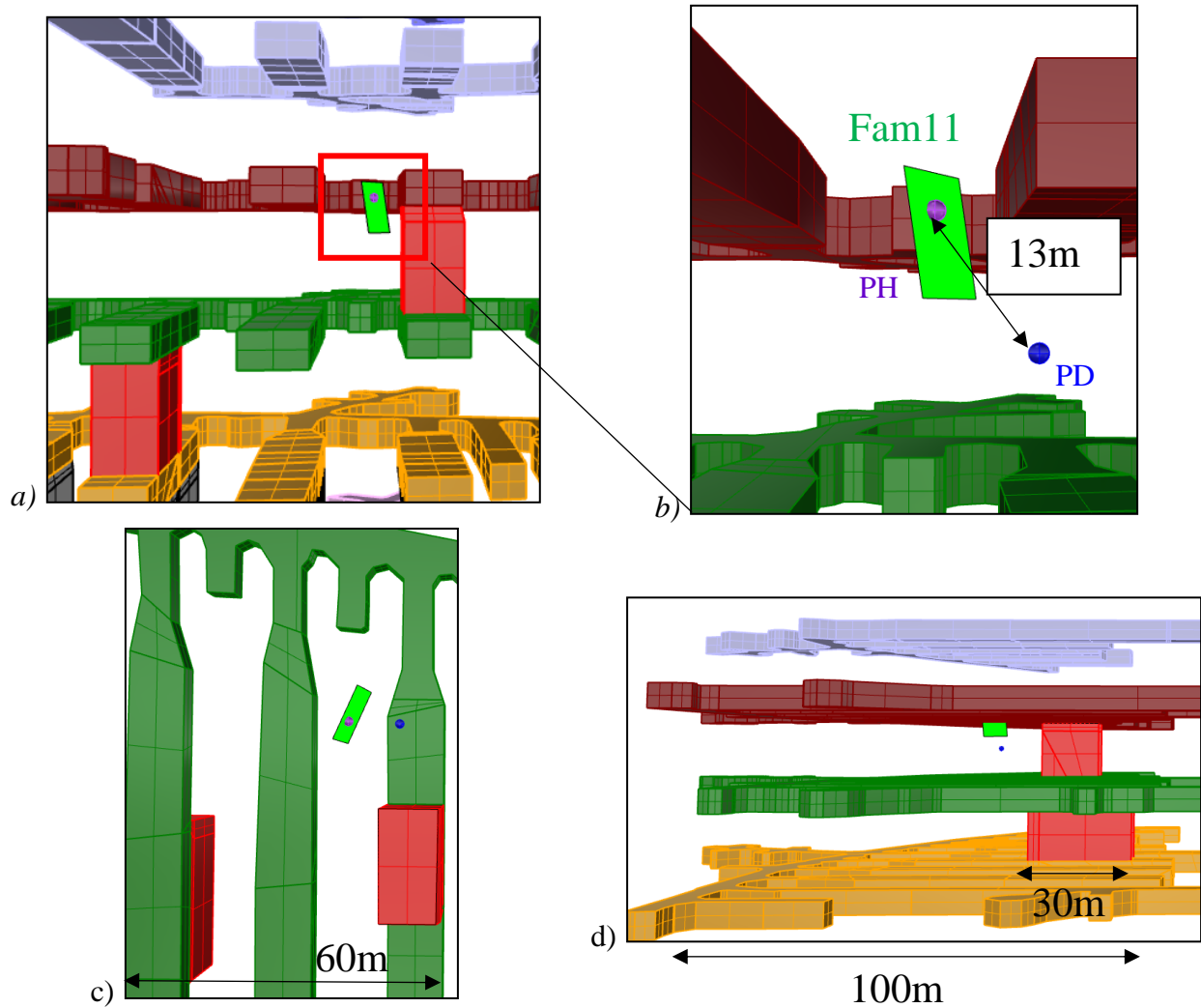


Fig. 5.17 - Location of family 11 and excavated stopes. On the left: location of the family 11 and the two stopes (in red) which induced both activation. Note that the represented stopes are the excavated or planned to be excavated stopes, whereas the blank in the figure is the rockmass. The whole stopes are shown in red to facilitate visualization. In reality, only a portion of the stope is excavated (middle portion) as the whole stope of 60meters is excavated in three different steps.

5.3.2 Comparison between post blast repeater rate and strain

For each hour of the entire month that the seismic repeaters were monitored, I calculated the strain tensor and principal strains ϵ_1 , ϵ_2 , ϵ_3 from the 12 gauges of the two cells PH and PD. For each principal strain curve, I also subtracted the glue creep rate, considering that the rate of the curves during the two days prior to the explosion is representative of the glue effect. By convention, shortening is positive and elongation is negative. In Figure 15, ϵ_1 and ϵ_3 (i.e. the main shortening and elongation values) are shown for the entire period when family 11 was active. Note that the accuracy of the cell is $\pm 5\mu\epsilon$ and that most of the highest values are around $2\mu\epsilon$, with maximum values of $8\mu\epsilon$ per hour.

Two very different strain evolution are observed for blast 1 and blast 2 (Fig. 5.18). The first blast induces a maximum immediate response of $60\mu\epsilon$ and a maximum cumulative value of $120\mu\epsilon$ (ϵ_1 on PH cell), whereas the second blast induces an immediate shift of deformation of around $350\mu\epsilon$ (ϵ_1 on PD cell). This difference is at least partially explained by the difference of distance from the blast. For the first blast, a main shortening on PH and a main extension on PD are observed. This is the contrary for the second blast, with a main extension on PH and a main shortening on PD.

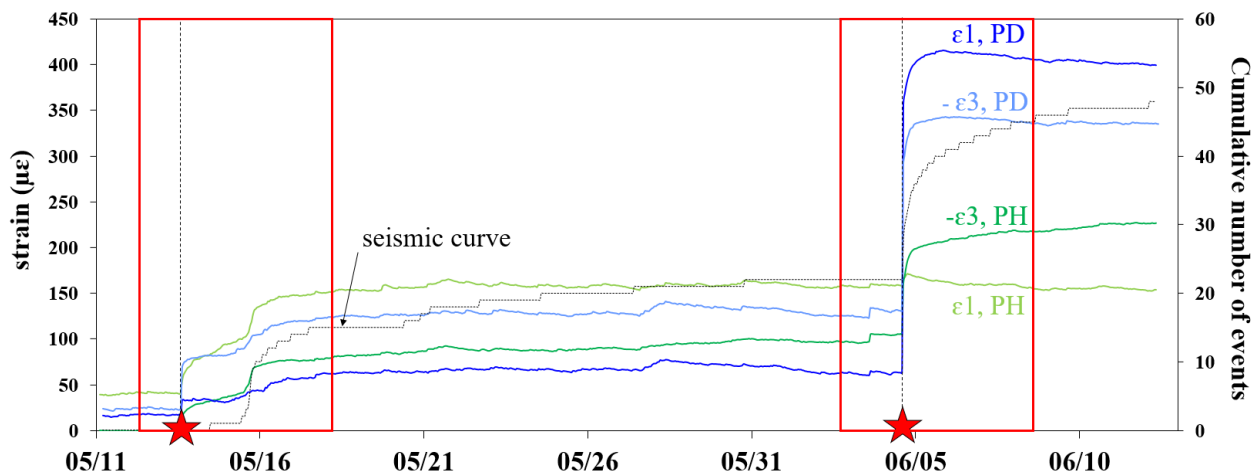


Fig. 5.18 - Main principal extensive (ϵ_3) and shortening (ϵ_1) strains on PH and PD cells for the period from 13/05/2016- until 12/06/2016. Blast inducing the shifts are shown in red stars. Dotted grey line shows the cumulative number of seismic events. Red squares indicate the intervals of first and second shifts which will be show in more details in the following.

During the first response, a remarkable creep curve was observed for ϵ_1 for the PH cell (light green curve in Fig. 5.19). Note that this curve is a creep curve with common geomechanical definition (i.e. increase of deformation with time under constant load), as the load is considered constant after the instantaneous impact of the excavation. The different phases commonly exhibited in creep curves on field or in laboratory are observed (Boukharov, 1996): a first immediate response just after the blast, a deceleration phase, a steady-state phase during a few hours, and an acceleration phase where most seismic events are monitored. During the steady phase (2 days), almost no

repeaters are monitored. A similar creeping response is observed on ϵ_3 of PH cell. Three phases are clearly visible in orientations of principal strains, calculated for the 12 gauges of each strain cells and for each hour (same method as the one described in section 5.2.2). First phase is the instantaneous response to blast directly impacted by the blast. At the second hour, the orientation changes suddenly and stays constant during the whole steady-phase period. The main extensive strain is almost aligned with the orientation of the nodal plane, and the main shortening strain is rotated at 90° on the horizontal plane from the nodal plane. The direction of the 3 principal strain axes seem constant during creep and seismic periods. However, there is an inversion between the orientations of ϵ_1 and ϵ_2 .

Interestingly the response differs for PD cell compared to PH cell for the first blast (blue curves on Fig. 5.19). Almost all the deformation is monitored during the first hour following the blast, and almost no creep curve is observed. This differs from PH cell where only a small portion of the deformation was monitored during the hour following the blast and continued to increase with time following a classic creep curve. This indicates that the rockmass was creeping at PH location but almost not at PD. This suggests creep is more localized in some regions than others, either due to a discontinuity or due to stiff and weak rocks at close vicinity (mica altered and stiff non-altered Micaquartzites).

For the second blast (closer to strain cells), the strongest deformation is monitored by the PD cell (Fig. 5.20). The strain response is instantaneous and almost all strain occur during the hour of blasting. Seismicity also starts instantaneously after blast, on the difference of the delayed response for the first blast. Unlike for the first blast, neither a steady state nor an acceleration phases of creep response are observed. This curve looks like usual mine response to excavation, where 50-100% of the strain change is monitored during the first minute of a mine blast (Hudyma et al., 1994). Two different orientations are observed in this second response. First, a clear orientation is observed during the few hours after blast on PH cell. Then, the same orientation as monitored for the first response is also monitored (with inversion between ϵ_2 and ϵ_3). The presence of two orientations is very consistent with the spatiotemporal migration of seismic events observed on family 11 by Kinscher et al (2020), which observed that repeaters from family 11 could be classified in two different sub groups.

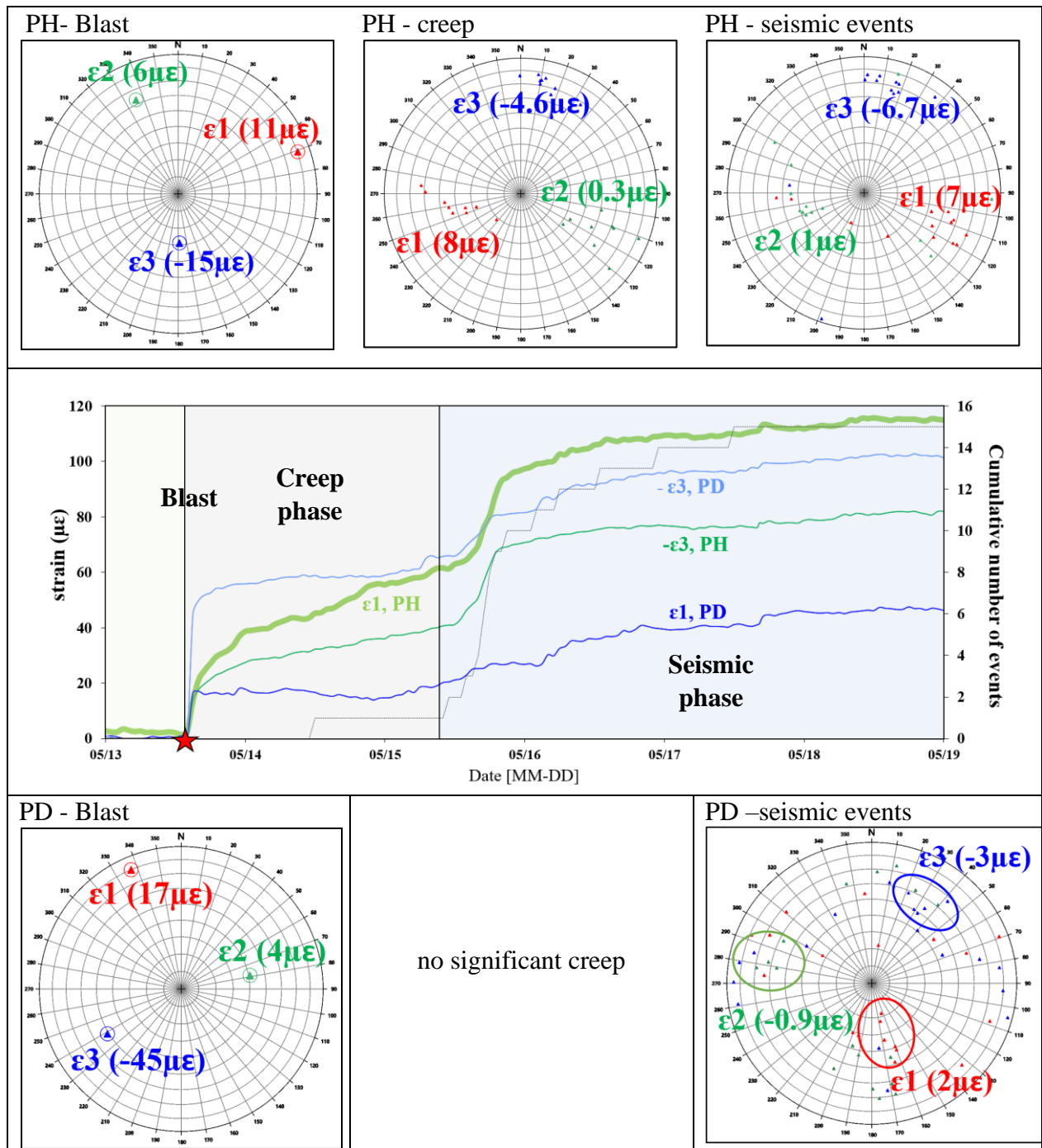


Fig. 5.19 - Zoom of the figure 15 during the first response post-blast, i.e. the period between 12/05 and 19/05/2016. As for figure 15, principal strains and the cumulative number of seismic events are shown. Same colors are used than in Fig. 5.18. Red bar indicates the time where the number of seismic events increase with time (accelerated phase of creep). Principal strain orientations for PH (above) and PD (below) cells are added. From left to right: strains measured during the hour of the excavation, creep during first shift, seismic events during first shift. On the figures, only data with strain $>2\mu\epsilon$ are used.

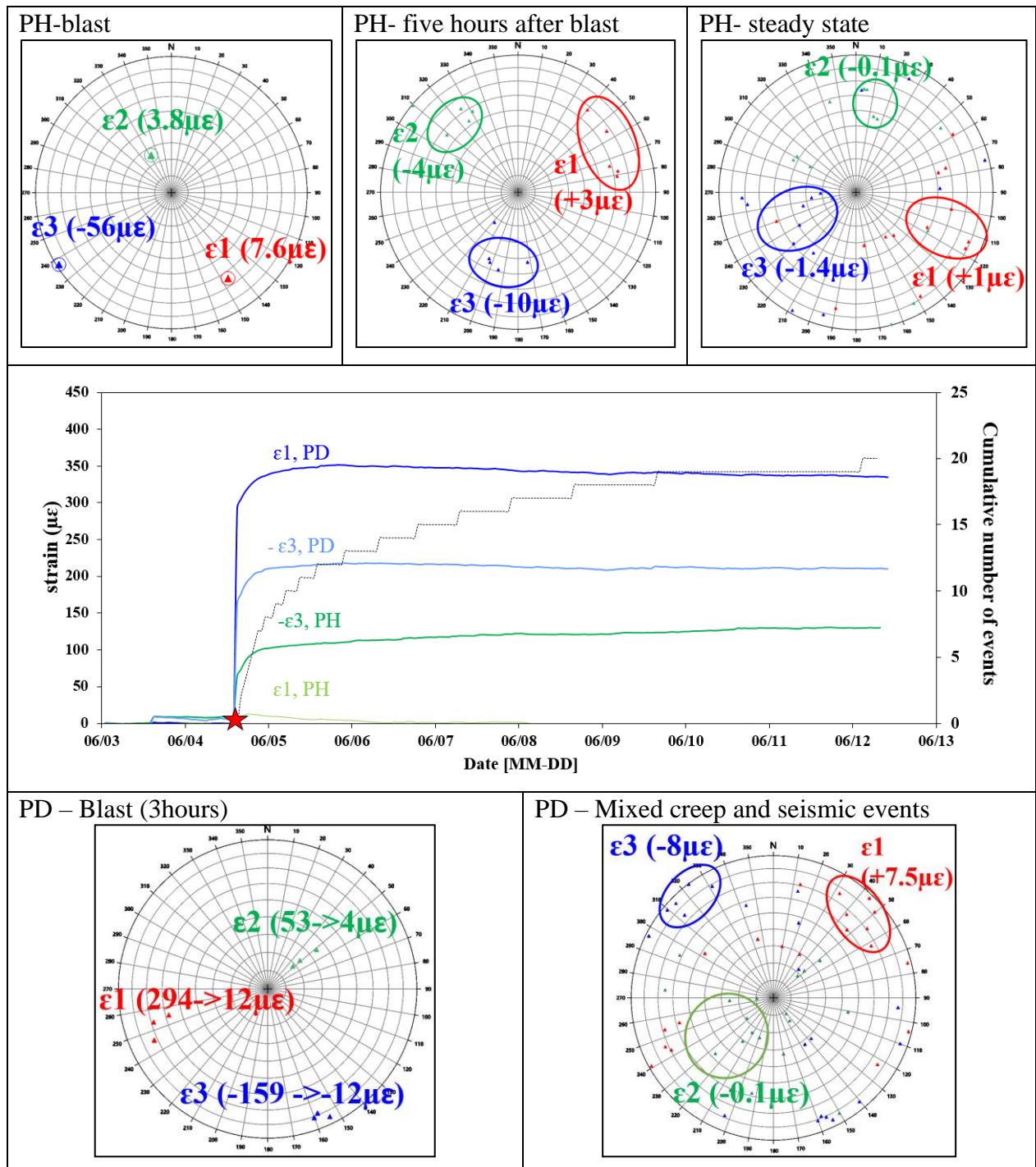


Fig. 5.20 - Zoom of the figure 15 during the first response post-blast, i.e. the period between 04/06 and 12/06/2016. Same colors and legends are used than in Fig. 5.19. The response is instantaneous and almost no creep is monitored. For PD blast, three orientations are shown because the influence of blast lasts during three hours (with strong decrease in strain values indicated by the two presented values). For other phases, maximum values of strain are shown. On the figures, only data with strain $>2\mu\epsilon$ are used.

5.3.3 Role of the excavation in the triggering of seismicity

In chapter three, It was shown that family 11 is likely to slip under the influence of the excavation, although temporality is not explained, considering stresses given by the 3D geomechanical model of De Santis (2019). Here, I followed same method but using strain cells instead of the 3D model. I assumed that the stress tensor calculated during blast was as an indicator of stresses acting on the fault plane during this hour, as PH is very close to the asperity. With same method that described in chapter three, stress paths during the 52 steps of excavation of the block 1250 were obtained (Fig. 5.21). Two different values of coefficient of friction were considered for the Coulomb criteria: $\mu=0,36$ and $\mu=0,23$. First value is a typical value on fractures, second one is representative of fractures with phyllosilicate infilling. Steps where seismicity is monitored are steps 34 and 37. Results show that all steps from 11 are likely to be activated, which is similar that what was observed in chapter three. Step 11 and step 29 play a major role. Step 11 clearly moves the fault plane towards rupture, whereas step 29 moves away the fault plane from rupture, even though it stays above the lower criteria of rupture.

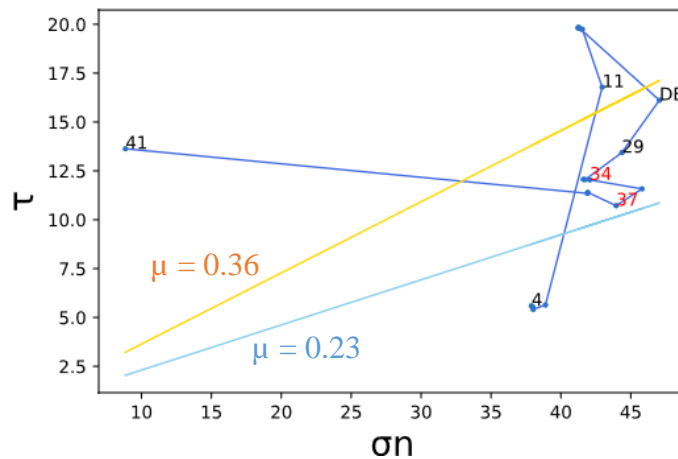


Fig. 5.21 - Stress paths for the thirteen main shifts of deformation monitored by PH cell during the 52 steps of excavation of the block 1250 between 2015 and 2016. Number refers to step of excavation. The two lines represent two different Coulomb criteria, for coefficient of friction $\mu = 0.36$ and $\mu = 0.23$. As mentioned in chapter 4, $\mu = 0.23$ is a low coefficient of friction consistent with phyllosilicate infilling. Steps 34 and 37 in red represents the steps which induced the first and second shifts of seismicity.

From step29, values of σ_1 decrease significantly (Fig. 5.22). Also, a change of orientation of the principal stresses is observed (same as principal strains as the medium is elastic and isotropic). From step 29, orientation of σ_1 is more consistent with focal mechanism, as they are within the dilatational quadrant (Lisle, 1992). Step 29 represents the excavation of the first portion of the last pillar of stope 13 (middle stope). Then, orientation seems to play a major role in the activation of the fault plane and could explain why seismicity occurs only after step 29 even though higher shifts can be monitored before. However, there is no explanation why seismicity appeared on steps 34

and 37 and not at other steps after step 29, which is probably due to the fact the asperity is close to rupture since step 29, and that a very small stress change can induce seismicity.

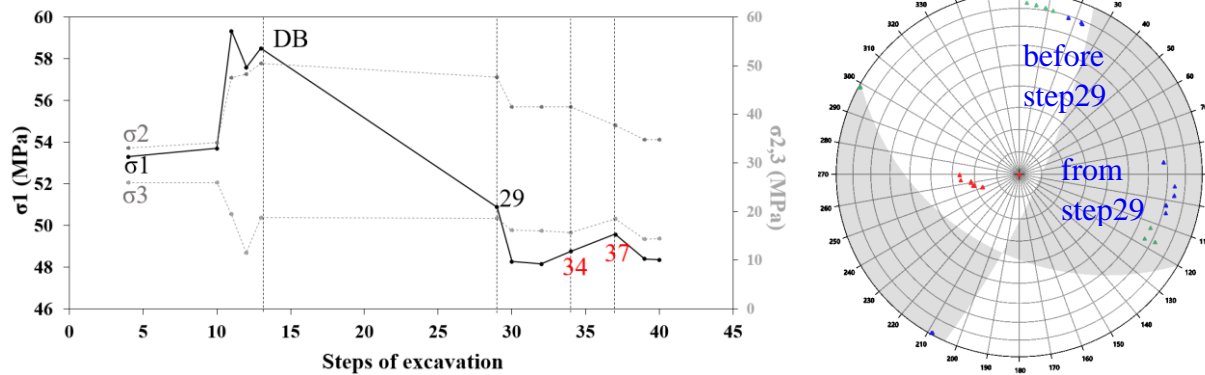


Fig. 5.22 - Values and orientations of principal stresses (positive compressions). On the left: strains values in function of steps of excavation. Continuous line represents σ_1 , dotted lines σ_2 and σ_3 . Evolution of stresses is clearly visible for σ_1 , with an increase of values until 60MPa, and then a decrease occurring during step 29. Seismicity occurs at step 34 and step 37. Change of orientations is clearly visible from step 29 on the right figure. Dilatational quadrants are shown in dark on the right figure (opposite at the usual convention with dark compressive quadrant).

5.3.4 Analyses and discussions

We observed two different responses of family 11 for two different blasts. The first one is induced by a distant blast and shows a creeping response with a progressive increase of strain. A value of $60\mu\epsilon$ is reached (ϵ_1) after two days, and the sequence of seismic repeaters starts associated with an increase of strain until $120\mu\epsilon$ (ϵ_1). A possible explanation is that the seismic asperity is first loaded by the progressive creep until the stress threshold needed to activate slip on the asperity is reached. Because stope is distant from the repeater family in the case of the first response, the threshold is not reached immediately after the blast. For the second blast, the excavated stope was very close from the repeater family and directly reached the threshold. Note that the seismic asperity was also probably close to rupture since the influence of the first blast was still ongoing.

An evolution of direction of main strains was clearly highlighted on PH cell during first response. Within an hour of the blast, strain directions directly changed and stayed constant during the whole creeping phase. Then, creep occurs immediately in one main direction. The orientation can be influenced for example by the presence of a discontinuity or an anisotropy in stresses. An inversion between ϵ_1 and ϵ_2 is observed during the seismic phase, compared to the aseismic phase. Then, creep orientation is not parallel to the orientation of seismic movement, which is not in agreement with Wallace and Bott hypothesis. It is not clear if this difference is an instrumentation artefact or whether it represents a field reality: differences between values of ϵ_1 and ϵ_2 suggest this is probably

not an artifact. If it is assumed that creep is located on a discontinuity, a possible interpretation is the presence of striation or other geometrical irregularities on the asperity, which influences slip direction (Kirkpatrick & Brodsky, 2014; Macklin et al., 2021).

A difference of creep orientations was observed for the responses after the first and the second blast, at least for the few hours following the second blast. This difference of strain orientations whereas seismic repeaters are monitored in both cases suggests that the creep doesn't occur on a unique fault plane but can be distributed in a rockmass volume. After a few hours, orientations of main strains are similar to the first blast (with inversion of ϵ_2 and ϵ_3). This means that creep starts as a diffuse mechanism in the rockmass and then progressively localized along a discontinuity. This is similar to progressive localization mechanism used to explain triggering of seismic events on large-scale fault planes in seismology, and highly consistent with creep tests in laboratory where seismic events are first diffuse in the sample and align along a shear plane (see chapter 1). When creep occurs in the rockmass, two main mechanisms are possible. First, slip can be induced by a localization of shear stresses along a pre-existing discontinuity, which corresponds to the progressive shear localization. Slip can also be induced by a progressive decrease of normal stress on a discontinuity, due to creep in the surrounding volume.

5.4 Conclusions

In this chapter, triggering mechanism of seismic repeaters were investigated, by combining local strain information with geological and geophysical data. I focused on the analysis of cell data for two repeater families close to strain cells. One of the family is located in the sill pillar and exhibits a quasi-periodic trend whereas the second family is located in an excavation panel and exhibits an Omori-like response.

For the first family, an inverse elastic dislocation model (Okada model), based on strain measurements monitored by strain cells during a unique seismic event, enabled to locate and constrain dimensions of the seismic asperity. The asperity was located outside the area reached by the drillings, which can explain why the asperity was not observed in the drillings. Assuming the asperity is located on a larger fault plane crossing the drillings, it was shown that the plane reaches the drillings where phyllosilicate filled faults have been observed. From these observations, it was deduced that the classical model based on an asperity on a creeping fault plane is consistent with field data.

For the second family (transient repeaters), temporal evolutions of values and orientation of principal strains were calculated in the rockmass surrounding the family, for the whole month where the family was active. Two different seismic and strain responses were observed for two different blasts (first blast was close to cells and second one further). The first response exhibited a delayed seismic response after a creep period of two days. Strain increased progressively during the creep phase. The second blast induced an immediate increase of both strain and seismic

responses, and almost all strain was monitored during the minute of the blast. For both blasts, strain orientation changes during and right after the blast, which highlight that two different mechanisms exist (inside the rockmass and a fault?). For both blasts, the same creep orientation is observed. However for the second blast, an additional creep orientation is observed during a few hours after blast, which suggests the presence of a diffuse mechanism in the rockmass with a progressive localization on a discontinuity, similar to progressive localization models used in seismology to explain triggering of foreshocks (Kato & Ben-Zion, 2021).

Conclusion and perspectives

This PhD is dedicated to understand what host seismic repeaters (plane or rock mass) and what are the loading mechanisms of the seismic asperities (i.e. static stress changes, aseismic creep), combining observations at different scales, using methodologies from geophysics, structural geology, geomechanics and numerical modeling. Such type of analysis on repeaters is rarely done in the mines, but it has been widely studied by seismologists at the geodynamics scale. They found that the definition of creep and asperities are scale-dependent, but the classical model for repeaters remains that it corresponds to a unique asperity on a fault plane loaded by creep on the surrounding area, and that creep and seismic behavior are deeply related to mechanical and physical properties of the faults, and to the state of stress (Mcllaskey & Yamashita, 2017; Saffer & Marone, 2003)

First, at the scale of the orebody, I have shown that seismic repeaters are statistically more localized in rocks containing phyllosilicate minerals, moderately fractured, and likely to support a certain amount of stress. However, these rocks are frequent in the orebody and other elements, such as discontinuities, must be involved to explain the presence of such repeaters. The use of a continuous large scale elastoplastic model provided by De Santis et al. (2020)) have shown that in some cases, stress changes induced by excavation steps could induce the activation of faults oriented as the nodal planes of repeaters. This indicates that, at large scale, a link can be made between fault hosting repeaters activity and the mine excavation. But it was not possible to explain the temporality of seismicity events with the excavation steps, and the scale of the study did not allow to get details on any mechanisms nor properties.

In a second step, I treated a dataset acquired from a local network centered on one specific repeater family and composed of 6 cored boreholes and 4 strains cells. Several fractured zones were identified and one family of fractures oriented like the nodal plane, and with phyllosilicate infilling (<1mm), possibly interpreted as the creeping part of the fault. Few markers of slip could be identified in the cores, but none of them have an orientation compatible with the preferential nodal plane inferred from seismic events alignments and focal mechanisms. No evidence was found in the cores, such as wear and roughness, intense deformation, or gouge on a surface, that could allow to appoint a specific zone as the asperity. Whether the drillings crossed it or not, this reveals the difficulty of catching and defining a mechanical asperity in a fractured rock mass from cored boreholes, for such small magnitude events.

In a third step, I took a closer look at the strain measurements, and at the cumulative number of seismic events on two repeaters families, including the one presented previously. The families present two different temporal recurrences: one is quasi-periodic (1 event every ~35 days since years), where the number of events for the second one follows an Omori law (decay in $1/t$, during a month). For the first family, I proposed a solution for a fault plane containing a seismic asperity (3 m in size) and a creeping area (>15 m in size), based on an inversion model using deformation

cells, Okada elastic dislocation model and borehole fractures orientations. The fact that a solution exists suggests that the classical model of repeaters, i.e. an asperity loaded by a creeping zone on a fault, may apply in that case. This also provides a value of asperity and loading zone sizes for a M_w -1 event.

For the second family, it was shown that a distant excavation blast induced a sudden strain step, followed by two days of strain increase (creep), itself followed by a seismic sequence. Strain tensors calculations showed a sudden change of principal strain axis during and after that blast, suggesting that the instantaneous strain and the creep are not supported by the same features (rock mass versus fault?). Then the creep seems to trigger the seismic sequences, with this time a permutation of the principal strain axis at the onset and during the seismic sequence. Here again, results show a difference between what occurs during creep and seismic event. This can be explained for example because creep occur in the rockmass and not on the fault, or because slip orientation differ from aseismic slip in the plane due to geometric striation which reorient the slip. PD cell monitors almost no creep, which shows that two cells at close proximity can monitor very different responses. This confirms that creep is localized in some regions, either on a discontinuity or inside weaker rockmasses. A second blast, closer to the strain cell, showed a concomitant and sudden strain and seismic increase. As for the difference than for the first blast, a change for principal strain axis orientations is observed during and right after the blast, even if less pronounced. Five hours after the second blast, the principal strain axis orientations get back the orientations observed during the creep phase of the first blast response, telling that two creep orientations exist.

Those results drive major conclusions regarding loading of asperities and creep response.

- First, different observations were made from three different cells, where the main difference is the loading of the area via either constant stresses, stress changes due to a distant blast or stress changes due to a close blast. The high difference between the observed strain responses shows that creep is highly dependent of the loading mechanism. Also, different responses were observed on PH and PD cells, which are very close to each other, which suggest that creep response is spatially heterogeneous in the rockmass.

- Creep can be interpreted either due to creep on a fault plane, or either due to creep in the rockmass. The two interpretations depend on whether that strain monitored on PH cell, very close to the repeater family, is considered representative of the aseismic slip on a fault or of the rockmass deformation in a volume at a few meters from the cell.

- Even for different blasts, creep aligns in same direction after a few hours, which suggests same predominant creep mechanism occur. For a close blast with high instantaneous strain increase, a first different creep orientation is observed for the first hours after blast, which also suggests a progressive localization mechanism, at least in some cases (i.e. diffuse creep in a whole rockmass volume and progressive localization along a discontinuity).

Studying small events in mines is not trivial, even with such a local installation at close vicinity from seismic source. It appears difficult to apply the same metrics, and empirical laws than for events on much larger faults, especially because the available dataset are not the same. For instance:

- Seismological studies on major faults are mostly based on geodetic measurements at the surface (near-field GNSS, InSAR, strainmeters). These measurements involve several points of measurements on large horizontal surfaces, whereas repeaters in the mine are observed directly at depth, with very local strain measurements in 3D.

- Measurements at geodynamic scale are made nearby large and well-identified fault planes. Small events in the mines can be hosted on small features, difficult to localize precisely, and strain gauges are unlikely to be very close to them.

- Seismological models assume repeaters are asperities on a larger fault plane. As mentioned in chapter 1, source mechanisms in mining are more diverse and might be associated with other mechanisms, and the famous double-couple model may not apply to interpret seismic data.

Recently the ANR research project FIMOPTIC aims at improving monitoring of seismic repeaters in Garpenberg by using comprehensive and innovative fiber optic technologies. This project gives precious perspectives on limitations just presented. In a first step, potential seismic repeater source are located in high accuracy by installing numerous geophones in Sill-Pillar as well as optical fibers interrogated by DAS (Distributed acoustic sensing). The precise location of seismic repeaters is a predominant data in this study, as drillings can easily miss the target asperity for an error location of a few meters. Once repeater location is known further on-off fault drillings and in-situ strain measurements will be performed using high sensitive optical strain-meters and a standard monitoring devices. Data from optical strain-meters is continuous in time and space and will be more suitable to include them in inverse seismological models.

Bibliography

- Ahmadi, O., Juhlin, C., Malehmir, A., & Munck, M. (2013). High-resolution 2D seismic imaging and forward modeling of a polymetallic sulfide deposit at Garpenberg, central Sweden. *Geophysics*, 78(6). <https://doi.org/10.1190/GEO2013-0098.1>
- Al-Jaroudi, S. S., Ul-Hamid, A., Mohammed, A. R. I., & Saner, S. (2007). Use of X-ray powder diffraction for quantitative analysis of carbonate rock reservoir samples. *Powder Technology*, 175(3), 115–121. <https://doi.org/10.1016/j.powtec.2007.01.013>
- Allmendinger, R. W. (2019). FaultKin 8.1 manual. In *FaultKin software*.
- Allmendinger, R. W., Cardozo, N., & Fisher, D. M. (2012). Structural geology algorithms: Vectors and tensors. In *Structural Geology Algorithms: Vectors and Tensors*. <https://doi.org/10.1017/CBO9780511920202>
- An, M., Zhang, F., Zhang, L., & Fang, Y. (2018). Proceedings of GeoShanghai 2018 International Conference: Rock Mechanics and Rock Engineering. *Proceedings of GeoShanghai 2018 International Conference: Rock Mechanics and Rock Engineering, March 2019*. <https://doi.org/10.1007/978-981-13-0113-1>
- Andrieux, P., Hudyma, M., O'Connor, C., Li, H., Cotesta, L., & Brummer, R. K. (2008). Calibration of large-scale three-dimensional non-linear numerical models of underground mines using microseismic data. *Continuum and Distinct Element Numerical Modeling in Geo-Engineering, June 2016*, 1–9.
- Angelier, J., & Mechler, P. (1977). Sur une methode graphique de recherche des contraintes principales egalement utilisables en tectonique et en seismologie: la methode des diedres droits. *Bull. Soc. Géol. France*, 1309–1318.
- Ashby, M. F., & Sammis, C. G. (1990). The damage mechanics of brittle solids in compression. *Pure and Applied Geophysics*, 133(3), 489–521.
- Askaripour, M., Saeidi, A., Rouleau, A., & Mercier-Langevin, P. (2022). Rockburst in underground excavations: A review of mechanism, classification, and prediction methods. *Underground Space (China)*, 7(4), 577–607. <https://doi.org/10.1016/j.undsp.2021.11.008>
- Avouac, J. P. (2015). From geodetic imaging of seismic and aseismic fault slip to dynamic modeling of the seismic cycle. *Annual Review of Earth and Planetary Sciences*, 43, 233–271. <https://doi.org/10.1146/annurev-earth-060614-105302>
- Bakun, W. H., King, G. C. P., & Cockerham, R. S. (2013). *Seismic Slip, Aseismic Slip, and the Mechanics of Repeating Earthquakes on the Calaveras Fault, California*. 37, 195–207. <https://doi.org/10.1029/gm037p0195>
- Barros, L. De, Daniel, G., Guglielmi, Y., Rivet, D., Caron, H., Payre, X., Bergery, G., Henry, P., Castilla, R., Dick, P., & Barbieri, E. (2016). *Journal of Geophysical Research : Solid Earth of fluid-induced fault reactivation*. 1–17. <https://doi.org/10.1002/2015JB012633>. Received
- Bedford, J., Moreno, M., Baez, J. C., Lange, D., Tilmann, F., Rosenau, M., Heidbach, O.,

- Oncken, O., Bartsch, M., Rietbrock, A., Tassara, A., Bevis, M., & Vigny, C. (2013). A high-resolution, time-variable afterslip model for the 2010 Maule Mw = 8.8, Chile megathrust earthquake. *Earth and Planetary Science Letters*, *383*, 26–36. <https://doi.org/10.1016/j.epsl.2013.09.020>
- Beroza, G. C., Cole, A. T., & Ellsworth, W. L. (1995). Stability of coda wave attenuation during the Loma Prieta, California, earthquake sequence. *Journal of Geophysical Research*, *100*(B3), 3977–3987. <https://doi.org/10.1029/94JB02574>
- Bohnhoff, M., Wollin, C., Domigall, D., Küperkoch, L., Martínez-Garzón, P., Kwiatek, G., & Malin, P. E. (2017). Repeating Marmara Sea earthquakes: Indication for fault creep. *Geophysical Journal International*, *210*(1), 332–339. <https://doi.org/10.1093/gji/ggx169>
- Boskovic, M. (2022). Challenges of resuming the production after a major seismic event at LKAB's Kiirunavaara mine. *10th International Symposium on Rockbursts and Seismicity in Mines (RaSiM10)*.
- Bott, B. M. H. P. (1959). The Mechanics of Oblique Slip Faulting. *Geol. Mag.*, *XCVI*(2).
- Boukharov, N. G. (1996). The three processes of brittle crystalline rock creep G. N. Boukharov, M. W. Chanda & N. G. Boukharov, *International Journal of Rock Mechanics & Mining Sciences*, *32*(4), 1995, pp 325–335. *International Journal of Rock Mechanics and Mining Science & Geomechanics Abstracts*, *33*(3), A117. <http://linkinghub.elsevier.com/retrieve/pii/0148906296869956>
- Bourouis, S., & Bernard, P. (2007a). Evidence for coupled seismic and aseismic fault slip during water injection in the geothermal site of Soultz (France), and implications for seismogenic transients. *Geophysical Journal International*, *169*(2), 723–732. <https://doi.org/10.1111/j.1365-246X.2006.03325.x>
- Bourouis, S., & Bernard, P. (2007b). Evidence for coupled seismic and aseismic fault slip during water injection in the geothermal site of Soultz (France), and implications for seismogenic transients. In *Geophysical Journal International* (Vol. 169, Issue 2, pp. 723–732). <https://doi.org/10.1111/j.1365-246X.2006.03325.x>
- Bradbury, K. K., Evans, J. P., Chester, J. S., Chester, F. M., & Kirschner, D. L. (2011). Lithology and internal structure of the San Andreas fault at depth based on characterization of Phase 3 whole-rock core in the San Andreas Fault Observatory at Depth (SAFOD) borehole. *Earth and Planetary Science Letters*, *310*(1–2), 131–144. <https://doi.org/10.1016/j.epsl.2011.07.020>
- Brantut, N., Baud, P., Heap, M. J., & Meredith, P. G. (2012). Micromechanics of brittle creep in rocks. *Journal of Geophysical Research: Solid Earth*, *117*(8), 1–12. <https://doi.org/10.1029/2012JB009299>
- Brown, L. G. (2018). *Quantification of Seismic Responses to Mining Using Novel Seismic Response Parameters*. 286.
- Brown, L. G. (2021). Quantifying discrete seismic responses to mining. *Canadian Geotechnical Journal*, *58*(7), 1023–1035. <https://doi.org/10.1139/cgj-2020-0248>
- Brown, S. R., & Scholz, C. H. (1985). Broad bandwidth study of the topography of natural rock

- surfaces. *Journal of Geophysical Research*, 90(B14).
<https://doi.org/10.1029/jb090ib14p12575>
- Bullock, R. J., De Paola, N., Holdsworth, R. E., & Trabucho-Alexandre, J. (2014). Lithological controls on the deformation mechanisms operating within carbonate-hosted faults during the seismic cycle. *Journal of Structural Geology*, 58, 22–42.
<https://doi.org/10.1016/j.jsg.2013.10.008>
- Burgmann, R., Schmidt, D., Nadeau, R. M., d'Alessio, M., Fielding, E., Manaker, D., McEvelly, T. V., & Murray, M. H. (2000). Earthquake potential along the Northern Hayward fault, California. *Science*, 289(5482), 1178–1182. <https://doi.org/10.1126/science.289.5482.1178>
- Byerlee, J. (1978). Friction of rocks. *Pure and Applied Geophysics PAGEOPH*, 116(4–5), 615–626. <https://doi.org/10.1007/BF00876528>
- Cai, M., Kaiser, P. K., & Martin, C. D. (2001a). Quantification of rock mass damage in underground excavations from microseismic event monitoring. *International Journal of Rock Mechanics and Mining Sciences*, 38(8), 1135–1145. [https://doi.org/10.1016/S1365-1609\(01\)00068-5](https://doi.org/10.1016/S1365-1609(01)00068-5)
- Cai, M., Kaiser, P. K., & Martin, C. D. (2001b). Quantification of rock mass damage in underground excavations from microseismic event monitoring. *International Journal of Rock Mechanics and Mining Sciences*, 38(8), 1135–1145. [https://doi.org/10.1016/S1365-1609\(01\)00068-5](https://doi.org/10.1016/S1365-1609(01)00068-5)
- Cappa, F., Guglielmi, Y., & De Barros, L. (2022). Transient evolution of permeability and friction in a slowly slipping fault activated by fluid pressurization. *Nature Communications*, 13(1), 1–9. <https://doi.org/10.1038/s41467-022-30798-3>
- Cappa, F., Scuderi, M. M., Collettini, C., Guglielmi, Y., & Avouac, J. P. (2019). Stabilization of fault slip by fluid injection in the laboratory and in situ. *Science Advances*, 5(3), 1–9. <https://doi.org/10.1126/sciadv.aau4065>
- Carpenter, B. M., Marone, C., & Saffer, D. M. (2011). Weakness of the San Andreas Fault revealed by samples from the active fault zone. *Nature Geoscience*, 4(4), 251–254. <https://doi.org/10.1038/ngeo1089>
- Chen, J., & Spiers, C. J. (2016). Rate and state frictional and healing behavior of carbonate fault gouge explained using microphysical model. *Journal of Geophysical Research: Solid Earth*, 121(12), 8642–8665. <https://doi.org/10.1002/2016JB013470>
- Chen, T., & Lapusta, N. (2009). Scaling of small repeating earthquakes explained by interaction of seismic and aseismic slip in a rate and state fault model. *Journal of Geophysical Research: Solid Earth*, 114(1), 1–12. <https://doi.org/10.1029/2008JB005749>
- Chlieh, M., Perfettini, H., Tavera, H., Avouac, J. P., Remy, D., Nocquet, J. M., Rolandone, F., Bondoux, F., Gabalda, G., & Bonvalot, S. (2011). Interseismic coupling and seismic potential along the Central Andes subduction zone. *Journal of Geophysical Research: Solid Earth*, 116(12), 1–21. <https://doi.org/10.1029/2010JB008166>
- Choi, J. H., Edwards, P., Ko, K., & Kim, Y. S. (2016). Definition and classification of fault damage zones: A review and a new methodological approach. *Earth-Science Reviews*, 152,

70–87. <https://doi.org/10.1016/j.earscirev.2015.11.006>

- Cirillo, D., Totaro, C., Lavecchia, G., Orecchio, B., De Nardis, R., Presti, D., Ferrarini, F., Bello, S., & Brozzetti, F. (2022). Structural complexities and tectonic barriers controlling recent seismic activity in the Pollino area (Calabria-Lucania, southern Italy)-constraints from stress inversion and 3D fault model building. *Solid Earth*, *13*(1), 205–228. <https://doi.org/10.5194/se-13-205-2022>
- Cook, N. G. W. (1976). Seismicity associated with mining. *Engineering Geology*, *10*(2–4), 99–122. [https://doi.org/10.1016/0013-7952\(76\)90015-6](https://doi.org/10.1016/0013-7952(76)90015-6)
- Cotesta, L., O'Connor, C., Brummer, R., & Punkkinen, A. (2014). Numerical modelling and scientific visualisation – integration of geomechanics into modern mine designs. *Proceedings of the Seventh International Conference on Deep and High Stress Mining*, 377–394. https://doi.org/10.36487/acg_rep/1410_25_cotesta
- Cronin, V. (2004). *Vince Cronin A Draft Primer on Focal Mechanism Solutions for Geologists A Draft Primer on Focal Mechanism Solutions for Geologists*. 1–14.
- Das, S., & Kostrov, B. V. (1983). Breaking of a single asperity: rupture process and seismic radiation. *Journal of Geophysical Research*, *88*(B5), 4277–4288. <https://doi.org/10.1029/JB088iB05p04277>
- De Barros, L., Cappa, F., Deschamps, A., & Dublanchet, P. (2020). Imbricated Aseismic Slip and Fluid Diffusion Drive a Seismic Swarm in the Corinth Gulf, Greece. *Geophysical Research Letters*, *47*(9), 1–9. <https://doi.org/10.1029/2020GL087142>
- De Santis, F. (2019). *Rock mass mechanical behavior in deep mines: in situ monitoring and numerical modelling for improving seismic hazard assessment Soutenuie* (Issue September).
- De Santis, F., Contrucci, I., Kinscher, J., Bernard, P., Renaud, V., & Gunzburger, Y. (2019). Impact of Geological Heterogeneities on Induced-Seismicity in a Deep Sublevel Stopping Mine. *Pure and Applied Geophysics*, *176*(2), 697–717. <https://doi.org/10.1007/s00024-018-2020-9>
- De Santis, F., Renaud, V., Gunzburger, Y., Kinscher, J., Bernard, P., & Contrucci, I. (2020). In situ monitoring and 3D geomechanical numerical modelling to evaluate seismic and aseismic rock deformation in response to deep mining. *International Journal of Rock Mechanics and Mining Sciences*, *129*. <https://doi.org/10.1016/j.ijrmms.2020.104273>
- Dieterich, J. (1994). A constitutive law for rate of earthquake production and its application to earthquake clustering. *Journal of Geophysical Research*, *99*(B2), 2601–2618. <https://doi.org/10.1029/93JB02581>
- Dieterich, J. H. (1979). Modeling of rock friction 1. Experimental results and constitutive equations. *Journal of Geophysical Research: Solid Earth*, *84*(B5), 2161–2168. <https://doi.org/10.1029/JB084iB05p02161>
- Dieterich, J. H. (2007). 4.04 - Applications of Rate- and State-Dependent Friction to Models of Fault Slip and Earthquake Occurrence. *Treatise on Geophysics: Volume 1-10, 1–10*, 107–129. <https://doi.org/10.1016/B978-044452748-6.00065-1>

- Doblas, M. (1998). Slickenside kinematic indicators. *Tectonophysics*, 295(1–2), 187–197. [https://doi.org/10.1016/S0040-1951\(98\)00120-6](https://doi.org/10.1016/S0040-1951(98)00120-6)
- Dublanchet, P. (2021). *Quantification and mechanical control of fault slip events : insights from physics based models To cite this version : HAL Id : tel-03499671 MINES ParisTech - Centre de Géosciences.*
- Dublanchet, P., Bernard, P., & Favreau, P. (2013). Creep modulation of Omori law generated by a Coulomb stress perturbation in a 3-D rate-and-state asperity model. *Journal of Geophysical Research E: Planets*, 118(9), 4774–4793. <https://doi.org/10.1002/jgrb.50311>
- Dublanchet, P., Godano, M., & Bernard, P. (2015). Inferring fault mechanical conditions from the source parameters of a complex microseismic multiplet in the Corinth rift, Greece. *Journal of Geophysical Research: Solid Earth*, 120(11), 7655–7682. <https://doi.org/10.1002/2015JB012259>
- Durand, V., Gualandi, A., Ergintav, S., Kwiatek, G., Haghshenas, M., Motagh, M., Dresen, G., & Martínez-Garzón, P. (2022). Deciphering aseismic deformation along submarine fault branches below the eastern Sea of Marmara (Turkey): Insights from seismicity, strainmeter, and GNSS data. *Earth and Planetary Science Letters*, 594, 117702. <https://doi.org/10.1016/j.epsl.2022.117702>
- Erguncu Güçlü, İ., Dineva, S., Mozaffari, S., & Nystrom, A. (2020). *Large seismic events ($M > 0$) in the Lappberget orebody, Garpenberg, Sweden: blast or non-blast-related?* 189–204. https://doi.org/10.36487/acg_repo/2035_06
- Fairhurst, C. (2004). Nuclear waste disposal and rock mechanics: Contributions of the Underground Research Laboratory (URL), Pinawa, Manitoba, Canada. *International Journal of Rock Mechanics and Mining Sciences*, 41(8 SPEC.ISS.), 1221–1227. <https://doi.org/10.1016/j.ijrmms.2004.09.001>
- Foulger, G. R., Wilson, M. P., Gluyas, J. G., Julian, B. R., & Davies, R. J. (2018). Earth-Science Reviews Global review of human-induced earthquakes. *Earth-Science Reviews*, 178(July 2017), 438–514. <https://doi.org/10.1016/j.earscirev.2017.07.008>
- French, M. E., Chester, F. M., & Chester, J. S. (2015). Micromechanisms of creep in clay-rich gouge from the Central Deforming Zone of the San Andreas Fault. *Journal of Geophysical Research: Solid Earth*, 120(2), 827–849. <https://doi.org/10.1002/2014JB011496>
- Geller, R. J., & Mueller, C. S. (1980). Four similar earthquakes in central California. *Geophysical Research Letters*, 7(10), 821–824.
- Gibowicz, S. (2009). Seismicity Induced by Mining: Recent Research. *Advances in Geophysics*, 51(C), 1–53. [https://doi.org/10.1016/S0065-2687\(09\)05106-1](https://doi.org/10.1016/S0065-2687(09)05106-1)
- Gibowicz, S. ., & Kijko, A. (1994). An introduction to Mining Seismology. In *Academic Press, San Diego*. [https://doi.org/10.1016/0148-9062\(74\)91552-6](https://doi.org/10.1016/0148-9062(74)91552-6)
- Glamheden, R., & Hökmark, H. (2010). *Creep in jointed rock masses - State of knowledge* (Issue June). www.skb.se.
- Glaser, S. D., & Doolin, D. M. (2000). *New directions in rock mechanics Ð report on a forum*

sponsored by the American Rock Mechanics Association. 37.

- Goldsby, D. L., & Tullis, T. E. (2002). Low frictional strength of quartz rocks at subseismic slip rates. *Geophysical Research Letters*, 29(17). <https://doi.org/10.1029/2002GL015240>
- Guglielmi, Y., Cappa, F., Avouac, J. P., Henry, P., & Elsworth, D. (2015). Seismicity triggered by fluid injection-induced aseismic slip. *Science*, 348(6240), 1224–1226. <https://doi.org/10.1126/science.aab0476>
- Hadizadeh, J., Mitterpergher, S., Gratier, J. P., Renard, F., Di Toro, G., Richard, J., & Babaie, H. A. (2012a). A microstructural study of fault rocks from the SAFOD: Implications for the deformation mechanisms and strength of the creeping segment of the San Andreas Fault. *Journal of Structural Geology*, 42, 246–260. <https://doi.org/10.1016/j.jsg.2012.04.011>
- Hadizadeh, J., Mitterpergher, S., Gratier, J. P., Renard, F., Di Toro, G., Richard, J., & Babaie, H. A. (2012b). A microstructural study of fault rocks from the SAFOD: Implications for the deformation mechanisms and strength of the creeping segment of the San Andreas Fault. *Journal of Structural Geology*, 42, 246–260. <https://doi.org/10.1016/j.jsg.2012.04.011>
- Hakala, M. (2018). *Boliden Mineral AB In Situ Stress Measurement with LVDT-cell in Boliden Garpenberg mine at 1314 m level (report)*.
- Hasegawa, A., Yoshida, K., Asano, Y., Okada, T., Iinuma, T., & Ito, Y. (2012). Change in stress field after the 2011 great Tohoku-Oki earthquake. *Earth and Planetary Science Letters*, 355–356, 231–243. <https://doi.org/10.1016/j.epsl.2012.08.042>
- Hasegawa, H. S., Wetmiller, R. J., & Gendzwill, D. J. (1989). Induced seismicity in mines in Canada—An overview. *Pure and Applied Geophysics PAGEOPH*, 129(3–4), 423–453. <https://doi.org/10.1007/BF00874518>
- Hayashi, M., & Hiramatsu, Y. (2013). Spatial distribution of similar aftershocks of a large inland earthquake, the 2000 Western Tottori earthquake, in Japan. *Earth, Planets and Space*, 65(12), 1587–1592. <https://doi.org/10.5047/eps.2013.09.002>
- Heimisson, E. R., Smith, J. D., Avouac, J. P., & Bourne, S. J. (2022). Coulomb threshold rate-and-state model for fault reactivation: Application to induced seismicity at Groningen. *Geophysical Journal International*, 228(3), 2061–2072. <https://doi.org/10.1093/gji/ggab467>
- Helmstetter, A., & Shaw, B. E. (2009). Afterslip and aftershocks in the rate-and-state friction law. *Journal of Geophysical Research: Solid Earth*, 114(1). <https://doi.org/10.1029/2007JB005077>
- Hillier, S. (2009). Quantitative Analysis of Clay and other Minerals in Sandstones by X-Ray Powder Diffraction (XRPD). In *Clay Mineral Cements in Sandstones* (Issue November). <https://doi.org/10.1002/9781444304336.ch11>
- Hiramatsu, Y., Hayashi, M., & Hayashi, A. (2011). Relation between similar aftershocks and ruptured asperity of a large inland earthquake: Example of the 2007 Noto Hanto earthquake. *Earth, Planets and Space*, 63(2), 145–149. <https://doi.org/10.5047/eps.2010.11.010>
- Holcombe, R. (2013). *Oriented drillcore: measurement, conversion, and qa/qc procedures for structural and exploration geologists* (Issue May).

- Holdsworth, R. E., van Diggelen, E. W. E., Spiers, C. J., de Bresser, J. H. P., Walker, R. J., & Bowen, L. (2011). Fault rocks from the SAFOD core samples: Implications for weakening at shallow depths along the San Andreas Fault, California. *Journal of Structural Geology*, 33(2), 132–144. <https://doi.org/10.1016/j.jsg.2010.11.010>
- Huang, X., Haimson, B. C., Plesha, M. E., & Qiu, X. (1993). An investigation of the mechanics of rock joints-Part I. Laboratory investigation. *International Journal of Rock Mechanics and Mining Sciences And*, 30(3), 257–269. [https://doi.org/10.1016/0148-9062\(93\)92729-A](https://doi.org/10.1016/0148-9062(93)92729-A)
- Hudson, J. A., & Harrison, J. . (2000). *Engineering Rock Mechanics: An Introduction to the Principles*. Elsevier Science Ltd.
- Hudyma, M. R. (2008). *Analysis and interpretation of clusters of seismic events in mines*. November, 409. https://repository.uwa.edu.au/view/singleviewer/single_viewer_toolbar2.jsp?frameId=1
- Hudyma, M. R., Heal D, & Mikula P. (2003). Seismic monitoring in mines — old Technology — new applications. *Proceedings of the First Australasian Ground Control in Mining Conference, November 2003*, 201–218.
- Igarashi, T., Matsuzawa, T., & Hasegawa, A. (2003). Repeating earthquakes and interplate aseismic slip in the northeastern Japan subduction zone. *Journal of Geophysical Research: Solid Earth*, 108(B5), 1–9. <https://doi.org/10.1029/2002jb001920>
- Ikari, M. J., Marone, C., & Saffer, D. M. (2011). On the relation between fault strength and frictional stability. *Geology*, 39(1), 83–86. <https://doi.org/10.1130/G31416.1>
- Ikari, M. J., Marone, C., Saffer, D. M., & Kopf, A. J. (2013). Slip weakening as a mechanism for slow earthquakes. *Nature Geoscience*, 6(6), 468–472. <https://doi.org/10.1038/ngeo1818>
- Ikari, M. J., Niemeijer, A. R., & Marone, C. (2011). The role of fault zone fabric and lithification state on frictional strength, constitutive behavior, and deformation microstructure. *Journal of Geophysical Research: Solid Earth*, 116(8), 1–25. <https://doi.org/10.1029/2011JB008264>
- Ikari, M. J., Saffer, D. M., & Marone, C. (2009). Frictional and hydrologic properties of clay-rich fault gouge. *Journal of Geophysical Research: Solid Earth*, 114(5), 1–18. <https://doi.org/10.1029/2008JB006089>
- Inbal, A., Ampuero, J. P., & Avouac, J. P. (2017). Locally and remotely triggered aseismic slip on the central San Jacinto Fault near Anza, CA, from joint inversion of seismicity and strainmeter data. *Journal of Geophysical Research: Solid Earth*, 122(4), 3033–3061. <https://doi.org/10.1002/2016JB013499>
- Iwasaki, T., & Sato, R. (1979). Strain field in a semi-infinite medium due to an inclined rectangular fault. *Journal of Physical Earth*, 27, 285–314.
- Jansson, N. (2011). The Origin of Iron Ores in Bergslagen , Sweden , and their Relationships with Polymetallic Sulphide Ores. In *Engineering*.
- Jansson, N. F., Zetterqvist, A., Allen, R. L., Billström, K., & Malmström, L. (2017). Genesis of the Zinkgruvan stratiform Zn-Pb-Ag deposit and associated dolomite-hosted Cu ore, Bergslagen, Sweden. *Ore Geology Reviews*, 82, 285–308.

<https://doi.org/10.1016/j.oregeorev.2016.12.004>

- Julian, B. R., Miller, A. D., & Foulger, G. R. (1998). Non-double-couple earthquakes. 1. Theory. *Reviews of Geophysics*, 36(4), 525–549. <https://doi.org/10.1029/98RG00716>
- Kagan, Y. Y. (1991). 3-D rotation of double-couple earthquake sources. *Geophysical Journal International*, 106(3), 709–716. <https://doi.org/10.1111/j.1365-246X.1991.tb06343.x>
- Kagan, Y. Y. (2007). Simplified algorithms for calculating double-couple rotation. *Geophysical Journal International*, 171(1), 411–418. <https://doi.org/10.1111/j.1365-246X.2007.03538.x>
- Kaiser, P. K., & Cai, M. (2012). Design of rock support system under rockburst condition. *Journal of Rock Mechanics and Geotechnical Engineering*, 4(3), 215–227. <https://doi.org/10.3724/sp.j.1235.2012.00215>
- Kaiser, P. K., McCreath, D. R., & Tannant, D. D. (1996). *Canadian Rockburst Support Handbook*. January, 314.
- Kaiser, P. K., Yazici, S., & Maloney, S. (2001). Mining-induced stress change and consequences of stress path on excavation stability - A case study. *International Journal of Rock Mechanics and Mining Sciences*, 38(2), 167–180. [https://doi.org/10.1016/S1365-1609\(00\)00038-1](https://doi.org/10.1016/S1365-1609(00)00038-1)
- Kampmann, T. C., Jansson, N. F., Stephens, M. B., Majka, J., & Lasskogen, J. (2017). Systematics of hydrothermal alteration at the Falun base metal sulfide deposit and implications for ore genesis and exploration, Bergslagen Ore District, Fennoscandian Shield, Sweden. *Economic Geology*, 112(5), 1111–1152. <https://doi.org/10.5382/econgeo.2017.4504>
- Kang, J. Q., Zhu, J. B., & Zhao, J. (2019). A review of mechanisms of induced earthquakes: from a view of rock mechanics. *Geomechanics and Geophysics for Geo-Energy and Geo-Resources*, 5(2), 171–196. <https://doi.org/10.1007/s40948-018-00102-z>
- Kato, A., & Ben-Zion, Y. (2021). The generation of large earthquakes. *Nature Reviews Earth and Environment*, 2(1), 26–39. <https://doi.org/10.1038/s43017-020-00108-w>
- Keneti, A., & Sainsbury, B. (2018). Review of published rockburst events and their contributing factors. *Engineering Geology*, 246(October), 361–373. <https://doi.org/10.1016/j.enggeo.2018.10.005>
- Kimura, H., Kasahara, K., Igarashi, T., & Hirata, N. (2006). Repeating earthquake activities associated with the Philippine Sea plate subduction in the Kanto district, central Japan: A new plate configuration revealed by interplate aseismic slips. *Tectonophysics*, 417(1–2), 101–118. <https://doi.org/10.1016/j.tecto.2005.06.013>
- Kinscher, J., Krüger, F., Woith, H., Lühr, B. G., Hintersberger, E., Irmak, T. S., & Baris, S. (2013). Seismotectonics of the Armutlu peninsula (Marmara Sea, NW Turkey) from geological field observation and regional moment tensor inversion. *Tectonophysics*, 608, 980–995. <https://doi.org/10.1016/j.tecto.2013.07.016>
- Kinscher, J. L., Broothaers, M., Schmittbuhl, J., de Santis, F., Laenen, B., & Klein, E. (2023). First insights to the seismic response of the fractured Carboniferous limestone reservoir at

- the Balmatt geothermal doublet (Belgium). *Geothermics*, 107(December 2022).
<https://doi.org/10.1016/j.geothermics.2022.102585>
- Kinscher, J. L., De Santis, F., Poiata, N., Bernard, P., Palgunadi, K. H., & Contrucci, I. (2020). Seismic repeaters linked to weak rock-mass creep in deep excavation mining. *Geophysical Journal International*, 222(1), 110–131. <https://doi.org/10.1093/gji/ggaa150>
- Kirkpatrick, J. D., & Brodsky, E. E. (2014). Slickenline orientations as a record of fault rock rheology. *Earth and Planetary Science Letters*, 408, 24–34.
<https://doi.org/10.1016/j.epsl.2014.09.040>
- Koketsu, K., Yokota, Y., Nishimura, N., Yagi, Y., Miyazaki, S., Satake, K., Fujii, Y., Miyake, H., Sakai, S., Yamanaka, Y., & Okada, T. (2011). A unified source model for the 2011 Tohoku earthquake. *Earth and Planetary Science Letters*, 310(3–4), 480–487.
<https://doi.org/10.1016/j.epsl.2011.09.009>
- Kozłowska, M., Orlecka-Sikora, B., Kwiatek, G., M. S. Boettcher, & Dresen, G. (2015). Nanoseismicity and picoseismicity rate changes from static stress triggering caused by a Mw 2.2 earthquake in Mponeng gold mine, South Africa. *Journal of Geophysical Research: Solid Earth*, 120, 290–307. <https://doi.org/10.1002/2014JB011410>
- Kulander, B. R., Dean, S. L., & Ward, B. J. (1990). Fractured Core Analysis : Interpretation, Logging, and Use of Natural and Induced Fractures in Core. In *AAPG Methods in Exploration Series*,.
- Lay, T. (2015). The surge of great earthquakes from 2004 to 2014. *Earth and Planetary Science Letters*, 409, 133–146. <https://doi.org/10.1016/j.epsl.2014.10.047>
- Leeman, J. R., Saffer, D. M., Scuderi, M. M., & Marone, C. (2016a). Laboratory observations of slow earthquakes and the spectrum of tectonic fault slip modes. *Nature Communications*, 7, 1–6. <https://doi.org/10.1038/ncomms11104>
- Leeman, J. R., Saffer, D. M., Scuderi, M. M., & Marone, C. (2016b). Laboratory observations of slow earthquakes and the spectrum of tectonic fault slip modes. *Nature Communications*, 7, 1–6. <https://doi.org/10.1038/ncomms11104>
- Lei, Q., Latham, J. P., Xiang, J., & Tsang, C. F. (2017). Role of natural fractures in damage evolution around tunnel excavation in fractured rocks. *Engineering Geology*, 231(August), 100–113. <https://doi.org/10.1016/j.enggeo.2017.10.013>
- Lengliné, O., & Marsan, D. (2009). Inferring the coseismic and postseismic stress changes caused by the 2004 Mw = 6 Parkfield earthquake from variations of recurrence times of microearthquakes. *Journal of Geophysical Research: Solid Earth*, 114(10), 1–19.
<https://doi.org/10.1029/2008JB006118>
- Linde, A. T., Gladwin, M. T., Johnston, M. J. S., Gwyther, R. L., & Bilham, R. G. (1996). A slow earthquake sequence on the San Andreas fault. *Nature*, 383, 65–68.
- Lisle, R. (2015). *A critical look at the Wallace-Bott hypothesis in fault-slip analysis A critical look at the Wallace-Bott hypothesis in fault-slip analysis*. July 2013.
<https://doi.org/10.2113/gssgfbull.184.4-5.299>

- Lisle, R. J. (1992). New method of estimating regional stress orientations: application to focal mechanism data of recent British earthquakes. *Geophysical Journal International*, 110(2), 276–282. <https://doi.org/10.1111/j.1365-246X.1992.tb00873.x>
- Lund Snee, J.-E., & Zoback, M. D. (2019). State of Stress in North American Unconventional Oil and Gas Producing Basins. *William C. Gussow Geoscience Conference, March 2020*, 1–7. <https://doi.org/10.6084/m9.figshare.12084771.v1>
- Ma, J., Dong, L., Zhao, G., & Li, X. (2018). Discrimination of seismic sources in an underground mine using full waveform inversion. *International Journal of Rock Mechanics and Mining Sciences*, 106(May), 213–222. <https://doi.org/10.1016/j.ijrmms.2018.04.032>
- Macklin, C., Kaneko, Y., & Kears, J. (2021). Coseismic slickenlines record the emergence of multiple rupture fronts during a surface-breaking earthquake. *Tectonophysics*, 808(October 2020), 228834. <https://doi.org/10.1016/j.tecto.2021.228834>
- Madariaga, R. (1976). Dynamics of an expanding circular fault. *Bulletin of the Seismological Society of America*, 66(3), 639–666. <https://doi.org/10.1785/bssa0660030639>
- Mai, P. M., Spudich, P., & Boatwright, J. (2005). Hypocenter locations in finite-source rupture models. *Bulletin of the Seismological Society of America*, 95(3), 965–980. <https://doi.org/10.1785/0120040111>
- Malan, D. F. (1998). *An investigation into the identification and modelling of time-dependent behaviour of deep level excavations in hard rock*.
- Malan, D. F. (1999). Time-dependent behaviour of deep level tabular excavations in hard rock. *Rock Mechanics and Rock Engineering*, 32(2), 123–155. <https://doi.org/10.1007/s006030050028>
- Malan, D. F., Vogler, U. W., & Drescher, K. (1997). Time-dependent behaviour of hard rock in deep level gold mines. *Journal of The South African Institute of Mining and Metallurgy*, 97(3), 135–147.
- Malek, F., Espley, S., Yao, M., Trifu, C., & Suorineni, F. (2008). Management of High Stress and Seismicity at Vale Inco Creighton Mine. *The 42nd U.S. Rock Mechanics Symposium (USRMS), 29 June-2 July, May 2015*, 8.
- Malovichko, D. (2012). Discrimination of blasts in mine seismology. *Proceedings of the Sixth International Seminar on Deep and High Stress Mining*, 161–172. https://doi.org/10.36487/acg_rep/1201_11_malovichko
- Manthei, G., & Plenkers, K. (2018). Review on in situ acoustic emission monitoring in the context of structural health monitoring in mines. *Applied Sciences (Switzerland)*, 8(9). <https://doi.org/10.3390/app8091595>
- Marone, C. J., Scholtz, C. H., & Bilham, R. (1991). On the mechanics of earthquake afterslip. *Journal of Geophysical Research*, 96(B5), 8441–8452. <https://doi.org/10.1029/91JB00275>
- Marrett, R., & Allmendinger, R. W. (1990). Kinematic analysis of fault-slip data. *Journal of Structural Geology*, 12(8), 973–986. [https://doi.org/10.1016/0191-8141\(90\)90093-E](https://doi.org/10.1016/0191-8141(90)90093-E)
- Marsan, D., Bean, C. ., Steacy, S., & McCloskey, J. (1999). Spatio-temporal analysis of stress

- diffusion in a mining-induced seismicity. *Geophysical Research Letters*, 26(24), 3697–3700.
- Martínez-Garzón, P., Durand, V., Bentz, S., Kwiatek, G., Dresen, G., Turkmen, T., Nurlu, M., & Bohnhoff, M. (2021). Near-Fault Monitoring Reveals Combined Seismic and Slow Activation of a Fault Branch within the Istanbul–Marmara Seismic Gap in Northwest Turkey. *Seismological Research Letters*, 92.
- Matsuzawa, T., Igarashi, T., & Hasegawa, A. (2002). Characteristic small-earthquake sequence off Sanriku, northeastern Honshu, Japan. *Geophysical Research Letters*, 29(11), 38-1-38–4. <https://doi.org/10.1029/2001GL014632>
- Matsuzawa, T., Uchida, N., Igarashi, T., Okada, T., & Hasegawa, A. (2004). Repeating earthquakes and quasi-static slip on the plate boundary east off northern Honshu, Japan. *Earth, Planets and Space*, 56(8), 803–811.
- McClure, M. W., & Horne, R. N. (2011). Investigation of injection-induced seismicity using a coupled fluid flow and rate/state friction model. *Geophysics*, 76(6). <https://doi.org/10.1190/geo2011-0064.1>
- McGarr, A. (2002). Case histories of induced and triggered seismicity: Chapter 40. In *International geophysics studies* (Vol. 81, Issue PartA, pp. 647–661). Elsevier.
- McGarr, A. (1976a). Dependence of magnitude statistics on strain rate. *Bulletin of the Seismological Society of America*, 66(1), 33–44.
- McGarr, A. (1976b). Seismic moments and volume changes. *Journal of Geophysical Research*, 81(8), 1487–1494. <https://doi.org/10.1029/jb081i008p01487>
- McKinnon, S. D. (2006). Triggering of seismicity remote from active mining excavations. *Rock Mechanics and Rock Engineering*, 39(3), 255–279. <https://doi.org/10.1007/s00603-005-0072-5>
- Mclasley, G. C., & Yamashita, F. (2017). Slow and fast ruptures on a laboratory fault controlled by loading characteristics. *Journal of Geophysical Research: Solid Earth*, 122(5), 3719–3738. <https://doi.org/10.1002/2016JB013681>
- Mesimeri, M., & Karakostas, V. (2018). Repeating earthquakes in western Corinth Gulf (Greece): Implications for aseismic slip near locked faults. *Geophysical Journal International*, 215(1), 659–676. <https://doi.org/10.1093/gji/ggy301>
- Moore, D. E., & Lockner, D. A. (1995). The role of microcracking in shear-fracture propagation in granite. *Journal of Structural Geology*, 17(1). [https://doi.org/10.1016/0191-8141\(94\)E0018-T](https://doi.org/10.1016/0191-8141(94)E0018-T)
- Morrow, C. A., Moore, D. E., & Lockner, D. A. (2000). The effect of mineral bond strength and adsorbed water on fault gouge frictional strength. *Geophysical Research Letters*, 27(6), 815–818. <https://doi.org/10.1029/1999GL008401>
- Murru, M., Akinci, A., Falcone, G., Pucci, S., Console, R., & Parsons, T. (2016). $M \geq 7$ earthquake rupture forecast and time-dependent probability for the sea of Marmara region, Turkey. *Journal of Geophysical Research: Solid Earth*, 121(4), 2679–2707. <https://doi.org/10.1002/2015JB012595>

- Na, Z., Lixin, M., Laigui, W., & Yibin, Z. (2022). Numerical simulation of creep fracture evolution in fractured rock masses. *Frontiers in Earth Science*, *10*(July), 1–13. <https://doi.org/10.3389/feart.2022.901742>
- Nadeau, R. M., Foxall, W., & McEvilly, T. V. (1995). Clustering and periodic recurrence of microearthquakes on the San Andreas fault at Parkfield, California. *Science*, *267*(5197), 503–507. <https://doi.org/10.1126/science.267.5197.503>
- Nadeau, R. M., & Johnson, L. R. (1998). Seismological studies at Parkfield VI: moment release rates and estimates of source parameters for small repeating earthquakes. *Bulletin of the Seismological Society of America*, *88*(3), 790–814. <https://doi.org/10.1785/bssa0880030790>
- Nadeau, R. M., & McEvilly, T. V. (1999). Fault slip rates at depth from recurrence intervals of repeating microearthquakes. *Science*, *285*(5428), 718–721. [https://doi.org/10.1016/s0016-0032\(26\)90726-6](https://doi.org/10.1016/s0016-0032(26)90726-6)
- Naoui, M., Nakatani, M., Igarashi, T., Otsuki, K., Yabe, Y., Kgarume, T., Murakami, O., Masakale, T., Ribeiro, L., Ward, A., Moriya, H., Kawakata, H., Nakao, S., Durrheim, R., & Ogasawara, H. (2015). Unexpectedly frequent occurrence of very small repeating earthquakes ($-5.1 \leq M_w \leq -3.6$) in a South African gold mine: Implications for monitoring intraplate faults. *Journal of Geophysical Research : Solid Earth*, *120*, 8478–8493. <https://doi.org/10.1002/2015JB012447>. Received
- Naoui, M., Nakatani, M., Otsuki, K., Yabe, Y., Kgarume, T., Murakami, O., Masakale, T., Ribeiro, L., Ward, A., Moriya, H., Kawakata, H., Durrheim, R., & gasawara, H. (2015). Steady activity of microfractures on geological faults loaded by mining stress. *Tectonophysics*, *649*, 100–114. <https://doi.org/10.1016/j.tecto.2015.02.025>
- Noël, C., Passelègue, F. X., Giorgetti, C., & Violay, M. (2019). Fault Reactivation During Fluid Pressure Oscillations: Transition From Stable to Unstable Slip. *Journal of Geophysical Research: Solid Earth*, *124*(11), 10940–10953. <https://doi.org/10.1029/2019JB018517>
- Nordström, E., Dineva, S., & Nordlund, E. (2020). Back Analysis of Short-Term Seismic Hazard Indicators of Larger Seismic Events in Deep Underground Mines (LKAB, Kiirunavaara Mine, Sweden). *Pure and Applied Geophysics*, *177*(2), 763–785. <https://doi.org/10.1007/s00024-019-02352-8>
- Okada, Y. (1992). Internal deformation due to shear and tensile faults in a half-space. *Bulletin - Seismological Society of America*, *82*(2), 1018–1040. <https://doi.org/10.1785/bssa0820021018>
- Orlecka-Sikora, B., Lasocki, S., Lizurek, G., & Rudziński, Ł. (2012). Response of seismic activity in mines to the stress changes due to mining induced strong seismic events. *International Journal of Rock Mechanics and Mining Sciences*, *53*, 151–158. <https://doi.org/10.1016/j.ijrmms.2012.05.010>
- Ortlepp, W. D. (1997). *RaSiM Comes of Age — A Review of the Contribution to the Understanding and Control of Mine Rockbursts*, SRK Consulting. 3–20.
- Ortlepp, W. D., & Stacey, T. R. (1994). *Rockburst Mechanisms in Tunnels and Shafts*. *9*(1), 59–65.

- Pacheco, J. F., Sykes, L. R., & Scholz, C. H. (1993). Nature of seismic coupling along simple plate boundaries of the subduction type. *Journal of Geophysical Research*, 98(B8). <https://doi.org/10.1029/93jb00349>
- Palgunadi, K. H., Poiata, N., Kinscher, J., Bernard, P., De Santis, F., & Contrucci, I. (2019). Methodology for full waveform near real-time automatic detection and localization of microseismic events using high (8 kHz) sampling rate records in mines: Application to the Garpenberg mine (Sweden). *Seismological Research Letters*, 91(1), 399–414. <https://doi.org/10.1785/0220190074>
- Paradigm Geophysical. (2009). *Gocad and SKUA Suite software*. <https://www.aspentech.com/en/acquisition/subsurface-science-and-engineering>
- Parsons, T. (2002). Global Omori law decay of triggered earthquakes: Large aftershocks outside the classical aftershock zone. *Journal of Geophysical Research: Solid Earth*, 107(B9), ESE 9-1-ESE 9-20. <https://doi.org/10.1029/2001jb000646>
- Peng, Z., & Ben-Zion, Y. (2005). Spatiotemporal variations of crustal anisotropy from similar events in aftershocks of the 1999 M7.4 İzmit and M7.1 Düzce, Turkey, earthquake sequences. *Geophysical Journal International*, 160(3), 1027–1043. <https://doi.org/10.1111/j.1365-246X.2005.02569.x>
- Peng, Z., & Gombert, J. (2010). An integrated perspective of the continuum between earthquakes and slow-slip phenomena. *Nature Geoscience*, 3(9), 599–607. <https://doi.org/10.1038/ngeo940>
- Perfettini, H., & Avouac, J.-P. (2004). Postseismic relaxation driven by brittle creep: A possible mechanism to reconcile geodetic measurements and the decay rate of aftershocks, application to the Chi-Chi earthquake, Taiwan. *Journal of Geophysical Research: Solid Earth*, 109(B2), 1–15. <https://doi.org/10.1029/2003jb002488>
- Perfettini, H., Frank, W. B., Marsan, D., & Bouchon, M. (2018). A Model of Aftershock Migration Driven by Afterslip. *Geophysical Research Letters*, 45(5), 2283–2293. <https://doi.org/10.1002/2017GL076287>
- Petit, J. P. (1987). Criteria for the sense of movement on fault surfaces in brittle rocks. *Journal of Structural Geology*, 9(5–6), 597–608. [https://doi.org/10.1016/0191-8141\(87\)90145-3](https://doi.org/10.1016/0191-8141(87)90145-3)
- Pondrelli, S., Salimbeni, S., Ekström, G., Morelli, A., Gasperini, P., & Vannucci, G. (2006). The Italian CMT dataset from 1977 to the present. *Physics of the Earth and Planetary Interiors*, 159(3–4), 286–303. <https://doi.org/10.1016/j.pepi.2006.07.008>
- Poupinet, G., Ellsworth, W. L., & Frechet, J. (1984). Monitoring velocity variations in the crust using earthquake doublets: an application to the Calaveras fault, California (USA). *Journal of Geophysical Research*, 89(B7), 5719–5731. <https://doi.org/10.1029/JB089iB07p05719>
- Power, W. L., Tullis, T. E., Brown, S. R., Boitnott, G. N., & Scholz, C. H. (1987). Roughness of natural fault surfaces. *Geophysical Research Letters*, 14(1), 29–32. <https://doi.org/10.1029/GL014i001p00029>
- Renard, F., McBeck, J., Kandula, N., Cordonnier, B., Meakin, P., & Ben-Zion, Y. (2019). Volumetric and shear processes in crystalline rock approaching faulting. *Proceedings of the*

- National Academy of Sciences of the United States of America*, 116(33), 16234–16239.
<https://doi.org/10.1073/pnas.1902994116>
- Rice, J. R. (1983). Constitutive relations for fault slip and earthquake instabilities. *PAGEOPH*, 121(3).
- Rice, J. R. (1992). Fault Stress States, Pore Pressure Distributions, and the Weakness of the San Andreas Fault. *International Geophysics*, 51(C), 475–503. [https://doi.org/10.1016/S0074-6142\(08\)62835-1](https://doi.org/10.1016/S0074-6142(08)62835-1)
- Rice, J. R. (1993). Spatio-temporal Complexity of Slip on a Fault Rate- dependent friction. *Journal of Geophysical Research*, 98(93), 9885–9907.
<http://citeseerx.ist.psu.edu/viewdoc/download?doi=10.1.1.161.6067&rep=rep1&type=pdf>
- Richardson, E., & Jordan, T. H. (2002). Seismicity in deep gold mines of South Africa: Implications for tectonic earthquakes. *Bulletin of the Seismological Society of America*, 92(5), 1766–1782. <https://doi.org/10.1785/0120000226>
- Ruina, A. (1983). Slip instability and state variable friction laws. *Journal of Geophysical Research*, 88(B12), 10359–10370.
<http://onlinelibrary.wiley.com/doi/10.1029/JB088iB12p10359/abstract>
- Saffer, D. M., & Marone, C. (2003). Comparison of smectite- and illite-rich gouge frictional properties: Application to the updip limit of the seismogenic zone along subduction megathrusts. *Earth and Planetary Science Letters*, 215(1–2), 219–235.
[https://doi.org/10.1016/S0012-821X\(03\)00424-2](https://doi.org/10.1016/S0012-821X(03)00424-2)
- Sagy, A., & Brodsky, E. E. (2009a). Geometric and rheological asperities in an exposed fault zone. *Journal of Geophysical Research: Solid Earth*, 114(2), 1–15.
<https://doi.org/10.1029/2008JB005701>
- Sagy, A., & Brodsky, E. E. (2009b). Geometric and rheological asperities in an exposed fault zone. *Journal of Geophysical Research: Solid Earth*, 114(2), 1–15.
<https://doi.org/10.1029/2008JB005701>
- Sainoki, A., & Mitri, H. . (2015). *Evaluation of fault-slip potential due to shearing of fault asperities*. 20(March), 1–31. <https://doi.org/10.3109/02699052.2011.624568>
- Sainoki, A., & Mitri, H. S. (2014). Dynamic behaviour of mining-induced fault slip. *International Journal of Rock Mechanics and Mining Sciences*, 66, 19–29.
<https://doi.org/10.1016/j.ijrmmms.2013.12.003>
- Sainoki, A., & Mitri, H. S. (2016). Instantaneous stress release in fault surface asperities during mining-induced fault-slip. *Journal of Rock Mechanics and Geotechnical Engineering*, 8(5), 619–628. <https://doi.org/10.1016/j.jrmge.2016.05.003>
- Sainoki, A., & Mitri, H. S. (2017). Influence of mining activities on the reactivation of a footwall fault. *Arabian Journal of Geosciences*, 10(5). <https://doi.org/10.1007/s12517-017-2913-4>
- Sainoki, A., Mitri, H. S., & Chinnasane, D. (2017). Characterization of Aseismic Fault-Slip in a Deep Hard Rock Mine Through Numerical Modelling: Case Study. *Rock Mechanics and Rock Engineering*, 50(10), 2709–2729. <https://doi.org/10.1007/s00603-017-1268-1>

- Sainsbury, B. A., & Kurucuk, N. (2020). Impact of intact rock properties on proneness to rockbursting. *Bulletin of Engineering Geology and the Environment*, 79(4), 1939–1946. <https://doi.org/10.1007/s10064-019-01670-4>
- Sammis, C. G., Nadeau, R. M., & Johnson, L. R. (1999). How strong is an asperity? *Journal of Geophysical Research: Solid Earth*, 104(B5), 10609–10619. <https://doi.org/10.1029/1999jb900006>
- Sato, R., & Matsu'ura, M. (1974). Strains and tilts on the surface of a semi-infinite medium. *Journal of Physical Earth*, 22, 213–221.
- Savage, J. C., & Burford, R. O. (1973). Geodetic determination of relative plate motion in central California. *Journal of Geophysical Research*, 78(5), 832–845.
- Savage, J. C., Svarc, J. L., & Yu, S. B. (2007). Postseismic relaxation and aftershocks. *Journal of Geophysical Research : Solid Earth*, 112(6). <https://doi.org/10.1029/2006JB004584>
- Schaff, D. P., Beroza, G. C., & Shaw, B. E. (1998). Postseismic response of repeating aftershocks. *Geophysical Research Letters*, 25(24), 4549–4552. <https://doi.org/10.1029/1998GL900192>
- Schleicher, A. M., van der Pluijm, B. A., & Warr, L. N. (2012). Chlorite-smectite clay minerals and fault behavior: New evidence from the San Andreas Fault Observatory at Depth (SAFOD) core. *Lithosphere*, 4(3), 209–220. <https://doi.org/10.1130/L158.1>
- Schmittbuhl, J., Karabulut, H., Lengliné, O., & Bouchon, M. (2016). Long-lasting seismic repeaters in the Central Basin of the Main Marmara Fault. *Geophysical Research Letters*, 43(18), 9527–9534. <https://doi.org/10.1002/2016GL070505>
- Scholz, C. H. (1998). Earthquakes and friction laws. *Nature*, 391(6662), 37–42. <https://doi.org/10.1038/34097>
- Schulz, S. E., & Evans, J. P. (2000). Mesoscopic structure of the Punchbowl Fault, Southern California and the geologic and geophysical structure of active strike-slip faults. *Journal of Structural Geology*, 22(7), 913–930. [https://doi.org/10.1016/S0191-8141\(00\)00019-5](https://doi.org/10.1016/S0191-8141(00)00019-5)
- Shimamoto, T., & Logan, J. M. (1981). Effects of simulated clay gouges on the sliding behavior of Tennessee sandston. *Tectonophysics*, 75(3–4), 243–255. [https://doi.org/10.1016/0040-1951\(81\)90276-6](https://doi.org/10.1016/0040-1951(81)90276-6)
- Sibek, V. (1963). On securing the safety of operating ore mines exposed to rockburst hazards. *Proc 3rd Int. Min. Congr., Salzburg- Safety in Mining*.
- Šílený, J., & Milev, A. (2008). Source mechanism of mining induced seismic events - Resolution of double couple and non double couple models. *Tectonophysics*, 456(1–2), 3–15. <https://doi.org/10.1016/j.tecto.2006.09.021>
- Simser, B. P. (2019). Rockburst management in Canadian hard rock mines. *Journal of Rock Mechanics and Geotechnical Engineering*, 11(5), 1036–1043. <https://doi.org/10.1016/j.jrmge.2019.07.005>
- Smeraglia, L., Bettucci, A., Billi, A., Carminati, E., Cavallo, A., Di Toro, G., Natali, M., Passeri, D., Rossi, M., & Elena, S. (2017). Microstructural evidence for seismic and aseismic slips

- along clay-bearing carbonate. *Journal of Geophysical Research : Solid Earth*.
- Smith, R. B. (1977). Formation of folds, boudinage, and mullions in non-Newtonian materials. *Bulletin of the Geological Society of America*, 88(2), 312–320. [https://doi.org/10.1130/0016-7606\(1977\)88<312:FOFBAM>2.0.CO;2](https://doi.org/10.1130/0016-7606(1977)88<312:FOFBAM>2.0.CO;2)
- Snelling, P. E., Godin, L., & McKinnon, S. D. (2013). The role of geologic structure and stress in triggering remote seismicity in Creighton Mine, Sudbury, Canada. *International Journal of Rock Mechanics and Mining Sciences*, 58, 166–179. <https://doi.org/10.1016/j.ijrmms.2012.10.005>
- Sobiesiak, M., Meyer, U., Schmidt, S., Götze, H. J., & Krawczyk, C. M. (2007). Asperity generating upper crustal sources revealed by b value and isostatic residual anomaly grids in the area of Antofagasta, Chile. *Journal of Geophysical Research: Solid Earth*, 112(12), 1–11. <https://doi.org/10.1029/2006JB004796>
- Sornette, D. (1999). Earthquakes: From chemical alteration to mechanical rupture. *Physics Report*, 313(5), 237–292. [https://doi.org/10.1016/s0370-1573\(98\)00088-x](https://doi.org/10.1016/s0370-1573(98)00088-x)
- Souley, M., Renaud, V., Al Heib, M., Bouffier, C., Lahaie, F., & Nyström, A. (2018). Numerical investigation of the development of the excavation damaged zone around a deep polymetallic ore mine. *International Journal of Rock Mechanics and Mining Sciences*, 106(April), 165–175. <https://doi.org/10.1016/j.ijrmms.2018.04.028>
- Srinivasan, C., Arora, S. K., & Yaji, R. K. (1997). Use of mining and seismological parameters as premonitors of rockbursts. *International Journal of Rock Mechanics and Mining Sciences*, 34(6), 1001–1008. [https://doi.org/10.1016/S1365-1609\(97\)80009-3](https://doi.org/10.1016/S1365-1609(97)80009-3)
- Stein, R. S. (1999). The role of stress transfer in earthquake occurrence. *Nature*, 402, 605–609.
- Steketee, J. A. (1958). On volterra's dislocations in a semi-infinite elastic medium. *Canadian Journal of Physics*, 36, 192–205.
- Stigsson, M., & Munier, R. (2013). Orientation uncertainty goes bananas: An algorithm to visualise the uncertainty sample space on stereonet for oriented objects measured in boreholes. *Computers and Geosciences*, 56, 56–61. <https://doi.org/10.1016/j.cageo.2013.03.001>
- Sykes, L. R., & Seeber, L. (1985). Great earthquakes and great asperities, San Andreas fault, southern California (USA). *Geology*, 13(12), 835–838. [https://doi.org/10.1130/0091-7613\(1985\)13<835:GEAGAS>2.0.CO;2](https://doi.org/10.1130/0091-7613(1985)13<835:GEAGAS>2.0.CO;2)
- Tape, W., & Tape, C. (2012). Angle between principal axis triples. *Geophysical Journal International*, 191(2), 813–831. <https://doi.org/10.1111/j.1365-246X.2012.05658.x>
- Titus, S. J., DeMets, C., & Tikoff, B. (2006). Thirty-five-year creep rates for the creeping segment of the San Andreas fault and the effects of the 2004 Parkfield earthquake: Constraints from alignment arrays, continuous global positioning system, and creepmeters. *Bulletin of the Seismological Society of America*, 96(4 B). <https://doi.org/10.1785/0120050811>
- Tiu, G., Jansson, N., Wanhainen, C., Ghorbani, Y., & Lilja, L. (2021). Ore mineralogy and trace

- element (re)distribution at the metamorphosed Lappberget Zn-Pb-Ag-(Cu-Au) deposit, Garpenberg, Sweden. *Ore Geology Reviews*, 104223. <https://doi.org/10.1016/j.oregeorev.2021.104223>
- Tocher, D. (1960). Creep on the San Andreas Fault: A Progress Report. Creep Rate and Related Measurements at Vineyard, California. *Bulletin of the Seismological Society of America*.
- Uchida, N. (2019). Detection of repeating earthquakes and their application in characterizing slow fault slip. *Progress in Earth and Planetary Science*, 6(1). <https://doi.org/10.1186/s40645-019-0284-z>
- Uchida, N., & Bürgmann, R. (2019). Repeating Earthquakes. *Annual Review of Earth and Planetary Sciences*, 47(May), 305–332. <https://doi.org/10.1146/annurev-earth-053018-060119>
- Uchida, N., Kalafat, D., Pinar, A., & Yamamoto, Y. (2019). Repeating earthquakes and interplate coupling along the western part of the North Anatolian Fault. *Tectonophysics*, 769(July), 228185. <https://doi.org/10.1016/j.tecto.2019.228185>
- Uchida, N., & Matsuzawa, T. (2013). Pre- and postseismic slow slip surrounding the 2011 Tohoku-oki earthquake rupture. *Earth and Planetary Science Letters*, 374, 81–91. <https://doi.org/10.1016/j.epsl.2013.05.021>
- Uchida, N., Matsuzawa, T., Hasegawa, A., & Igarashi, T. (2003). Interplate quasi-static slip off Sanriku, NE Japan, estimated from repeating earthquakes. *Geophysical Research Letters*, 30(15).
- Urbancic, T. I., & Trifu, C. I. (2000). Recent advances in seismic monitoring technology at Canadian mines. *Journal of Applied Geophysics*, 45(4), 225–237. [https://doi.org/10.1016/S0926-9851\(00\)00030-6](https://doi.org/10.1016/S0926-9851(00)00030-6)
- Vallejos, J. A., & McKinnon, S. D. (2011). Correlations between mining and seismicity for re-entry protocol development. *International Journal of Rock Mechanics and Mining Sciences*, 48(4), 616–625. <https://doi.org/10.1016/j.ijrmms.2011.02.014>
- van Koppen, M. (2008). *Estimation of the Risk for Mine Induced Seismicity in Large Scale Mining in the Garpenberg Mine (Master thesis)*. Delft University of Technology, Netherlands.
- Vazaios, I., Vlachopoulos, N., & Diederichs, M. S. (2019). Assessing fracturing mechanisms and evolution of excavation damaged zone of tunnels in interlocked rock masses at high stresses using a finite-discrete element approach. *Journal of Rock Mechanics and Geotechnical Engineering*, 11(4), 701–722. <https://doi.org/10.1016/j.jrmge.2019.02.004>
- Waldhauser, F., & Schaff, D. P. (2021). A Comprehensive Search for Repeating Earthquakes in Northern California: Implications for Fault Creep, Slip Rates, Slip Partitioning, and Transient Stress. *Journal of Geophysical Research: Solid Earth*, 126(11), 1–22. <https://doi.org/10.1029/2021JB022495>
- Wallace, R. E. . (1951). Geometry of Shearing Stress and Relation to Faulting. *The Journal of Geology*, 59(2), 118–130.

- Wan, W., Liu, J., & Liu, J. (2018). Effects of Asperity Angle and Infill Thickness on Shear Characteristics Under Constant Normal Load Conditions. *Geotechnical and Geological Engineering*, 36(4), 2761–2767. <https://doi.org/10.1007/s10706-018-0447-5>
- Wang, G., Wu, X., Zhang, X., Zhang, Z., Zhao, Z., Han, W., Wang, Y., & Zhao, C. (2020). Macro–Microscopic Study on the Shear Characteristics of Filled Joints with Different Roughnesses. *Arabian Journal for Science and Engineering*, 45(10), 8331–8348. <https://doi.org/10.1007/s13369-020-04705-1>
- White, B., & Whyatt, J. (1999). Role of fault slip on mechanisms of rock burst damage, Lucky Friday Mine, Idaho, USA. *2nd Southern African Rock Engineering Symposium*, 169–178. <http://198.246.124.22/niosh/mining/UserFiles/works/pdfs/rofso.pdf>
- Wintsch, R. P., Christoffersen, R., & Kronenberg, A. K. (1995). Fluid-rock reaction weakening of fault zones. *Journal of Geophysical Research*, 100(B7). <https://doi.org/10.1029/94jb02622>
- Wong, R. H. C., Lin, P., Tang, C. A., & Chau, K. T. (2002). Creeping damage around an opening in rock-like material containing non-persistent joints. *Engineering Fracture Mechanics*, 69(17), 2015–2027. [https://doi.org/10.1016/S0013-7944\(02\)00074-7](https://doi.org/10.1016/S0013-7944(02)00074-7)
- Wu, W. (2021). A review of unloading-induced fault instability. *Underground Space (China)*, 6(5), 528–538. <https://doi.org/10.1016/j.undsp.2020.11.001>
- Yamaguchi, J., Naoi, M., Nakatani, M., Moriya, H., Igarashi, T., Murakami, O., Yabe, Y., Durrheim, R., & Ogasawara, H. (2018). Emergence and disappearance of very small repeating earthquakes on a geological fault in a gold mine in South Africa. *Tectonophysics*, 747–748(November 2017), 318–326. <https://doi.org/10.1016/j.tecto.2018.10.014>
- Ylmefors, A., Zhang, P., & Mozaffari, S. (2022). Classification of mining induced seismicity at the Kiirunavaara mine. *10th International Symposium on Rockbursts and Seismicity in Mines (RaSiM10)*.
- Yoshida, K., Hasegawa, A., Okada, T., & Iinuma, T. (2014). Changes in the stress field after the 2008 M7.2 Iwate-Miyagi Nairiku earthquake in northeastern Japan. *Journal of Geophysical Research: Solid Earth*, 119, 9016–9030.
- Zaliapin, I., & Ben-Zion, Y. (2013). Earthquake clusters in southern California I: Identification and stability. *Journal of Geophysical Research: Solid Earth*, 118(6), 2847–2864. <https://doi.org/10.1002/jgrb.50179>
- Zhang, Q., Wu, C., Fei, X., Jang, B. A., & Liu, D. (2019). Time-dependent behavior of rock joints considering asperity degradation. *Journal of Structural Geology*, 121(December 2018), 1–9. <https://doi.org/10.1016/j.jsg.2019.01.004>
- Zoback, M. Lou. (2006). The 1906 earthquake and a century of progress in understanding earthquakes and their hazards. *GSA Today*, 16(4–5), 4–11. <https://doi.org/10.1130/GSAT01604.1>
- Zoback, M., Hickman, S., & Ellsworth, W. (2011). Scientific drilling into the San Andreas fault zone - An overview of SAFOD's first five years. *Scientific Drilling*, 1, 14–28. <https://doi.org/10.2204/iodp.sd.11.02.2011>

Annex A

Lithological groups	Types of rocks
Schists	Talc Schist
	Chlorite/ sericite schist/ biotite/ tremolite/ chlorite-biotite/ chlorite-talc schists
	Mica schist
	Schales (phlogopite, mica-talc schale, sericite, etc)
Mica-Quartzites	Siltstone
	Quartzite ; Chert ; Sandstone; Qtz sandstone
	Sericite/ phlogopite/ biotite/ mica/ chlorite/ zoisite/ cordierite quartzites; ore quartzite
Dacite	Dacite
Dolomite	Dolomite; Limestone dolomite
Breccia	Sedimentary Breccia; Breccia
Skarns	Skarn
	Tremolite skarn
	Garnet skarn; Diopside skarn
	Actinolite skarn; Hornblende skarn
	Skarn-Dolomite Breccia
Massive Sulphides	Massive sulphides
	Semi-massive sulphides
	Massive Oxydes
	Autres (Massph, Masspy, Masmag)
Quartz mineral	Quartz mineral
Limestone	Limestone
	Limestone Breccia
	Carbonate rocks; Ca, Ka
VolcanoClastics	Metavolcanic Rock
	Clastic Sediment
	Tuffite; Tuff; Volcanique; Pyroclastiques; Pumice
	Rhyolite
Mafics (et Dyke)	Basalt; Andesite
	Métabasite
	Diabas

Table A.1. The classification of the eleven main lithological groups. The different types of rocks are the ones found both in the drillings and on the 2D geological maps drawn by geologists. They were assigned to the main lithological groups based on discussions with geologists. The different groups are homogeneous geomechanically, except for the mica-quartzite group which presents a heterogeneity due to the presence of different types and amount of micas minerals.

Annex B

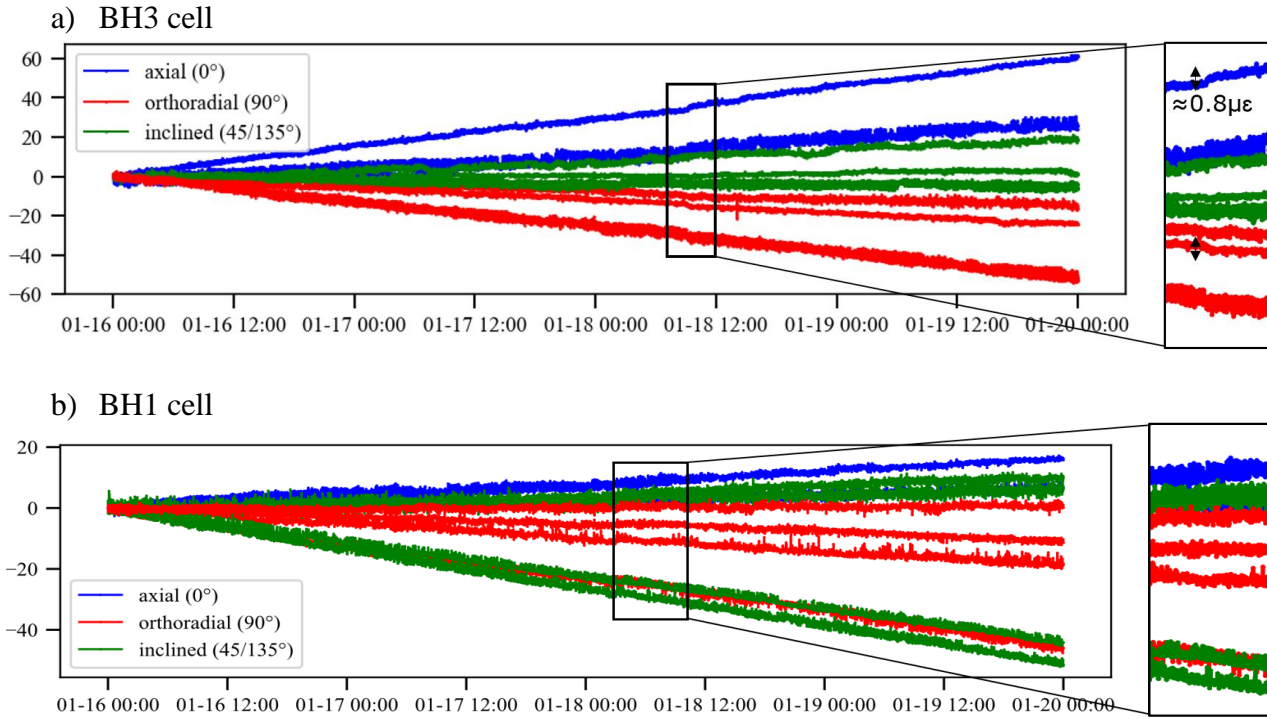


Figure B.1. Strain data for BH3 cell (top figure) and BH1 cell (bottom figure), between the 16th and 20th of January 2022. Dark square shows the time of the seismic event of M-1 occurring the 18th of January, monitored by BH4 cell and shown in 5.2.1. BH3 cell monitored a tiny shift of around 0.6μ ϵ and BH1 cell monitored no shift.

Annex C

In the framework of this thesis, an article has been submitted to the International Journal of Rock Mechanics and Mining sciences. Reviewers recommended reconsideration of the article following minor revisions. The version shown here is the version sent after revising the manuscript, with a status of “with editor” at the time of writing.

1 In-situ search for the origin of seismic repeaters in a deep mine, using
2 geological and geomechanical measurements.

3
4 **Emeline Lhoumaud^{a,*}, Yann Gunzburger^a, Marianne Conin^a, Jannes Kinscher^b, Aurélien Eglinger^c**

5
6 ^a*GeoRessources lab, Université de Lorraine - CNRS, Mines Nancy, Campus ARTEM, BP14234, 54042 Nancy Cedex, France*

7 ^b*Institut National de l'Environnement Industriel et des Risques (INERIS), Campus ARTEM CS14234, 54042 Nancy Cedex, France*

8 ^c*GeoRessources lab, Université de Lorraine - CNRS, CREGU, 54000 Nancy Cedex, France*

9 *Corresponding author

10 *E-mail address:* emeline.lhoumaud@univ-lorraine.fr

11
12 **Abstract**

13
14 Repeaters are repetitive seismic events with highly similar waveforms. They have been studied for decades
15 by seismologists in natural environments and are commonly associated with the occurrence of aseismic slip
16 (*i.e.* creep), loading seismogenic asperities on fault planes. Recently, long lasting repeater sequence (days
17 to years) have been also observed in the active Garpenberg underground mine, Sweden. The presence of
18 these phenomena may indicate that aseismic deformation induced by mining plays a role in triggering mine
19 seismicity and thus has to be considered in seismic hazard assessment. To better understand the origin of
20 these repeaters, we target one of the permanent repeater source located in the (~25 m thick) horizontal sill
21 pillar at 1 km depth using drilling cores and installation of strain cells in boreholes. By this in-situ
22 investigation, we aim at observing structures and mechanisms responsible for the occurrence of repeaters,
23 combining geological, geomechanical and geophysical observation. A clear co-seismic strain (~ 6 $\mu\epsilon$) during
24 the occurrence of one repeater event enabled us to constrain the location of that source asperity, outside the
25 area reached by the drillings. We show that the presence of an aseismic fault plane with at least one
26 seismogenic asperity is consistent with field observations and that the drillings have probably crossed the

27 aseismic portion of the fault plane. Finally, we discuss limitations of our installation, even if local and
28 unique, to clearly identify the source mechanism behind the observed seismicity.

29

30 **Keywords:** Induced seismicity, deep mine, seismic repeaters, strain cells, creep

31

32 1. Introduction

33

34 Seismic monitoring is commonly used in deep, hard-rock mines, for studying rock damage,^{1,2}
35 preventing rock-bursts³ and ensuring the miners safety. Seismic events are due to a release of energy during
36 fracturing inside the rock mass or when instability occurs on pre-existing geological structures.⁴ They have
37 been classified in two categories in deep mines⁵⁻⁸: (i) seismic events directly induced by excavation and
38 following the advance of the mining front and (ii) seismic events associated with shear or rupture along
39 inherited planar structures (*e.g.* fault plane, shear zones). The latter can be spatially and temporally distant
40 to the excavation front and induce high magnitude seismic events.⁹⁻¹² However, a rigorous two-type
41 classification of the seismic events is not always straight forward, and identifying source mechanism of
42 seismicity is far from being obvious.^{13,14} As an example, *Snelling et al.*¹⁵ observe no correlation between
43 main geological structures and remotely-monitored seismicity in the Creighton mine in Sudbury, Canada.

44 Recently, certain event types have been related to mechanism involving aseismic slip. Sainoki *et*
45 *al.*¹⁶ used a microseismic database and a 3D numerical model to show that a fault in Copper Cliff Rock,
46 Canada, slips widely aseismically, and emphasizes the importance of differentiating aseismic from seismic
47 slip for optimizing support systems. Naoi *et al.*¹⁷ and Yamaguchi *et al.*¹⁸ suggested a potential link between
48 very small microseismic events ($M_w < -4$) in the Cooke 4 gold mine, South Africa, and stable and aseismic
49 fault slip. The authors referred the seismic events as seismic repeaters (i.e. seismic signals with highly
50 similar waveforms), well-known in natural seismology and commonly associated to the shearing of
51 asperities loaded by a slow and aseismic slip on fault planes.¹⁹⁻²³ Some famous examples of seismic
52 repeaters have been studied at active plate margins as the San Andreas Fault in California, USA,²⁴ the North

53 Anatolian fault in Turkey,²⁵ the Northeastern subduction zone in Japan²⁶ but also in man-made reservoirs
54 and geothermal fields.²⁷⁻²⁹

55 Seismicity at the Garpenberg underground mine, in Sweden, was previously investigated using
56 geophysical and geotechnical in-situ data as well as 3D geomechanical modeling, and evidenced two
57 principal event types : (i) a proximal seismic activity, directly induced by local stress changes due to mining,
58 and (ii) a distant one, influenced by geological heterogeneities³⁰ both ranging in magnitude between $-2 <$
59 $M_w < 1$ (moment magnitude). However, subsequent studies on seismic data and strain measurements
60 showed that seismicity is widely associated with the occurrence of seismic multiplets and repeaters,
61 persisting in time over several weeks to months and partially over years whose recurrence rates and
62 triggering seemed to be link to creeping behavior of the rock mass.^{30,31} In agreement with the classical
63 interpretation, Kinscher *et al.*³¹ explain the presence of repeaters as a consequence of a slow and aseismic
64 slip on pre-existing structures, caused by the redistribution of stresses after stope excavation, and loading
65 asperities. In this hypothesis, the seismic asperity is seen as a brittle friction part of a creeping fault plane,
66 able to slip dynamically.³¹ Seismic repeaters of a same family are induced by the repetitive breaking of the
67 same asperity loaded by continuous and slow slip on aseismic portions of the fault. However, the exact
68 geological nature of these asperities and of the creeping material remained unknown from this model³¹ and
69 need to be understood in detail in order to involves the potential underlying seismic-aseismic coupling
70 process in seismic hazard assessment in the mine.

71 To observe the structures and investigate the mechanisms responsible for the generation of seismic
72 repeaters, we installed a dense and local network centered on one particular repeater family located at 1km
73 depth. Six boreholes have been drilled through the location of seismic events, and strain sensors (CSIRO
74 Hi12 cells) were installed inside the boreholes. This adds proximal geological and geomechanical data to
75 the geophysical observations, and enables us to explore the origin of repeaters in our zone of interest. Drill
76 cores and strain measurements are analyzed and compared with seismic source mechanism and seismic
77 location. In our method, seismic parameters calculated from previous analyses (source location, orientation
78 and parameters) as used as a reference for the comparison, keeping in mind they contain biases. Then, a

79 model is built to discuss the presence of a seismogenic asperity on a creeping fault plane, and constrain its
80 location. Our results show that field observations are compatible with the existence of an asperity on a
81 creeping fault plane. However, our study also illustrates how difficult it may be to conclude on the geological
82 origin of the monitored seismicity, even with such a unique, in-situ installation.

83

84 **2. Study area and local monitoring network**

85

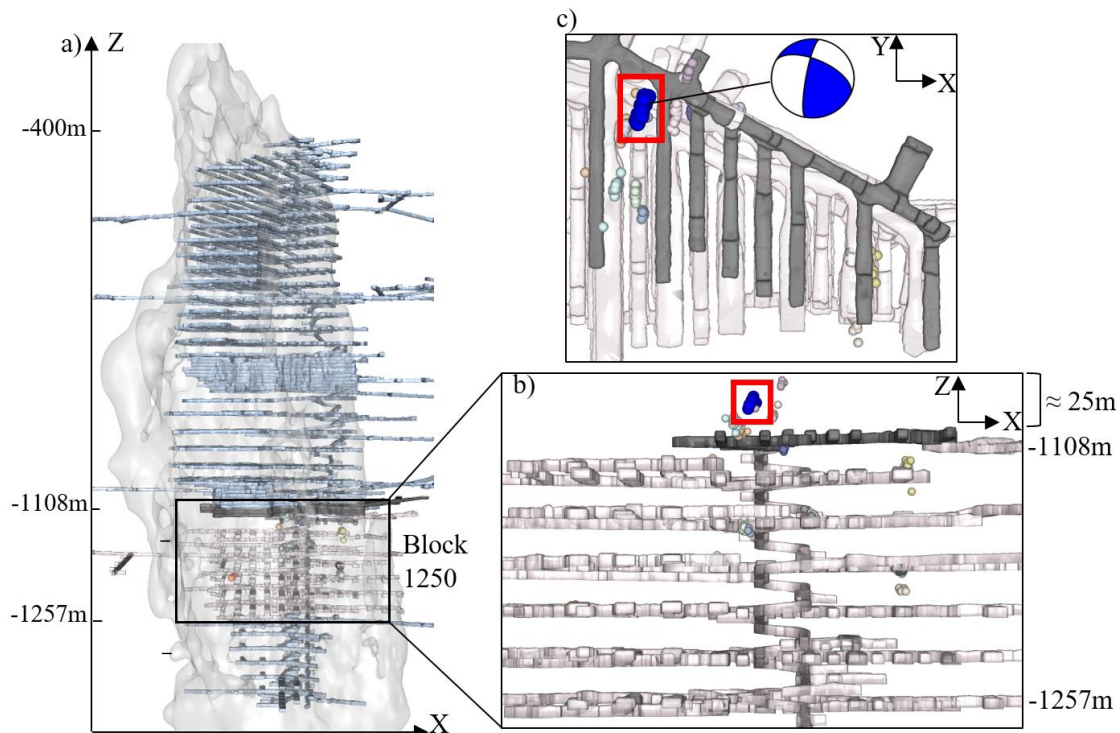
86 *2.1. Study area*

87

88 The Garpenberg mine is a deep polymetallic mine located in central Sweden, operated by Boliden
89 mining company. The Lappberget deposit is currently the largest Zn-Pb-Ag-(Cu-Au) sulfide deposit in the
90 mine.³² Lithologies described within the mine are mainly composed of felsic metavolcanites, characterized
91 by a moderate to intense K-Mg-Fe±Si-rich alteration expressed by mica and quartz,³³ with an overlying unit
92 dominated by calcitic to dolomitic marble.³³ Mineralization occurs as massive sulfide steeply lenses and is
93 mostly concentrated on the limbs of the upright structural dome.³⁴ Orebodies are dominated by an
94 assemblage of sphalerite, galena and pyrite with pyrrhotite and chalcopyrite as minor components and
95 locally magnetite.^{34,35} Few mineralized northeast-trending shear zones are also described as cross-cutting
96 the massive sulfide mineralization and are associated with talc and chlorite alteration.³⁴

97 The main mining method is sublevel stoping. Study area of our target repeater source is located in
98 the sill-pillar (around 25 meters in height) right above one excavated panel ranging from -1108m to -1257m
99 in depth (figure 1). It is located at the limit between (i) breccias in calcitic marble and metasediments and
100 (ii) the intensely quartz-mica-altered and silicified metavolcanites containing mineralized veins. Silicified
101 rocks are stiff, but their properties vary as a function of their mica content. Two stress measurements in the
102 mine panel below the sill-pillar provide Young's modulus of 44 GPa and 64 GPa. Metasediments and
103 calcitic marble are more homogeneous, with a Young's modulus estimated around 55 GPa.³⁰ Tectonic
104 foliation expressed as schistosity is more penetrative in more coarse-grained and mica-rich rocks, which

105 gives anisotropy to the rock mass. For the following, we use the local, mine coordinates X, Y and Z. When
 106 we adopt strike orientation (N-S), North is oriented along the Y-axis of the mine.



107
 108 Figure 1. The ore body of Lappberget and the area of monitoring of Ineris since 2015. a) is vertical section showing
 109 the whole ore body with drifts of excavation, b) is a zoom of the area monitored by Ineris and c) is a plane view of the
 110 area. Upper and lower levels of the sill pillar are in grey (height around 25m). Note only the lower level of the sill-
 111 pillar is showed in images b) and c) to facilitate visualization. Spheres of different colors represent the 17th families of
 112 repeaters detected by the previous network. Plane view shows an alignment slightly inclined from Y-direction of the
 113 mine. Red square indicates the family of repeaters (dark blue spheres) described in table 1, which is the target family
 114 of the installation described in the following and the main object of the paper. The focal mechanism was determined
 115 from the moment tensor double-couple (DC) solutions (colored = compressive quadrant, white = extensive quadrant).
 116

117 *2.2. Seismic analysis from seismic catalogue (2015-2017)*

118
 119 Seventeen main families of repeaters have been identified within the rock volume³¹ (block 1250)
 120 monitored by Ineris (the French National Institute for Industrial Environment and Risks) since 2015 (figure
 121 1). Some repeater families are regularly reactivated over very long periods of time (up to several years). As
 122 creep is usually linked to the presence of a weak-material infilling (i.e, with low shear resistance) inside a

123 fault,^{36,37} Kinscher *et al.*³¹ assumed that the repeaters in the mine are due to the breaking of asperities within
124 creeping talc-filled pre-existing fractures.

125 The procedure to determine repeaters and parameters is detailed by Kinscher *et al.*³¹, and we remind
126 here key points. The data used to identify repeaters are events monitored during the period 2015-2017 by a
127 network installed in the excavation panel below the sill pillar (Z from -1108m until -1257m). The network
128 was composed of four 3-components and five 1-component 14 Hz geophones, and operated in a triggered
129 mode with a 8000 Hz sampling rate. The grouping in families with similar waveforms was done by means
130 of wave form cross-correlation, and threshold of the cross-correlation coefficient $C > 0.8$ was used.³¹ Event
131 location was performed by using P- and S-wave arrival times and P-wave polarization angles, and a
132 relocation was performed following the double difference (DD) principle.³¹ Source parameters, such as
133 corner frequency and seismic moment of the seismic events, have been calculated by using a source
134 spectrum fitting method using 3-components stations of the network. Source radii were derived from the
135 corner frequency using Madariaga's model.³¹ Finally an analysis of source overlap (using relative event
136 location and source radii) was applied in order to classify and distinguish between exact seismic repeaters
137 (repeat rupture of the same source) and multiplets (rupture of closely neighbored sources). In the context of
138 this article, we consider the 17 main families identified by Kinscher *et al.*³¹ as repeater families, because all
139 source locations are within a radius of 1-10m (i.e. of same dimensions than families with exact same source)
140 even though they don't overlap perfectly.

141 Source mechanisms, determined from the moment tensor double-couple (DC) solutions, show a
142 predominance of strike-slip movement with a significant reverse component for most of the repeaters³¹.
143 Fault planes seem to strike along the Y-direction of the mine as indicated by the alignment of the relocated
144 seismic event cloud of each family (figure 1). Source radii calculation indicate that seismogenic asperities
145 have dimensions in the range 1-10 m, with a maximum slip of several millimeters for the strongest events,
146 magnitudes M_w between -1.2 and 2, and stress drops between 0.1 and 10MPa.³¹ Time periodicity is around
147 1 month, but can be decreased by the occurrence of mine blasts. For repeaters of the target family in the sill
148 pillar, slip values mainly range between 0.3 and 2mm with an average value of 1mm. The family has a

149 recurrence time of 35 days, which partially decreases following some local stopping events.³¹ Main
 150 parameters of target repeater family, active since 2016, are presented in Table 1. These parameters,
 151 determined with seismic analyses, are used as reference in this article and compared with geomechanical
 152 and geological data.

Strike	Dip	Rake	Source mechanism	Mw average	Slip average	Stress drop	Mean source radius
190°	75°	130°	Strike-slip with reverse component	-0.3	1mm	≈1MPa	5.8m

153 Table 1. Characteristics of the nodal plane associated with the targeted family.³¹ Strike is defined clockwise from Y-
 154 axis of the mine and follows the right-hand rule. The rake corresponds to the slip direction on the fault plane, defined
 155 with Aki Richards convention. Mw-average is the average moment magnitude of the events and slip-average is the
 156 average amount of seismic slip during one seismic event. Note that the orientation of the nodal plane, amongst the two
 157 possible orientations given by focal mechanism, was chosen as the one parallel to the alignment of seismic events
 158 along this plane. This choice is explained in more details by Kinscher *et al.*³¹

159

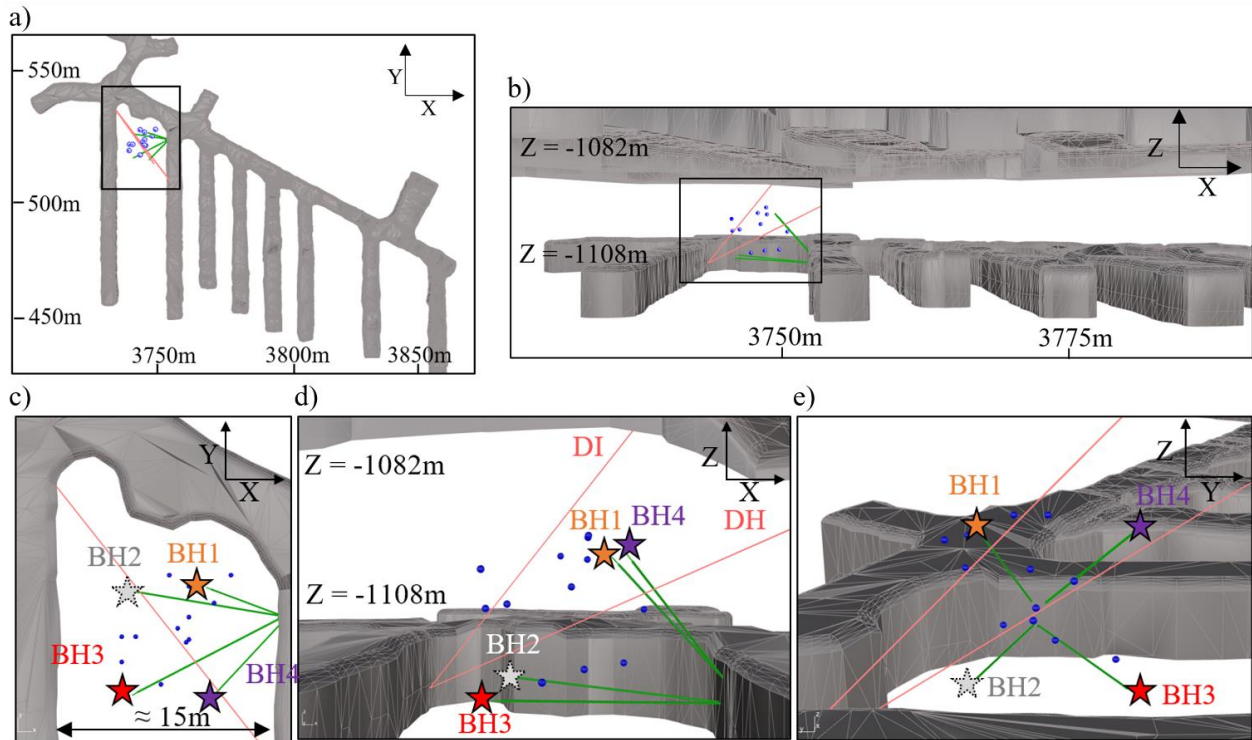
160 2.3. *In-situ local monitoring system*

161

162 To improve absolute location of the target and other repeaters, a local seismic network composed of
 163 seven stations has been installed in the Sill Pillar in 2020, in which full wave form based method is used to
 164 assure automatic seismic event detected and location.³⁸ Amongst newly detected events, events with most
 165 similar wave forms than the target family has been identified and located based on P and S wave arrival
 166 times.

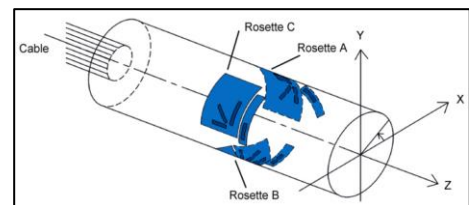
167 Based on the absolute location of the newly detected seismic repeaters, several boreholes were
 168 drilled in November 2021 in the volume of highest events concentration, to try to crosscut the fault plane
 169 associated with the target repeater family. Four permanent CSIRO Hollow Inclusion (HI12) strain cells were
 170 installed at the bottom of 10-meters long boreholes BH1, BH3, BH3 and BH4 (Figure 2). Cells were
 171 previously tested in laboratory to ensure an accuracy about ±5 micro-strains (με).³⁹ Strains are measured
 172 every minute. Each cell includes 12 strain gauges with different orientations (Table 2), allowing to get the

173 complete strain tensor at the location of the cell.^{40,41} Two additional boreholes (DI and DH, respectively 30
 174 and 35 meters long) were drilled to get lithological and structural information. BH2 was not operational,
 175 due to a problem of installation (the cell is not entirely located within the small pilot hole, which was visible
 176 from borehole cameras). Coordinates of strain cells and dimensions of the area are showed table 2.



177
 178 Figure 2. Local monitoring network installed in the sill-pillar. Upper images a) and b) show plane view (Z = -1108m)
 179 and front view at the scale of the whole sill pillar. Below images c), d) and e) show a zoom on the installation: plane
 180 view, front view and side view. Excavated drifts are in grey. Blue dots represent the absolute location of newly
 181 repeaters between October 2020 and November 2021. BH1, BH3 and BH4 refer to the 3 correctly installed CSIRO
 182 cells (colored stars) and the associated drillings (in green). BH2 is showed in grey as it was not functional. In red:
 183 additional drillings DH and DI.

	BH1	BH2	BH3	BH4	Main event detected	dimensions of the area
X	3740	3733	3733	3740	3735	≈ 15m
Y	522	522	513	513	515	≈ 20m
Z	-1097	-1105	-1105	-1097	-1099	≈ 25m



184 Table 2. On the left: coordinates of: the four cells, a main event of M-1 detected by the network (occurred on the 18th
 185 of January 2022 and further mentioned in the article) and dimensions of the area. On the right: scheme of one csiro
 186 cell, with the orientations of the twelve different gauges (radial, inclined and orthoradial).

187 **3. Field data analysis**

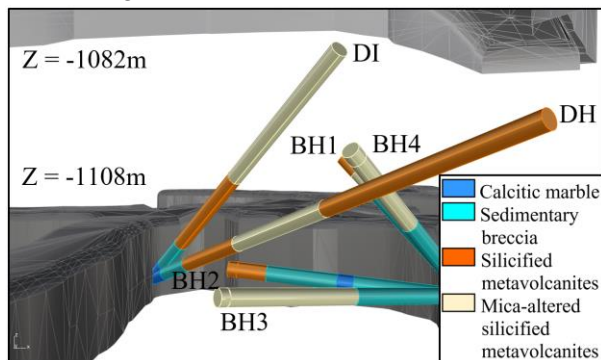
188

189 **3.1. Fracture density and fracture orientation**

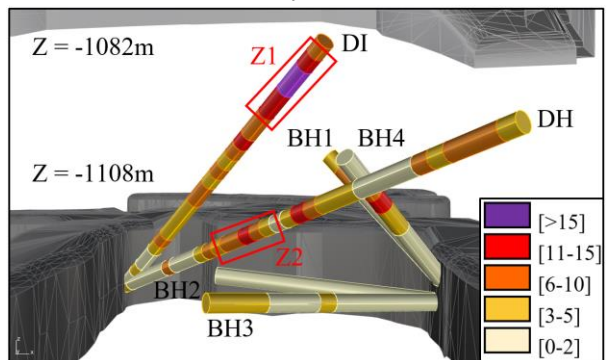
190

191 In this section, we describe the fracturation of the area, and compare the orientation of the fractures
192 with the seismic nodal plane given by seismic data (table 1). Drill cores in the study area, with a total length
193 of about one hundred meters and with different orientations, show the presence of metasedimentary rocks,
194 and siliceous rocks with different amounts of micas and hosting mineralized veins. Such lithologies are very
195 common in the mine and similar to what is usually observed elsewhere. Rocks are of good quality and drill
196 cores are not much fractured (linear density usually less than 10 fractures per meter). Two zones of higher
197 fracture density are observed: Z1 and Z2 (figure 3).

a) Lithologies



b) Linear fracture density



c) Zone of fracturation Z1



d) Zone of fracturation Z2

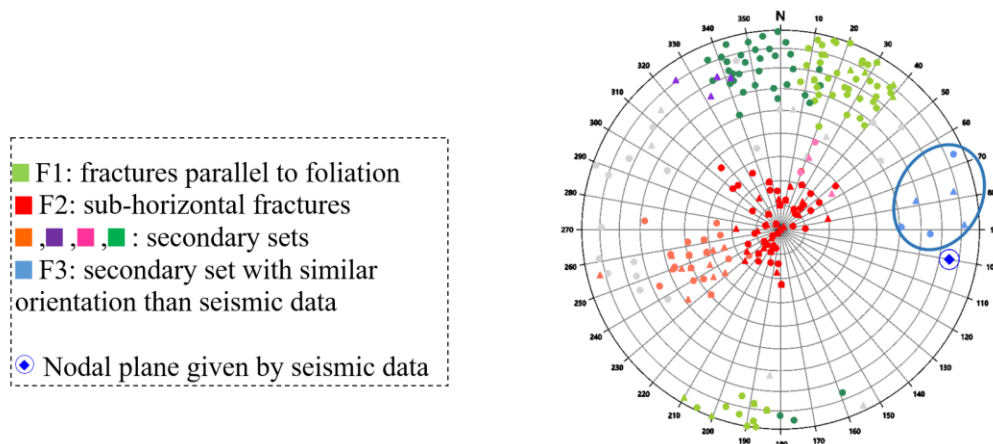


198 Figure 3. a) Lithologies logged in the drill-cores. b) Linear fracture density (number of fractures per meter) along the
199 drill-cores in the sill-pillar. Highlighted by red rectangles, the two main zones of fractures: Z1 and Z2. Mine
200 excavations are in grey. c) and d) Photos of the two main fracture zones.

201

202 Drill cores have been cautiously oriented using endoscope images and in-situ orientations of the
203 fractures were properly determined from the oriented drill cores using the method proposed by Holcombe

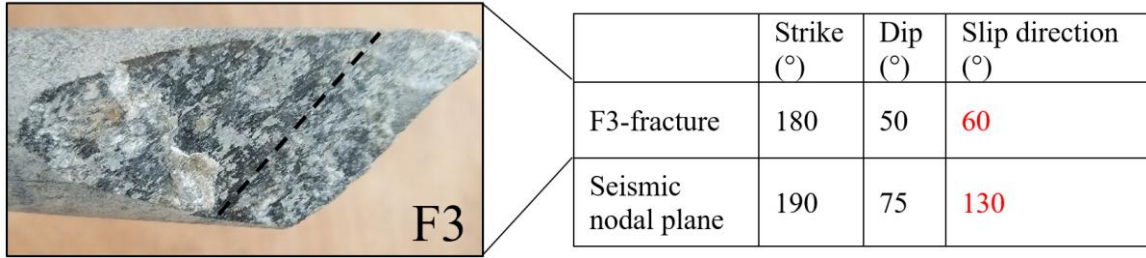
204 (2013). The method is based on the measurement of two angles on the cores, measured with protractor
 205 templates, which provide the orientation of fractures relative to the drill core axis and to a reference line
 206 along the core. Two main sets of fractures have been intersected by at least 5 drillings and are visible all
 207 along the cores: F1 and F2 (figure 4). These sets correspond to the main structures already identified by the
 208 geologists of the mine. Secondary sets of fractures are also observed. Set F3, mainly located inside Z2 zone
 209 of fracturation, is the only one whose orientation is compatible with that of the seismic nodal plane.



210
 211 Figure 4. Orientation of natural fractures in the boreholes. Each set is represented by a different color. In dark blue:
 212 the nodal plane deduced from seismic analysis. Dots represent fractures and triangles represent veins. In grey, fractures
 213 not belonging to any set.

214
 215 3.2. *Mineralogy of fracture infillings and evidence of shear movement along F3 fractures*

216
 217 X-ray diffraction (XRD) analyses were conducted at the GeoRessources laboratory (Nancy, France)
 218 to identify the nature of the infilling minerals and assess if fracture planes tend to slip aseismically. Most of
 219 F3 fractures contain laumontite (zeolite), and muscovite and chlorite that usually have low friction
 220 coefficients⁴³ and could be good candidate for creeping material. Moreover, F3 fractures present slickenside
 221 lineations. However, the direction of slip on F3 fractures measured from these lineations (Figure 5) is very
 222 different from the one expected by the seismic rake, as the rake of the seismic nodal plane indicates a reverse
 223 plus right-lateral displacement and the geological fracture indicates a reverse plus left-lateral displacement.
 224 Even if those two slip directions are incompatible, the presence of lineations indicates that F3 have slipped
 225 in the past and may still do but without leaving slickensides lineation while creeping at this specific
 226 location.



228
 229 Figure 5. Comparison between F3-set and the seismic nodal plane. At the left, one F3-fracture from the drill cores.
 230 From slickensides lineation (dashed dark line), slip direction of the fracture is measured. Slip direction of the seismic
 231 nodal plane is deduced from the seismic focal mechanism (seismic rake). Table on the right shows strike, dip and slip
 232 direction from both F3-fractures and the seismic nodal plane. Slip direction is strongly different, as 60° indicates a left-
 233 lateral displacement and 130° a right-lateral displacement (Aki Richards convention).

234
 235 *3.3. State of stress*

236
 237 Several stress measurements have been performed in the mine. All of them are likely influenced by
 238 the presence of galleries, except for one,⁴⁴ that we selected to infer the stress state. Principal stresses σ_1 and
 239 σ_3 of these measurements were dipping horizontally and oriented at 155° and 65° from the Y axis,
 240 respectively, while σ_2 is vertical. Normal and shear stresses on fracture planes derived from this stress state
 241 are plotted on figure 6. The seismic nodal plane appears most favorably oriented to slip for the assumed
 242 stress state. Here, we assume that the whole target fault plane (with both aseismic portions and at least one
 243 asperity) has the same orientation as the nodal plane. The coefficient of friction has to be as low as 0.3 for
 244 the fault to slip, which is coherent with what is usually observed in chlorite gauge with aseismic slip.⁴⁵

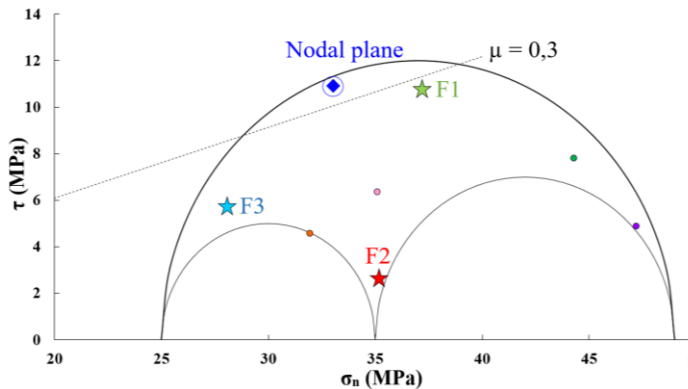
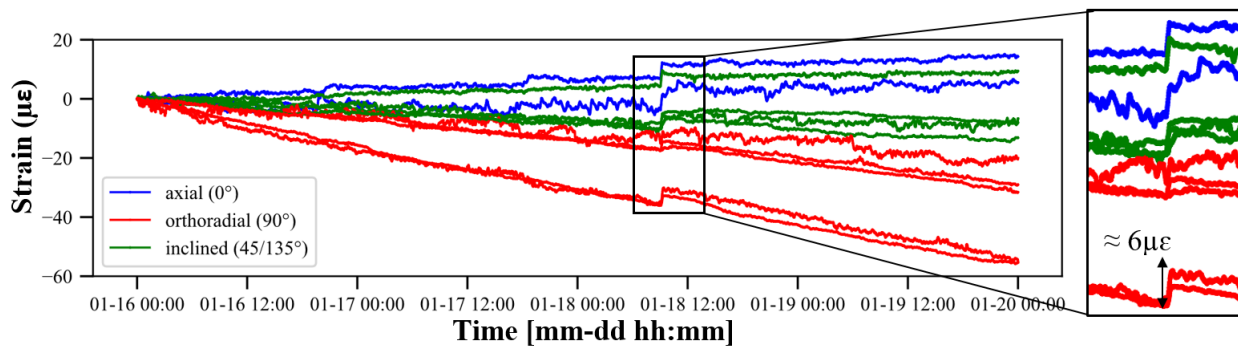


Figure 6. Mohr plot of the stress vector on fracture planes and on the nodal plane. Stars represent F1, F2 and F3 sets of fractures and dots the secondary structures. Blue diamond is the nodal plane given by seismic data. The dotted line is the Coulomb failure criterion $\tau = \mu * \sigma_n$, with a friction coefficient of 0.3 (no cohesion). Note that F3 set is less favorable oriented to slip (i.e. is in more stable condition) than the seismic nodal plane, whereas they have similar orientation. This is due to the high sensitivity of the calculation to small changes in orientation.

245 3.4. Strain monitoring

246
247 One seismic event of magnitude $M=1$ was detected by the strain cells on January 18, 2022. This
248 event is one order of magnitude higher than the other seismic events monitored during a period of 8 months.
249 Correlation between seismic waveforms of this event and the target family shows that it belongs to the target
250 family. During the event occurrence, a co-seismic shift of 6 micro-strains ($\mu\epsilon$) was monitored by the BH4
251 strain cell (figure 7). BH1 did not monitor any deformation and BH3 monitored one tiny shift of around
252 $0,8\mu\epsilon$. This latter shift is below the resolution of $5\mu\epsilon$ ensured by the technicians in charge of cell installation,
253 but was visible because the noise level before and after the shift is $< 0.8\mu\epsilon$. This suggests that the asperity
254 is located very close to BH4, not too far from BH3 and sufficiently far from BH1 to not be detected.



255
256 Figure 7. Recordings of the 12 strain gauges of the BH4 CSIRO cell, between the January 16 and 20, 2022. In red: the
257 orthoradial gauges, in blue the axial gauges and in green the inclined gauges. The shift of deformation occurred the
258 18th of January, mainly between 9:08am and 9:09am. Strain curves show a constant drift, explained by the creep of the
259 glue.⁴⁶ Here, only the co-seismic shift is of interest and the drift is neglected as the co-seismic movement occurs over
260 a very short period compared to the creep characteristic timescale. Because of the short duration of the shift, we exclude
261 the influence of the creep of the glue during the minute of the seismic event. On some gauges, some stair-stepped shape
262 as well as potential post-seismic deformation are visible. Because we work at the limit of the resolution of the cell, we
263 only focus on what occurred during the minute of the main seismic event. Further investigation plan to install high
264 resolution optic fiber to study in more details pre and post seismic deformation.

265
266 A reliable co-seismic strain tensor could be derived using the 12 CSIRO Hi12 strain gauges from BH4,
267 following the inversion method described by Worotnicki.⁴⁰ The geometry of the strain gauges inside the
268 device is shown table 2. Amplitudes and orientations of the three principal strain axes (figure 8) demonstrate

269 a main elongation along ϵ_3 ($-6,6\mu\epsilon$) with an azimuth of 48° from Y-direction and a dip of 22° . The coseismic
270 strain data recorded at BH3 was too noisy to obtain reliable orientations of principal strains.

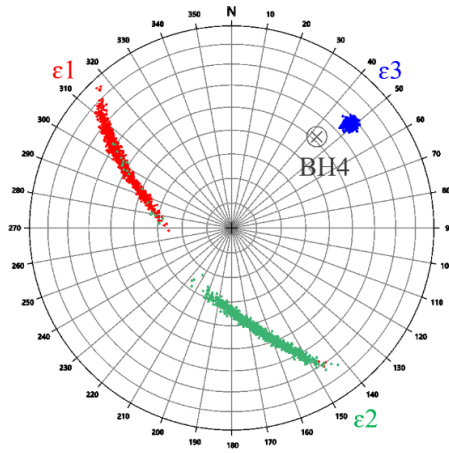


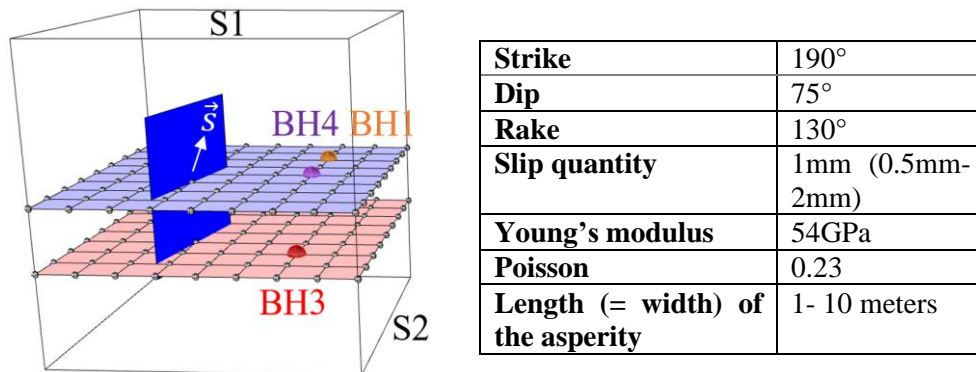
Figure 8. Principal co-seismic strain orientations during the shift of the 18th of January. Dots on the figure come from a random set of other potential solutions considering the error attached to the estimation of the tensor. Values are $\epsilon_3 = -6,6\mu\epsilon$ (extension), $\epsilon_2 = +0,96\mu\epsilon$ (shortening), $\epsilon_1 = +1,7\mu\epsilon$ (shortening). One major extensive strain is observed within the direction of the drilling.

271
272 **4. Evaluation of the presence of a coupled seismic/aseismic fault plane**
273
274 This section aims at evaluating the compatibility of the seismic source location and mechanism with
275 the co-seismic strain measurements and the observations from the drill cores. We distinguish the seismic
276 asperity, whose dynamic slip caused the seismic source of the event of the 18th of January, from the whole
277 creeping fault plane. Strain records were modelled using Okada's finite fault approach model to evaluate
278 compatibility between seismic nodal plane (i.e. the asperity) and deformation measurements; and to localize
279 the seismic asperity.

280
281 *4.1. Elastic model of dislocation*

282
283 We use the dislocation model by Okada allowing to calculate analytically the strain tensors in the
284 vicinity of a finite fault ⁴⁷ to simulate slip on the seismic asperity. We extract strain tensors at the location
285 of the strain cells and we compare them with CSIRO in-situ measurements (figure 9). The medium is
286 approximated as a homogenous half-space and is supposed to be elastic and isotropic. Details on the method
287 can be found in Van Zwieten *et al.* ⁴⁸ We used the Coulomb3 software to build the Okada model. ⁴⁹ Geometry

288 of the model is chosen according to the dimensions of the sill pillar: X in the range 3500m to 3900m; Y in
 289 the range 500m to 540m; Z from the surface until down to a depth of -1120m. Rock parameters come from
 290 bi-axial tests performed on samples from the mine panel below the sill-pillar.⁵⁰ As the co-seismic shift of
 291 deformation is induced by slip on one asperity, we only include the seismic asperity in the model and not
 292 the whole fault plane. Parameters of the asperity are taken from the seismic nodal plane derived from seismic
 293 source analysis by Kinscher *et al.*³¹ The size of the asperity varies between 1 and 10 meters, with length and
 294 width of same dimensions. As discussed further in next section, the centroid of the asperity corresponds to
 295 the seismic centroid (and error location).



296 Figure 9. Schematic geometry of the elastic model of dislocation (not to scale) and associated parameters. The planar
 297 free surface (S1) of the medium is traction-free and the borders of the half space (S2) are displacement-free. The
 298 asperity is represented by the blue rectangular surface, \vec{s} is the slip vector on the asperity with specific orientation
 299 (rake) and value (1mm). Purple and red surfaces indicate horizontal surfaces at BH4 and BH3 levels, with a mesh
 300 resolution of 0,5m. Strain tensors are extracted at BH1, BH3 and BH4 cells (orange, red and purple dots). Strike is the
 301 most reliable data, dip uncertainty is estimated to be approximately 30°, rake uncertainty cover values indicating strike-
 302 slip and/or right lateral movements, the amount of slip can be up to a few mm. A few tests, by varying each parameter
 303 individually, have showed no significant changes in the interpretation of the results presented next section. Length of
 304 the asperity comes from the source radius estimated from corner frequency using Madariaga's model, by Kinscher *et*
 305 *al.*³¹

306

307 4.2. Location of the asperity

308

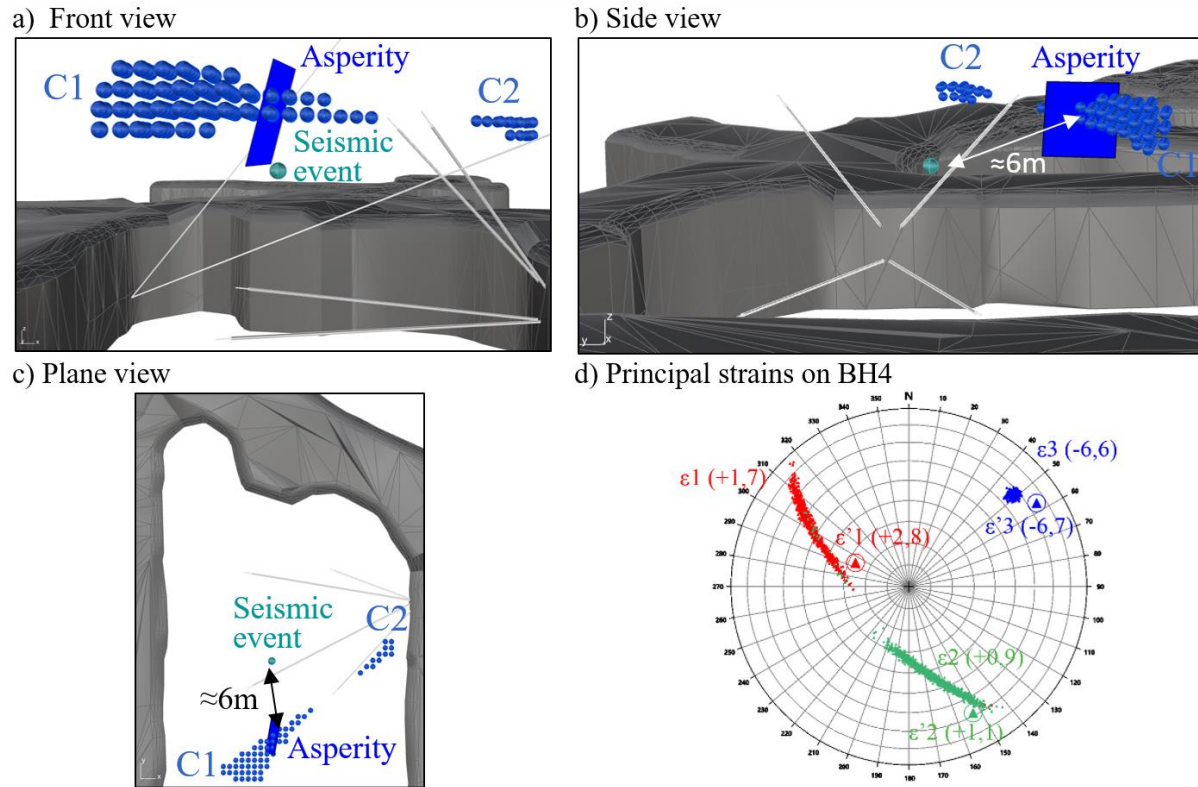
309 The location of the asperity is constrained using an inversion approach. The asperity should be
 310 within a radius of 10 meters from the seismic hypocenter of the January 18th event which corresponds to the

311 location error estimated from probabilistic analysis based on observed and theoretical P and S wave arrival
312 times⁵¹. We tested locations over grid with 0.5 m resolution (total of 34248 points). For each configuration,
313 strain tensors are extracted at the cell positions and compared with monitored data.

314 Most likely fault location are then found by comparison (error minimization) with the principal
315 strains recorded by the BH4 cell. In addition, the absence of significant strain at BH1 and BH3 was also
316 used to constrain the fault location by imposing the modelled principal strain to be below the recording
317 sensitivity of the strain cells. More specifically for BH4, we selected locations which gave modeled principal
318 strains within the uncertainty range of the cell, of similar sign (i.e. extension or shortening) than the
319 measured ones, with a ratio greater than 2 between the major and intermediate principal strains, and
320 corresponding to a slip of 0.5 to 2 mm on the fault. For the latter, we selected locations which gave a major
321 principal strain between $-12 \mu\epsilon$ and $-3 \mu\epsilon$, since the model was built for a slip of 1mm and because slip and
322 strain values are proportional (the major principal strain measured by BH4 is $-6\mu\epsilon$).

323 Results show the existence of solutions to our inversion model, and thus the existence of asperity
324 locations consistent with both seismic parameters and monitored strains. They show that most likely asperity
325 locations are concentrated to two areas (figure 10). None of these areas is crosscut by the drillings, what
326 eventually explain the apparent absence of fractures with markers of movement consistent with seismic
327 source mechanism in the drill cores. The area located to the west is generally closer to the seismic event
328 location and is thus assumed to be the most likely asperity location. Average distance between the events is
329 2m and the maximal distance is 8m. On figure 10, we show one possible location of the asperity within the
330 cluster and the associated dimensions. This location is the one which gives strain values closest to the ones
331 monitored by BH4, based on the model inversion. The chosen asperity is at 6 m from the seismic event of
332 the 18th of January, which is reasonable considering seismic event location error. Its dimensions are 3m*3m,
333 also based on the model results. Orientations of the main strains are within the ranges of uncertainties of the
334 BH4 cell. The asperity displayed on Figure 10 corresponds to the smallest misfit with measured strains for
335 a fault slip of 1mm. However, all locations in the cluster and all dimensions in the range 1-10m are

336 considered equally plausible. In fact, the exact location of the asperity depends on the fault slip value, which
 337 is an uncertain seismic parameter.

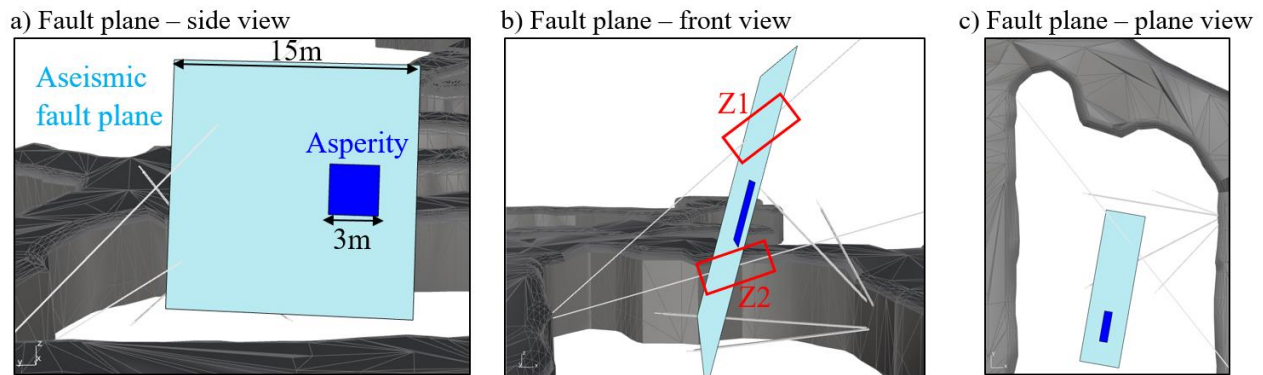


338
 339 Figure 10. a), b), c) The two clusters of possible locations for the asperity (blue dots), given by the inverse resolution.
 340 The chosen location of the asperity is shown by a blue surface. Light blue dot represent the seismic event of the 18th
 341 January. d) Values and orientation of principal strains, for the BH4 cell and for the model after slip on the asperity. ϵ_1 ,
 342 ϵ_2 , ϵ_3 are given by the cell. ϵ'_1 , ϵ'_2 , ϵ'_3 are obtained from the model at the location of the cell.

343
 344 *4.3. Compatibility with drill core observations*

345
 346 The localized asperity is expected to be part of a fault plane, and embedded between creeping zones
 347 along that plane. Dimensions of the fault plane hosting the asperity are chosen large enough to be crossed
 348 by the drillings, which gives a fault plane of 15m*15m. These dimensions are below the size of the main
 349 shear zones observed in the mine, crossing the whole ore body over hundreds of meters. Interestingly, the
 350 fault plane is crossed by the drillings in Z1 and Z2 zones of fracturation identified in the drill cores (figure

351 11). Z2 contains F3-fractures, with chlorite/muscovite infilling and similar orientation to the seismic nodal
352 plane. This finally is an excellent agreement between geophysical, geological and geomechanical data.



353
354 Figure 11. Aseismic fault plane (light blue surface) crossed by the drillings. Z1 and Z2 are the two highest zones of
355 fracturation within the drill cores. The asperity (dark blue) has been placed arbitrarily on the fault plane. The fault
356 plane is assumed to have same orientation than the seismic nodal plane.

357

358 5. Discussions

359

360 The origin of seismic repeaters has been investigated from an insitu measurements, combining
361 geophysical, geological and geo-mechanical data. Based on the data we evaluated the hypothesis that
362 repeaters are related to the repeat rupture of one single asperity loaded by creeping portions on a fault plane.
363 Following this conceptual model, co-seismic deformation recorded by the strain cells indicate that the size
364 of the asperity (seismic part of the fault plane) is likely a few meters, as consistent with estimates from
365 seismic source parameters (source radius estimated from corner frequency). Furthermore, the strain data and
366 geological observation indicate that the seismic asperity has been unfortunately missed by the drillings. On
367 the other hand, drill cores highlighted a potential aseismic part of the same fault zone associated with the
368 asperity. Indeed, drillings highlighted a fractured zone coherent in orientation and location with respect to
369 the asperity and characterized by weak creep prone material (chlorite, muscovite) and a low friction
370 coefficient.

371 Despite this general agreement between the model and the multiparameter data set, these findings
372 need to be further confirmed and detailed by future investigations due to the underlying uncertainties of our

373 data analysis and data completeness. Accordingly, the geological and rheological nature of the seismic
374 asperity (not crosscut by our drillings) and the involved seismic-aseismic coupling mechanisms remain
375 uncertain. Main shortcoming is the significant location error of the seismic events which is a fundamental
376 prerequisite to reach the key zones by the drillings. The co-seismic deformation might also have been
377 influenced by instrumentation sensitivity, and the seismic nodal plane orientation include uncertainties due
378 to instrumentation and simplified models. Regarding the considered state of stresses, two other
379 measurements within the panel of excavation below the sill-pillar are not able to explain the activation of
380 the seismic nodal plane,⁵⁰ which highlights the difficulty to rely on one single stress state considering such
381 a variable environment.

382 Apart from the geomechanical processes expected from the evaluated model (i.e. aseismic creep),
383 we found evidence that the geological nature of creeping zones might be associated with strongly fractured
384 zones without involving weak creep prone materials (e.g. chlorite infillings). Indeed, at its northernmost
385 extent, the extrapolated fault plane crosscuts the highly fractured zone Z1 (figure 11) which does not show
386 any evidence of potential creep-prone weak-material. Observations from temporary DTTS Brillouin based
387 strain monitoring (not presented as it was not operational during the event of 18th of January) along an
388 optical fiber installed in the borehole DI crosscutting Z1 indicated initiation of continuous deformation in
389 this particular zone associated with strain rate of two micro strain /day over around weeks following the 18th
390 of January event. In this case, we thus assume that this highly fractured zone could represent a weak zone
391 in the rock mass susceptible to host time-dependent movement loading same locked parts in the area.

392

393 **6. Conclusion**

394

395 In this study we investigated the geological and geomechanical origin of seismic repeaters in the
396 mine of Garpenberg, Sweden. Determining their origin is crucial to evaluate the role of aseismic creep
397 induced by mining in the triggering of mine seismicity, and to improve seismic hazard assessment in deep
398 mines. In seismology, repeaters are commonly associated with the repeat rupture of a seismic asperity

399 continuously loaded on widely creeping fault. A local in situ experiment has been conducted targeting one
400 repeater family accessible from the mine drifts. The newly acquired geological data and results from strain
401 monitoring suggest the presence of a fault plane consistent in orientation and size with seismic source
402 characteristics. Unfortunately, the data set did not allow to conclude entirely on the detailed seismic-
403 aseismic coupling mechanisms along the fault, since drillings seemed to have missed its seismogenic part
404 (asperity). However, drillings seem to have reached aseismic moving parts of the plane which are possibly
405 related to the presence of chlorite and muscovite infillings. Future experiments are planned based on a much
406 denser seismic network and fiber optic technology to increase location of seismic events. Furthermore,
407 additional drillings and comprehensive optic fiber based strain monitoring devices around and within the
408 fault zone may allow to better understand and quantify the involved seismic – aseismic coupling mechanism.
409

410 **Declaration of competing interest**

411
412 The authors declare that they have no known competing financial interests or personal relationships that
413 could have appeared to influence the work reported in this paper.

414
415 **Acknowledgment**

416
417 This work was performed at the GeoRessources laboratory of the “Université de Lorraine” in France. It is
418 part of a collaboration between Boliden and Ineris which was initiated in the framework of the European
419 FP7 I2MINE project and continued with a four-year bipartite scientific collaboration. This work was
420 supported by the Region Grand Est (project 19_GE6_089) and Ineris. We acknowledge Anders Nyström,
421 rock mining engineer from Garpenberg and Pascal Bernard, seismologist at IPGP for the precious
422 discussions and advices. We acknowledge geologists of Boliden for being available to answer questions and
423 Francesca De Santis, research engineer at Ineris, for sharing her data and experience. We acknowledge
424 Daniele Bartier, assistant professor at GeoRessources, for her very precious help with the DRX analyses.
425 We acknowledge Nicolas Spitzensteder, technician at Ineris, for explaining the instrumentation, and Laura
426 Sicard and Guy-Aurèle Fiévet for their participation in the measurements on the cores.

427

428 **7. References:**

- 429
- 430 1. Cai M, Kaiser PK, Martin CD. Quantification of rock mass damage in underground excavations
431 from microseismic event monitoring. *Int J Rock Mech Min Sci.* 2001;38(8):1135-1145.
432 doi:10.1016/S1365-1609(01)00068-5
- 433 2. Hudyma MR, Heal D, Mikula P. Seismic monitoring in mines — old Technology — new
434 applications. *Proc First Australas Gr Control Min Conf.* 2003;(November 2003):201-218.
- 435 3. Srinivasan C, Arora SK, Yaji RK. Use of mining and seismological parameters as premonitors of
436 rockbursts. *Int J Rock Mech Min Sci.* 1997;34(6):1001-1008. doi:10.1016/S1365-1609(97)80009-3
- 437 4. Urbancic TI, Trifu CI. Recent advances in seismic monitoring technology at Canadian mines. *J*
438 *Appl Geophys.* 2000;45(4):225-237. doi:10.1016/S0926-9851(00)00030-6
- 439 5. Gibowicz S., Kijko A. *An Introduction to Mining Seismology.*; 1994. doi:10.1016/0148-
440 9062(74)91552-6
- 441 6. Gibowicz S. Seismicity Induced by Mining: Recent Research. *Adv Geophys.* 2009;51(C):1-53.
442 doi:10.1016/S0065-2687(09)05106-1
- 443 7. McGarr A. Seismic moments and volume changes. *J Geophys Res.* 1976;81(8):1487-1494.
444 doi:10.1029/jb081i008p01487
- 445 8. Richardson E, Jordan TH. Seismicity in deep gold mines of South Africa: Implications for tectonic
446 earthquakes. *Bull Seismol Soc Am.* 2002;92(5):1766-1782. doi:10.1785/0120000226
- 447 9. Brown LG. Quantifying discrete seismic responses to mining. *Can Geotech J.* 2021;58(7):1023-
448 1035. doi:10.1139/cgj-2020-0248
- 449 10. Hudyma MR. Analysis and interpretation of clusters of seismic events in mines.
450 2008;(November):409.
451 https://repository.uwa.edu.au/view/singleviewer/single_viewer_toolbar2.jsp?frameId=1
- 452 11. McKinnon SD. Triggering of seismicity remote from active mining excavations. *Rock Mech Rock*
453 *Eng.* 2006;39(3):255-279. doi:10.1007/s00603-005-0072-5
- 454 12. Sainoki A, Mitri HS. Dynamic behaviour of mining-induced fault slip. *Int J Rock Mech Min Sci.*
455 2014;66:19-29. doi:10.1016/j.ijrmms.2013.12.003
- 456 13. Ma J, Dong L, Zhao G, Li X. Discrimination of seismic sources in an underground mine using full
457 waveform inversion. *Int J Rock Mech Min Sci.* 2018;106(May):213-222.
458 doi:10.1016/j.ijrmms.2018.04.032
- 459 14. Alber M, Fritschen R, Bischoff M, Meier T. Rock mechanical investigations of seismic events in a
460 deep longwall coal mine. *Int J Rock Mech Min Sci.* 2009;46(2):408-420.
461 doi:10.1016/j.ijrmms.2008.07.014
- 462 15. Snelling PE, Godin L, McKinnon SD. The role of geologic structure and stress in triggering remote

- 463 seismicity in Creighton Mine, Sudbury, Canada. *Int J Rock Mech Min Sci.* 2013;58:166-179.
464 doi:10.1016/j.ijrmms.2012.10.005
- 465 16. Sainoki A, Mitri HS, Chinnasane D. Characterization of Aseismic Fault-Slip in a Deep Hard Rock
466 Mine Through Numerical Modelling: Case Study. *Rock Mech Rock Eng.* 2017;50(10):2709-2729.
467 doi:10.1007/s00603-017-1268-1
- 468 17. Naoi M, Nakatani M, Otsuki K, et al. Steady activity of microfractures on geological faults loaded
469 by mining stress. *Tectonophysics.* 2015;649:100-114. doi:10.1016/j.tecto.2015.02.025
- 470 18. Yamaguchi J, Naoi M, Nakatani M, et al. Emergence and disappearance of very small repeating
471 earthquakes on a geological fault in a gold mine in South Africa. *Tectonophysics.* 2018;747-
472 748(November 2017):318-326. doi:10.1016/j.tecto.2018.10.014
- 473 19. Bakun WH, King GCP, Cockerham RS. Seismic Slip, Aseismic Slip, and the Mechanics of
474 Repeating Earthquakes on the Calaveras Fault, California. 2013;37:195-207.
475 doi:10.1029/gm037p0195
- 476 20. Chen T, Lapusta N. Scaling of small repeating earthquakes explained by interaction of seismic and
477 aseismic slip in a rate and state fault model. *J Geophys Res Solid Earth.* 2009;114(1):1-12.
478 doi:10.1029/2008JB005749
- 479 21. Nadeau RM, McEvilly T V. Fault slip rates at depth from recurrence intervals of repeating
480 microearthquakes. *Science (80-).* 1999;285(5428):718-721. doi:10.1016/s0016-0032(26)90726-6
- 481 22. Poupinet G, Ellsworth WL, Frechet J. Monitoring velocity variations in the crust using earthquake
482 doublets: an application to the Calaveras fault, California (USA). *J Geophys Res.*
483 1984;89(B7):5719-5731. doi:10.1029/JB089iB07p05719
- 484 23. Rice JR. Spatio-temporal Complexity of Slip on a Fault Rate- dependent friction. *J Geophys Res.*
485 1993;98(93):9885-9907.
486 <http://citeseerx.ist.psu.edu/viewdoc/download?doi=10.1.1.161.6067&rep=rep1&type=pdf>
- 487 24. Nadeau RM, Foxall W, McEvilly T V. Clustering and periodic recurrence of microearthquakes on
488 the San Andreas fault at Parkfield, California. *Science (80-).* 1995;267(5197):503-507.
489 doi:10.1126/science.267.5197.503
- 490 25. Uchida N, Kalafat D, Pinar A, Yamamoto Y. Repeating earthquakes and interplate coupling along
491 the western part of the North Anatolian Fault. *Tectonophysics.* 2019;769(July):228185.
492 doi:10.1016/j.tecto.2019.228185
- 493 26. Igarashi T, Matsuzawa T, Hasegawa A. Repeating earthquakes and interplate aseismic slip in the
494 northeastern Japan subduction zone. *J Geophys Res Solid Earth.* 2003;108(B5):1-9.
495 doi:10.1029/2002jb001920
- 496 27. Bourouis S, Bernard P. Evidence for coupled seismic and aseismic fault slip during water injection
497 in the geothermal site of Soultz (France), and implications for seismogenic transients. *Geophys J*

- 498 *Int.* 2007;169(2):723-732. doi:10.1111/j.1365-246X.2006.03325.x
- 499 28. Guglielmi Y, Cappa F, Avouac JP, Henry P, Elsworth D. Seismicity triggered by fluid injection-
500 induced aseismic slip. *Science (80-)*. 2015;348(6240):1224-1226. doi:10.1126/science.aab0476
- 501 29. Kinscher JL, Broothaers M, Schmittbuhl J, de Santis F, Laenen B, Klein E. First insights to the
502 seismic response of the fractured Carboniferous limestone reservoir at the Balmatt geothermal
503 doublet (Belgium). *Geothermics*. 2023;107(December 2022).
504 doi:10.1016/j.geothermics.2022.102585
- 505 30. De Santis F, Renaud V, Gunzburger Y, Kinscher J, Bernard P, Contrucci I. In situ monitoring and
506 3D geomechanical numerical modelling to evaluate seismic and aseismic rock deformation in
507 response to deep mining. *Int J Rock Mech Min Sci*. 2020;129. doi:10.1016/j.ijrmms.2020.104273
- 508 31. Kinscher JL, De Santis F, Poiata N, Bernard P, Palgunadi KH, Contrucci I. Seismic repeaters
509 linked to weak rock-mass creep in deep excavation mining. *Geophys J Int*. 2020;222(1):110-131.
510 doi:10.1093/gji/ggaa150
- 511 32. De Santis F, Contrucci I, Kinscher J, Bernard P, Renaud V, Gunzburger Y. Impact of Geological
512 Heterogeneities on Induced-Seismicity in a Deep Sublevel Stopping Mine. *Pure Appl Geophys*.
513 2019;176(2):697-717. doi:10.1007/s00024-018-2020-9
- 514 33. Jansson N. *The Origin of Iron Ores in Bergslagen , Sweden , and Their Relationships with*
515 *Polymetallic Sulphide Ores.*; 2011.
- 516 34. Tiu G, Jansson N, Wanhainen C, Ghorbani Y, Lilja L. Ore mineralogy and trace element
517 (re)distribution at the metamorphosed Lappberget Zn-Pb-Ag-(Cu-Au) deposit, Garpenberg,
518 Sweden. *Ore Geol Rev*. Published online 2021:104223. doi:10.1016/j.oregeorev.2021.104223
- 519 35. De Santis F. Rock mass mechanical behavior in deep mines: in situ monitoring and numerical
520 modelling for improving seismic hazard assessment Soutenuue. 2019;(September).
- 521 36. Carpenter BM, Marone C, Saffer DM. Weakness of the San Andreas Fault revealed by samples
522 from the active fault zone. *Nat Geosci*. 2011;4(4):251-254. doi:10.1038/ngeo1089
- 523 37. Saffer DM, Marone C. Comparison of smectite- and illite-rich gouge frictional properties:
524 Application to the updip limit of the seismogenic zone along subduction megathrusts. *Earth Planet*
525 *Sci Lett*. 2003;215(1-2):219-235. doi:10.1016/S0012-821X(03)00424-2
- 526 38. Palgunadi KH, Poiata N, Kinscher J, Bernard P, De Santis F, Contrucci I. Methodology for full
527 waveform near real-time automatic detection and localization of microseismic events using high (8
528 kHz) sampling rate records in mines: Application to the Garpenberg mine (Sweden). *Seismol Res*
529 *Lett*. 2019;91(1):399-414. doi:10.1785/0220190074
- 530 39. Souley M, Renaud V, Al Heib M, Bouffier C, Lahaie F, Nyström A. Numerical investigation of the
531 development of the excavation damaged zone around a deep polymetallic ore mine. *Int J Rock*
532 *Mech Min Sci*. 2018;106(April):165-175. doi:10.1016/j.ijrmms.2018.04.028

- 533 40. Worotnicki G. Csiro Triaxial Stress Measurement Cell. In: Hudson JA, ed. *Comprehensive Rock*
534 *Engineering*. Pergamon Press Ltd, Oxford; 1993:329-394.
- 535 41. Amadei B, Stephansson O. Rock stress and its measurement. In: Chapman and Hall, ed. ;
536 1997:201-276.
- 537 42. Holcombe R. *Oriented Drillcore: Measurement, Conversion, and Qa/Qc Procedures for Structural*
538 *and Exploration Geologists.*; 2013.
- 539 43. den Hartog SAM, Faulkner DR, Spiers CJ. Low Friction Coefficient of Phyllosilicate Fault Gouges
540 and the Effect of Humidity: Insights From a New Microphysical Model. *J Geophys Res Solid*
541 *Earth*. 2020;125(6):1-12. doi:10.1029/2019JB018683
- 542 44. Hakala M. *Boliden Mineral AB In Situ Stress Measurement with LVDT-Cell in Boliden*
543 *Garpenberg Mine at 1314 m Level (Report).*; 2018.
- 544 45. Ikari MJ, Saffer DM, Marone C. Frictional and hydrologic properties of clay-rich fault gouge. *J*
545 *Geophys Res Solid Earth*. 2009;114(5):1-18. doi:10.1029/2008JB006089
- 546 46. Lahaie F, Gunzburger Y, Ben Ouanas A, Barnichon JD, Bigarré P, Pigué JP. Impact of epoxy glue
547 curing time on the quality of overcoring stress measurements in low-temperature environments.
548 *Rock Stress Earthquakes - Proc 5th Int Symp In-Situ Rock Stress*. 2010;(January 2015):161-166.
549 doi:10.1201/9780415601658-26
- 550 47. Okada Y. Internal deformation due to shear and tensile faults in a half-space. *Bull - Seismol Soc*
551 *Am*. 1992;82(2):1018-1040. doi:10.1785/bssa0820021018
- 552 48. Van Zwieten GJ, Hanssen RF, Gutiérrez MA. Overview of a range of solution methods for elastic
553 dislocation problems in geophysics. *J Geophys Res Solid Earth*. 2013;118(4):1721-1732.
554 doi:10.1029/2012JB009278
- 555 49. Toda S, Stein SR, Sevilgen V, Lin J. Coulomb 3.3 Graphic-rich deformation and stress-change
556 software for earthquake, tectonic, and volcano research and teachin. *USGS Open-File Rep*.
557 Published online 2011:1-63.
- 558 50. Bouffier C, Lahaie F, Bigarré P. *Stress Measurement Campaign and Stress Monitoring Experiment*
559 *in the Lappberget Mining Area, at Garpenberg Mine, Boliden Technical Note : Ref. : DRS-15-*
560 *127363-05867A.*; 2015.
- 561 51. Contrucci I, Klein E, Bigarré P, Lizeur A, Lomax A, Bennani M. Management of post-mining
562 large-scale ground failures: Blast swarms field experiment for calibration of permanent
563 microseismic early-warning systems. *Pure Appl Geophys*. 2010;167(1-2):43-62.
564 doi:10.1007/s00024-009-0005-4